nagra.

Arbeitsbericht NAB 21-22

TBO Bözberg-2-1: Data Report

Dossier VIII
Rock Properties, Porewater Characterisation and Natural Tracer Profiles

April 2022

T. Gimmi, L. Aschwanden, L. Camesi,
E. Gaucher, A. Jenni, M. Kiczka, U. Mäder,
M. Mazurek, D. Rufer, H.N. Waber,
P. Wersin, C. Zwahlen & D. Traber

National Cooperative
for the Disposal of
Radioactive Waste

Hardstrasse 73
P.O. Box 280
5430 Wettingen
Switzerland
Tel. +41 56 437 11 11

www.nagra.ch

nagra.

Arbeitsbericht NAB 21-22

TBO Bözberg-2-1: Data Report

Dossier VIII
Rock Properties, Porewater Characterisation and Natural Tracer Profiles

April 2022

T. Gimmi[1], L. Aschwanden[1], L. Camesi[1], E. Gaucher[1], A. Jenni[1], M. Kiczka[1], U. Mäder[1], M. Mazurek[1], D. Rufer[1], H.N. Waber[1], P. Wersin[1], C. Zwahlen[1] & D. Traber[2]

[1] Rock-Water Interaction, Institute of Geological Sciences, University of Bern

[2] Nagra

Keywords:
BOZ2-1, Jura Ost, TBO, deep drilling campaign, rock properties, petrophysical parameters, water content, porosity, mineralogy, clay content, clay mineral composition, sulphate minerals, porewater chemistry, natural tracer profiles

National Cooperative for the Disposal of Radioactive Waste

Hardstrasse 73
P.O. Box 280
5430 Wettingen
Switzerland
Tel. +41 56 437 11 11

www.nagra.ch

Nagra Arbeitsberichte ("Working Reports") present the results of work in progress that have not necessarily been subject to a comprehensive review. They are intended to provide rapid dissemination of current information.

This NAB aims at reporting drilling results at an early stage. Additional borehole-specific data will be published elsewhere.

In the event of inconsistencies between dossiers of this NAB, the dossier addressing the specific topic takes priority. In the event of discrepancies between Nagra reports, the chronologically later report is generally considered to be correct. Data sets and interpretations laid out in this NAB may be revised in subsequent reports. The reasoning leading to these revisions will be detailed there.

This Dossier was prepared by the Rock-Water Interaction Group of the University of Bern (authors are listed in the individual chapters). D. Traber was the responsible Nagra project manager.

The authors warmly acknowledge the laboratory work of:
P. Bähler and C. Pichler efficiently produced a substantial part of the data presented in this report.
U. Eggenberger, J. Krbanjevic, M. Wolffers, Anna Zappatini and Frank Gfeller provided data for mineralogical and BET analyses as well as evaluation tools.
T. Oyama (CRIEPI, Japan) kindly collaborated in the context of porewater squeezing.

We also acknowledge the experimental and analytical work performed at Hydroisotop GmbH and at the French Geological Survey (BRGM) who conducted a large number of isotope diffusive-exchange and aqueous leaching experiments, respectively.

We are also grateful for the excellent work of the drill-site team who successfully provided sealed core samples according to our specifications.

We thank P. Blaser and M. Unger for editorial work.

The comments and suggestions of Andreas Gautschi on the manuscript are gratefully acknowledged.

Table of Contents

List of Tables

List of Figures

Electronic Appendices

App. A: Comprehensive database with results of laboratory analyses (xls format)

App. B: Detailed documentation of advective displacement experiments (xls format)

App. C: Hydroisotop GmbH data report (pdf format)

App. D: BRGM data report (pdf format)

Note: Appendices C and D are only included in the digital version of this report and can be found under the paper clip symbol. The other Appendices are available upon request.

1 Introduction

1.1 Context

To provide input for site selection and the safety case for deep geological repositories for radioactive waste, Nagra has drilled a series of deep boreholes ("Tiefbohrungen", TBO) in Northern Switzerland. The aim of the drilling campaign is to characterise the deep underground of the three remaining siting regions located at the edge of the Northern Alpine Molasse Basin (Fig. 1-1).

In this report, we present the results from the Bözberg-2-1 borehole.

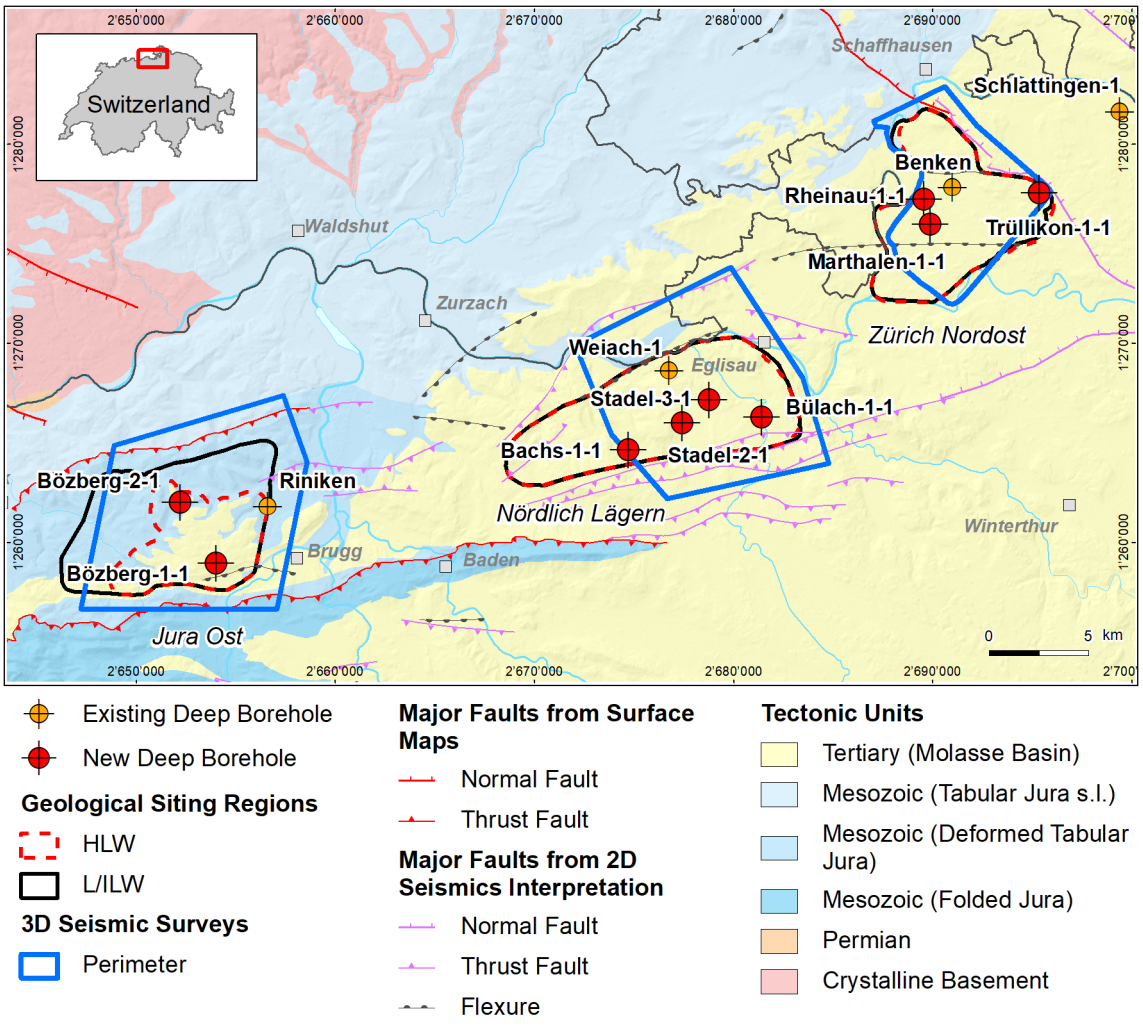

Fig. 1-1: Tectonic overview map with the three siting regions under investigation

1.2 Location and specifications of the borehole

The Bözberg-2-1 (BOZ2-1) exploratory borehole is the fifth borehole drilled within the framework of the TBO project. The drill site is located in the northern part of the Jura Ost siting region (Fig. 1-2). The vertical borehole reached a final depth of 829.11 m (MD)[1]. The borehole specifications are provided in Tab. 1-1.

Tab. 1-1: General information about the BOZ2-1 borehole

Siting region	Jura Ost
Municipality	Bözberg (Canton Aargau / AG), Switzerland
Drill site	Bözberg-2 (BOZ2)
Borehole	Bözberg-2-1 (BOZ2-1)
Coordinates	LV95: 2'652'218.764 / 1'261'985.437
Elevation	Ground level = top of rig cellar: 624.33 m above sea level (asl)
Borehole depth	829.11 m measured depth (MD) below ground level (bgl)
Drilling period	11th August – 14th December 2020 (spud date to end of rig release)
Drilling company	Daldrup & Söhne AG
Drilling rig	Wirth B 152t
Drilling fluid	Water-based mud with various amounts of different components such as[2]: 0 – 370 m: Bentonite & polymers 370 – 615 m: Potassium silicate & polymers 615 – 829.11 m: Pure-Bore®

The lithostratigraphic profile and the casing scheme are shown in Fig. 1-3. The comparison of the core versus log depth[3] of the main lithostratigraphic boundaries in the BOZ2-1 borehole is shown in Tab. 1-2.

[1] Measured depth (MD) refers to the position along the borehole trajectory, starting at ground level, which for this borehole is the top of the rig cellar. For a perfectly vertical borehole, MD below ground level (bgl) and true vertical depth (TVD) are the same. In all Dossiers depth refers to MD unless stated otherwise.

[2] For detailed information see Dossier I.

[3] Core depth refers to the depth marked on the drill cores. Log depth results from the depth observed during geophysical wireline logging. Note that the petrophysical logs have not been shifted to core depth, hence log depth differs from core depth.

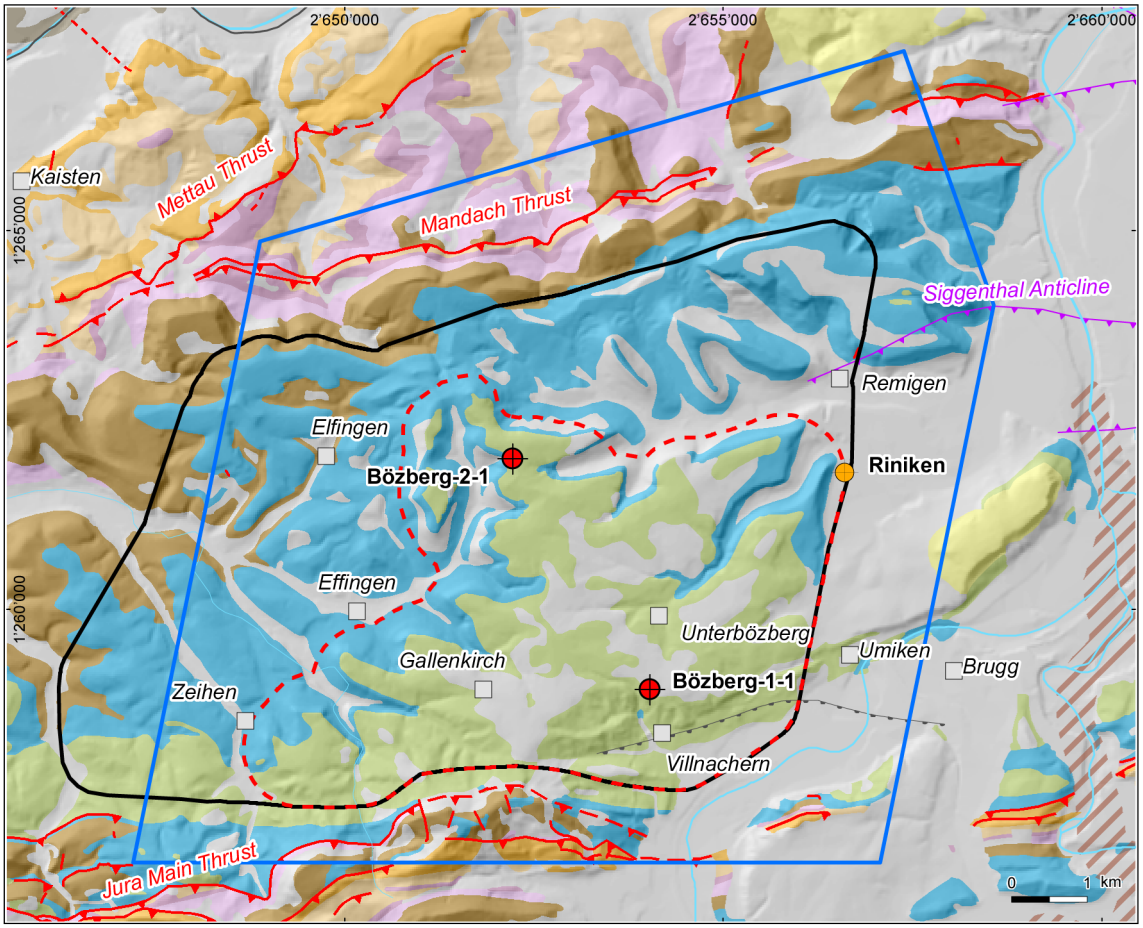

Fig. 1-2: Overview map of the investigation area in the Jura Ost siting region with the location of the BOZ2-1 borehole in relation to the boreholes Riniken and BOZ1-1

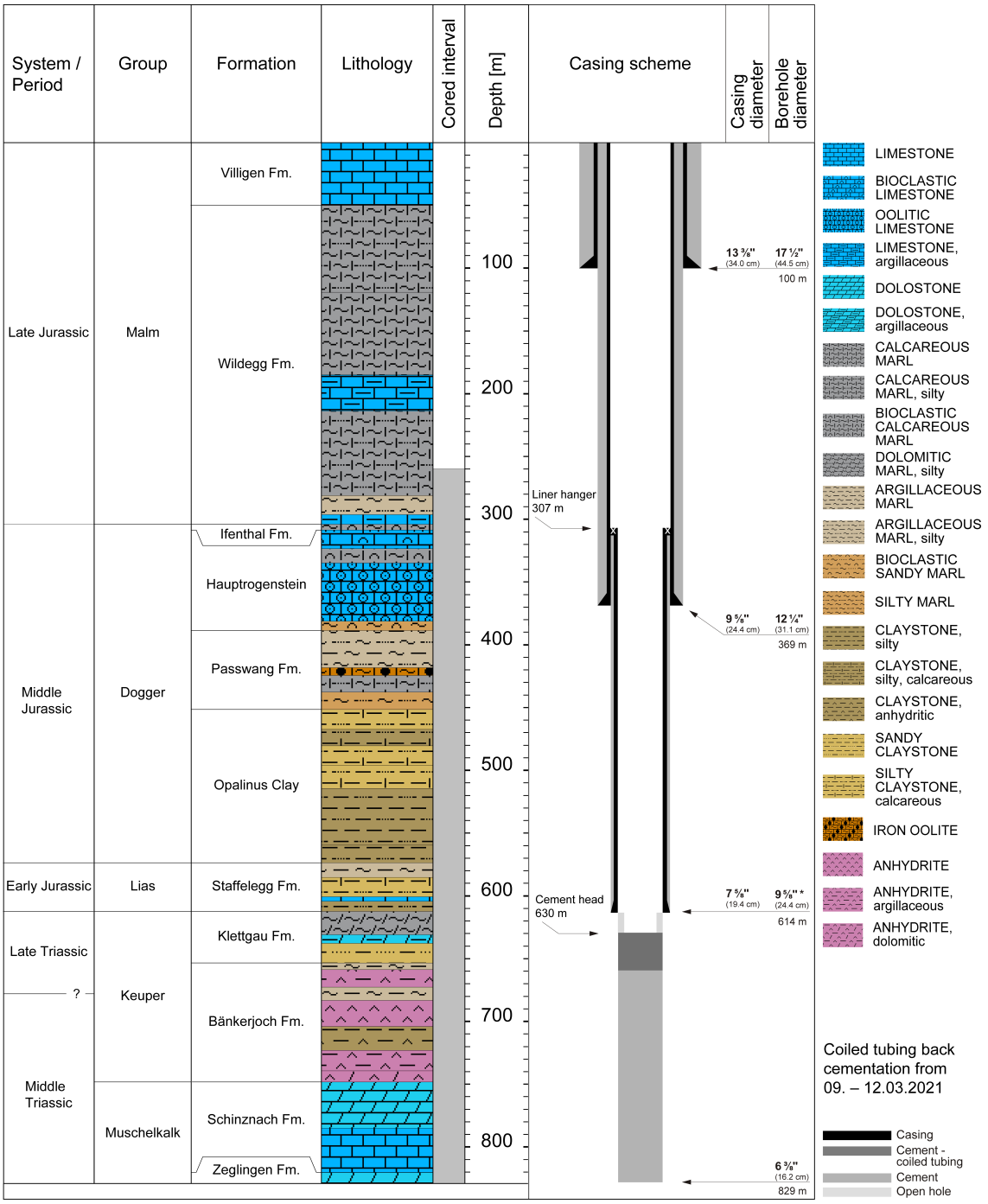

Fig. 1-3: Lithostratigraphic profile and casing scheme for the BOZ2-1 borehole[4]

[4] For detailed information see Dossier I and III.

Tab. 1-2: Core and log depth for the main lithostratigraphic boundaries in the BOZ2-1 borehole[5]

System / Period	Group	Formation	Core depth in m (MD)	Log depth in m (MD)	
Jurassic	Malm	Villigen Formation	50.0		—
		Wildegg Formation	303.95	304.38	—
	Dogger	Ifenthal Formation	308.70	309.07	—
		Hauptrogenstein	388.54	388.97	—
		Passwang Formation	451.54	451.90	—
		Opalinus Clay	573.68	573.89	—
	Lias	Staffelegg Formation	**612.46**	**612.76**	—
Triassic	Keuper	Klettgau Formation	653.45	654.70	—
		Bänkerjoch Formation	748.27	749.52	—
	Muschelkalk	Schinznach Formation	820.32	821.09	—
		Zeglingen Formation	829.11 final depth	829.88	—

[5] For details regarding lithostratigraphic boundaries see Dossier III and IV; for details about depth shifts (core goniometry) see Dossier V.

1.3 Documentation structure for the BOZ2-1 borehole

NAB 21-22 documents the majority of the investigations carried out in the BOZ2-1 borehole, including laboratory investigations on core material. The NAB comprises a series of stand-alone dossiers addressing individual topics and a final dossier with a summary composite plot (Tab. 1-3).

This documentation aims at early publication of the data collected in the BOZ2-1 borehole. It includes most of the data available approximately one year after completion of the borehole. Some analyses are still ongoing (e.g. diffusion experiments, analysis of veins, hydrochemical interpretation of water samples) and results will be published in separate reports.

The current borehole report will provide an important basis for the integration of datasets from different boreholes. The integration and interpretation of the results in the wider geological context will be documented later in separate geoscientific reports.

Tab. 1-3: List of dossiers included in NAB 21-22

Black indicates the dossier at hand.

Dossier	Title	Authors
I	TBO Bözberg-2-1: Drilling	P. Hinterholzer-Reisegger
II	TBO Bözberg-2-1: Core Photography	D. Kaehr & M. Gysi
III	TBO Bözberg-2-1: Lithostratigraphy	P. Jordan, P. Schürch, H. Naef, M. Schwarz, R. Felber, T. Ibele & M. Gysi
IV	TBO Bözberg-2-1: Microfacies, Bio- and Chemostratigraphic Analyses	S. Wohlwend, H.R. Bläsi, S. Feist-Burkhardt, B. Hostettler, U. Menkveld-Gfeller, V. Dietze & G. Deplazes
V	TBO Bözberg-2-1: Structural Geology	A. Ebert, L. Gregorczyk, S. Cioldi, E. Hägerstedt & M. Gysi
VI	TBO Bözberg-2-1: Wireline Logging, Micro-hydraulic Fracturing and Pressure-meter Testing	J. Gonus, E. Bailey, J. Desroches & R. Garrard
VII	TBO Bözberg-2-1: Hydraulic Packer Testing	R. Schwarz, M. Willmann, S. Reinhardt, S.M.L. Hardie, M. Voß & A. Pechstein
VIII	TBO Bözberg-2-1: Rock Properties, Porewater Characterisation and Natural Tracer Profiles	T. Gimmi, L. Aschwanden, L. Camesi, E. Gaucher, A. Jenni, M. Kiczka, U. Mäder, M. Mazurek, D. Rufer, H.N. Waber, P. Wersin, C. Zwahlen & D. Traber
IX	TBO Bözberg-2-1: Rock-mechanical and Geomechanical Laboratory Testing	E. Crisci, L. Laloui & S. Giger
X	TBO Bözberg-2-1: Petrophysical Log Analysis	S. Marnat & J.K. Becker
	TBO Bözberg-2-1: Summary Plot	Nagra

1.4 Scope and objectives of this dossier

The dossier at hand summarises the laboratory work of the Rock-Water Interaction Group (RWI) at the Institute of Geological Sciences of the University of Bern, of the French Geological Survey (BRGM) and of Hydroisotop GmbH dedicated to rock and porewater characterisation of core materials obtained from the BOZ2-1 borehole. The level of ambition is to document observations and measurements and to provide a quality-assured dataset. Closely related data obtained by other laboratories (CEC data by PSI) are integrated with our data.

Data are evaluated and discussed to some degree, including consistency and plausibility checks. An in-depth discussion, sophisticated modelling efforts and regional comparisons with data from other sites are beyond the scope of this report. Additional data obtained by other groups (e.g. hydraulic tests, groundwater sampling, geophysical borehole and core logging, structural logging) are considered in several cases but not in a comprehensive way. An integrated interpretation of all available data is deferred to a later stage of the TBO programme, when results from several boreholes can be synthesised for a siting region.

Throughout this report, rock samples used for analysis are identified by their mid-sample depth in meter MD.

2 Geoscientific data of interest and drilling conditions for the BOZ2-1 borehole

Thomas Gimmi, Lukas Aschwanden

2.1 Geological information

The BOZ2-1 borehole is located towards the northern part of the siting region Jura Ost (Fig. 1-1), northwest of the village of Oberbözberg. Jura Ost lies in the Deformed Tabular Jura between the autochthonous Tabular Jura in the NW and the Folded Jura in the south. The Deformed Tabular Jura is delineated by the E-W running Jura Main Thrust about 5 km south of BOZ2-1 and the Mandach Thrust (WSW-ENE) about 3 km NNW of BOZ2-1 (Fig. 1-2). Tectonically, the Deformed Tabular Jura is compressively overprinted by the Alpine forefront. This is for example manifested by a thrust of the Mesozoic sediments to the north with an estimated transport distance of about 200 m (Egli et al. 2017), which is assumed to have occurred on the Triassic salt layers of the Zeglingen Formation (Muschelkalk; Nagra 2014).

According to seismic interpretations, no relevant faults have been identified in the Mesozoic layers at the borehole location (Dossier V). However, field and seismic data indicate the occurrence of NNE-SSW striking subvertical strike-slip faults (Madritsch & Hammer 2012). The regional dip of the Mesozoic layers is subhorizontal towards the SE.

2.2 Structural logging

The results of the structural core logging are documented in Dossier V, where the following types of structural features are distinguished:

- Fault planes and fault zones (shear structures); these are mainly oriented subparallel to bedding (SE-dipping)
- Brittle extensional fractures (structures without shear or slip indication, e.g. joints, veins, tension gashes); these exhibit large variation in orientation and dip (1 – 90°)
- Stylolites; two classes with different orientation and dipping trend: 1) parallel or subparallel to bedding (SE- to S-dipping) and 2) subvertical with variable dip direction
- Larger open pores

The interpreted structures are unevenly distributed among the stratigraphic units (*cf.* Tab. 2-1 and Dossier V).

Tab. 2-1: Fault zones in the cored section of the BOZ2-1 borehole

From Dossier V.

Top [m MD log depth]	**Bottom** [m MD log depth]	**Thickness** [m]	**Unit**
270.84	271.28	0.44	Wildegg Formation
508.03	508.04	0.01	Opalinus Clay
510.26	510.74	0.48	Opalinus Clay
530.51	532.25	1.74	Opalinus Clay
561.65	562.22	0.57	Opalinus Clay
562.42	562.47	0.05	Opalinus Clay
604.47	604.49	0.02	Staffelegg Formation
625.85	627.66	1.81	Klettgau Formation
627.38	627.66	0.28	Klettgau Formation
639.31	641.73	2.42	Klettgau Formation
645.73	645.75	0.02	Klettgau Formation
736.67	736.68	0.01	Bänkerjoch Formation
740.31	740.36	0.05	Bänkerjoch Formation
746.19	746.22	0.03	Bänkerjoch Formation
746.42	746.43	0.01	Bänkerjoch Formation
746.46	746.50	0.04	Bänkerjoch Formation

2.3 Hydrogeological conditions

Tab. 2-2 gives a summary of the hydraulic tests performed. The results of the hydraulic packer tests in the BOZ2-1 borehole are documented in Dossier VII.

In the Hauptrogenstein, the packed-off interval extended from 334.30 to 365.93 m depth. The main flow zone in this interval was at about 352 m depth, indicated by mud logging. A prominent single subvertical fracture, characterised as an open joint, was observed at this depth. In the Keuper, the packed-off interval extended from 631.40 – 658.00 m depth, including Gansingen and Ergolz Members as potential permeable units. In the Muschelkalk, the packed-off interval was between 747.50 and 805.50 m depth. Here, hydrotesting was decided based on mud losses observed when reaching 805 m depth.

Tab. 2-2: Results of hydraulic packer tests in borehole BOZ2-1

The best estimates for transmissivity *T*, hydraulic conductivity *K* and hydraulic head are indicated. Hydraulic heads in the clay-rich formations are believed to be affected by transient hydromechanical processes. See Dossier VII for further details.

Top [m MD]	**Bottom** [m MD]	**Length** [m]	**Geological units**	***T*** [m^2/s]	***K*** [m/s]	**(Apparent) Head** [m asl]	**Test name**
334.3	365.93	31.63	Hauptrogenstein (aquifer)	4×10^{-07}	1×10^{-08}	463	HRO1
429.3	452.32	23.02	Passwang Fm.	7×10^{-13}	3×10^{-14}	672	PWF1
402.5	425.52	23.02	Passwang Fm.	4×10^{-13}	2×10^{-14}	849	PWF2
527.5	550.52	23.02	Opalinus Clay	1×10^{-12}	6×10^{-14}	868	OPA1
455	478.02	23.02	Opalinus Clay	8×10^{-13}	3×10^{-14}	790	OPA2
559.18	566.16	6.98	Opalinus Clay	1×10^{-13}	1×10^{-14}	1'210	OPA3
507.2	513.55	6.35	Opalinus Clay	8×10^{-14}	1×10^{-14}	1'144	OPA4a
598	615	17	Staffelegg Fm.	8×10^{-12}	5×10^{-13}	638	LIA1
631.4	658	26.6	Klettgau Fm. (Keuper aquifer)	1×10^{-04}	6×10^{-06}	450	KEU1
747.5	805.5	58	Schinznach Fm. (Muschelkalk aquifer)	9×10^{-05}	2×10^{-06}	383	MUK1

2.4 Groundwater samples

Groundwater samples with variable degrees of drilling-fluid contamination were obtained from the Hauptrogenstein, Keuper and Muschelkalk aquifers. For the present report, values for the chemically conservative parameters Cl and Br and the water-isotope ratios $\delta^{18}O$ and $\delta^{2}H$ are of major interest, as these represent boundary conditions for the porewater data. These values were corrected by Lorenz (*in prep.*) for (minor) drilling-fluid contamination and are reproduced in Tab. 2-3 along with information on the chemical water type and mineralisation of the groundwaters.

Tab. 2-3: Conservative parameters for waters from the Hauptrogenstein, Keuper and Muschelkalk aquifers in borehole BOZ2-1 corrected for drilling-fluid contamination

From Lorenz (*in prep.*).

Parameter	**Unit**	**Hauptrogenstein aquifer**	**Keuper aquifer**	**Muschelkalk aquifer**
Chemical type		**Na-SO_4-Cl**	**Na-SO_4-HCO_3**	**Na-Cl**
Mineralisation (TDS)	[g/L]	4.3 *	1.1 *	12.2 *
Chloride (Cl^-)	[mg/L]	710 **	13.1 **	5'826 ***
Bromide (Br^-)	[mg/L]	2.3 **	0.036 **	1.17 ***
$\delta^{18}O$ of water	[‰$_{VSMOW}$]	–7.89 **	–10.17 **	–10.26 ***
$\delta^{2}H$ of water	[‰$_{VSMOW}$]	–57.4 **	–69.7 **	–73.8 ***
Test interval	[m MD]	334.30 – 365.93	631.40 – 658.00	747.50 – 805.50

* Last sample

** Corrected based on ^3H-H_2O

*** Corrected based on uranine

2.5 Drilling conditions and drilling fluids

Water-based muds with various amounts of additional components were used as drilling fluids (*cf.* Tabs. 1-1 and 2-4). From 0 – 370 m, additives included bentonite and polymers, from 370 – 615 m potassium silicate and polymers, and from 615 – 829 m Pure-Bore®.

Losses of drilling mud were recorded at several places during the drilling operations in BOZ2-1 (Tab. 2-4 and Dossier I). Relevant losses of 93 m^3 in total occurred at a depth of 351.70 m MD (log depth) in the Hauptrogenstein; they correspond to a single open subvertical fracture observed in the drill cores. Some mud losses with a constantly increasing pumping pressure occurred also at ~ 583 m MD (~ 24 m^3), eventually related to a technical issue (Section 3.5.3 in Dossier I). Further mud losses were observed in the Schinznach and Zeglingen Formations from 805 m to 829 m MD (core depth). The losses at this depth amounted to 273 m^3 in total and were caused by steeply dipping open fractures observed in the cores.

Tab. 2-4: Drilling muds and main mud loss events

Based on Dossier I.

Depth interval [m]	**Geological unit**	**Additives of wate-based drilling mud**	**Comments**
0 – 370	Quaternary – Hauptrogenstein	Bentonite, polymers	Destructive drilling 0 – 260 m; large mud loss (93 m^3) at 351.5 m, open fracture / joint
370 – 615	Hauptrogenstein – Klettgau Fm.	K silicate, polymers	Mud loss (24 m^3) with increasing pumping pressure at ~ 583 m (Staffelegg Fm.), eventually related to technical issue (see text)
615 – 829	Klettgau Fm. – Zeglingen Fm.	Pure-Bore®, polymers	Large mud loss (up to 273 m^3) at 805.50 – 829.11 m in fracture zone in Schinznach and Zeglingen Fm.

3 Sampling and applied methods

3.1 Sampling strategy

Thomas Gimmi

A suite of 8 different sample types were investigated (Tab. 3-1). Sample types and the general procedures of core sampling, sample conditioning and storage are described by Rufer (2019).

Tab. 3-1: Sample types and sampling strategy

The table includes on-site conditioned samples relevant for the present report.

Sample type	**Main study targets**	**Sampling (by on-site team)**
PW (porewater chemistry), RP (various rock properties)	Characterisation of porewater chemistry and rock	Sample lithology representative of the current lithofacies and the sampled core section (usually 3 m). Sampling with about regular spacing in order to obtain a representative dataset
SQ (squeezing)	Characterisation of porewater chemistry	Focussed on clay-rich lithologies due to methodological constraints
AD (advective displacement)	Characterisation of porewater chemistry	Focussed on clay-rich lithologies due to methodological constraints
OD (out-diffusion)	Out-diffusion experiments (diffusion coefficient for Cl^-, Cl^- concentration in bulk porewater)	Focussed on clay-poor lithologies due to methodological constraints. Experiments are not part of this investigation
DI (diffusion experiments)	Diffusion coefficients (at PSI)	Focussed on upper and lower confining units, i.e., restricted range of lithologies
NG (noble gas analysis)	Concentrations and isotopic compositions of dissolved noble and reactive gases	Sampling with a regular spacing, with situational tightening of the sampling interval close to potentially water-conducting features. Reported separately.
GM (geomechanics)	Mineralogy and grain density of samples studied for their geomecha-nical properties by other laboratories	Sampling with about regular spacing; data not yet/only partly available

3.2 Laboratory programme

Thomas Gimmi

In total, 147 PW, RP, SQ, AD, DI and OD samples were investigated, and additional 108 NG and GM samples were taken (see overview in Tab. 3-2). The PW and RP samples were analysed at different laboratories: 40 PW or RP samples were investigated by the French Geological Survey (BRGM), 51 by Hydroisotop GmbH (HI), and 29 by the Rock-Water Interaction Group (RWI) at the University of Bern. This also allowed for an inter-laboratory comparison. Samples of types SQ, AD, DI were investigated by RWI, the additional measurements for sample types NG and

GM are being made when the material is available (main studies of DI and GM samples were performed by other laboratories; see Tab. 3-1). OD samples are kept for possible later analysis. In Tab. 3-3, the analytical programme for the various sample types and the different laboratories are shown in more detail.

As in the previous boreholes, the investigations were focused on the section Dogger and Liassic. Because the borehole provided clear evidence of the Keuper aquifer, it was decided not to analyse the lower sections (below the top of the Bänkerjoch Formation) for porewater and natural tracers.

Tab. 3-2: Numbers of samples analysed or collected for the different geological units

In the case of the NG samples and the GM samples, the number refers to the total number of samples collected (RWI: Rock-Water Interaction Group of the University of Bern, BRGM: French Geological Survey, HI: Hydroisotop GmbH).

Times	**PW, RP**			**SQ**	**AD**	**DI**	**NG**	**GM**	**OD**	**Total** *
	RWI	BRGM	HI	RWI	RWI	RWI	RWI	RWI	RWI	
Malm	1	1	2				2	4		**4/6**
«Brauner Dogger»	13	16	19	1	1	4	11	19	2	**56/30**
Opalinus Clay	7	16	20	2	1		7	17		**46/24**
Staffelegg Fm.	2	4	6	1	1	4	3	4	2	**20/7**
Klettgau Fm.	4	3	4				3	6		**11/9**
Bänkerjoch Fm.	2					2	5	11		**4/16**
Schinznach Fm.							4	9		**0/13**
Zeglingen Fm.							2	1		**0/3**
All	**29**	**40**	**51**	**4**	**3**	**10**	**37**	**71**	**4**	**147/108**

* Total of PW, RP, SQ, AD, DI, and OD samples/total of NG and GM samples

Tab. 3-3: Analytical programme performed for the different sample types

×× = standard programme, × = selected samples only

Method	**PW, RP** (RWI)	**PW, RP** (BRGM)	**RP** (HI)	**SQ**	**AD**	**DI**	**NG**	**GM**
Bulk mineralogical composition incl. CNS analysis	××	××**		××	××	××		××***
Clay mineralogy	×	×			××	××		
Bulk wet density	××	××			××	××	××***	
Grain density	××	××			××	××		××***
Water content	××	××	××	××	××	××	××***	
BET surface area						××		
Cation-exchange properties	×*				××			
Sorption measurements								
Aqueous extraction	××	××		××	××			
Porewater squeezing				××				
Advective displacement of porewater					××			
Water isotopes	××		××	××	××			
Dissolved noble gases							×	
Dissolved reactive gases							×	

* Subsamples collected during sample preparation, re-packed and sent to PSI for analysis

** Analyses performed by RWI on remaining rock material from experiments of BRGM

*** Analyses to be performed by RWI on remaining rock material (currently only partly available)

3.3 Analytical methods and methods of raw-data processing

Thomas Gimmi

Experimental procedures of RWI and associated analytical methods, formalisms to process measured data and quantification of propagated errors are documented in Waber (ed.) (2020) and are not repeated here. Moreover, Mazurek et al. (2021) provide additional information for situations where the current practice is not documented or deviates from that described in Waber (ed.) (2020).

Water contents (gravimetry and isotope mass balance) and isotope data from diffusive-exchange experiments by Hydroisotop GmbH were obtained using the same protocol as that applied by the University of Bern, documented in Waber (ed.) (2020) and slightly extended in Mazurek et al. (2021). BRGM used different protocols for sample preparation and for the quantification of petrophysical parameters, as presented in Section 3.4 and in their data report provided in the electronic Appendix D, but followed the protocol of Waber (ed.) (2020) for the aqueous extracts.

3.4 Petrophysical parameters studied by BRGM

Thomas Gimmi

Sample preparation

The samples were cut open from the Al/plastic seals in a glovebox under N_2 atmosphere. All preparation using hammer and chisel was performed in the glovebox. The drying oven to measure water content was also placed within the glovebox, meaning that rock oxidation during drying could be completely suppressed.

Bulk wet density and water content $WC_{dry\ 2d}$

An aliquot of the sample was weighed as received (wet mass, $m_{init\ 1}$), then immersed in kerosene until bubbles disappeared at the surface. Then the immersed material was taken out of the kerosene, wiping the excess petroleum residue on the surface with a tissue. The water- and kerosene-saturated aliquot was weighed again ($m_{init\ 2}$). Subsequently, the aliquot was immersed into kerosene again and weighed according to Archimedes' principle ($m_{in\ kerosene}$; Monnier et al. 1973, Charpentier et al. 2003, Gaboreau et al. 2011). Together with the known density of liquid kerosene ($\rho_{kerosene}$), the bulk volume ($V_{bulk} = [m_{init\ 2} - m_{in\ kerosene}]/\rho_{kerosene}$) of the aliquot and therefore bulk wet density of the aliquot ($\rho_{bulk\ wet} = m_{init\ 1}/V_{bulk}$) were obtained. Note that according to this definition the obtained bulk wet density refers to that of the sample prior to immersion in kerosene. If some degree of evaporation occurred during sample preparation, bulk wet density is slightly underestimated. Finally, the aliquot was dried in an oven at 105 °C for 48 h (2 d), which was expected to remove both porewater and kerosene, so that the dry rock mass (m_{dry}) was obtained by subsequent weighing. From this, the water contents $WC_{wet,\ 2d} = (m_{init\ 1} - m_{dry})/\ m_{init\ 1}$ and $WC_{dry,\ 2d} = (m_{init\ 1} - m_{dry})/\ m_{dry}$ were calculated.

Water content $WC_{dry\ 28d}$

Two other aliquots of each sample (150 – 200 g) were weighed and then dried for 28 d at 105 °C. Sample mass was measured recurrently, and all samples reached a mass plateau that did not further change over time. This is a minor difference to the experience made by the University of Bern where sample mass reaches a minimum and then increases weakly (typically < 0.02% over 1 – 2 weeks) due to ongoing oxidation. This latter process was minimised in BRGM's campaign because drying was performed under oxygen-free conditions in the glovebox.

Comparison of water contents $WC_{dry\ 2d}$ and $WC_{dry\ 28d}$

The data are compared in Fig. 3.4-1, which shows that on average $WC_{dry\ 28d}$ exceeds $WC_{dry\ 2d}$ (less clear for samples with very low water contents), indicating that the drying process is not complete after 2 d. In that sense, $WC_{dry\ 28d}$ is probably more appropriate.

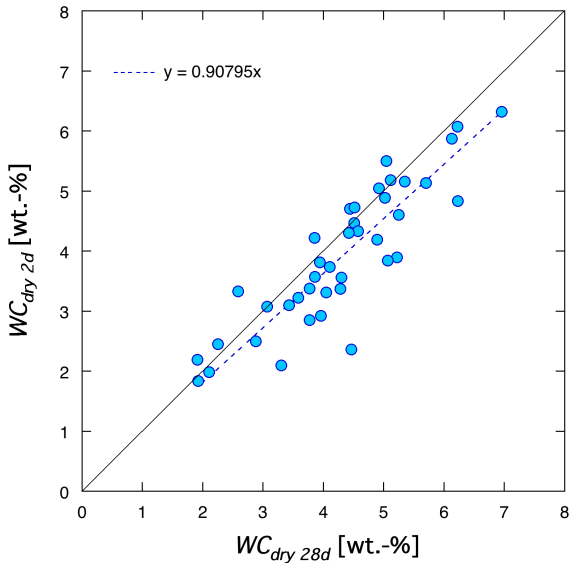

Fig. 3.4-1: Comparison of water contents WC_{dry} obtained by BRGM by drying at 105 °C over 2 d and over 28 d

Stippled blue line is a linear regression of the data.

Aqueous extraction

Aqueous extracts at S/L ≈ 1 were prepared from yet another aliquot of the sample, applying the same protocols as described in Waber (ed.) (2020). Samples were extracted as received, i.e., they were not dried before extraction. Cl and SO_4 were quantified by ion chromatography, while ICP-MS was used for Br. Cations were not investigated. All manipulations were performed in a glovebox under N_2 atmosphere.

Ratio of water-loss porosity and pycnometer porosity and comparison with data from University of Bern

Formally, the ratio ϕ_{WL}/ϕ_{pyc} between water-loss porosity and pycnometer porosity obtained for a given sample corresponds to the water saturation $S_w = V_{water}/V_{pores}$ of that sample. The two parameters ϕ_{WL} and ϕ_{pyc} are, however, generally determined on two different aliquots of a sample. The error of saturation values $S_w = \phi_{WL}/\phi_{pyc}$ is thus typically large, possibly affected by heterogeneity between different aliquots. Such heterogeneity is only partly represented in the propagated error (through standard deviation of 2 or 3 water content subsamples at BRGM and University of Bern, respectively). Thus, absolute numbers of this ratio must be interpreted with care.

When comparing porosity obtained from water content with pycnometer porosity, minor to major discrepancies were identified for individual samples (Figs. 3.4-2, 3.4-3). The University of Bern dataset tends to larger values in the Opalinus Clay, and generally shows more outliers and more values with large propagated errors compared to the BRGM dataset for samples dried during 28 d. The latter is related to the fact that the University of Bern dataset includes comparably more samples from the confining units (see depth profile in Fig. 3.4-3), some of which have low porosity and/or comparably large heterogeneity at the sample scale, leading to larger uncertainties. Overall, the University of Bern data and the BRGM data for samples dried during 28 d are both centred around 1 (BRGM 28 d: 0.99 ± 0.10; University of Bern: 0.98 ± 0.16). This is

different compared to an earlier investigation (TRU1-1 borehole; Aschwanden et al. 2021), where water-loss porosities obtained by BRGM for samples dried at 28 d tended to be lower than pycnometer porosities, in many cases substantially so. It was hypothesised that the differences could be related to the dry N_2 atmosphere in the glovebox, in which the BRGM samples were processed (the University of Bern samples were processed under atmospheric conditions). According to their report, the processing of the BRGM samples from BOZ2-1 was identical to that for the earlier investigation, so the reason for the different observations remains unclear.

Fig. 3.4-2 presents additionally the ratio between water-loss porosity and pycnometer porosity for BRGM samples dried during 2 d. This dataset shows a slight tendency of decreasing values with decreasing pycnometer porosity, and the mean value is 0.94±0.08. This confirms the above statement that the drying process may not be complete after 2 d, and that the water content or the water-loss porosity after drying for 28 d is probably more appropriate.

Partial desaturation of aliquots, if occurring, would mean that all quantities that refer to the wet mass are somewhat biased compared to a saturated sample. For instance, the measured bulk wet density would be slightly underestimated. However, the calculated bulk dry density is independent of the degree of saturation (unless sample shrinkage occurred due to partial desaturation). Also, a comparison in terms of water contents per dry mass is then more reliable than a comparison in terms of water contents per wet mass. If water-loss porosities were considerably larger than pycnometer porosities, this could hint to some water uptake during the preparation of the water-loss samples (e.g., due to a high relative humidity of the surrounding air), or to an underestimation of the pycnometer porosity (for unknown reasons), but it could also just be related to sample heterogeneities. A careful inspection of trends of these data is then required as is done for instance in Figs. 3.4-2 and 3.4-3.

Any uptake or loss of water during preparation of water-loss samples could be corrected for by using the derived value of S_w when calculating quantities depending on the water content (e.g., Cl concentrations in aqueous extracts, *cf.* Equation 6-1 in Waber (ed.) 2020). Alternatively, the pycnometer porosity could be used instead of the water-loss porosity in corresponding calculations, or a water content derived from the pycnometer porosity instead of the measured one according to $WC_{dry} = \phi_{pyc}\, \rho_{water}/\rho_{bulk\ dry}$. This is done for comparison in Section 5.2 (see also Section 4.4) when presenting the anion profiles. Interestingly, the datasets obtained at the two laboratories (University of Bern and BRGM) match better when using the pycnometer porosities instead of the water-loss porosities, which has not been observed in earlier investigations. This is, however, not a proof that water uptake did occur for the University of Bern samples (mainly Opalinus Clay) during the sample preparation. It just shows that mainly in this formation there is a slight but systematic difference in the measured water contents between RWI and BRGM, but not in the measured pycnometer porosities.

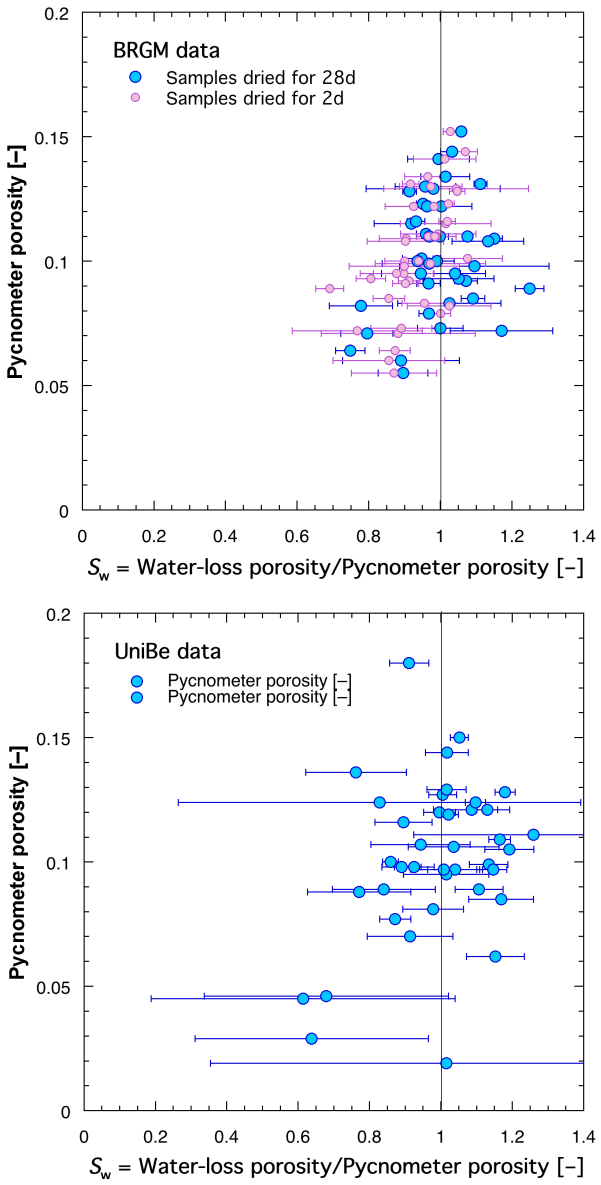

Fig. 3.4-2: Comparison of ratios of water-loss porosity (calculated from $WC_{dry\ 28d}$ and $WC_{dry\ 2d}$ in the case of BRGM) and pycnometer porosity obtained from measurements at BRGM and at the University of Bern

Propagated error based on standard deviation of water content measurements in duplicate (BRGM) or in triplicate (UniBe). The UniBe data include comparably more samples from the confining units with typically larger errors.

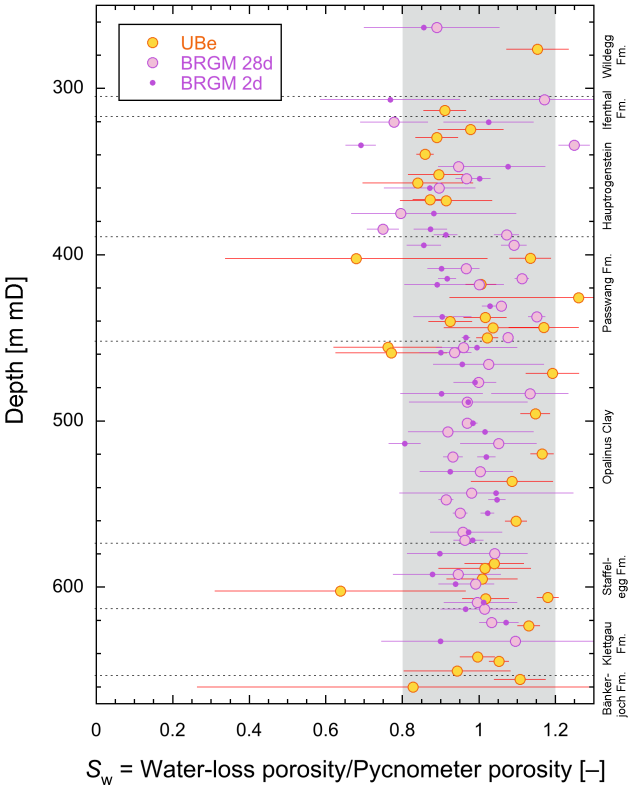

Fig. 3.4-3: Depth profile of ratios of water-loss porosity (calculated from $WC_{dry\ 28d}$ and $WC_{dry\ 2d}$ in the case of BRGM) and pycnometer porosity obtained from measurements at BRGM and at the University of Bern

Propagated error based on standard deviation of water content measurements in duplicate (BRGM) or in triplicate (UBe). The UBe data include comparably more samples from the confining units with typically larger error.

4 Results

4.1 Documentation of measured and calculated data

Thomas Gimmi

Raw data collected by the three different laboratories in the frame of the analytical programme of the BOZ2-1 borehole are organised in a FileMaker database, including raw-data files, graphics and photographs. The main purpose of this database is to ensure the full documentation and traceability of original and derived data presented in this report. From this database, the relevant data were exported into a comprehensive Excel sheet, which is attached in Appendix A (the full datasets of Hydroisotop GmbH and BRGM are provided in their data reports in Appendices C and D, respectively). The objective of this Excel sheet is not to fully document all analyses made but, per parameter and sample, to indicate the "best" or most representative value in case multiple measurements were made, and to list parameters calculated from the original measurements. For example, only one composition is given for squeezed and advectively displaced porewaters in a sample, even though multiple aliquots were collected and analysed. Explanory notes to this sheet follow here.

Bulk mineralogy (X-ray diffraction and CNS analysis)

- Contents of minerals not detected by X-ray diffraction are set to 0, as the actual detection limits are difficult to quantify. "tr" = present in trace amounts.
- Clay-mineral content is not measured directly but is calculated by difference to 100%.
- Pyrite content is calculated from the measured S content, assuming that pyrite is the main S reservoir in the rock. This is not the case in anhydrite-bearing rocks, which are typically free of pyrite. Here, the S is used to calculate the content of anhydrite.
- Column "Füchtbauer name" refers to the nomenclature of clastic rocks as defined in Naef et al. (2019). Names are listed only for rock compositions that have < 10 wt.-% minerals not represented in the Füchtbauer triangle (i.e., minerals other than clays, calcite, dolomite/ ankerite, siderite, quartz, K-feldspar, plagioclase). In particular, this means that evaporitic rocks are not given a Füchtbauer name. If a rock contains ≥ 90 wt.-% minerals represented in the Füchtbauer triangle but also contains anhydrite, this is stated in brackets.
- The Füchtbauer triangle does not distinguish between limestones and dolostones. When the content of calcite exceeds that of dolomite/ankerite, the terms "limestone" or "calcareous" are used in this report, and "dolostone" or "dolomitic" are used if the opposite applies.

Clay mineral groups

- All data refer to wt.-% of the total rock.
- Illite/smectite ML (85-90) refers to a mixed-layer phase with 85-90% illite layers, Chl/Sm ML (85-95) designates a chlorite-smectite mixed-layer phase with 85-95% chlorite (analogous for the other listed mixed-layer phases).

End-member clays

- All data refer to wt.-% of the total rock.
- Illite, smectite and chlorite partially occur in mixed-layer phases. Here, the respective total contents of the end-members are calculated. For example, if a sample contains 10 wt.-% illite and 8 wt.-% illite/smectite mixed layers containing 75% illite, the end-member illite content would be 16 wt.-%.

Petrophysical parameters

- Bulk wet density was measured, and bulk dry density was calculated using equation 5-14 in Waber (ed.) (2020).
- Pycnometer porosity was calculated from densities using equation 5-16 in Waber (ed.) (2020).
- Water content (dry) was calculated from water content (wet) using $w_d = w_w/(1-w_w)$; see eq. 12 in Appendix A of Waber (ed.) (2020).
- Water-loss porosity was calculated using bulk wet density (equation 5-9 in Waber (ed.) 2020) or grain density (equation 5-7 in Waber (ed.) 2020).
- The formalisms to calculate water content from isotope diffusive-exchange experiments are given in equation 76 of Appendix A of Waber (ed.) (2020) and are detailed in Mazurek et al. (2021).

Cl^- and Br^- from aqueous extracts recalculated to pore-water concentrations using water content

- Concentrations are given relative to bulk porewater as well as relative to various assumptions regarding anion accessibility in the pore space. The calculation is made using equation 6-1 in Waber (ed.) (2020). The variants pertaining to the dependence of anion accessibility on clay-mineral content are discussed in Chapter 5.
- In most cases, water content and aqueous extract data were obtained from separate aliquots of a sample. In some cases, previously dried subsamples on which water contents had been determined were used to extract just Cl and Br concentrations

Errors

- The error columns refer to analytical uncertainty or instrument precision for measured parameters and to propagated errors for calculated parameters, following the formalisms documented in Waber (ed.) (2020) and Appendices A and B.

4.2 Mineralogical composition

Martin Mazurek

4.2.1 Whole rock data

A total of 86 mineralogical analyses were performed in the section Wildegg Formation (Malm) – Bänkerjoch Formation (Keuper). The full dataset is documented in Appendix A, and Tab. 4.2-1 provides formation-specific summaries. Plots against depth for the most relevant minerals are shown in Fig. 4.2-1, and a representation in the Füchtbauer triangle is given in Fig. 4.2-3.

The Triassic section is lithologically heterogeneous, mainly due to the variable contents of dolomite and anhydrite. Given the limited number of samples, systematic depth trends cannot be resolved. The overlying Dogger-Lias section is discussed in detail further below. In the studied lower part of the Wildegg Formation, an upward trend of decreasing clay-mineral contents and increasing calcite contents is seen, even though weakly defined by just 3 analyses. Note that in the BOZ1-1 profile, the reverse trends were observed in this part of the profile (Wersin et al. 2022).

Minor or trace amounts of the following phases have been identified:

- Magnesite in the Bänkerjoch Formation
- Celestite in the Hauptrogenstein, Klettgau and Bänkerjoch Formations
- Barite in the Klettgau Formation
- Goethite in the Ifenthal Formation, upper Hauptrogenstein ('Movelier Beds' + 'Spatkalk') and Staffelegg Formation
- Haematite in the upper Hauptrogenstein ('Movelier Beds' + 'Spatkalk').

The depth profiles of the contents of S and N (based on CNS analysis) are shown in Fig. 4.2-2, and they are remarkably similar to those of BOZ1-1. Variable but often high S contents are seen in the Staffelegg Formation. In both boreholes, a relative minimum occurs in the lower part of the Opalinus Clay. Conversely, N contents show a maximum approximately at that position and decrease systematically upwards until the top of the Passwang Formation. The highest N contents are observed in the Staffelegg Formation, likely due to the presence of abundant organic matter.

Tab. 4.2-1: Bulk-rock mineralogy: formation-specific means, medians, standard devations and ranges [wt.-%]

In addition to the listed phases, one sample from the lower Hauptrogenstein, one from the Klettgau Formation and one from the Bänkerjoch Formation contain traces of celestite. Two samples from the Klettgau Formation contain traces of barite. For the calculation of statistical parameters, values below detection were set to 0. In several cases, systematic depth trends of mineral contents were observed (see below). This means that in these cases the data do not follow a Gaussian distribution, which is a pre-requisite for the calculation of meaningful standard deviations. In such cases, the ranges (also listed) are more meaningful.

Formation (number of analyses)	**Member**		**S** [wt.-%]	**N** [wt.-%]	**C(inorg)** [wt.-%]	**C(org)** [wt.-%]	**Quartz** [wt.-%]	**K-feldspar** [wt.-%]	**Plagioclase** [wt.-%]	**Calcite** [wt.-%]	**Dolomite/Ank.** [wt.-%]	**Siderite** [wt.-%]	**Magnesite** [wt.-%]	**Anhydrite** [wt.-%]	**Goethite** [wt.-%]	**Haematite** [wt.-%]	**Pyrite** [wt.-%]	**Clay minerals** [wt.-%]
Wildegg Fm. (2)		Mean	0.00	0.00	8.86	0.37	5.0	0.7	0.0	73.9	0.0	0.0	0.0	0.0	0.0	0.0	0.0	20.1
		Median	0.00	0.00	8.86	0.37	5.0	0.7	0.0	73.9	0.0	0.0	0.0	0.0	0.0	0.0	0.0	20.1
		Stdev	0.00	0.00	0.59	0.01	0.4	1.0	0.0	4.9	0.0	0.0	0.0	0.0	0.0	0.0	0.0	4.4
		Min	0.00	0.00	8.45	0.36	4.7	0.0	0.0	70.4	0.0	0.0	0.0	0.0	0.0	0.0	0.0	17.0
		Max	0.00	0.00	9.28	0.38	5.3	1.4	0.0	77.3	0.0	0.0	0.0	0.0	0.0	0.0	0.0	23.2
Ifenthal Fm. (1)		Mean	0.22	0.00	7.76	0.41	2.9	0.0	0.0	61.6	1.5	1.7	0.0	0.0	2.0	0.0	0.4	29.5
Haupt-rogen-stein (all) (16)		Mean	0.25	0.00	9.10	0.44	4.4	0.7	0.2	70.7	4.7	0.0	0.0	0.0	0.7	0.1	0.5	17.6
		Median	0.18	0.00	9.60	0.32	3.7	0.0	0.0	72.1	3.0	0.0	0.0	0.0	0.0	0.0	0.3	16.3
		Stdev	0.29	0.00	1.84	0.34	4.5	1.5	0.6	14.1	4.9	0.0	0.0	0.0	2.4	0.5	0.5	8.5
		Min	0.00	0.00	4.51	0.16	0.0	0.0	0.0	37.6	0.0	0.0	0.0	0.0	0.0	0.0	0.0	6.4
		Max	0.92	0.00	11.13	1.42	17.9	5.1	2.0	91.4	14.0	0.0	0.0	0.0	9.6	1.8	1.7	35.0
Haupt-rogen-stein (5)	Upper ('Movelier Beds' + 'Spatkalk')	Mean	0.39	0.00	8.14	0.42	4.7	1.1	0.2	64.6	3.1	0.0	0.0	0.0	2.3	0.4	0.7	22.6
		Median	0.33	0.00	7.47	0.30	4.7	0.0	0.0	59.4	0.0	0.0	0.0	0.0	0.0	0.0	0.6	25.9
		Stdev	0.33	0.00	1.65	0.36	3.6	1.7	0.5	15.3	5.5	0.0	0.0	0.0	4.2	0.8	0.6	9.0
		Min	0.00	0.00	6.80	0.16	1.1	0.0	0.0	53.7	0.0	0.0	0.0	0.0	0.0	0.0	0.0	6.7
		Max	0.92	0.00	10.97	1.04	8.9	3.8	1.1	91.4	12.7	0.0	0.0	0.0	9.6	1.8	1.7	28.3
Haupt-rogen-stein (11)	Lower	Mean	0.18	0.00	9.53	0.45	4.3	0.5	0.2	73.5	5.4	0.0	0.0	0.0	0.0	0.0	0.3	15.3
		Median	0.13	0.00	9.82	0.33	3.3	0.0	0.0	76.9	5.3	0.0	0.0	0.0	0.0	0.0	0.2	16.1
		Stdev	0.26	0.00	1.83	0.35	5.1	1.5	0.6	13.3	4.7	0.0	0.0	0.0	0.0	0.0	0.5	7.7
		Min	0.00	0.00	4.51	0.22	0.0	0.0	0.0	37.6	0.0	0.0	0.0	0.0	0.0	0.0	0.0	6.4
		Max	0.92	0.00	11.13	1.42	17.9	5.1	2.0	87.0	14.0	0.0	0.0	0.0	0.0	0.0	1.7	35.0
Passwang Fm. (18)		Mean	0.59	0.02	3.06	0.62	26.9	4.5	2.9	24.6	0.8	0.1	0.0	0.0	0.0	0.0	1.1	38.6
		Median	0.51	0.00	3.09	0.58	26.2	4.4	2.9	22.5	0.0	0.0	0.0	0.0	0.0	0.0	0.9	38.8
		Stdev	0.37	0.02	1.69	0.23	9.7	1.1	1.0	13.7	2.1	0.3	0.0	0.0	0.0	0.0	0.7	10.9
		Min	0.03	0.00	0.51	0.24	12.6	1.8	1.6	4.2	0.0	0.0	0.0	0.0	0.0	0.0	0.1	16.2
		Max	1.51	0.06	7.28	0.96	46.1	6.6	5.3	59.1	8.9	1.1	0.0	0.0	0.0	0.0	2.8	64.8
Passwang Fm. (8)	Rothenfluh Mb.	Mean	0.83	0.02	4.46	0.70	18.1	4.1	2.3	36.5	0.6	0.0	0.0	0.0	0.0	0.0	1.6	36.2
		Median	0.86	0.02	4.25	0.69	17.6	4.0	2.1	34.5	0.0	0.0	0.0	0.0	0.0	0.0	1.6	38.5
		Stdev	0.38	0.02	1.22	0.22	3.2	1.2	0.5	9.8	0.9	0.0	0.0	0.0	0.0	0.0	0.7	6.8
		Min	0.25	0.00	3.43	0.33	12.6	1.8	1.6	28.6	0.0	0.0	0.0	0.0	0.0	0.0	0.5	22.3
		Max	1.51	0.05	7.28	0.95	23.2	5.9	3.0	59.1	1.8	0.0	0.0	0.0	0.0	0.0	2.8	42.7
Passwang Fm. (10)	Waldenburg + lower part of	Mean	0.40	0.02	1.93	0.55	34.0	4.8	3.3	15.0	0.9	0.1	0.0	0.0	0.0	0.0	0.7	40.5
		Median	0.47	0.00	2.07	0.47	34.3	5.0	3.7	16.7	0.0	0.0	0.0	0.0	0.0	0.0	0.9	39.8
		Stdev	0.23	0.02	1.03	0.22	6.5	1.0	1.1	7.2	2.8	0.3	0.0	0.0	0.0	0.0	0.4	13.4
		Min	0.03	0.00	0.51	0.24	20.1	3.3	1.6	4.2	0.0	0.0	0.0	0.0	0.0	0.0	0.1	16.2

Formation (number of analyses)	**Member**		**S** [wt.-%]	**N** [wt.-%]	**C(inorg)** [wt.-%]	**C(org)** [wt.-%]	**Quartz** [wt.-%]	**K-feldspar** [wt.-%]	**Plagioclase** [wt.-%]	**Calcite** [wt.-%]	**Dolomite/Ank.** [wt.-%]	**Siderite** [wt.-%]	**Magnesite** [wt.-%]	**Anhydrite** [wt.-%]	**Goethite** [wt.-%]	**Haematite** [wt.-%]	**Pyrite** [wt.-%]	**Clay minerals** [wt.-%]
	Brüggli Mb.	Max	0.78	0.06	3.62	0.96	46.1	6.6	5.3	22.9	8.9	1.1	0.0	0.0	0.0	0.0	1.5	64.8
Opalinus Clay (26)	All	Mean	0.49	0.06	1.61	0.92	21.9	4.2	2.6	10.4	0.2	2.6	0.0	0.0	0.0	0.0	0.9	56.3
		Median	0.43	0.06	1.31	0.94	21.8	4.4	2.6	8.0	0.0	2.8	0.0	0.0	0.0	0.0	0.8	59.3
		Stdev	0.49	0.02	1.01	0.23	6.0	1.4	0.8	8.2	0.7	2.8	0.0	0.0	0.0	0.0	0.9	11.7
		Min	0.00	0.00	0.53	0.21	11.5	0.0	0.0	1.6	0.0	0.0	0.0	0.0	0.0	0.0	0.0	27.1
		Max	2.42	0.09	4.82	1.34	36.2	6.0	4.2	40.2	2.6	11.3	0.0	0.0	0.0	0.0	4.5	73.6
Opalinus Clay (8)	Sub-unit with silty calcar-eous beds	Mean	0.94	0.05	2.37	0.97	25.1	4.0	2.6	17.6	0.0	0.4	0.0	0.0	0.0	0.0	1.8	47.7
		Median	0.84	0.06	1.84	1.12	25.9	4.1	2.6	15.4	0.0	0.0	0.0	0.0	0.0	0.0	1.6	45.6
		Stdev	0.66	0.02	1.49	0.41	3.0	1.3	0.4	11.1	0.0	1.0	0.0	0.0	0.0	0.0	1.2	12.5
		Min	0.23	0.00	0.74	0.21	20.6	1.9	1.9	6.2	0.0	0.0	0.0	0.0	0.0	0.0	0.4	27.1
		Max	2.42	0.07	4.82	1.34	28.5	5.5	3.3	40.2	0.0	2.9	0.0	0.0	0.0	0.0	4.5	63.6
Opalinus Clay (3)	Upper silty sub-unit	Mean	0.35	0.06	1.83	0.89	23.1	4.6	2.7	11.3	0.9	3.5	0.0	0.0	0.0	0.0	0.6	52.3
		Median	0.42	0.06	1.79	0.90	22.3	4.6	2.7	11.2	0.0	3.5	0.0	0.0	0.0	0.0	0.8	52.4
		Stdev	0.32	0.00	0.59	0.10	1.9	0.9	0.2	3.8	1.5	0.8	0.0	0.0	0.0	0.0	0.6	6.7
		Min	0.00	0.05	1.27	0.79	21.8	3.7	2.6	7.6	0.0	2.6	0.0	0.0	0.0	0.0	0.0	45.6
		Max	0.62	0.06	2.45	0.98	25.3	5.5	2.9	15.2	2.6	4.2	0.0	0.0	0.0	0.0	1.2	58.9
Opalinus Clay (12)	Mixed clay-silt-carbon-ate sub-unit	Mean	0.23	0.07	1.15	0.88	21.2	4.6	2.8	6.4	0.2	3.5	0.0	0.0	0.0	0.0	0.4	60.1
		Median	0.19	0.07	1.09	0.90	19.9	4.9	2.7	5.6	0.0	3.6	0.0	0.0	0.0	0.0	0.4	60.4
		Stdev	0.17	0.01	0.37	0.10	7.2	1.0	0.7	3.5	0.7	3.5	0.0	0.0	0.0	0.0	0.3	9.2
		Min	0.00	0.05	0.53	0.68	12.4	2.5	1.8	1.6	0.0	0.0	0.0	0.0	0.0	0.0	0.0	45.1
		Max	0.59	0.09	1.70	1.00	36.2	6.0	4.2	13.2	2.5	11.3	0.0	0.0	0.0	0.0	1.1	72.9
Opalinus Clay (3)	Clay-rich sub-unit	Mean	0.47	0.07	1.21	0.93	15.0	2.7	1.5	6.8	0.0	3.8	0.0	0.0	0.0	0.0	0.9	68.4
		Median	0.48	0.07	1.25	0.92	15.9	3.3	1.8	5.8	0.0	3.0	0.0	0.0	0.0	0.0	0.9	70.4
		Stdev	0.02	0.00	0.19	0.02	3.1	2.5	1.4	1.7	0.0	1.4	0.0	0.0	0.0	0.0	0.0	6.4
		Min	0.44	0.07	1.00	0.92	11.5	0.0	0.0	5.8	0.0	2.9	0.0	0.0	0.0	0.0	0.8	61.3
		Max	0.49	0.07	1.37	0.96	17.5	4.9	2.8	8.8	0.0	5.3	0.0	0.0	0.0	0.0	0.9	73.6
Staffel-egg Fm. (12)		Mean	0.85	0.04	2.26	0.96	25.9	3.7	1.8	17.2	1.4	0.0	0.0	0.0	0.1	0.0	1.6	47.3
		Median	0.45	0.04	1.27	0.74	25.4	4.2	2.2	10.6	0.0	0.0	0.0	0.0	0.0	0.0	0.8	44.9
		Stdev	0.81	0.04	2.89	0.67	18.1	1.9	1.0	21.3	2.8	0.0	0.0	0.0	0.3	0.0	1.5	20.6
		Min	0.00	0.00	0.70	0.20	0.8	0.0	0.0	5.8	0.0	0.0	0.0	0.0	0.0	0.0	0.0	6.7
		Max	2.48	0.10	11.17	2.68	54.1	6.1	2.8	82.6	9.6	0.0	0.0	0.0	1.0	0.0	4.6	75.2
Klettgau Fm. (7)		Mean	0.10	0.01	4.32	0.44	14.6	6.6	5.3	1.1	32.1	0.0	0.0	0.0	0.0	0.0	0.2	39.6
		Median	0.04	0.00	5.34	0.22	11.3	5.9	4.5	0.0	41.0	0.0	0.0	0.0	0.0	0.0	0.1	39.7
		Stdev	0.13	0.02	3.40	0.51	10.8	3.3	3.5	2.4	25.7	0.0	0.0	0.0	0.0	0.0	0.2	14.6
		Min	0.00	0.00	0.00	0.08	2.5	3.1	1.3	0.0	0.0	0.0	0.0	0.0	0.0	0.0	0.0	22.6
		Max	0.32	0.04	8.99	1.47	36.4	11.2	11.3	6.5	69.0	0.0	0.0	0.0	0.0	0.0	0.6	68.3
Bänker-joch Fm. (4)		Mean	10.55	0.00	1.73	0.39	7.5	3.8	1.1	0.5	12.2	0.0	0.5	44.3	0.0	0.0	0.1	29.7
		Median	11.55	0.00	0.45	0.38	5.9	3.7	0.8	0.0	2.2	0.0	0.0	48.2	0.0	0.0	0.0	27.4
		Stdev	9.41	0.00	2.72	0.15	6.5	4.4	1.3	0.9	21.6	0.0	1.0	40.0	0.0	0.0	0.1	17.7
		Min	0.11	0.00	0.23	0.23	1.8	0.0	0.0	0.0	0.0	0.0	0.0	0.0	0.0	0.0	0.0	12.7
		Max	19.00	0.00	5.80	0.59	16.5	7.9	2.6	1.9	44.5	0.0	2.0	80.7	0.0	0.0	0.2	51.4

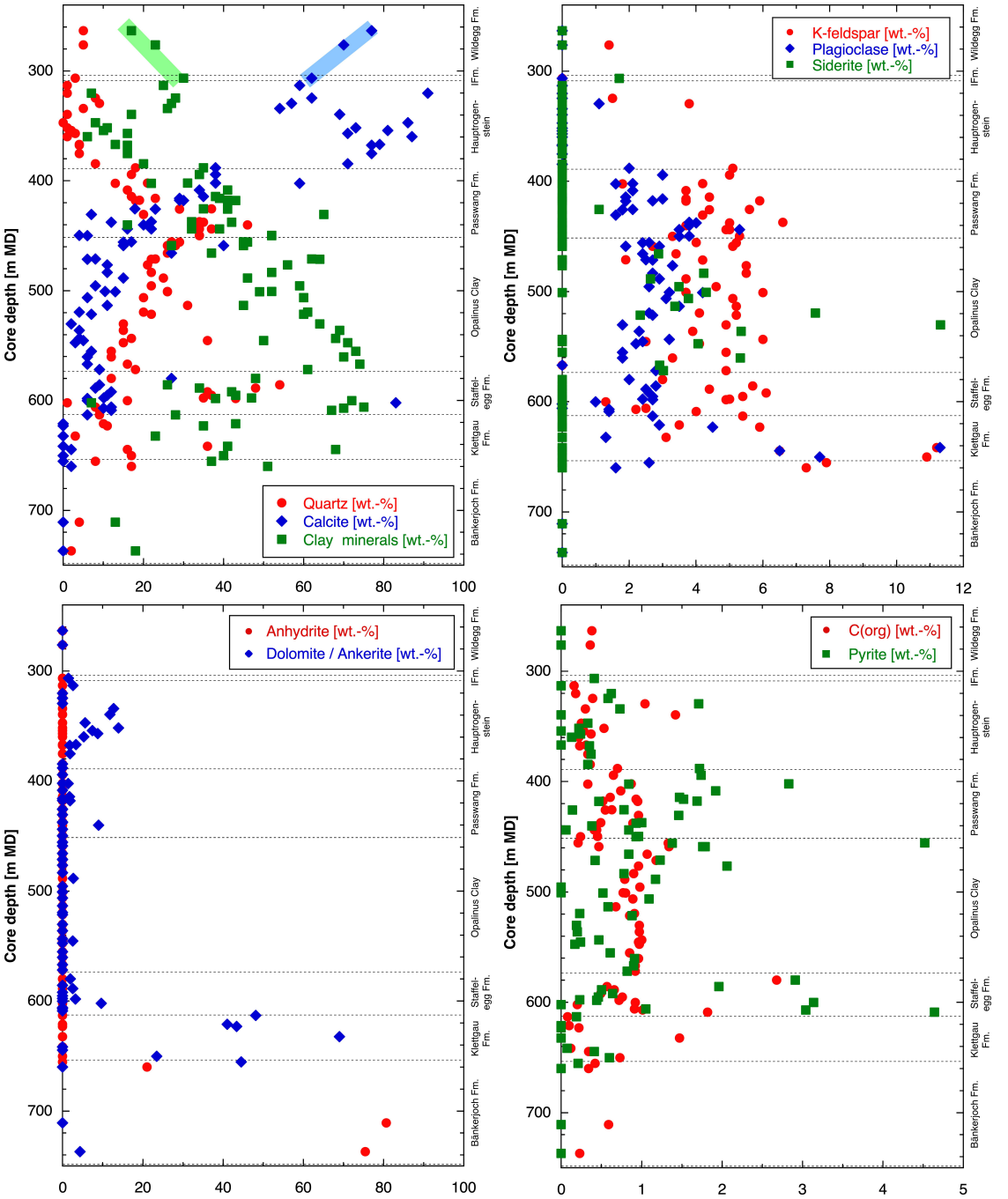

Fig. 4.2-1: Mineral contents in the bulk rock as a function of depth

Observed trends for the main minerals are only indicated for the Malm and Triassic sections where present, the Dogger and Lias are detailed in Fig. 4.2-4.

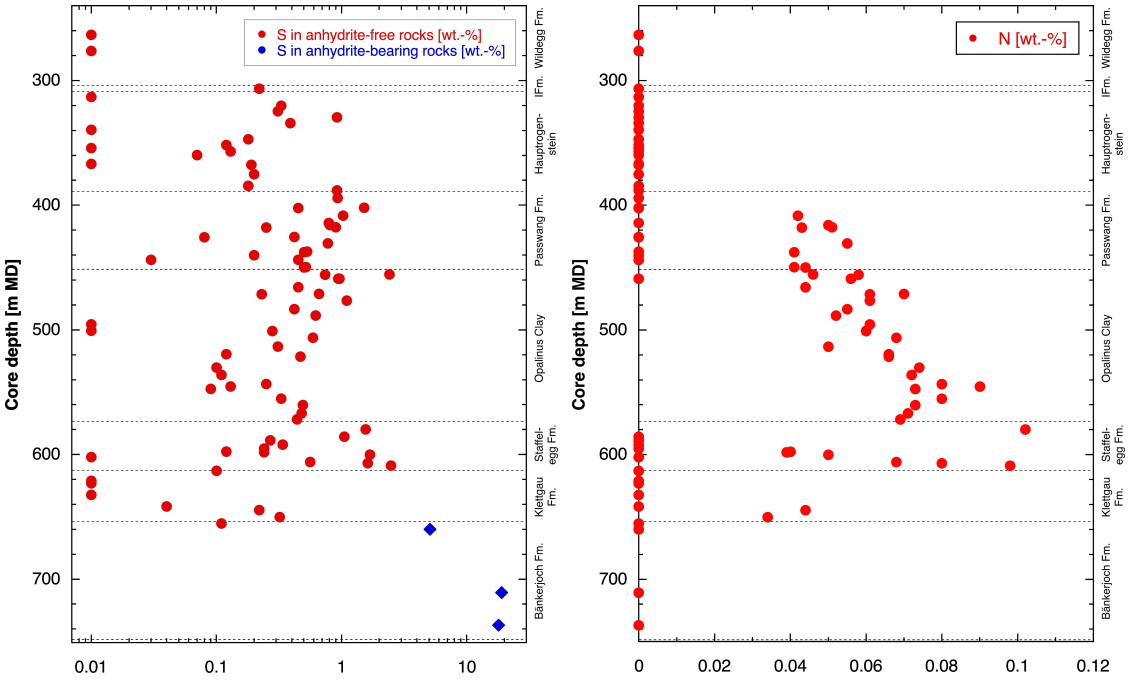

Fig. 4.2-2: Contents of S and N in the bulk rock as a function of depth

S contents below the detection limit of 0.05 wt.-% are represented by data points shown at 0.01 wt.-%. N contents below the detection limit of 0.01 wt.-% are represented by data points shown at 0 wt.-%.

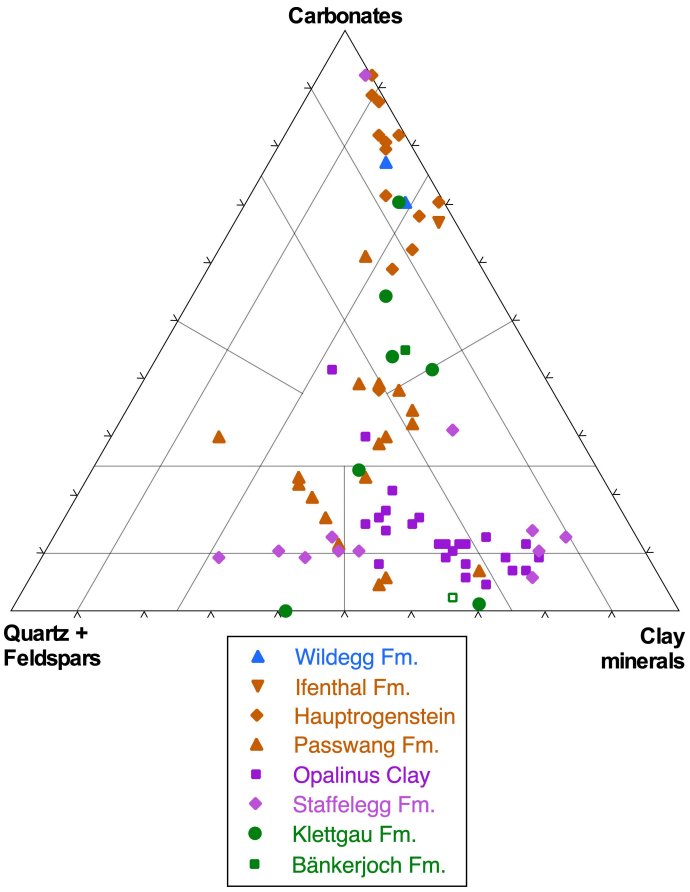

Fig. 4.2-3: Mineralogical composition of studied samples in the Füchtbauer triangle

Open symbols indicate samples containing 10 – 50 wt.-% minerals other than those represented by the Füchtbauer triangle (which are clays, calcite, dolomite/ankerite, siderite, magnesite, quartz, K-feldspar, plagioclase). Samples with > 50 wt.-% of such minerals are excluded.

A closer look at the section Staffelegg Formation – Opalinus Clay – Passwang Formation – Hauptrogenstein

The graphs shown in Fig. 4.2-4 indicate systematic depth trends of the contents of quartz, clay minerals, calcite, dolomite and C(org), whereas other minerals show no evident systematic variability.

Staffelegg Formation

Lithological heterogeneity is a characteristic in the Staffelegg Formation, which, according to the Füchtbauer nomenclature, contains claystone, marl, limestone and sandstone/siltstone. A trend of strongly decreasing clay-mineral, strongly increasing quartz/clay ratio and mildly decreasing calcite contents from the base of the formation to the top of the Frick Member can be seen. High contents of pyrite and organic C are observed in some samples (not only in the Rietheim Member).

Opalinus Clay

Informal sub-units within the Opalinus Clay were defined by Mazurek & Aschwanden (2020) on a regional basis. This scheme was successfully applied to the BOZ2-1 core (Dossier III), and the sub-unit boundaries are included in Fig. 4.2-4.

- Clay-mineral contents decrease from the base to the top of the mixed clay-silt-carbonate sub-unit. This is a difference to the findings in borehole BOZ1-1 where this interval can be sub-divided in two sections with different trends. However, note that such a subdivision can be seen for calcite in BOZ2-1 (Fig. 4.2-4a).
- Depth trends are weakly defined or absent in the upper part of the Opalinus Clay.
- Siderite occurs almost exclusively in the Opalinus Clay, and no depth trends can be traced.

Passwang Formation

In comparison to the Opalinus Clay, heterogeneity on the scale of metres is larger. Reasonably well-defined trends of decreasing quartz and increasing calcite contents from base to top can be identified and are clearer than in borehole BOZ1-1.

Hauptrogenstein

- Similar to BOZ1-1, quartz and clay minerals decrease upwards within the lower Hauptrogenstein, while dolomite/ankerite increases.
- Goethite (up to 10 wt.-%) is a frequent accessory phase in the upper Hauptrogenstein ('Movelier Beds' + 'Spatkalk').

Conclusion

A number of mineralogical discontinuities and changes in depth trends were identified and generally correlate well with the lithostratigraphic subdivision defined in Dossier III.

Quartz, clay-mineral and calcite contents show the most pronounced trends and discontinuities in their depth profiles. Let us note that the sub-units of the Opalinus Clay are not zones with constant properties but rather zones with constant trends, i.e. depositional cycles.

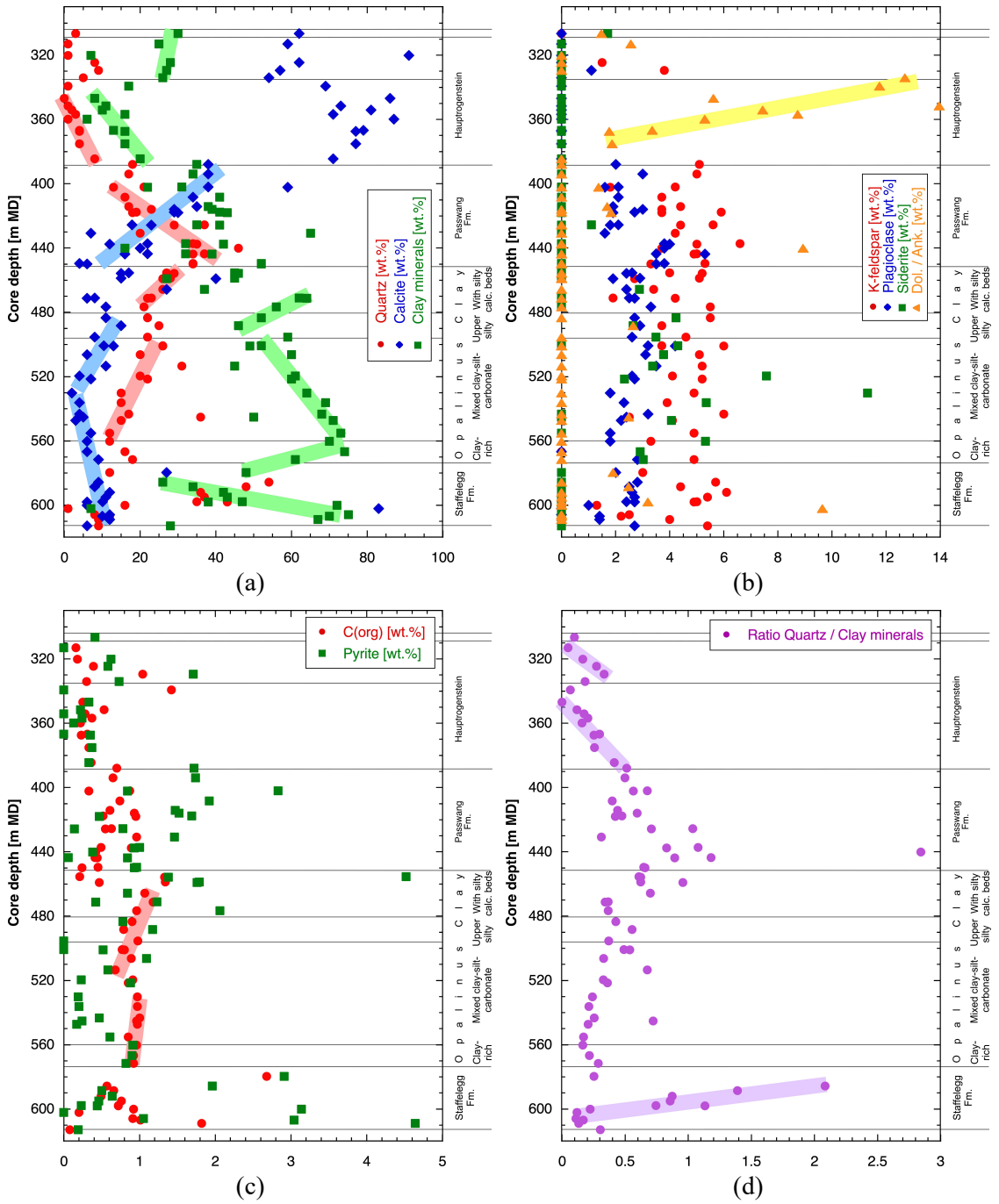

Fig. 4.2-4: Depth trends of mineral contents in the bulk rock in the Lias – Dogger interval
Coloured bars highlight systematic trends.

4.2.2 Clay minerals

A total of 33 mineralogical analyses of the clay fraction were performed in the section Hauptrogenstein – Bänkerjoch Formation. The full dataset is documented in Appendix A. Tab. 4.2-2 provides formation-specific summaries, normalising the contents of individual clay phases to the sum of all clay minerals.

The identified clay-mineral species include illite, smectite, illite/smectite mixed layers, kaolinite, chlorite and chlorite/smectite mixed layers. The identification of chlorite/smectite mixed layers in all samples is in contrast with previous data from northern Switzerland where this mineral was rarely reported (Mazurek 2017). However, this is not a real difference but due to the improved methodology of the evaluation of X-ray patterns that was applied for the TBO campaign (details in Waber (ed.) 2020). Because the chlorite/smectite mixed-layer phase contains 85 – 95% chlorite layers, its XRD reflections are close to those of pure chlorite. The new methodology also allows to better resolve the fraction of smectite layers in the illite/smectite mixed-layer phase. As seen in Tab. 4.2-2, illite-rich mixed layers dominate, but minor amounts of illite-poorer mixed layers also occur. Given the fact that the contents of mixed-layer phases and the smectite fractions in these are known, the end-member compositions of illite, smectite, chlorite and kaolinite (whether in mixed layers or as a discrete phase) can be calculated and are also listed in Tab. 4.2-2.

Depth trends of the relative proportions of clay minerals are shown graphically in Fig. 4.2-5 for individual clay phases (a) and end-member clays (b). The depth plot of the latter is less noisy than that of the individual clay minerals. Variability of the smectite end-member is limited, except for some high values in the Passwang Formation (as in borehole BOZ1-1), one value in the Staffelegg Formation (limestone of the Beggingen Member or 'Arietenkalk') and values in the Bänkerjoch Formation. Chlorite varies more strongly, except in the Opalinus Clay.

The relative proportions of the two main end-member clays, namely illite and kaolinite, vary substantially over the profile. The Bänkerjoch Formation is characterised by the dominance of the illite end-member, while the proportions of kaolinite are low. The overlying Dogger–Lias interval will be explored in more detail below.

The relative proportions of the illite, smectite and kaolinite end-members as shown in Fig. 4.2-6 illustrate the homogeneous clay composition in the Opalinus Clay when compared to the overlying units.

Tab. 4.2-2: Mineralogical composition of the clay fraction: formation-specific means, medians, standard deviations and ranges

In some cases, systematic depth trends of clay-mineral contents are observed. This means that in these cases the data do not follow a Gaussian distribution, which is a pre-requisite for the calculation of meaningful standard deviations. In such cases, the ranges (also listed) are more meaningful.

Formation (number of analyses)	**Member**		**Individual clay phases** [wt.-% of clay fraction]										**End-member clays** [wt.-% of clay fraction]			
			Illite	**Ill/Sm ML (85-90)**	**Ill/Sm ML (75-80)**	**Ill/Sm ML (50-70)**	**Ill/Sm ML (20-40)**	**Total Ill/Sm**	**Smectite**	**Kaolinite**	**Chlorite**	**Chl/Sm ML (85-95)**	**Illite**	**Smectite**	**Kaolinite**	**Chlorite**
Hauptrogenstein (all) (2)		Mean	22.1	0.4	1.7	8.9	1.0	11.9	2.3	28.7	26.5	8.7	29.0	8.3	28.7	34.2
		Median	22.1	0.4	1.7	8.9	1.0	11.9	2.3	28.7	26.5	8.7	29.0	8.3	28.7	34.2
		Stdev	17.8	0.6	2.3	2.1	1.3	2.5	1.5	7.1	18.3	3.7	19.7	2.1	7.1	14.6
		Min	9.5	0.0	0.0	7.4	0.0	10.1	1.2	23.6	13.5	6.1	15.0	6.8	23.6	23.8
		Max	34.7	0.8	3.3	10.3	1.9	13.6	3.3	33.7	39.4	11.3	42.9	9.7	33.7	44.5
Upper Hauptrogenstein ('Movelier Beds' + 'Spatkalk') (1)		Mean	9.5	0.8	0.0	7.4	1.9	10.1	1.2	33.7	39.4	6.1	15.0	6.8	33.7	44.5
Lower Hauptrogenstein (1)		Mean	34.7	0.0	3.3	10.3	0.0	13.6	3.3	23.6	13.5	11.3	42.9	9.7	23.6	23.8
Passwang Fm. (9)		Mean	36.8	13.5	13.7	12.5	0.0	39.6	1.3	10.2	5.9	6.1	65.8	12.7	10.2	11.3
		Median	37.5	10.0	13.8	11.7	0.0	39.1	0.0	11.8	6.3	5.0	65.5	11.7	11.8	10.4
		Stdev	5.2	12.5	11.6	6.2	0.1	8.0	2.4	4.7	2.0	3.3	3.6	4.8	4.7	4.3
		Min	26.4	0.0	0.0	3.7	0.0	30.8	0.0	2.1	3.5	0.9	58.9	7.4	2.1	6.7
		Max	41.9	38.3	29.0	20.4	0.2	57.0	6.6	16.8	9.3	10.4	70.4	21.1	16.8	18.7
Passwang Fm. (5)	Rothenfluh Mb.	Mean	37.5	19.8	7.7	15.1	0.0	42.7	2.2	8.8	5.0	3.9	68.1	14.7	8.8	8.4
		Median	41.0	21.6	0.0	18.7	0.0	42.0	0.0	8.9	4.5	4.6	68.3	13.5	8.9	7.9
		Stdev	6.5	13.0	10.6	7.1	0.1	9.5	3.1	6.0	1.5	1.9	2.0	5.8	6.0	1.7
		Min	26.4	7.0	0.0	3.7	0.0	30.8	0.0	2.1	3.5	0.9	65.1	7.4	2.1	6.7
		Max	41.9	38.3	20.1	20.4	0.2	57.0	6.6	16.8	6.7	5.6	70.4	21.1	16.8	10.8
Passwang Fm. (4)	Waldenburg + lower part of Brüggli Mb.	Mean	36.0	5.6	21.1	9.1	0.0	35.8	0.2	12.0	7.1	8.8	62.9	10.1	12.0	15.0
		Median	37.1	5.1	21.1	9.7	0.0	35.8	0.0	12.0	7.2	10.0	63.6	9.8	12.0	15.5
		Stdev	3.5	6.4	8.7	2.9	0.0	3.6	0.3	1.6	2.0	2.7	2.8	1.5	1.6	3.6
		Min	30.9	0.0	13.4	5.4	0.0	31.7	0.0	10.1	4.7	4.7	58.9	8.8	10.1	10.4
		Max	38.9	12.2	29.0	11.7	0.0	40.1	0.6	14.1	9.3	10.4	65.5	12.0	14.1	18.7
Opalinus Clay (10)	All	Mean	29.5	11.2	11.4	3.1	0.0	25.7	0.0	33.4	4.3	7.1	50.0	6.1	33.4	10.5
		Median	29.8	9.4	11.8	3.3	0.0	24.8	0.0	33.5	4.1	7.2	49.6	5.9	33.5	10.3
		Stdev	1.9	6.4	6.3	1.4	0.0	3.0	0.0	3.1	1.5	0.8	2.1	0.7	3.1	1.8
		Min	25.3	5.2	0.1	1.2	0.0	22.3	0.0	28.8	2.2	5.9	47.2	5.2	28.8	8.5
		Max	31.3	25.4	20.5	5.7	0.0	31.2	0.0	37.7	6.7	8.3	55.0	7.4	37.7	13.9

Tab. 4.2-2: (continued)

Formation (number of analyses)	**Member**		**Individual clay phases** [wt.-% of clay fraction]										**End-member clays** [wt.-% of clay fraction]			
			Illite	**Ill/Sm ML (85-90)**	**Ill/Sm ML (75-80)**	**Ill/Sm ML (50-70)**	**Ill/Sm ML (20-40)**	**Total Ill/Sm**	**Smectite**	**Kaolinite**	**Chlorite**	**Chl/Sm ML (85-95)**	**Illite**	**Smectite**	**Kaolinite**	**Chlorite**
Opalinus Clay (3)	Sub-unit with silty calcareous beds	Mean	31.0	11.0	11.8	3.4	0.0	26.2	0.0	30.5	4.5	7.8	51.8	6.3	30.5	11.3
		Median	31.0	8.6	11.3	3.4	0.0	25.3	0.0	29.2	4.3	8.3	51.4	5.9	29.2	11.6
		Stdev	0.2	6.2	8.5	0.3	0.0	3.6	0.0	2.6	2.1	0.9	3.0	0.8	2.6	2.7
		Min	30.8	6.3	3.6	3.2	0.0	23.1	0.0	28.8	2.5	6.8	49.0	5.8	28.8	8.5
		Max	31.1	18.0	20.5	3.7	0.0	30.2	0.0	33.5	6.7	8.3	55.0	7.3	33.5	13.9
Opalinus Clay (1)	Upper silty sub-unit	Mean	29.5	10.1	12.2	3.3	0.0	25.6	0.0	33.5	5.1	5.9	50.2	6.0	33.5	10.3
Opalinus Clay (5)	Mixed clay-silt-carbonate sub-unit	Mean	28.6	12.8	9.8	3.1	0.0	25.6	0.0	34.4	4.4	6.8	49.1	6.0	34.4	10.4
		Median	29.2	11.7	11.1	2.7	0.0	24.0	0.0	33.9	3.8	7.2	49.2	5.9	33.9	10.2
		Stdev	2.4	7.8	6.4	1.9	0.0	3.6	0.0	2.6	1.1	0.6	1.3	0.8	2.6	1.4
		Min	25.3	5.7	0.1	1.2	0.0	22.3	0.0	31.6	3.4	5.9	47.2	5.2	31.6	8.6
		Max	31.3	25.4	16.7	5.7	0.0	31.2	0.0	37.7	6.0	7.2	50.6	7.4	37.7	12.3
Opalinus Clay (1)	Clay-rich sub-unit	Mean	29.4	5.2	17.4	1.7	0.0	24.3	0.0	36.9	2.2	7.3	48.7	5.7	36.9	8.6
Staffelegg Fm. (10)		Mean	33.6	16.9	8.7	6.3	1.4	33.3	1.5	18.3	4.7	8.5	59.7	9.6	18.3	12.4
		Median	36.9	16.8	3.8	4.3	0.0	33.3	0.0	18.7	4.8	7.3	61.6	7.8	18.7	10.5
		Stdev	9.6	11.7	10.6	6.1	4.0	4.3	4.6	4.3	2.2	6.4	10.6	7.1	4.3	7.1
		Min	8.9	0.0	0.0	1.2	0.0	28.4	0.0	7.7	0.9	3.6	30.5	5.1	7.7	8.1
		Max	44.2	31.2	29.9	21.1	12.8	41.1	14.5	22.8	8.8	26.2	68.4	29.5	22.8	32.3
Bänkerjoch Fm. (2)		Mean	31.7	5.1	0.0	2.7	23.4	31.1	5.2	3.5	1.4	27.2	46.2	25.3	3.5	25.1
		Median	31.7	5.1	0.0	2.7	23.4	31.1	5.2	3.5	1.4	27.2	46.2	25.3	3.5	25.1
		Stdev	11.8	7.1	0.0	2.6	19.9	29.6	7.3	4.9	2.0	13.6	5.4	3.5	4.9	13.8
		Min	23.3	0.0	0.0	0.8	9.3	10.1	0.0	0.0	0.0	17.5	42.4	22.8	0.0	15.3
		Max	40.0	10.1	0.0	4.5	37.4	52.0	10.3	7.0	2.8	36.8	50.0	27.7	7.0	34.8

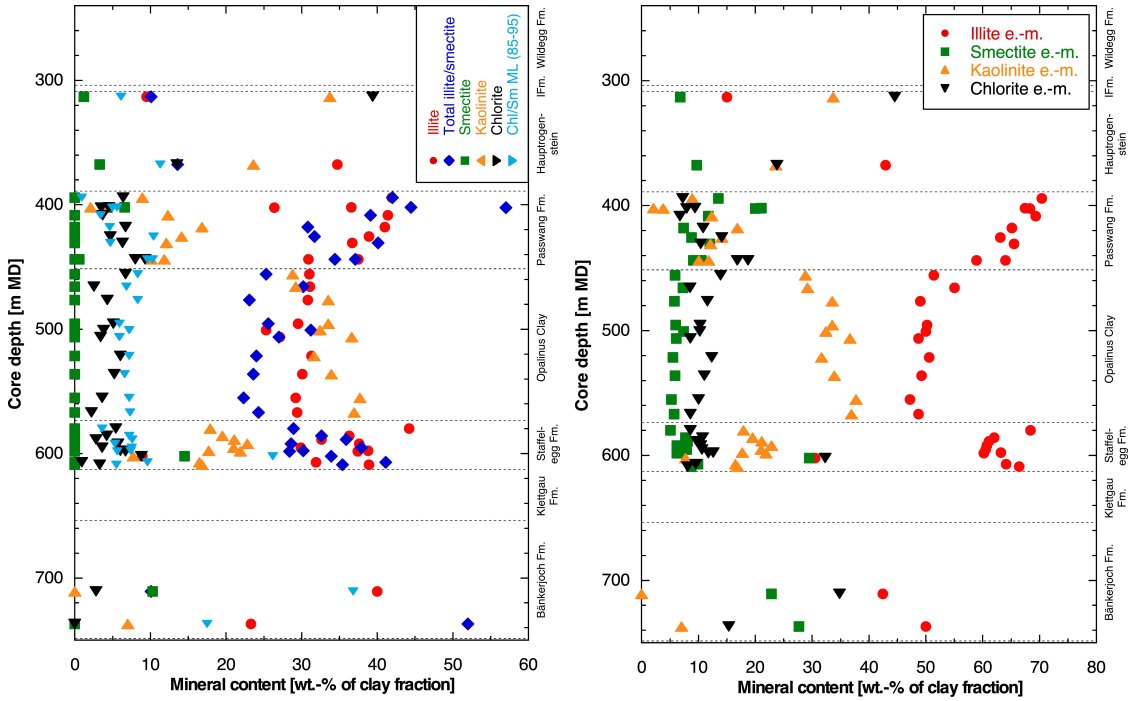

Fig. 4.2-5: Mineralogical composition of the clay fraction as a function of depth; (a) individual clay minerals, (b) end-member clays

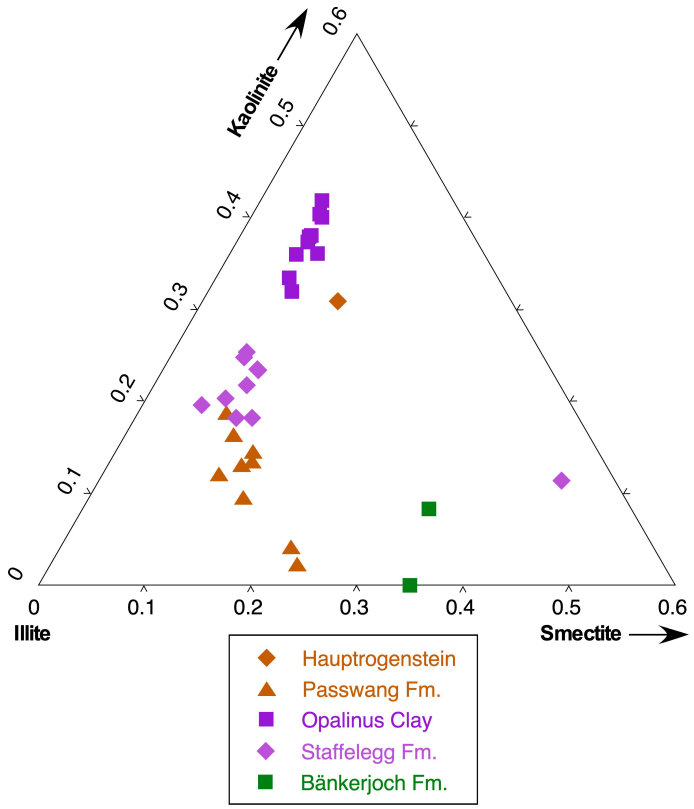

Fig. 4.2-6: Relative mass proportions of illite, smectite and kaolinite end-member clays

One sample from the Hauptrogenstein is outside the range of the diagram (kaolinite-rich and illite-poor).

A closer look at the section Staffelegg Formation – Opalinus Clay – Passwang Formation – Hauptrogenstein

The composition of the clay fraction in this interval shows some depth trends (Figs. 4.2-7 and 4.2-8). The ratio illite to kaolinite end-member is low and remarkably constant in the Opalinus Clay when compared to the underlying Staffelegg Formation. The Passwang Formation is characterised by increasing illite and, less evident, decreasing kaolinite fractions from base to top. The chlorite fraction also clearly decreases. These trends are more systematic in comparison with the findings in borehole BOZ1-1. In the Passwang Formation, the ratio illite/kaolinite end-members reaches the highest values in the whole profile, in particular in the Rothenfluh Member.

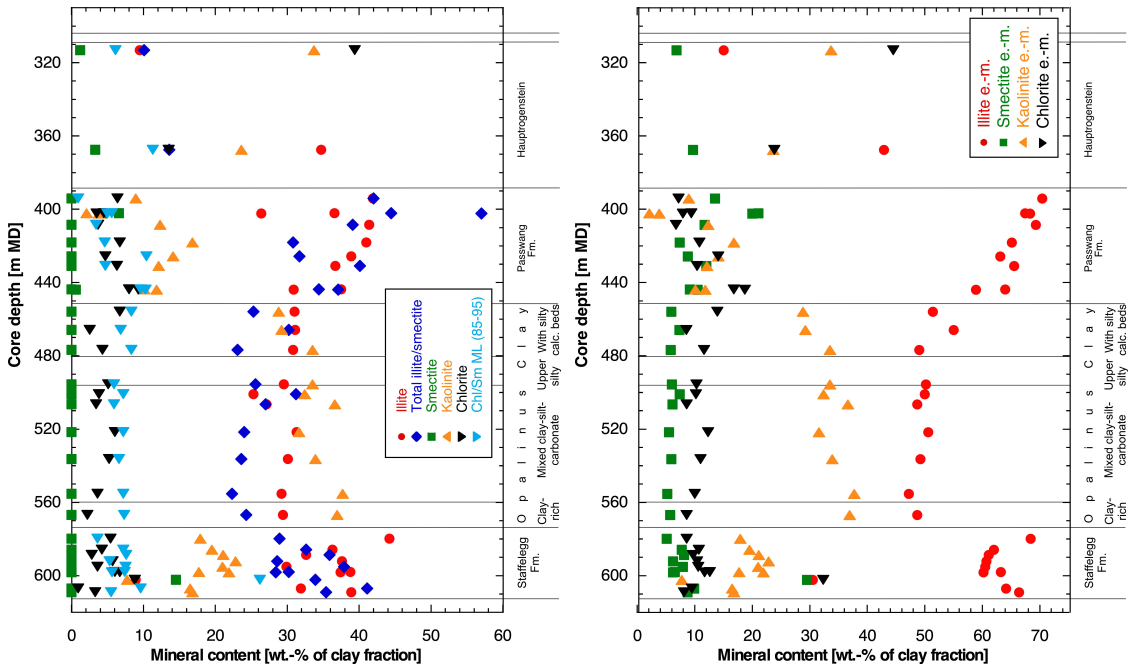

Fig. 4.2-7: Mineralogical composition of the clay fraction as a function of depth in the Lias – Dogger interval; (a) individual clay minerals, (b) end-member clays

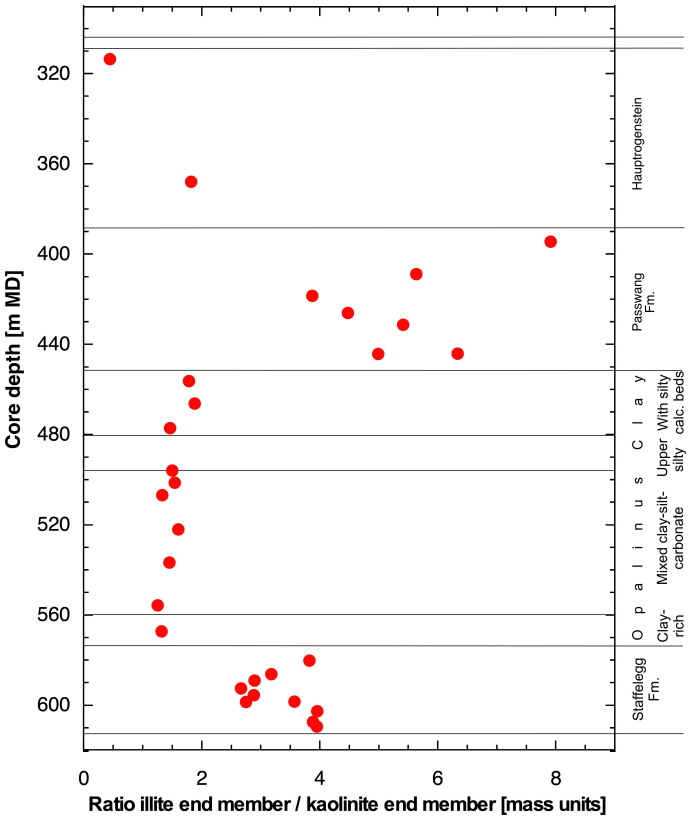

Fig. 4.2-8: Ratio of the illite to kaolinite end-member clays as a function of depth

Two samples from the Rothenfluh Member of the Passwang Formation have high values of 18 – 32 and fall outside the range shown in the graphic.

4.3 Petrophysical parameters

Martin Mazurek, Lukas Aschwanden & Thomas Gimmi

Petrophysical parameters were obtained by 3 different laboratories, and the analytical programme is listed in Tab. 4.3-1.

Tab. 4.3-1: Analytical programme for petrophysical measurements

	University of Bern	**BRGM**	**Hydroisotop GmbH**
Bulk wet density	42	40	
Grain density	42	40	
Gravimetric water content	46	40	51
Water content based on isotope diffusive exchange	29		51
N_2 adsorption isotherm	10		

The formalisms to calculate additional parameters from measured data (such as porosity) are detailed in Waber (ed.) (2020). The analytical protocols used for the quantification of petrophysical parameters were identical for the University of Bern and Hydroisotop GmbH data, and therefore these two datasets are merged in tables and figures. On the other hand, BRGM used different protocols, which are described in Section 3.4. The BRGM dataset is therefore treated separately. Formation-specific statistical data are summarised in Tab. 4.3-2 for University of Bern / Hydroisotop GmbH and in Tab. 4.3-3 for BRGM. The full dataset is documented in Appendix A.

In case of the TRU1-1 campaign, porosity obtained by BRGM from water content was typically markedly lower than pycnometer porosity, which was explained by partial sample desaturation prior to the measurement of the water content (Aschwanden et al. 2021). Consequently, water-content data from BRGM were screened out and not used for further considerations. In case of the BOZ2 data discussed here, such a discrepancy is not evident. As shown in Fig. 4.3-10, BRGM's water-loss and pycnometer porosities agree well and are also in agreement with data produced at University of Bern. Thus, in contrast to TRU1, all data from BRGM are used in case of BOZ2. Given the fact that BRGM states that they used identical protocols for both campaigns, the observed discrepancy remains unexplained at this stage.

Tab. 4.3-2: Summary of measured and calculated petrophysical data obtained by University of Bern and Hydroisotop GmbH

Listed water contents (wet) are averages of measurements performed on typically 2 – 3 subsamples (see Section 4.3.1 below). n = number of samples.

							Gravimetry				Isotope mass balance			
Formation	**Member**		**Bulk wet density** [g/cm³]	**Bulk dry density, calculated** [g/cm³]	**Grain density** [g/cm³]	**Pycnometer porosity** [–]	**Water content (wet) (105 °C)** [wt.-%]	**Water content (dry) (105 °C)** [wt.-%]	**Water-loss porosity using bulk wet density** [–]	**Water-loss porosity using grain density** [–]	**Water content (wet) based on isotope diffusive exchange** [wt.-%]	**Porosity based on isotope diffusive exchange using bulk wet density** [–]	**Porosity based on isotope diffusive exchange using grain density** [–]	**External surface area (BET)** [m²/g dry rock]
Wildegg Fm.		Mean	2.590	2.518	2.686	0.062	3.777	3.933	0.072	0.095	4.167	0.082	0.105	
		Median					3.823	3.975		0.097	4.114		0.104	
		Stdev					0.978	1.056		0.024	1.045		0.025	
		Min					2.777	2.856		0.071	3.149		0.080	
		Max					4.732	4.967		0.118	5.238		0.130	
		n	1	1	1	1	3	3	1	3	3	1	3	0
Haupt-rogenstein	All	Mean	2.566	2.476	2.756	0.101	3.523	3.667	0.091	0.090	3.698	0.086	0.094	7.96
		Median	2.574	2.492	2.741	0.093	3.344	3.459	0.083	0.085	3.481	0.085	0.091	7.96
		Stdev	0.025	0.054	0.056	0.035	1.197	1.311	0.032	0.029	0.979	0.011	0.023	1.34
		Min	2.534	2.370	2.717	0.070	2.322	2.377	0.064	0.060	2.519	0.074	0.065	7.01
		Max	2.596	2.532	2.889	0.180	6.462	6.908	0.164	0.166	6.574	0.104	0.160	8.91
		n	8	8	8	8	17	17	8	17	15	6	15	2
Haupt-rogenstein	Upper ('Movelier Beds' + 'Spatkalk')	Mean	2.552	2.442	2.778	0.119	4.277	4.489	0.110	0.108	4.294	0.085	0.108	8.91
		Median	2.547	2.460	2.727	0.098	3.438	3.560	0.087	0.088	4.072	0.085	0.103	
		Stdev	0.022	0.065	0.097	0.053	1.461	1.614	0.047	0.036	1.211	0.006	0.028	
		Min	2.534	2.370	2.717	0.081	3.073	3.170	0.079	0.079	3.190	0.081	0.082	
		Max	2.576	2.497	2.889	0.180	6.462	6.908	0.164	0.166	6.574	0.090	0.160	
		n	3	3	3	3	7	7	3	7	6	2	6	1

Tab. 4.3-2: (continued)

Formation	Member		Bulk wet density [g/cm³]	Bulk dry density, calculated [g/cm³]	Grain density [g/cm³]	Pycnometer porosity [–]	Gravimetry: Water content (wet) (105 °C) [wt.-%]	Gravimetry: Water content (dry) (105 °C) [wt.-%]	Gravimetry: Water-loss porosity using bulk wet density [–]	Gravimetry: Water-loss porosity using grain density [–]	Isotope mass balance: Water content (wet) based on isotope diffusive exchange [wt.-%]	Isotope mass balance: Porosity based on isotope diffusive exchange using bulk wet density [–]	Isotope mass balance: Porosity based on isotope diffusive exchange using grain density [–]	External surface area (BET) [m²/g dry rock]
Haupt-rogenstein	Lower	Mean	2.575	2.495	2.744	0.090	2.995	3.091	0.079	0.077	3.302	0.086	0.085	7.01
		Median	2.574	2.500	2.743	0.089	2.876	2.961	0.074	0.075	3.155	0.084	0.081	
		Stdev	0.025	0.041	0.015	0.019	0.611	0.652	0.016	0.015	0.564	0.013	0.014	
		Min	2.534	2.430	2.723	0.070	2.322	2.377	0.064	0.060	2.519	0.074	0.065	
		Max	2.596	2.532	2.764	0.116	4.115	4.292	0.104	0.106	4.089	0.104	0.105	
		n	5	5	5	5	10	10	5	10	9	4	9	1
Passwang Fm.	All	Mean	2.531	2.424	2.702	0.103	4.093	4.283	0.107	0.103	4.683	0.128	0.117	18.79
		Median	2.525	2.410	2.705	0.107	4.374	4.574	0.111	0.110	4.910	0.136	0.122	18.79
		Stdev	0.035	0.063	0.016	0.024	1.197	1.282	0.030	0.029	1.124	0.020	0.027	6.45
		Min	2.481	2.349	2.665	0.046	1.207	1.222	0.032	0.032	2.181	0.100	0.057	14.23
		Max	2.614	2.582	2.726	0.129	5.507	5.828	0.140	0.136	5.899	0.150	0.145	23.36
		n	10	10	10	10	21	21	10	21	17	7	17	2
Passwang Fm.	Rothenfluh Mb.	Mean	2.557	2.466	2.713	0.091	3.814	3.983	0.091	0.096	4.509	0.130	0.113	14.23
		Median	2.550	2.437	2.708	0.099	4.405	4.608	0.113	0.111	4.910	0.130	0.122	
		Stdev	0.054	0.105	0.011	0.041	1.325	1.415	0.052	0.032	1.178	0.020	0.028	
		Min	2.507	2.379	2.706	0.046	1.207	1.222	0.032	0.032	2.374	0.116	0.062	
		Max	2.614	2.582	2.726	0.127	5.090	5.363	0.128	0.128	5.773	0.145	0.143	
		n	3	3	3	3	9	9	3	9	7	2	7	1
Passwang Fm.	«Humphriesi-Sch.»	Mean					4.285	4.476		0.108	4.714		0.118	
		n	0	0	0	0	1	1	0	1	1	0	1	0
Passwang Fm.	Walden-burg + lower part of Brüggli Mb.	Mean	2.520	2.405	2.697	0.108	4.305	4.512	0.115	0.108	4.815	0.127	0.120	23.36
		Median	2.521	2.406	2.703	0.108	4.374	4.574	0.110	0.110	5.429	0.136	0.135	
		Stdev	0.020	0.030	0.016	0.014	1.157	1.243	0.017	0.028	1.201	0.022	0.028	
		Min	2.481	2.349	2.665	0.085	1.338	1.356	0.091	0.035	2.181	0.100	0.057	
		Max	2.543	2.438	2.712	0.129	5.507	5.828	0.140	0.136	5.899	0.150	0.145	
		n	7	7	7	7	11	11	7	11	9	5	9	1
Opalinus Clay	All	Mean	2.524	2.409	2.712	0.112	4.688	4.925	0.114	0.117	5.134	0.129	0.127	
		Median	2.518	2.405	2.713	0.111	4.977	5.237	0.119	0.123	5.299	0.139	0.131	
		Stdev	0.019	0.036	0.038	0.016	0.748	0.815	0.022	0.018	0.785	0.025	0.018	
		Min	2.504	2.372	2.663	0.088	2.491	2.555	0.068	0.065	3.285	0.091	0.084	
		Max	2.554	2.486	2.787	0.136	5.550	5.876	0.136	0.137	6.295	0.159	0.155	
		n	8	8	8	8	30	30	8	30	27	7	27	0
Opalinus Clay	With silty calc. beds	Mean	2.524	2.425	2.725	0.110	4.078	4.261	0.099	0.103	4.408	0.111	0.111	
		Median	2.511	2.407	2.726	0.105	4.165	4.345	0.104	0.107	4.145	0.103	0.106	
		Stdev	0.026	0.054	0.062	0.024	0.955	1.032	0.029	0.023	0.858	0.025	0.019	
		Min	2.508	2.383	2.663	0.088	2.491	2.555	0.068	0.065	3.285	0.091	0.084	
		Max	2.554	2.486	2.787	0.136	5.038	5.305	0.125	0.125	5.531	0.139	0.136	
		n	3	3	3	3	9	9	3	9	8	3	8	0
Opalinus Clay	Upper silty	Mean	2.526	2.415	2.673	0.097	4.534	4.749	0.111	0.113	4.934	0.123	0.123	
		Median					4.488	4.699		0.113	4.962		0.124	
		Stdev					0.177	0.195		0.005	0.066		0.002	
		Min					4.384	4.585		0.109	4.858		0.120	
		Max					4.730	4.964		0.118	4.981		0.124	
		n	1	1	1	1	3	3	1	3	3	1	3	0

Tab. 4.3-2: (continued)

Formation	Member		Bulk wet density [g/cm³]	Bulk dry density, calculated [g/cm³]	Grain density [g/cm³]	Pycnometer porosity [–]	Gravimetry: Water content (wet) (105 °C) [wt.-%]	Gravimetry: Water content (dry) (105 °C) [wt.-%]	Gravimetry: Water-loss porosity using bulk wet density [–]	Gravimetry: Water-loss porosity using grain density [–]	Isotope mass balance: Water content (wet) based on isotope diffusive exchange [wt.-%]	Isotope mass balance: Porosity based on isotope diffusive exchange using bulk wet density [–]	Isotope mass balance: Porosity based on isotope diffusive exchange using grain density [–]	External surface area (BET) [m²/g dry rock]
Opalinus Clay	Mixed clay-silt-carb.	Mean	2.523	2.399	2.709	0.114	4.988	5.252	0.124	0.124	5.491	0.146	0.136	
		Median	2.515	2.403	2.706	0.112	5.104	5.379	0.127	0.127	5.708	0.146	0.141	
		Stdev	0.024	0.026	0.010	0.006	0.486	0.537	0.010	0.011	0.512	0.000	0.012	
		Min	2.504	2.372	2.700	0.109	4.065	4.237	0.112	0.103	4.564	0.146	0.114	
		Max	2.550	2.423	2.720	0.121	5.550	5.876	0.132	0.137	6.050	0.146	0.148	
		n	3	3	3	3	15	15	3	15	13	2	13	0
Opalinus Clay	Clay-rich	Mean	2.520	2.384	2.722	0.124	5.173	5.455	0.136	0.129	5.726	0.159	0.141	
		Median					5.140	5.418		0.128	5.739		0.141	
		Stdev					0.222	0.247		0.006	0.576		0.013	
		Min					4.970	5.229		0.124	5.143		0.128	
		Max					5.409	5.718		0.135	6.295		0.155	
		n	1	1	1	1	3	3	1	3	3	1	3	0
Staffelegg Fm.		Mean	2.547	2.444	2.714	0.099	4.111	4.307	0.102	0.103	4.823	0.139	0.120	23.84
		Median	2.533	2.434	2.698	0.097	3.929	4.090	0.101	0.099	4.341	0.139	0.109	22.63
		Stdev	0.063	0.104	0.023	0.036	1.354	1.462	0.044	0.033	1.181	0.040	0.027	19.13
		Min	2.487	2.340	2.694	0.029	0.698	0.703	0.019	0.019	3.746	0.111	0.095	1.73
		Max	2.685	2.666	2.747	0.144	6.202	6.612	0.151	0.151	6.682	0.167	0.162	48.37
		N	7	7	7	7	14	14	7	14	8	2	8	4
Klettgau Fm.		Mean	2.516	2.387	2.727	0.125	4.807	5.059	0.129	0.120	4.992	0.134	0.125	
		Median	2.514	2.391	2.736	0.121	4.918	5.173	0.128	0.122	5.111	0.134	0.126	
		Stdev	0.043	0.050	0.042	0.018	0.944	1.043	0.024	0.022	0.942	0.024	0.022	
		Min	2.470	2.337	2.671	0.107	3.467	3.591	0.101	0.088	3.825	0.107	0.097	
		Max	2.568	2.431	2.767	0.150	6.315	6.741	0.158	0.156	6.361	0.159	0.157	
		N	4	4	4	4	8	8	4	8	8	4	8	0
Bänker-joch Fm.		Mean	2.716	2.654	2.848	0.069	2.360	2.443	0.062	0.062	5.624	0.144	0.141	4.91
		Median	2.730	2.667	2.855	0.067	2.349	2.425	0.063	0.063	5.624	0.144	0.141	4.91
		Stdev	0.166	0.210	0.085	0.047	1.788	1.876	0.045	0.045	2.064	0.049	0.046	2.10
		Min	2.521	2.418	2.761	0.019	0.670	0.675	0.019	0.019	4.165	0.110	0.108	3.43
		Max	2.885	2.866	2.922	0.124	4.073	4.246	0.103	0.105	7.083	0.179	0.174	6.39
		n	4	4	4	4	4	4	4	4	2	2	2	2

Tab. 4.3-3: Summary of measured and calculated petrophysical data obtained by BRGM

Listed water contents and bulk wet densities are averages of measurements performed on 2 aliquots of the same sample. n = number of samples per geological unit.

Formation	Member		Bulk wet density [g/cm³]	Bulk dry density, calculated [g/cm³]	Grain density [g/cm³]	Pycnometer porosity [–]	Gravimetry			
							Water content (wet) (105 °C) [wt.-%]	Water content (dry) (105 °C) [wt.-%]	Water-loss porosity using bulk wet density [–]	Water-loss porosity using grain density [–]
Wildegg Fm.		Mean	2.576	2.523	2.683	0.060	2.061	2.104	0.053	0.053
		n	1	1	1	1	1	1	1	1
Ifenthal Fm.		Mean	2.634	2.549	2.747	0.072	3.197	3.303	0.084	0.083
		n	1	1	1	1	1	1	1	1
Haupt-rogenstein	All	Mean	2.572	2.497	2.713	0.079	2.918	3.014	0.075	0.075
		Median	2.572	2.497	2.708	0.081	2.750	2.829	0.070	0.071
		Stdev	0.025	0.035	0.020	0.015	0.943	1.003	0.024	0.023
		Min	2.534	2.449	2.692	0.055	1.877	1.913	0.048	0.049
		Max	2.607	2.557	2.744	0.101	4.275	4.466	0.111	0.109
		n	8	8	8	8	8	8	8	8
Haupt-rogenstein	Upper ('Movelier Beds' + 'Spatkalk')	Mean	2.571	2.483	2.716	0.086	3.400	3.529	0.088	0.087
		Median	2.571	2.483	2.716	0.086	3.400	3.529	0.088	0.087
		Stdev	0.051	0.018	0.034	0.005	1.237	1.325	0.034	0.031
		Min	2.534	2.470	2.692	0.082	2.526	2.591	0.064	0.065
		Max	2.607	2.496	2.740	0.089	4.275	4.466	0.111	0.109
		n	2	2	2	2	2	2	2	2
Haupt-rogenstein	Lower	Mean	2.573	2.502	2.711	0.077	2.757	2.843	0.071	0.071
		Median	2.572	2.508	2.708	0.075	2.590	2.660	0.067	0.067
		Stdev	0.019	0.039	0.017	0.017	0.903	0.957	0.023	0.022
		Min	2.548	2.449	2.697	0.055	1.877	1.913	0.048	0.049
		Max	2.606	2.557	2.744	0.101	3.889	4.046	0.099	0.098
		n	6	6	6	6	6	6	6	6
Passwang Fm.	All	Mean	2.527	2.413	2.702	0.107	4.555	4.790	0.115	0.114
		Median	2.528	2.410	2.696	0.109	4.665	4.893	0.118	0.117
		Stdev	0.043	0.075	0.014	0.027	1.344	1.479	0.032	0.031
		Min	2.468	2.307	2.687	0.073	2.798	2.878	0.073	0.073
		Max	2.596	2.523	2.721	0.152	6.505	6.958	0.161	0.159
		n	7	7	7	7	7	7	7	7
Passwang Fm.	Rothenfluh Mb.	Mean	2.544	2.444	2.700	0.095	3.938	4.115	0.100	0.099
		Median	2.548	2.458	2.695	0.088	3.546	3.676	0.090	0.090
		Stdev	0.047	0.078	0.014	0.025	1.333	1.461	0.032	0.031
		Min	2.483	2.338	2.690	0.073	2.798	2.878	0.073	0.073
		Max	2.596	2.523	2.721	0.131	5.863	6.229	0.146	0.144
		n	4	4	4	4	4	4	4	4
Passwang Fm.	Walden-burg + lower part of Brüggli Mb.	Mean	2.505	2.371	2.705	0.123	5.378	5.691	0.135	0.133
		Median	2.520	2.395	2.707	0.110	4.963	5.222	0.125	0.123
		Stdev	0.033	0.056	0.016	0.025	0.988	1.109	0.023	0.023
		Min	2.468	2.307	2.687	0.109	4.665	4.893	0.118	0.117
		Max	2.528	2.410	2.720	0.152	6.505	6.958	0.161	0.159
		n	3	3	3	3	3	3	3	3

Tab. 4.3-3: (continued)

Formation	Member		Bulk wet density [g/cm³]	Bulk dry density, calculated [g/cm³]	Grain density [g/cm³]	Pycnometer porosity [–]	Gravimetry			
							Water content (wet) (105 °C) [wt.-%]	Water content (dry) (105 °C) [wt.-%]	Water-loss porosity using bulk wet density [–]	Water-loss porosity using grain density [–]
Opalinus Clay	All	Mean	2.504	2.395	2.698	0.112	4.386	4.591	0.110	0.110
		Median	2.501	2.395	2.692	0.113	4.350	4.548	0.109	0.109
		Stdev	0.043	0.048	0.041	0.014	0.516	0.563	0.012	0.012
		Min	2.445	2.328	2.657	0.083	3.320	3.434	0.085	0.085
		Max	2.596	2.470	2.835	0.130	5.077	5.348	0.126	0.127
		n	16	16	16	16	16	16	16	16
Opalinus Clay	With silty calc. beds	Mean	2.513	2.414	2.685	0.101	3.933	4.096	0.099	0.099
		Median	2.516	2.414	2.688	0.105	4.017	4.186	0.100	0.100
		Stdev	0.034	0.043	0.021	0.013	0.506	0.548	0.012	0.012
		Min	2.469	2.362	2.657	0.083	3.320	3.434	0.085	0.085
		Max	2.552	2.468	2.708	0.111	4.378	4.578	0.110	0.110
		n	4	4	4	4	4	4	4	4
Opalinus Clay	Upper silty	Mean	2.532	2.423	2.702	0.104	4.311	4.508	0.109	0.108
		Median	2.532	2.423	2.702	0.104	4.311	4.508	0.109	0.108
		Stdev	0.007	0.012	0.006	0.006	0.729	0.796	0.019	0.017
		Min	2.527	2.414	2.698	0.099	3.795	3.945	0.096	0.096
		Max	2.537	2.431	2.707	0.108	4.826	5.071	0.122	0.121
		n	2	2	2	2	2	2	2	2
Opalinus Clay	Mixed clay-silt-carb.	Mean	2.504	2.392	2.709	0.117	4.496	4.710	0.113	0.113
		Median	2.489	2.380	2.698	0.119	4.506	4.719	0.112	0.113
		Stdev	0.051	0.053	0.054	0.012	0.403	0.441	0.010	0.010
		Min	2.445	2.328	2.659	0.093	3.809	3.960	0.098	0.097
		Max	2.596	2.470	2.835	0.129	4.988	5.249	0.126	0.127
		n	8	8	8	8	8	8	8	8
Opalinus Clay	Clay-rich	Mean	2.461	2.339	2.678	0.126	4.930	5.186	0.121	0.122
		Median	2.461	2.339	2.678	0.126	4.930	5.186	0.121	0.122
		Stdev	0.002	0.004	0.014	0.006	0.207	0.229	0.005	0.005
		Min	2.459	2.337	2.668	0.122	4.784	5.024	0.118	0.118
		Max	2.462	2.342	2.687	0.130	5.077	5.348	0.125	0.126
		n	2	2	2	2	2	2	2	2
Staffelegg Fm.		Mean	2.451	2.344	2.627	0.108	4.369	4.577	0.107	0.107
		Median	2.452	2.345	2.649	0.097	4.033	4.203	0.099	0.099
		Stdev	0.047	0.060	0.058	0.022	0.959	1.057	0.022	0.022
		Min	2.400	2.285	2.543	0.095	3.636	3.773	0.090	0.091
		Max	2.501	2.403	2.669	0.141	5.775	6.129	0.140	0.140
		n	4	4	4	4	4	4	4	4
Klettgau Fm.		Mean	2.558	2.428	2.776	0.125	5.119	5.402	0.131	0.130
		Median	2.537	2.389	2.790	0.134	5.394	5.701	0.136	0.135
		Stdev	0.059	0.077	0.027	0.024	0.909	1.006	0.021	0.021
		Min	2.513	2.378	2.745	0.098	4.105	4.281	0.108	0.107
		Max	2.625	2.517	2.792	0.144	5.859	6.224	0.149	0.148
		n	3	3	3	3	3	3	3	3

4.3.1 Water content

Martin Mazurek & Lukas Aschwanden

The distribution of gravimetric water content in the studied section Malm – Keuper is shown in Fig. 4.3-1. Note that the University of Bern data reflect averages of 3 aliquots of the same sample – 2 from isotope diffusive exchange plus 1 separate measurement. On the other hand, the data of Hydroisotop GmbH reflect the average of the 2 aliquots from isotope diffusive-exchange experiments only. A third, separate measurement was also performed for each sample but, for operational reasons, is not considered in Tab. 4.3-3 and in the graphics of this section. Variability among the different aliquots is generally small (error bars in Fig. 4.3-1 reflect 1σ deviation among the different aliquots of a sample, i.e., they are a measure of the lithological heterogeneity of the sample on the cm scale) and thus, the effect of a third measurement is marginal. Nevertheless, for reasons of completeness, all three measurements of Hydroisotop GmbH are considered in Appendix A.

No systematic depth trends are evident in the Malm and in the Keuper, and the Dogger – Lias section is detailed further below.

Water contents from gravimetry and from isotope diffusive exchange correlate well (Fig. 4.3-2), but the latter are mostly somewhat higher. One sample from the Bänkerjoch Formation (a mixture of anhydrite and clay minerals) deviates from the regression line due to sample heterogeneity on the cm scale, also highlighted by the large error bars and the core photograph in Fig. 4.3-3.

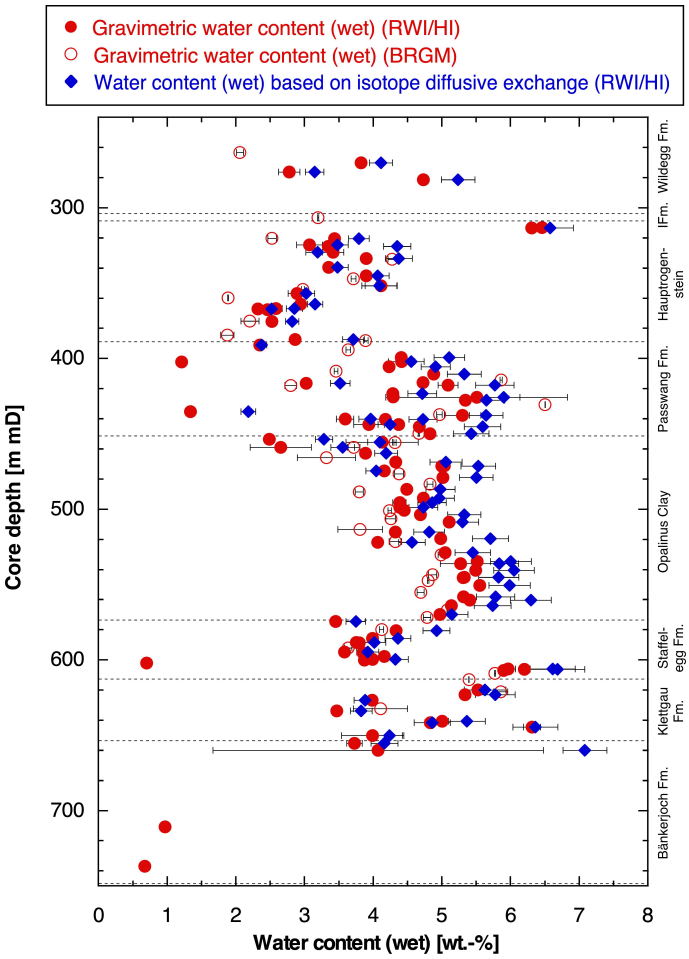

Fig. 4.3-1: Water content as a function of depth

Black bars for gravimetric water content indicate 1σ variability among 2 (BRGM/ Hydro-isotop GmbH HI) or 3 (University of Bern, RWI) aliquots of the same sample. Black bars for water content from isotope diffusive exchange represent the propagated analytical error.

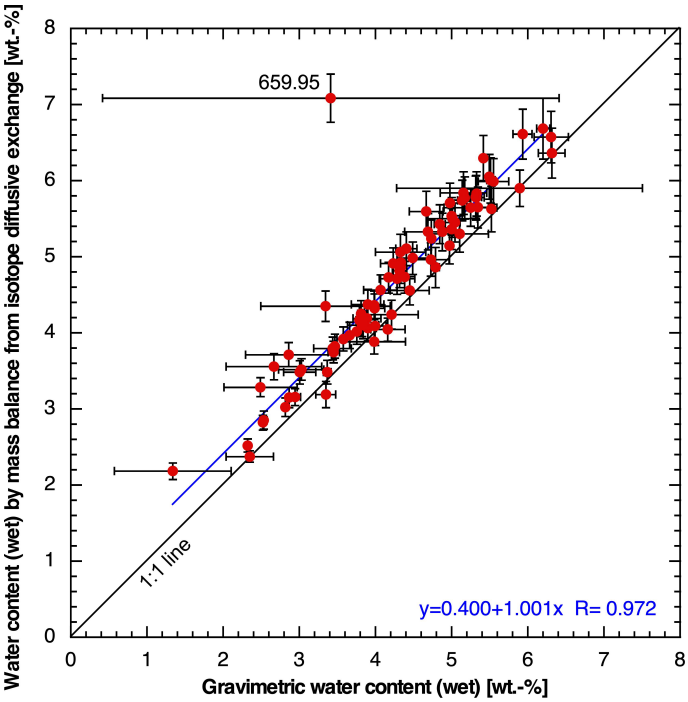

Fig. 4.3-2: Correlation of water contents based on gravimetry and on isotope diffusive exchange

All data originate from University of Bern / Hydroisotop GmbH. Note that only the gravimetric water contents obtained from the aliquots used for the isotope diffusive-exchange experiments are considered in this graph, so the correlation refers to identical sample materials. Black bars for gravimetric water content indicate 1σ variability among these 2 aliquots. Black bars for water content from isotope diffusive exchange represent the propagated analytical error. Blue regression line excludes the labelled outlier. See Fig. 4.8-2 for a more detailed comparison.

Fig. 4.3-3: Core photograph of heterogeneous sample 659.95 from the Bänkerjoch Formation
Width of photograph is 10 cm.

A closer look at the clay-rich Lias – Dogger section

As shown in Fig. 4.3-4, water contents in the Lias-Dogger section show some systematic trends with depth. These are similar for gravimetric water content and that obtained from isotope mass balance:

- A moderately well-defined trend of water content decreasing upwards is observed in the lower part of the Staffelegg Formation, reaching a minimum within the Frick Member. From there, a well-expressed increase is found until the top of the Clay-rich sub-unit of the Opalinus Clay. Both these trends mirror analogous trends in the clay-mineral contents (Fig. 4.2-4a).
- Similar to borehole BOZ1-1, water content decreases within the Mixed clay-silt-carbonate sub-unit of the Opalinus Clay, again correlated with clay-mineral content.
- A sharp upward decrease of water content is seen in the Sub-unit with silty calcareous beds, which is not observed in BOZ1-1.
- Distinct depth trends are not evident in the Passwang Formation, except possibly at the base.
- A weakly defined increase is inferred within the lower part of the Hauptrogenstein and is best explained by the degree of dolomitisation that distinctly increases upwards (Fig. 4.2-4b).

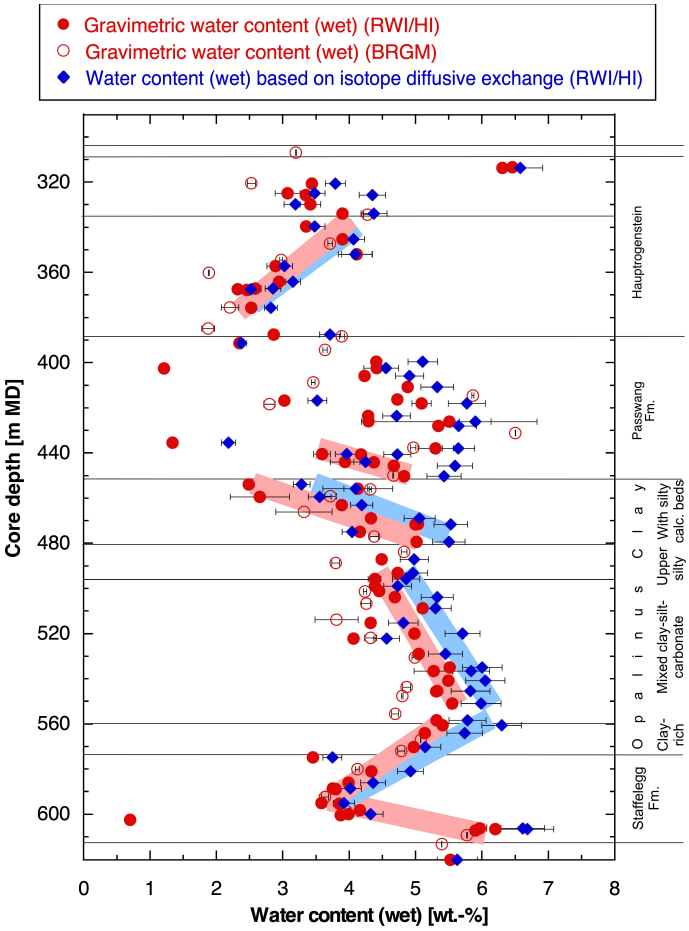

Fig. 4.3-4: Water content (wet) as a function of depth in the Lias – Dogger interval

Black bars for gravimetric water content indicate 1σ variability among 3 aliquots of the same sample. Black bars for water content from isotope diffusive exchange represent the propagated analytical error.

4.3.2 Grain density

Martin Mazurek & Lukas Aschwanden

The grain-density profile is shown in Fig. 4.3-5. Throughout the Malm and Dogger units, values are around 2.7 g/cm^3, with only limited scatter. The upwards increasing trend within the lower Hauptrogenstein reflects the increasing degree of dolomitisation (Fig. 4.2-4b). An outlier in the uppermost Hauptrogenstein ('Spatkalk') is due to 12 wt.-% goethite and haematite, and another outlier in the uppermost Opalinus Clay is due to the presence of 5 wt.-% pyrite. Another sample with a high value at 543.40 m cannot be explained by the mineralogical data. One low value in the Rietheim Member of the Staffelegg Formation (Posidonienschiefer) is due to the presence of 3.5 wt.-% organic carbon. In the Keuper, values become larger, as does variability. This reflects the lithological heterogeneity, in particular the variable contents of dolomite and anhydrite with

their high mineral densities. Fig. 4.3-6 shows the correlation between grain density and dolomite/ ankerite contents. Grain density increases linearly with dolomite concentration (black trend line in Fig. 4.3-6), and most outliers can be explained by the abundance of other high-density minerals.

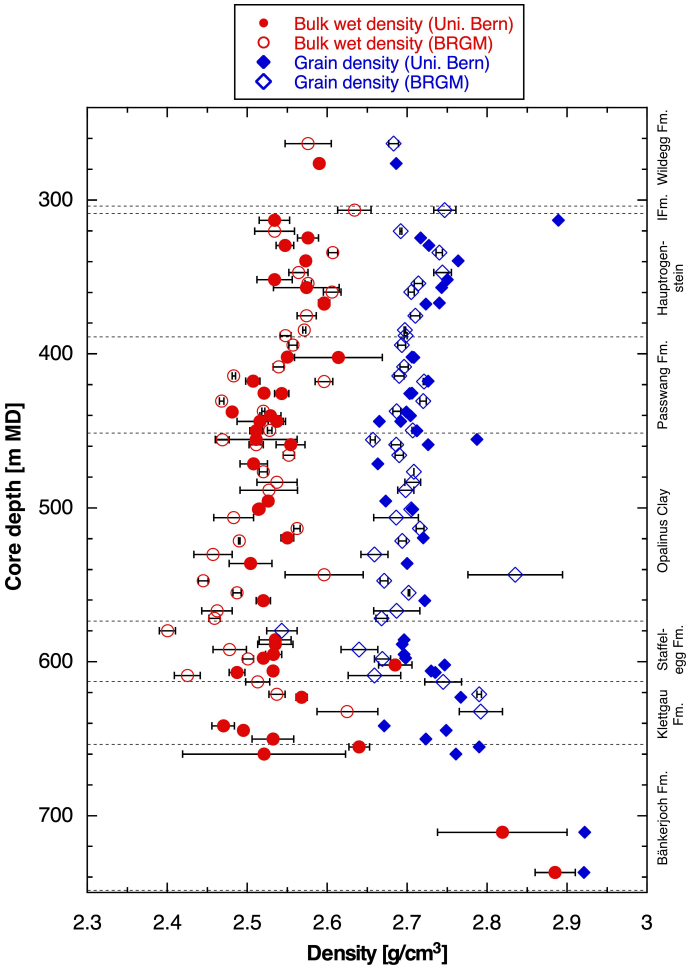

Fig. 4.3-5: Depth profile of bulk wet and grain densities

Black bars for bulk wet density (both labs) and for grain density (BRGM) indicate 1σ variability among several (2 – 3) pieces of the same sample. Analytical error bars for grain density measured at Unversity of Bern are smaller than the symbol size.

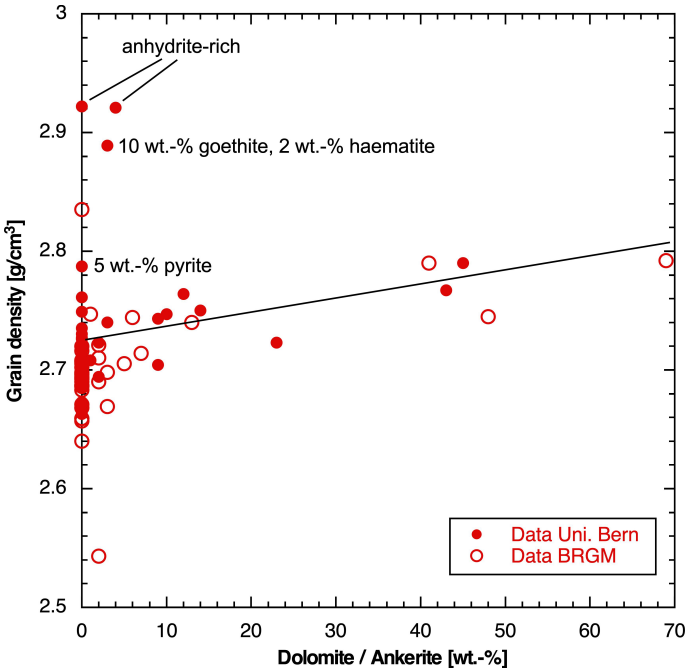

Fig. 4.3-6: Grain density as a function of the contents of dolomite/ankerite

All mineralogy data are from University of Bern, density data are from Unversity of Bern and BRGM.

4.3.3 Bulk wet density

Martin Mazurek & Lukas Aschwanden

All available data are shown in Fig, 4.3-5 as a function of depth. Large error bars for some samples reflect heterogeneity on the cm – dm scale.

4.3.4 Porosity

Martin Mazurek & Lukas Aschwanden

Three different approaches were used to constrain rock porosity (for details see Waber (ed.) 2020):

- *Water-loss porosity:* calculation from the gravimetric water content using either bulk wet or grain density.
- *Porosity from isotope diffusive exchange:* calculation from the water content obtained by mass balance using either bulk wet or grain density.
- *Pycnometer porosity:* calculation from bulk dry and grain densities; bulk dry density is calculated from bulk wet density and water content.

Water-loss porosity and porosity from isotope diffusive exchange were calculated using bulk wet density by default. If the latter was not available, grain density was used, by which full water saturation of the pore space is assumed. The graphic in Fig. 4.3-7 shows that the two densities yield near-identical porosities, so the choice of the type of density for the calculation incurs no additional uncertainty.

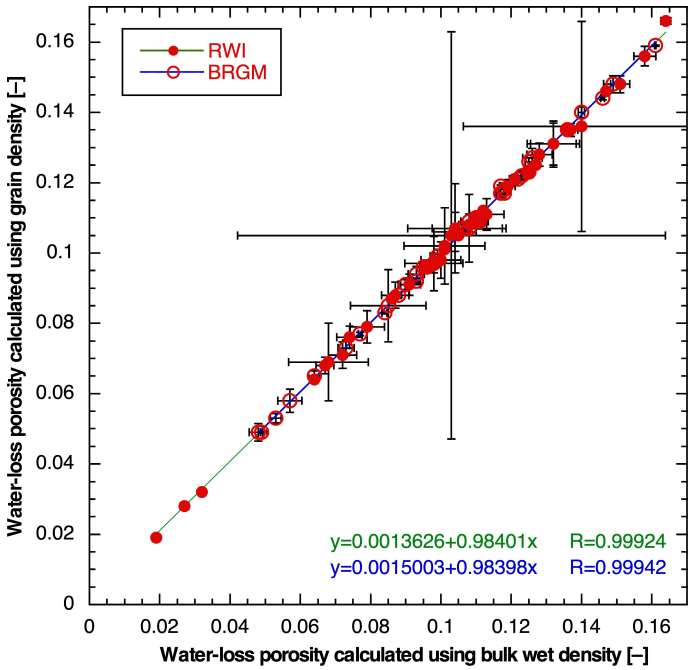

Fig. 4.3-7: Water-loss porosity calculated from gravimetric water content using either bulk wet or grain density

Bars indicate propagated errors, which are dominated by local heterogeneity of the water content. The fit lines for the data of the two laboratories overlap completely.

Comparison of porosities obtained by different methods

- An excellent linear correlation is observed between water-loss porosity and porosity from isotope diffusive exchange (Fig. 4.3-8, based on data from University of Bern and Hydro-isotop GmbH). The latter yields slightly higher values. One outlier from the Triassic is likely due to sample heterogeneity (Fig. 4.3-3).
- A markedly less well-defined linear correlation is found between pycnometer porosity and porosity from isotope diffusive exchange (Fig. 4.3-9, based on data from University of Bern). On the average, the latter yields slightly higher values.
- The correlation between water-loss and pycnometer porosity is shown in Fig. 4.3-10 (based on data from University of Bern and BRGM). The slope of the regression line is markedly below 1.

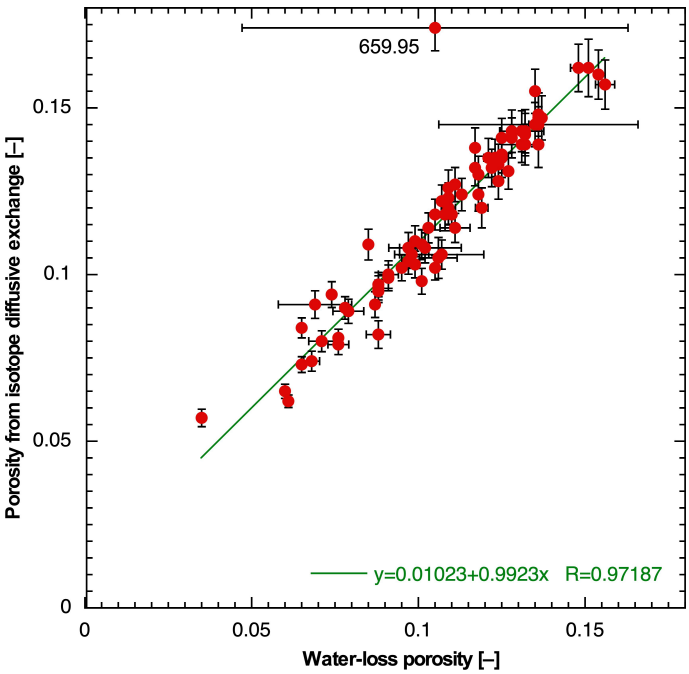

Fig. 4.3-8: Correlation of water-loss porosity and porosity from isotope diffusive exchange

All data from University of Bern and Hydroisotop GmbH. Bars indicate propagated errors. Regression line excludes the labelled outlier. In the absence of grain-density data for the Hydroisotop GmbH samples, a value of 2.7 g/cm^3 was used.

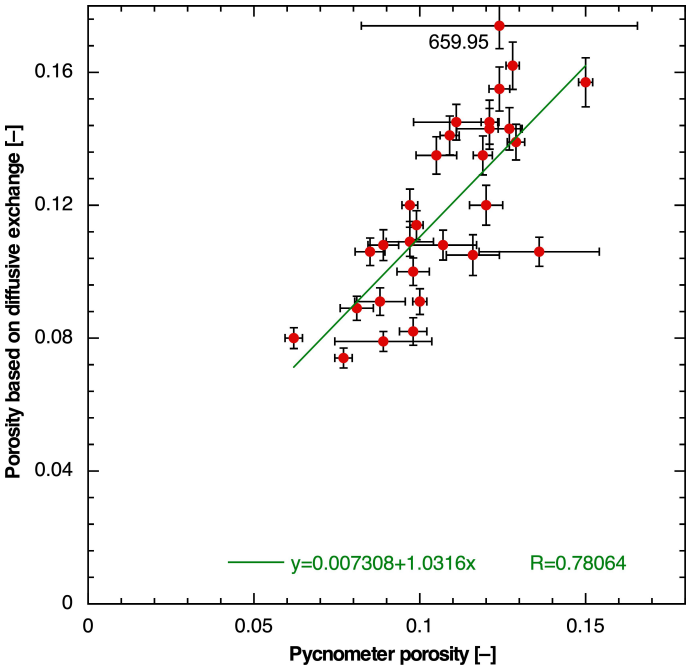

Fig. 4.3-9: Correlation of pycnometer porosity and porosity from isotope diffusive exchange

All data from University of Bern. Bars indicate propagated errors. Regression line excludes the labelled outlier.

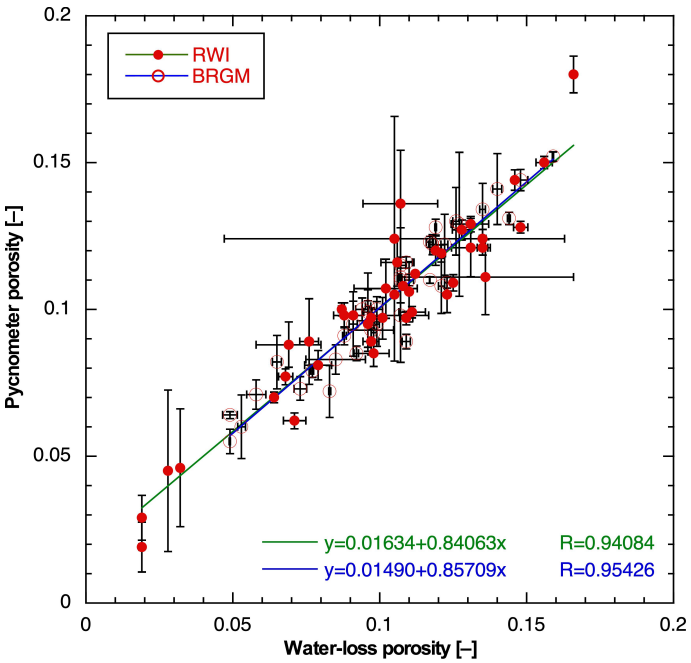

Fig. 4.3-10: Correlation of water-loss and pycnometer porosity

Bars indicate propagated errors.

Depth trends

In Fig. 4.3-11, porosity is shown as a function of depth. The shape of the profile is similar to that of water content (Fig. 4.3-1). The comments made on the distribution of water content with depth (Section 4.3.1) also apply to porosity.

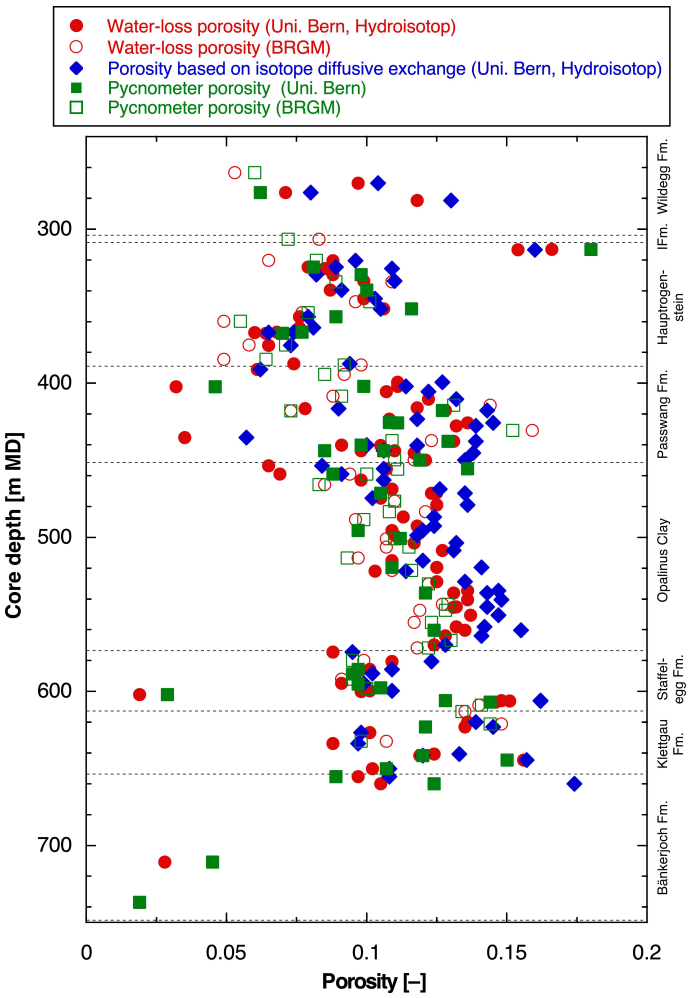

Fig. 4.3-11: Depth trends of porosities obtained by different methods and laboratories

Porosity as a function of mineralogical composition

The correlation of porosity with clay-mineral content is shown in Fig. 4.3-12. A general positive correlation can be identified, but scatter is substantial. The slope of the data is steeper for clay-mineral contents in the range 0 – 30 wt.-% and becomes flatter at higher clay-mineral contents. Samples that fall out of the general trend towards higher porosity include Fe-oolithic units (such as the 'Spatkalk'), dolomite-rich lithologies (such as the Gruhalde Member of the Klettgau Formation) or some limestones from the lower part of the Hauptrogenstein.

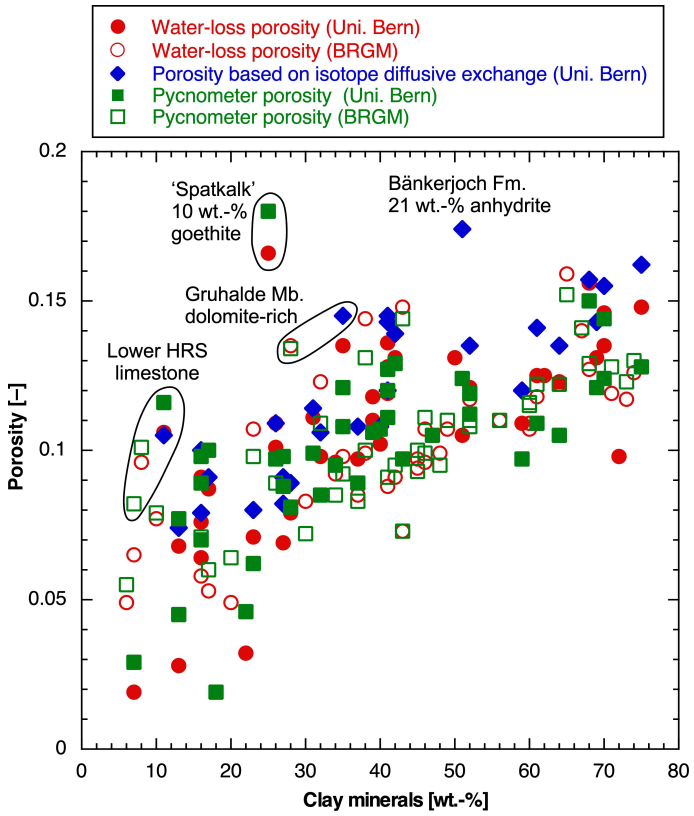

Fig. 4.3-12: Porosity as a function of clay-mineral content

4.3.5 Specific surface area and pore size distributions from N_2 ad-/desorption

Thomas Gimmi

Depth trends

Nitrogen adsorption data were only obtained for the 10 samples from the upper and lower confining units of Opalinus Clay on which through-diffusion experiments (PSI, Van Loon & Glaus *in prep.*) were performed (Tab. 4.3-2). Two samples are from the Hauptrogenstein, two from the Passwang Formation, four from the Staffelegg Formation and two from the Bänkerjoch Formation. They show strong lithological variability, but claystone samples are underrepresented (one sample).

Due to the comparably small number of samples and the lack of data from the Opalinus Clay, the depth trends of the specific surface area S_{BET} are not very clear (Fig. 4.3-13). However, a comparison with the data obtained from the BOZ1-1 borehole (right plot in Fig. 4.3-13) shows that the variation with the rock formation is similar in both boreholes (note that in the BOZ1-1 borehole, the upper and lower parts of the Hauptrogenstein are separated by a section belonging to the Klingnau Formation).

As N_2 cannot reach any interlayer pores of smectites, S_{BET} represents surfaces of external (non-interlayer) pores. The largest value of about 50 m^2/g was found for the claystone sample (70 wt.-% clay mineral fraction) from the lower part of the Staffelegg Formation. Values in the range of about 20 to 25 m^2/g were measured for other clay-rich units from the lower Passwang Formation and the upper part of the Staffelegg Formation. Low values (< ~ 9 m^2/g) were found in the Hauptrogenstein and for the two anhydrite-dominated samples from the Bänkerjoch Formation, and the lowest value was reported for the limestone sample from the Staffelegg Formation (602.23 m, ~ 2 m^2/g). The scatter in the values from the Staffelegg Formation is remarkable, as they cover the highest and the lowest measured values within a vertical distance of ~ 5 m. The variability in the reported S_{BET} is linked to the heterogeneity of the clay-mineral contents (Fig. 4.2-1) and of other parameters defining the texture and the pore structure of the sample, which are related to heterogeneities regarding depositional environment and diagenesis.

The variation of the specific surface area S_{BET} with depth is generally related to trends observed in other physical and mineralogical properties of samples from the BOZ2-1 borehole, such as the bulk dry density, the gravimetric water content, the water-loss porosity or the clay-mineral content. For comparison purposes, in some plots the general trends seen for the larger dataset from BOZ1-1 are also shown (but a more careful analysis should be based on the individual data of the two boreholes, not just on the possibly oversimplified general trends).

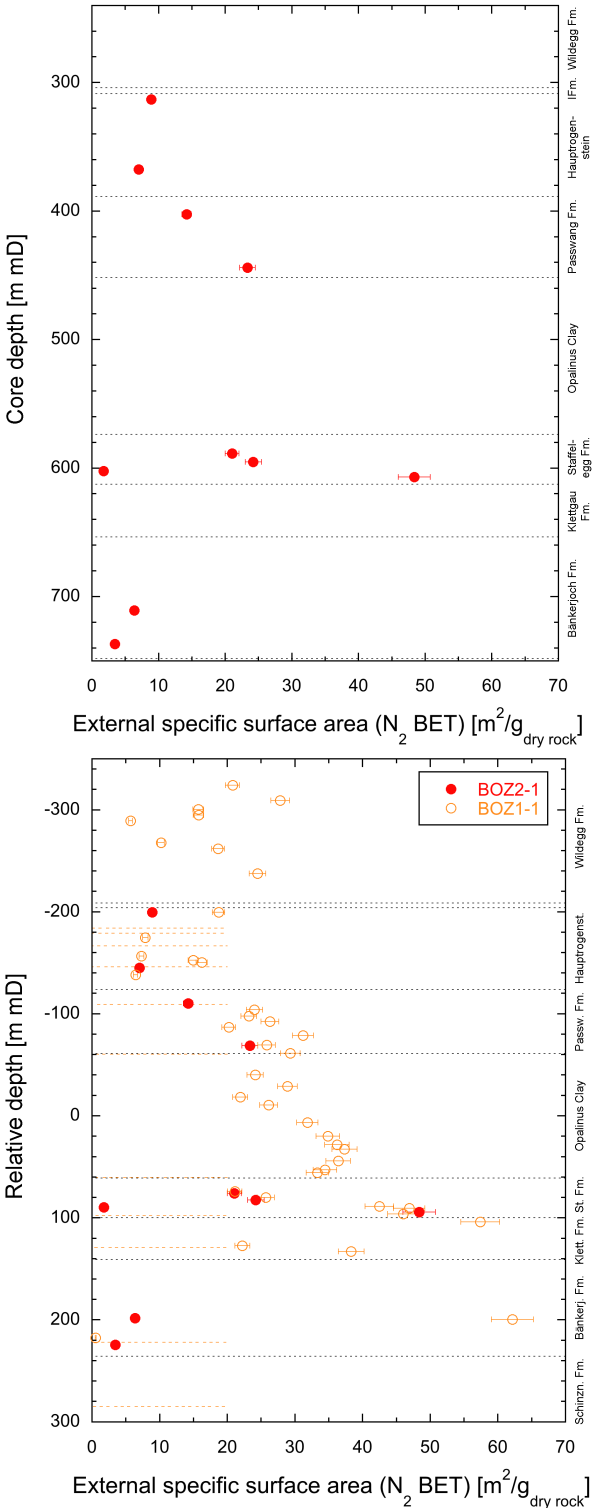

Fig. 4.3-13: Specific surface area (S_{BET}) derived from N_2 adsorption as a function of depth

Left: Data from BOZ2-1. Right: Comparison of data from BOZ2-1 with those from BOZ1-1, with depth relative to centre of Opalinus Clay. S_{BET} represents external surfaces only. The total specific surface area, including interlayer surfaces, would be larger depending on the smectite content of the sample. Errors resulting from sample preparation and handling are estimated to be ± 5% in general and ± 10% for $S_{BET} < 2$ m^2 g^{-1}, as given by the error bars. In the right plot, the orange dashed lines show formation boundaries for BOZ1-1 (names not given).

Correlation of S_{BET} with water content and clay mineral content

The S_{BET} tends to increase with the gravimetric water content relative to the dry sample mass (Fig. 4.3-14). The correlation is, however, very weak, which is related to the small number and the lithological differences between the chosen samples from the confining units.

The largest S_{BET} value for the claystone in the Staffelegg Formation (606.95 m) is related to a large water content. A large water content was also obtained for the sample at 313.13 m in the upper part of the Hauptrogenstein ('Movelier Beds' and 'Spatkalk'), but this sample as well as the other sample from the Hauptrogenstein have comparably low specific surface areas (~ 9 m^2/g and ~ 7 m^2/g, respectively). The Hauptrogenstein sample has a goethite content of 10 wt.-% and a reddish, rusty color, distinct from the surrounding greyish colors, similarly as the samples from the same formation in BOZ1-1. The limestone sample in the Staffelegg Formation (602.23 m) with the lowest S_{BET} has also a very low water content of 0.7 wt.-%.

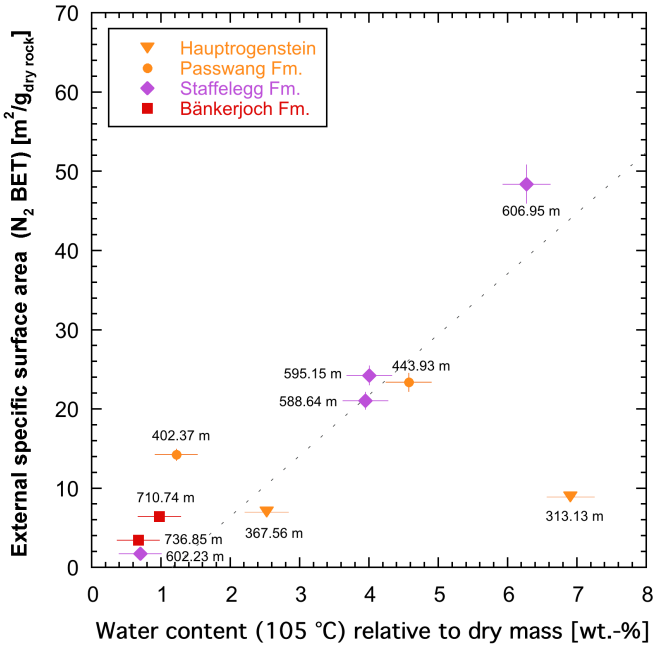

Fig. 4.3-14: Specific surface area (S_{BET}) derived from N_2 adsorption plotted against the gravimetric water content relative to the dry mass of the samples

Error bars show estimated errors for the water content (based on standard deviations of other samples) and estimated errors for S_{BET}. The dotted line shows the regression obtained for the BOZ1-1 data which include samples from all formations (a regression for the speficially chosen samples from BOZ2-1 alone is considered as less meaningful).

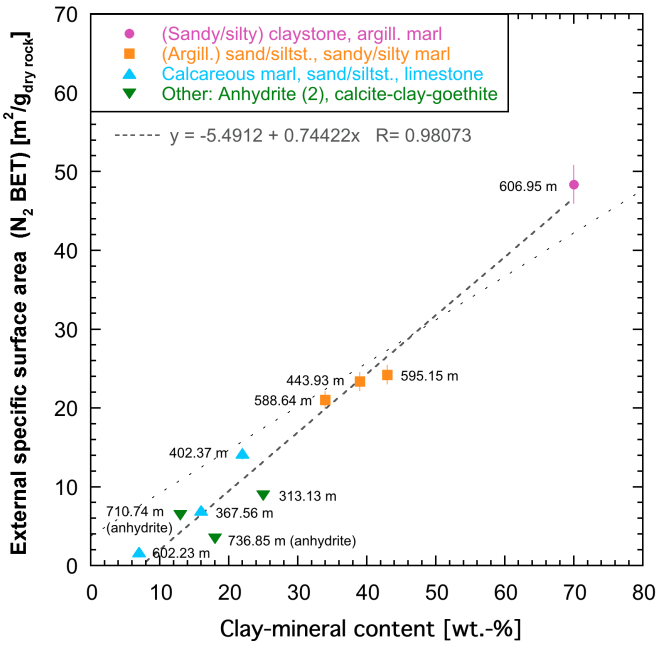

Fig. 4.3-15: Relation between external specific surface area (S_{BET}) derived from N_2 adsorption and content of clay minerals

The samples are assigned to four classes according to their positions in the Füchtbauer diagram (i.e., according to lithological rock types). The fourth group includes samples without a Füchtbauer name (two samples dominated by anhydrite, one sample with considerable amounts of goethite). The dashed line is a regression on the BOZ2-1 data which do not include any samples from the Opalinus Clay; the dotted line shows the regression obtained for the BOZ1-1 data including samples from all formations

The specific surface area S_{BET} is more clearly correlated with the total content of clay minerals (Fig. 4.3-15) than with the water content for the limited number of samples from the BOZ2-1 borehole. The single claystone sample from the Staffelegg Formation (606.95 m) shows the largest S_{BET} value. The different lithological subgroups (claystone, very argillaceous sandstone/siltstone, limestone and other for this sample set, the last including the two thin-layered anhydrite-claystone samples at 710.74 m and 736.84 m and the sample at 313.13 m) tend to plot in different regions in Fig. 4.3-15.

A positive correlation of S_{BET} exists also with the contents of the illite end-member (Fig. 4.3-16), with the samples at 313.13 m and 736.84 m plotting somewhat above and below the correlation, respectively. This correlation (slope of 1.033) is very similar to that obtained for the BOZ1-1 data (slope of 1.035). No clear correlation with the kaolinite, smectite and chlorite end-member contents is visible for the limited dataset of BOZ2-1. The individual data plot in a very similar range compared to the data from BOZ1-1, with the Hauptrogenstein samples and the two anhydrite-dominated samples from BOZ2-1 having comparably larger clay end-member contents compared to the dataset from BOZ1-1.

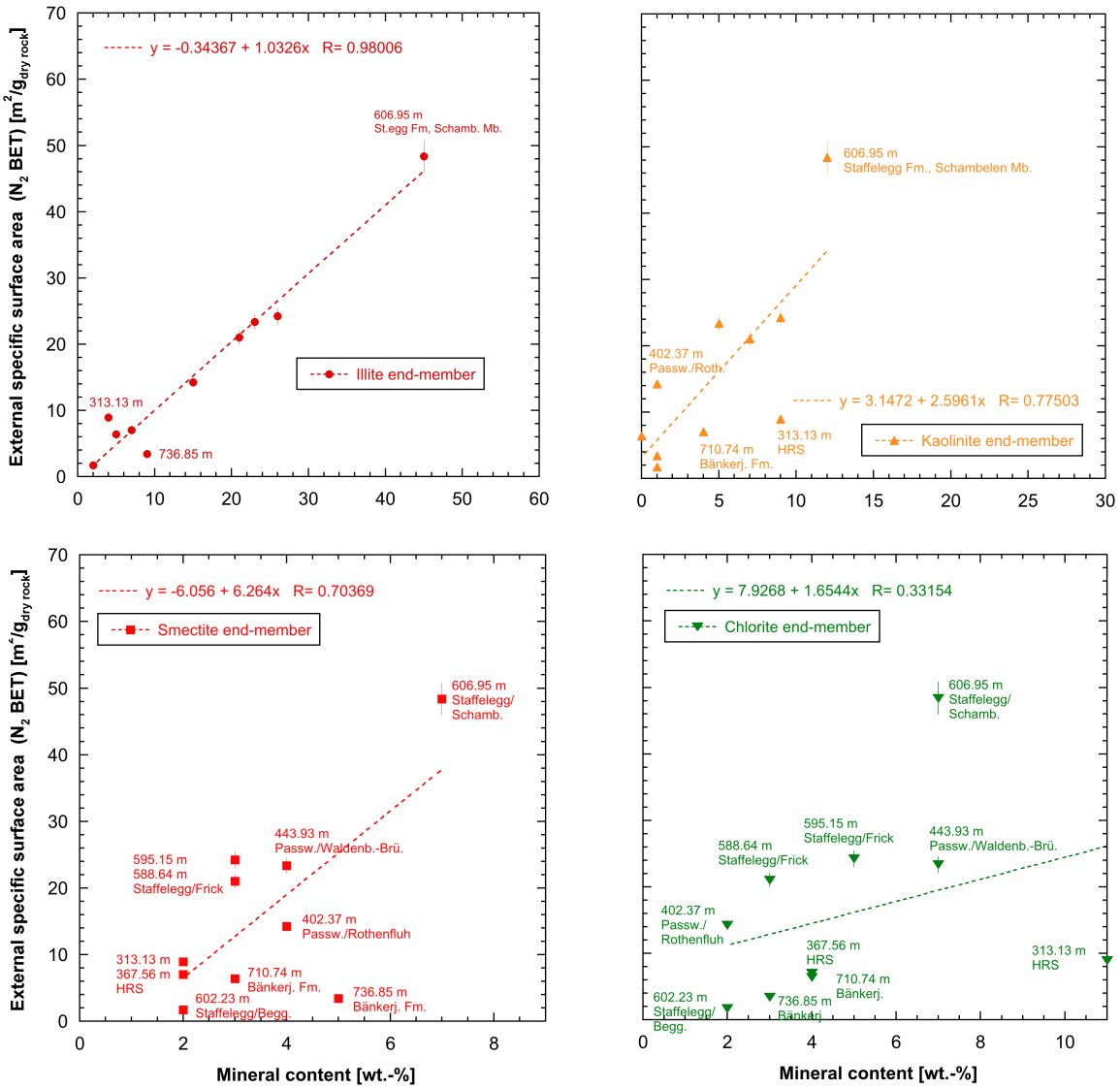

Fig. 4.3-16: Relation between external specific surface area (S_{BET}) derived from N_2 adsorption and contents of specific clay mineral end-members

Average sizes of external pores derived from S_{BET}

Average sizes of external pores were estimated from the specific surface area S_{BET} and the water content per dry mass WC_d as:

$$\overline{r_{ext}} = WC_d/(\rho_w S_{BET})$$

with ρ_w the water density taken to be 1 g/mL. This calculation assumes negligible pore volumes in interlayer pores, i.e. it attributes the measured water content to external pores only (which is not appropriate for samples with relevant smectite end-member contents).

From the inverse of the slope of the linear relation in Fig. 4.3-14 (the slope represents S_{BET}/WC_d), we obtain an overall average layer thickness (or radius) of external pores for the 10 samples from BOZ2-1 of 2.5 nm, which corresponds to about 8 to 10 water layers. A smaller average value was obtained for the samples from BOZ1-1, which included many claystone samples.

Instead of calculating an overall average from the linear regression, it is more interesting to derive an average layer thickness for each sample. Fig. 4.3-17 plots average external pore radii (attributing all water to external surfaces) for each sample as a function of the gravimetric water content per dry solid mass (a) and as a function of the total clay-mineral content (b). The lowest radius of 0.86 nm (diameter of ~ 1.7 nm) is obtained for the limestone sample from the upper part of the Passwang Formation (402.37 m, Rothenfluh Member), the largest radius of 7.8 nm (diameter of ~ 15.5 nm) for the sample from the upper part of the Hauptrogenstein (313.13 m, 'Movelier Beds' and 'Spatkalk') having also a comparably large water content. All other samples have radii between ~ 1 – 4 nm. The values for the different formations and lithologies are broadly consistent with the larger dataset obtained for the BOZ1-1 borehole. That is, they have a tendency of decreasing values with increasing clay-mineral contents, and thus also with increasing water contents, and the limestones and calcareous marls show a comparably large variability. Also, the ironoolithic Hauptrogenstein sample at 313.13 m ('Movelier Beds' and 'Spatkalk') is an outlier especially when plotted as a function of the water content, similarly as the comparable ironoolithic Hauptrogenstein sample from BOZ1-1 at 416.35 m ('Spatkalk').

The claystone sample at 606.95 m with a large clay-mineral fraction and a smectite end-member fraction of ~ 7 wt.-% has certainly some interlayer water. Accordingly, the calculated average external pore radius of ~ 1.3 nm represents a maximum value. A correction of average external pore size that accounts for the volume of interlayer water based on the smectite end-member content could be made assuming typical smectite particle geometries. However, in view of the involved uncertainties this is not done at present.

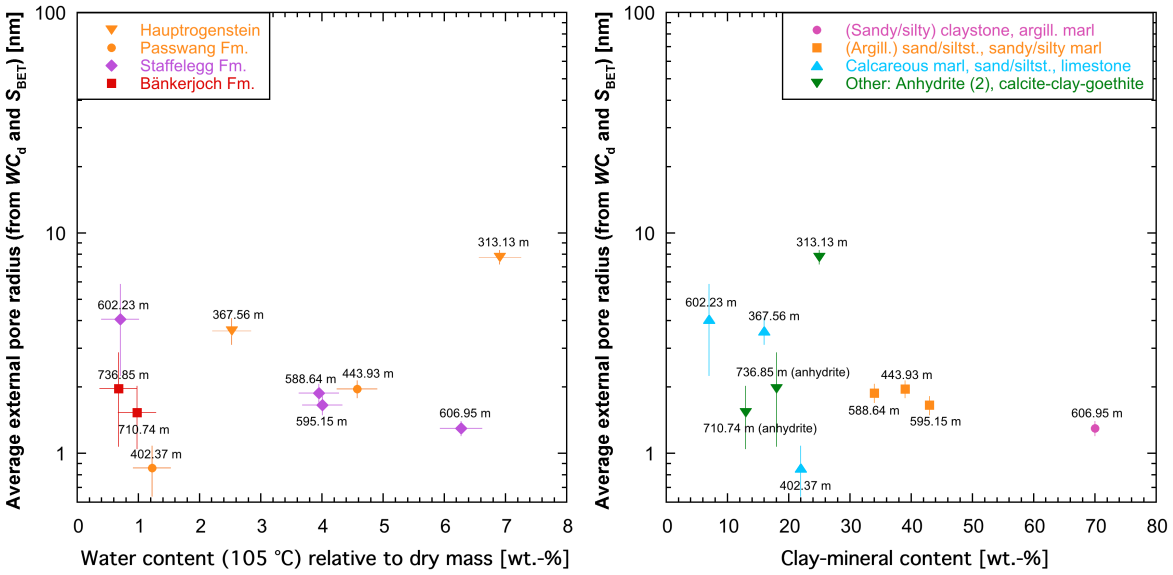

Fig. 4.3-17: Average external pore radius calculated from S_{BET} and the gravimetric water content (assuming insignificant interlayer pore volume) plotted against the gravimetric water content per dry mass of the samples (a) and against the total clay-mineral content (b)

Samples are grouped according to geological units (a) or according to rock lithology (b). Error bars show estimated errors for the water content (based on standard deviations of other samples) and propagated errors for the average external pore radius.

Distribution of external pore sizes derived from N_2 isotherms

Pore size distributions (diameters) of external pores were derived by the standard BJH algorithm from N_2 ad- and desorption isotherms. The figures in the following present results from N_2 desorption for the samples of the different formations, grouped according to rock lithology. Most samples show more or less prominent peaks at a diameter of about 4 nm in the curves derived from desorption. These peaks are typically related to the closure of the hysteresis of the isotherm and are thus attributed to liquid instabilities (instability of the configuration of liquid nitrogen) rather than to a distinct pore volume in this size range. Such hysteresis is generally interpreted as indicating a relatively complex pore architecture (e.g., Thommes et al. 2015).

Fig. 4.3-18a presents the pore size (diameter) distribution for the sample at 313.13 m (ironoolith from the Hauptrogenstein, 'Movelier Beds' and 'Spatkalk'), which appeared often as an outlier in the above figures. It is exceptional with respect to the broad width of the distribution, peaking at a diameter of ~ 40 nm, and the comparably small hysteresis peak at 4 nm. The sample is characterised by a calcite content of 59 wt.-%, a clay content of 25 wt.-%, and a goethite content of 10 wt.-%. Its pore size distribution is very similar to that of the ironoolithic sample at 416.35 m from the BOZ1-1 borehole, characterised by a similar mineralogy including goethite (but only 6 wt.-%, thus classified as limestone according to the Füchtbauer nomenclature).

The diameter distributions of the three calcite-rich and clay-poor samples, classified as limestones according to the Füchtbauer nomenclature, have all a broad peak at 60 – 100 nm (Fig. 4.3-18b). Two of these samples have also a second broad peak or a shoulder at smaller diameters (< 10 – 30 nm) and hysteresis peaks at 4 nm, while the sample at 602.33 m with the lowest S_{BET} and a lower clay-mineral content compared to the other two limestone samples has no such peaks.

The very argillaceous sandstone/siltstone samples according to the Füchtbauer nomenclature (Fig. 4.3-18c) have also two peaks (or a shoulder and a peak) near 10 nm and near 60 – 100 nm, but the peaks at the lower sizes are more important compared to the limestone samples. The hysteresis peaks tend to be more significant than for the limestones, meaning that the pore architecture is more complex.

The claystone sample (Fig. 4.3-18d) has a considerable amount of small pores (important peak at diameters of ~ 3 – 8 nm) as well as of larger pores (broader peak at ~ 60 nm), and furthermore a very strong hysteresis peak hinting to a complex pore architecture. Its pore size distribution is about consistent with those obtained for claystone samples from the BOZ1-1 borehole.

The two fine-layered anhydrite-claystone samples (Fig. 4.3-18e, no Füchtbauer name, 81 wt.-% and 75 wt.-% anhydrite) are characterised mainly by a rather narrow peak at a diameter of ~ 100 nm, a notable hysteresis peak, and a very minor peak at ~ 10 nm. The distribution is different from that of the anhydrite sample from the BOZ1-1 borehole at 808.61 m (97 wt.-% anhydrite). That sample had a lower water content and thus generally smaller peaks, with only a weakly expressed hysteresis peak and a broad peak centered at a diameter of ~ 40 nm.

The reliability of the pore size distribution results can be tested by comparing maximum adsorbed amounts of N_2 at highest N_2 pressures, expressed as wt.-% H_2O, with the samples' water contents (Fig. 4.3-19). In general, the values agree approximately, lending confidence to the derived size distributions. The value for the limestone sample from 402.37 m plots somewhat above the 1:1 line. This could indicate that some pore size fractions (presumably those of large sizes) derived from the N_2 isotherms are slightly overestimated, but it could also be related to heterogeneity at the cm scale, because different samples were used to determine the water content and the N_2 isotherms. Conversely, the values of the samples at 313.13 m and 443.93 m plot somewhat below the 1:1 line, meaning that some of the pores (presumably with larger sizes) are underestimated.

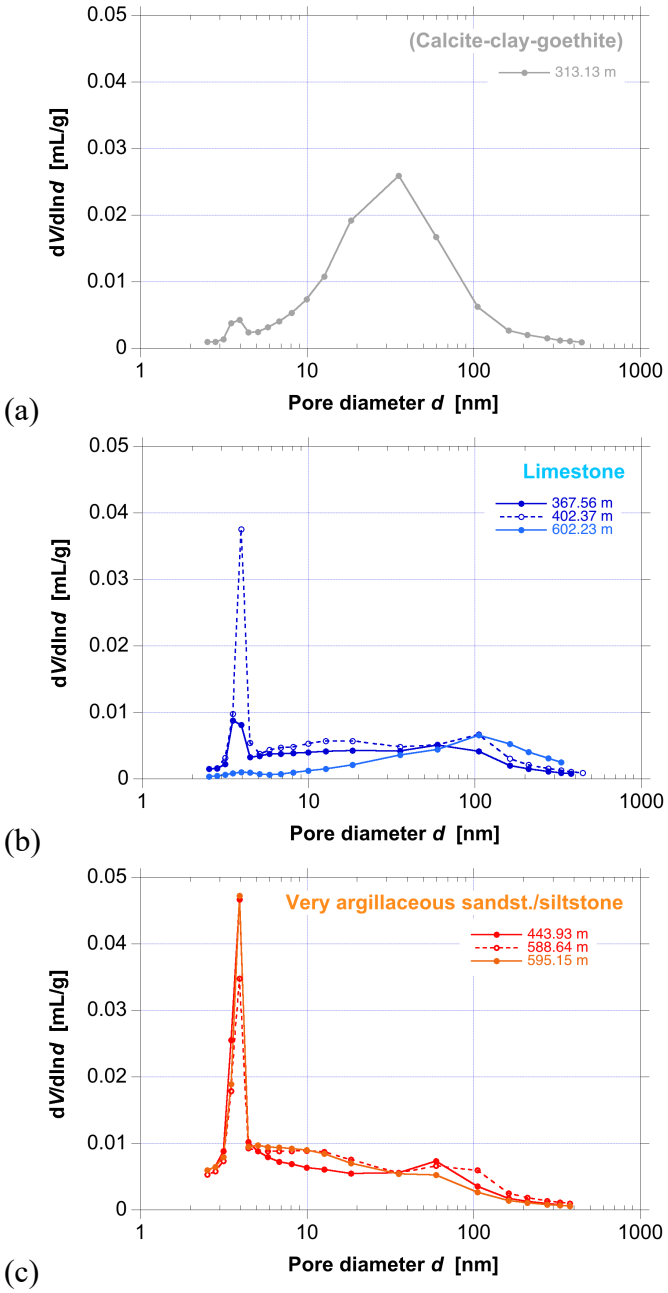

Fig. 4.3-18: Distribution of (external) pore diameters derived from N_2 desorption

(a) Sample with 59 wt.-% calcite, 25 wt.-% clay minerals, and 10 wt.-% goethite (313.13 m, no Füchtbauer name), (b) limestone samples (367.56 m, 402.37 m, 602.23 m), (c) very argillaceous sandstone/siltstone samples (443.93 m, 588.64 m, 595.15 m).

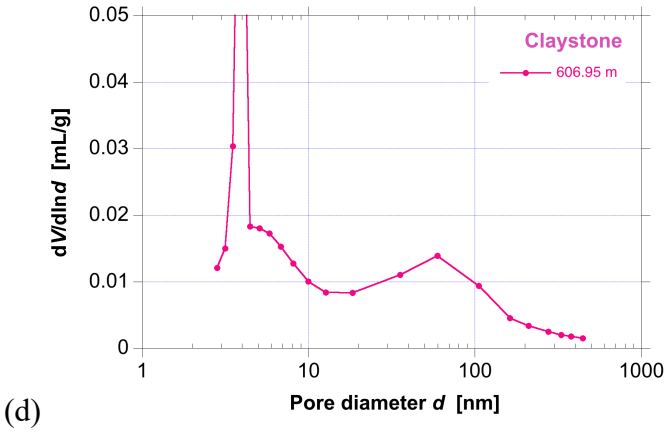

(d)

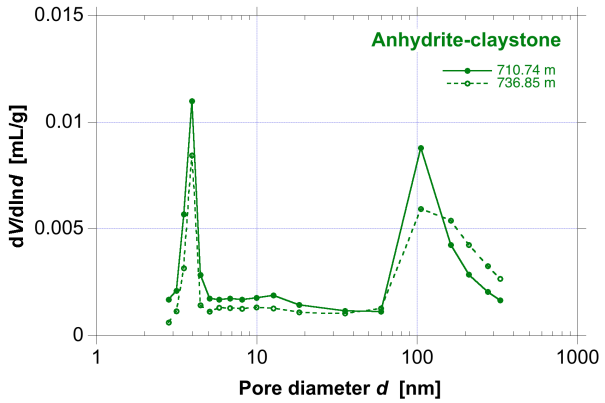

(e)

Fig. 4.3-18: (continued)

(d) claystone sample (606.95 m), and (e) thin-layered anhydrite-claystone samples (710.74 m, 81 wt.-% anhydrite; 736.85 m, 75 wt.-% anhydrite; note the 3.3 times smaller y-axis range compared to the other subfigures).

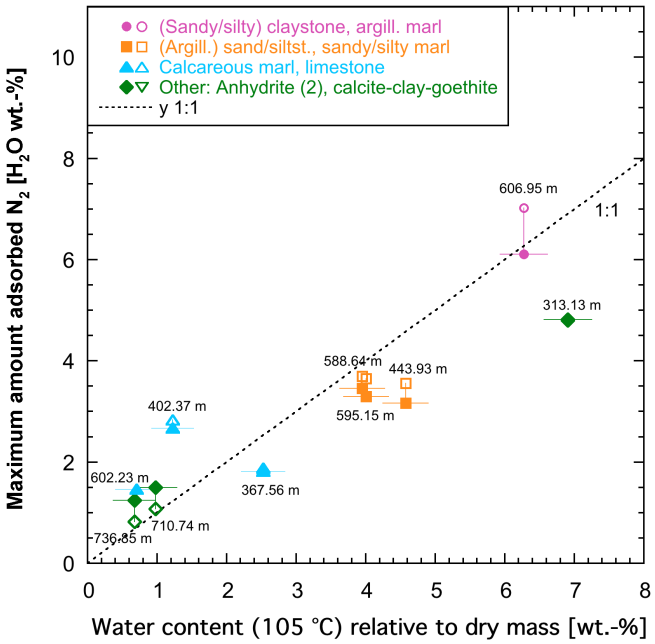

Fig. 4.3-19: Comparison of maximum amount of adsorbed N_2 (recalculated to H_2O wt.-%) with water content per dry sample mass

Open symbols: adsorption, closed symbols: desorption. The samples at 710.74 m and 736.85 m are dominated by anhydrite, the sample at 313.13 m is mainly composed of calcite, clay minerals and goethite.

Average sizes of external pores based on pore size distributions calculated from the N_2 isotherms

Average sizes of external pores cannot only be derived from S_{BET} and the water content as shown above but also from the pore size distribution derived from N_2 isotherms. In both cases, it is assumed that interlayer pore volumes (which are not probed by N_2 adsorption) are insignificant. Radii directly derived by averaging the BJH pore size distributions (Fig. 4.3-20) are somewhat larger when compared with the average radii determined from S_{BET} and the gravimetric water content (Fig. 4.3-17) but show the same tendencies: smaller radii (around 2 – 4 nm for the samples here) for the claystone and the three very argillaceous sandstones/siltstones and larger radii, but with scatter, for the limestones (around 3 – 6 nm for the samples at 367.56 m and at 402.37 m and a large value of ~ 16 nm for the sample at 602.23 m). A large radius of 10 – 11 nm was also derived for the sample at 313.13 m, while the radii for the anhydrite-rich samples at 710.74 m and 736.85 m range between 3 – 8 nm. Overall, the variation with lithology for the few samples from the BOZ2-1 borehole is similar as that for the samples from the BOZ1-1 borehole.

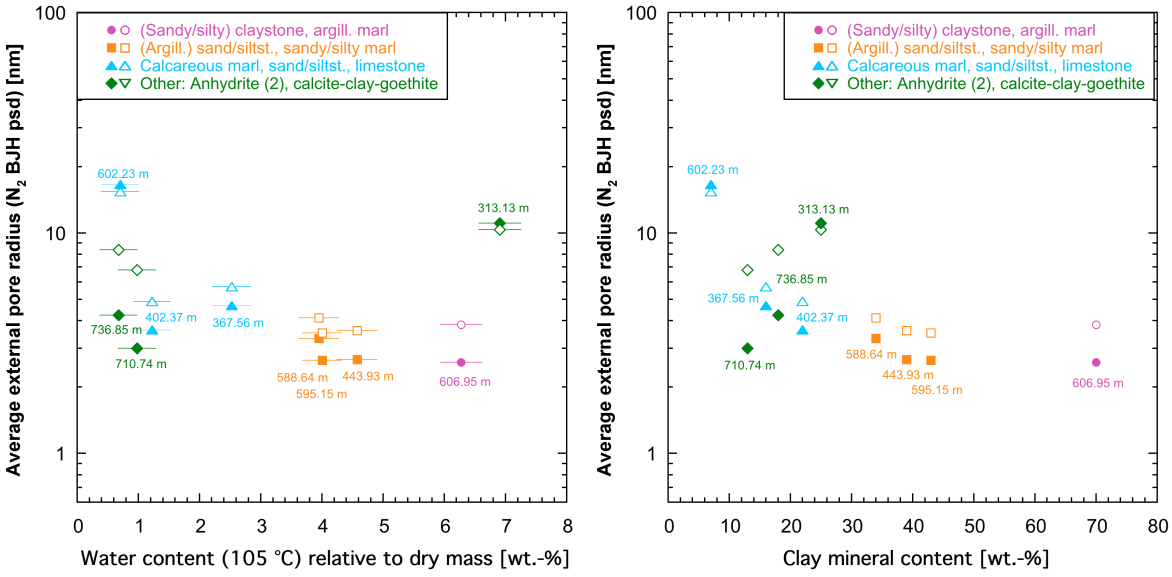

Fig. 4.3-20: Average external pore radius (assuming insignificant interlayer pore volume) based on the BJH pore size distribution from the N_2 isotherms (closed symbols: adsorption; open symbols: desorption) plotted against the gravimetric water content per dry mass of the samples (a) and against the total clay-mineral content (b)

Samples are grouped according to rock lithology. Error bars show estimated errors for the water content per dry mass (based on standard deviations of other samples)

4.4 Data from aqueous extraction tests

Carmen Zwahlen

Aqueous extraction (AqEx) tests are a simple but useful method to improve the understanding of the porewater – rock system across a sequence of sedimentary rocks if carried out at regular intervals. In this section, we present the data from aqueous extraction tests performed at a solid to liquid ratio of approximately 1. The data are discussed further in Chapter 5. The full dataset can be found in Appendix A, and details about the method are given in Waber (ed.) (2020).

4.4.1 Sample material and overview of analytical work

A total of 62 moisture-preserved drill core samples (PW and AD) from the Malm to the Bänkerjoch Formation and 14 dried drill core samples (PW and SQ) from the Hauptrogenstein to the Staffelegg Formation were subjected to aqueous extraction tests. Half of the investigated samples were processed and analysed at BRGM in Orléans (France), the remaining samples at RWI, University of Bern. The two laboratories followed the method described in Waber (ed.) (2020) but see discussion of slight differences in Section 3.4.

Additionally, data produced by RWI of the wet extracted solutions were used to model the mineral saturation states and the partial pressure of CO_2. These parameters were calculated with the PHREEQC Version 3 code (Parkhurst & Appelo 2013) and the PSI/Nagra thermodynamic database (Thoenen et al. 2014) assuming a temperature of 25 °C.

Tab. 4.4-1 Summary of analytical work performed on samples for aqueous extraction tests from the different geological formations (excluding duplicate and post-mortem extracts of AD and SQ experiments; *cf.* Sections 4.7.4 and 4.6.5)

Sample type: PW: porewater sample, AD: Advective displacement sample, SQ: Sqeezing sample, AqEx: aqueous extraction tests, S/L: solid to liquid ratio.

Group	**Formation**	**Sample type**	**Laboratory**	**AqEx at S/L ~ 1 (pH, Alkalinity, Cations, Anions)**
Malm	Wildegg Fm.	PW	BRGM, RWI	2
Malm	Ifenthal Fm.	PW	BRGM	1
Dogger	Hauptrogenstein	PW	BRGM, RWI	14
Dogger	Passwang Fm.	PW, AD, SQ	BRGM, RWI	16
Dogger	Opalinus Clay	PW, AD, SQ	BRGM, RWI	26
Lias	Staffelegg Fm.	PW, AD, SQ	BRGM, RWI	8
Keuper	Klettgau Fm.	PW	BRGM, RWI	7
Keuper	Bänkerjoch Fm.	PW	RWI	2
Total		**PW, AD, SQ**	**BRGM, RWI**	**76**

4.4.2 Aqueous extraction tests at a *S*/*L* of ~1

Ion concentrations in aqueous extracts have a limited significance if they are not recalculated to porewater concentrations. For cations possibly involved in reactions (ion exchange/sorption, dissolution/precipitation), this is not a simple task. For conservative anions, ion concentrations in porewaters can be calculated based on the measured water content (leading to bulk porewater concentrations) or additionally corrected for anion exclusion (leading to concentrations in the anion-accessible porewater, here called 'free' porewater concentrations). For chemically conservative compounds, this recalculation is established in Chapter 5. Thus, in this section only ion ratios are presented, which are – for conservative anions – independent of the recalculation formalisms, as well as bulk porewater concentrations for Cl and Br.

4.4.2.1 Anions

The Cl concentrations in the aqueous extracts range from 3.3 to 54.7 mg/L or 0.09 and 1.53 mmol/L and reach maximum values in the Staffelegg Formation and Hauptrogenstein. The Br concentrations vary from the limit of detection to 0.24 mg/L or 0.003 mmol/L in the Hauptrogenstein and include an outlier at 64 mg/L or 0.008 mmol/L.

All samples from the Wildegg to the Bänkerjoch Formation exhibit a molar Br/Cl ratio close to the seawater ratio, either slightly below or above with the exception of 4 samples from the Hauptrogenstein and one sample from the Wildegg Formation with ratios substantially above the seawater ratio (Fig. 4.4-1).

The depth profile of the Br/Cl ratio (Fig. 4.4-2) displays a trend with decreasing Br/Cl ratios from the Wildegg Formation to the base of the Opalinus Clay. There is good agreement between the wet extracted solution data from BRGM and RWI, however, most aqueous extracts from dry material have systematically lower ratios compared to neighbouring wet extracts due to lower Br concentrations. This suggests that Br is not behaving conservatively after drying and that some Br is retained during subsequent extraction (e.g. binding with solid organic matter). The Br/Cl ratios increase from the top of the Staffelegg Formation and reach similarly high values as in the Hauptrogenstein in the middle of the Klettgau Formation. Subsequently the ratios drop to lower values at the top of the Bänkerjoch Formation, where the profile ends. While scatter in the data is small in the Staffelegg Formation and the Opalinus Clay, it is notable in the Passwang Formation and the Hauptrogenstein. This increase in scatter was observed in the BOZ1-1 borehole but is presently not understood.

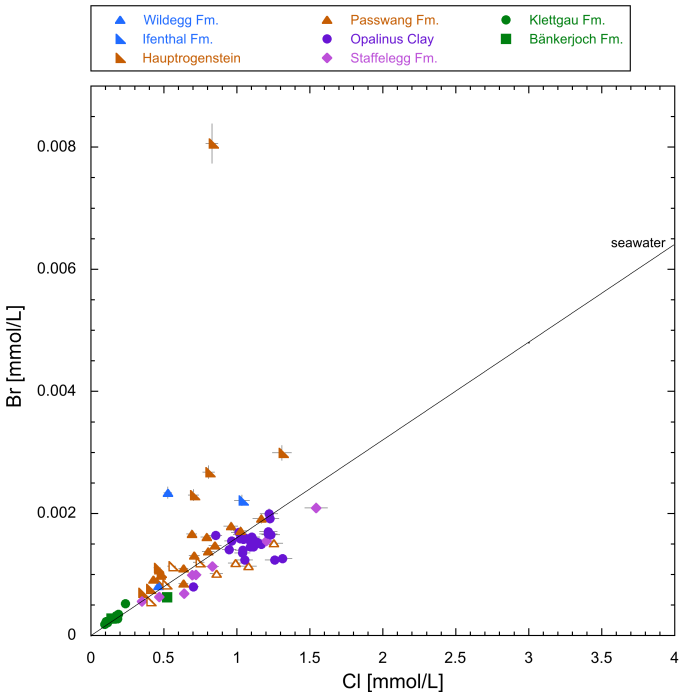

Fig. 4.4-1: Molar Br versus Cl concentrations in aqueous extracts at a S/L ratio of about 1
Open symbols mark dry aqueous extracts.

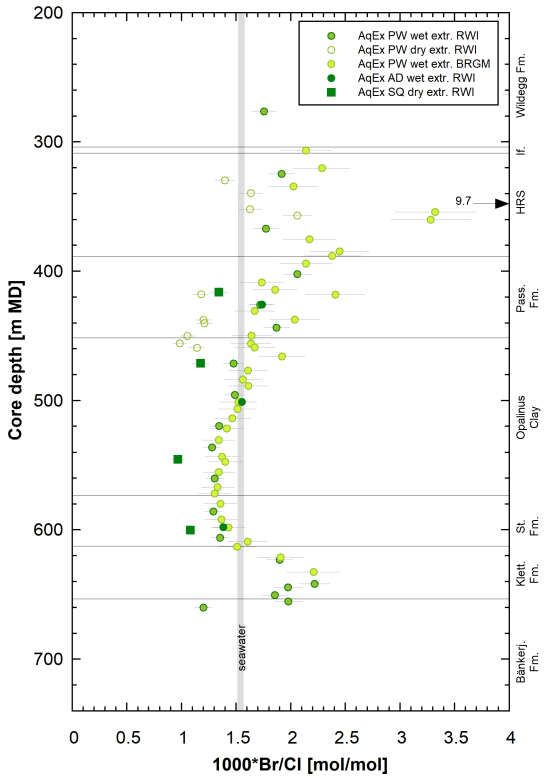

Fig. 4.4-2: Depth profile of the molar Br/Cl ratio in aqueous extracts at a S/L ratio of about 1

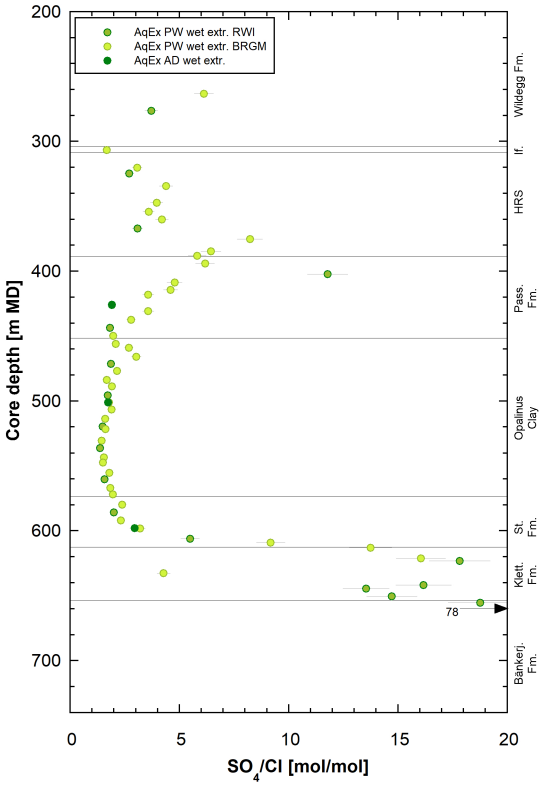

Fig. 4.4-3: Depth profile of SO_4/Cl molar concentration ratio in aqueous extracts at a S/L ratio of about 1

The SO_4 concentration varies between 97 and 539 mg/L with the exception of an anhydrite-bearing sample in the Bänkerjoch Formation where a concentration of 3'891 mg/L is reached. The depth profile of the SO_4/Cl ratio in aqueous extract solutions (Fig. 4.4-3) presents a continuous decrease from the Wildegg Formation to the bottom of the Opalinus Clay with the exception of a positive excursion at the boundary between the Hauptrogenstein and the Passwang Formation. From the lower part of the Opalinus Clay the ratio increases until reaching maximum values in the Bänkerjoch Formation. The data from the two different laboratories fit well together.

The F concentrations in aqueous extracts range between 1.6 and 5.6 mg/L across the whole depth profile (not shown) with the highest values being in the Hauptrogenstein and the Passwang Formation. The NO_3 concentrations are between 0.2 and 10 mg/L with maximum values reached in the lower part of the Passwang Formation and the top part of the Opalinus Clay. The alkalinity varies between 0.7 and 5.1 meq/L. The pH (not shown) is fairly constant from the Passwang to the Staffelegg Formation but presents more scatter and lower values above the Passwang Formation and in the Hauptrogenstein, Klettgau and Bänkerjoch Formations. The values range from 7.6 up to 10.1.

4.4.2.2 Cations

The Na concentrations in the aqueous extracts vary between 69 and 1'038 mg/L with maximum values reached in the Bänkerjoch Formation. The Na/Cl ratios (Fig. 4.4-4) show little variability throughout the Malm and Dogger section of the depth profile beside some scatter in the Hauptrogenstein. Subsequently, the ratios increase in the Staffelegg Formation until reaching a maximum in the Klettgau and Bänkerjoch Formation.

The K concentrations range from 1.8 mg/L up to 30.3 mg/L in the Bänkerjoch Formation. The Na/K ratios (Fig. 4.4-5) present a scattered depth profile with the highest ratios in the Opalinus Clay and lower ratios above and below. The BRGM and AD data plot systematically to the left of adjacent PW data from RWI, due to slightly higher K concentrations. The excess of K is likely related to a small contamination by the drilling fluid. In AD samples the contamination could arise from dry cutting the samples in contrast to the PW samples which are disintegrated solely by hammering. However, the extent of contamination is not large enough to affect any other ion concentrations.

The Sr concentrations range from the limit of detection to 27.9 mg/L with maximum values reached in the Hauptrogenstein. The Sr/Cl ratios (Fig. 4.4-6) plot in a narrow range throughout the Malm, Dogger and Lias sections with some outliers in the Hauptrogenstein and the Passwang Formation. In the Klettgau Formation, the Sr/Cl ratios increase up to a maximum in the Bänkerjoch Formation. This can be explained by the release of Sr from the dissolution of anhydrite or celestite during aqueous extraction. Celestite was detected in the anhydrite-bearing sample in the Bänkerjoch Formation and in one of the samples from the Hauptrogenstein with a high Sr/Cl ratio.

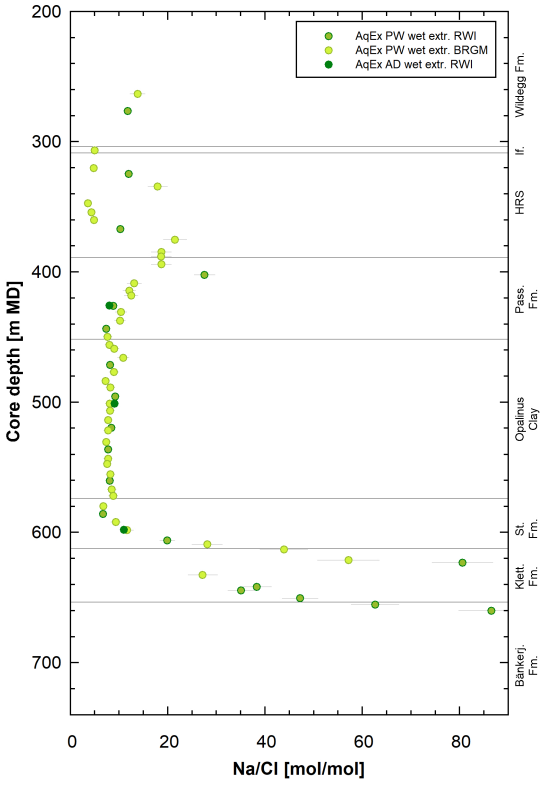

Fig. 4.4-4: Depth profile of the Na/Cl molar concentration ratio in aqueous extracts at a S/L ratio of about 1

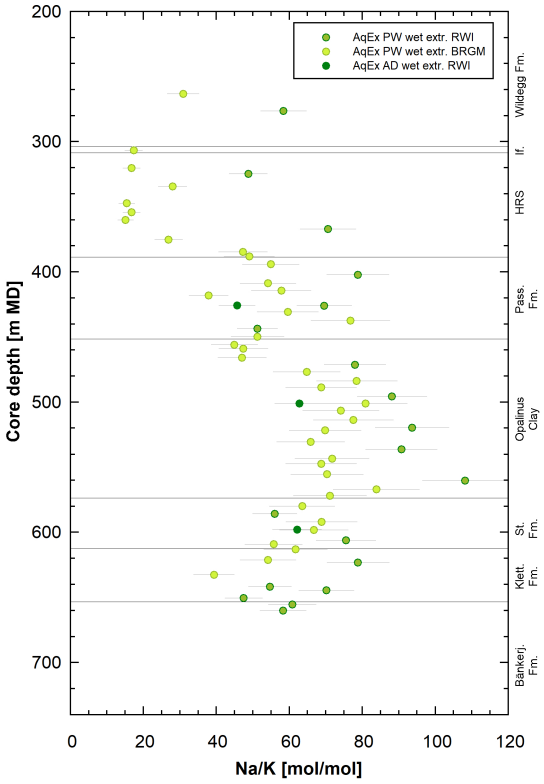

Fig. 4.4-5: Depth profile of the Na/K molar concentration ratio in aqueous extracts at a S/L ratio of about 1

Note that aqueous extracts of AD samples from RWI and PW samples from BRGM show lower Na/K ratios compared to those of neighbouring PW samples from RWI due to higher K concentrations. This could be related to a minor contamination by the K-silicate drilling fluid.

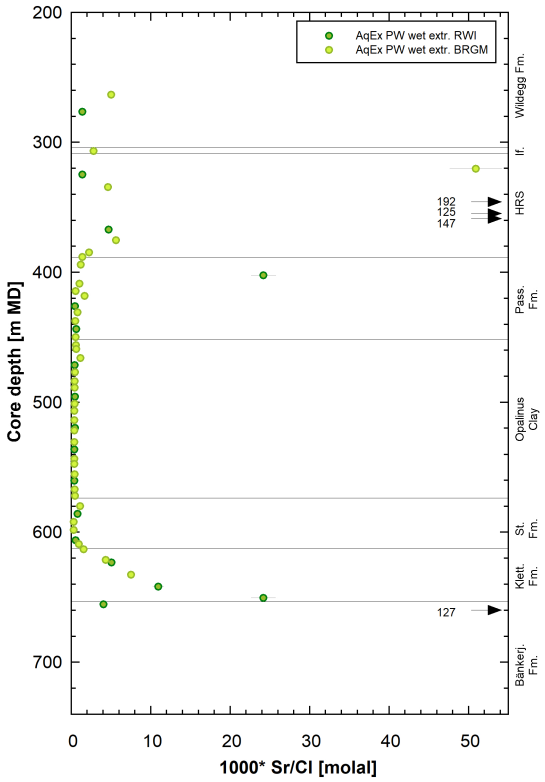

Fig. 4.4-6: Depth profile of the Sr/Cl molar concentration ratio in aqueous extracts at a S/L ratio of about 1

4.4.2.3 Saturation indices

The data produced by RWI of the wet extracted solutions were used to model the mineral saturation states and the partial pressure of CO_2 (alkalinity measurements are missing in the BRGM dataset). Most aqueous extract solutions from the Malm and Dogger are saturated or close to saturation with respect to calcite, but mostly undersaturated with respect to dolomite (disordered and ordered) (Tab. 4.4-2). The saturation indices for calcite vary in the Staffelegg, Klettgau and Bänkerjoch Formations from –1.95 to 0.9, with distinct over- and undersaturation reached in many samples from all these formations. Calcite oversaturation is expected for anhydrite-bearing samples where dissolution of Ca-sulphate is producing excess Ca that cannot be precipitated as calcite sufficiently fast. The considerably undersaturated sample with respect to calcite does not contain detectable amounts of calcite (641 m depth, Klettgau Formation). The samples at 598 and 660 m depth contain 10 and 2 wt.-% calcite, respectively, despite showing an undersaturation of –0.2. This might be caused by partial calcite dissolution during the aqueous extraction leading to a P_{CO2} level below atmospheric concentrations and a subsequent decrease in pH due to CO_2 equilibration during filtration and titration.

The sulphate minerals gypsum, anhydrite and celestite are undersaturated by 1 to 3 orders of magnitude in all extract solutions with the exception of one sample from the Bänkerjoch Formation. This exceptional sample contains 20 wt.-% anhydrite and 1 wt.-% celestite and is saturated with respect to gypsum and celestite and not far from saturation with respect to anhydrite. Saturation indices are missing for the sample at 644.57 m depth because the Ca concentration is below the detection limit.

Tab. 4.4-2 Saturation indices for calcite, dolomite (disordered and ordered), gypsum, anhydrite and celestite at a S/L ~ 1, pH and partial pressure of CO_2

Mineral saturation indices were calculated with the PHREEQC Version 3 code (Parkhurst & Appelo 2013) and the PSI/Nagra thermodynamic database (Thoenen et al. 2014) assuming a temperature of 25° C. Fm. stands for Formation, Wil for Wildegg Formation, HRS for Hauptrogenstein, Pas for Passwang Formation, Opa for Opalinus Clay, Sta for Staffelegg Formation, Kl for Klettgau Formation, Bä for Bänkerjoch Formation, S/L for solid/liquid, Cc for Calcite, Do for Dolomite (ordered or disordered), Gy for gypsum, An for Anhydrite and Ce for Celestite.

Fm.	**Depth** [m]	**S/L**	**SI Cc**	**SI Do (dis)**	**SI Do (ord)**	**SI Gy**	**SI An**	**SI Ce**	**pH**	**$\log_{10} P_{CO2}$** [bar]
Wil	276.33	0.94	0.06	-0.47	0.08	-2.73	-2.96	-2.45	9.11	-4.11
HRS	324.68	0.94	0.22	-0.27	0.28	-3.02	-3.24	-2.67	9.32	-4.28
HRS	366.91	0.95	0.04	-0.69	-0.14	-2.81	-3.03	-1.95	9.15	-4.20
Pas	402.15	0.91	0.02	-0.66	-0.11	-2.10	-2.33	-0.89	8.79	-3.72
Pas	425.69	0.92	0.18	-0.50	0.05	-2.98	-3.20		9.30	-4.16
Pas	425.92	0.89	0.16	-0.46	0.09	-3.10	-3.33	-2.75	9.33	-4.15
Pas	443.71	0.92	0.14	-0.53	0.02	-2.96	-3.18	-2.50	9.29	-4.17
Opa	471.37	0.90	-0.03	-0.92	-0.37	-2.86	-3.09	-2.58	8.87	-3.56
Opa	495.66	0.93	0.02	-0.82	-0.27	-2.98	-3.20	-2.68	8.87	-3.48
Opa	500.93	0.91	-0.03	-0.91	-0.36	-2.88	-3.10		8.67	-3.19
Opa	519.74	0.90	-0.02	-0.85	-0.30	-3.05	-3.27	-2.69	8.85	-3.43
Opa	536.30	0.90	0.08	-0.67	-0.12	-3.02	-3.24	-2.68	8.95	-3.55
Opa	560.29	0.90	0.06	-0.71	-0.16	-2.99	-3.21	-2.67	8.97	-3.60
Sta	585.84	0.93	0.05	-0.78	-0.23	-2.71	-2.94	-2.19	9.11	-4.02
Sta	597.93	0.96	-0.16	-1.19	-0.64	-2.91	-3.13		8.89	-3.65
Sta	606.13	0.90	0.20	-0.41	0.14	-2.78	-3.01	-2.78	9.15	-3.87
Kl	623.21	0.90	0.42	0.00	0.55	-2.69	-2.91	-2.51	9.05	-3.65
Kl	641.88	0.92	-1.95	-4.62	-4.07	-3.09	-3.32	-2.15	7.84	-3.21
Kl	644.57	0.89							8.20	-3.60
Kl	650.40	0.93	0.89	1.07	1.62	-2.37	-2.59	-1.52	9.69	-4.64
Bä	655.49	0.93	0.35	-0.03	0.52	-2.44	-2.67	-2.40	8.95	-3.65
Bä	659.95	0.92	-0.17	-1.33	-0.78	0.02	-0.20	0.12	7.62	-3.12

4.4.3 Chloride and bromide concentrations in bulk porewater

The formalisms to recalculate Cl and Br concentrations in aqueous extracts to concentrations in bulk porewater are given in Waber (ed.) (2020). In clay-free rocks, this recalculation to bulk water content delivers the transport relevant porewater concentrations of Cl and Br directly. In clay-bearing rocks, the anion-exclusion effect has to be considered as well in order to result in 'free' porewater concentrations. The derivation of the Cl and Br accessible porosity proportion and calculation of 'free' porewater concentrations is established in Chapter 5.

The recalculation of Cl and Br concentrations in aqueous extracts to concentrations in bulk porewater (Figs. 4.4-7 and 4.4-8) requires the knowledge of the water content of the rocks, which is obtained by calculating the average of three gravimetric water contents (one regular sample and two subsamples used for diffusive-exchange experiments) for the extracts prepared from wet samples. Additional aqueous extraction tests were carried out on 14 selected dried regular water content subsamples from Dogger to Lias in order to reduce the uncertainty regarding the variability of the water contents.

The depth profiles of Cl and Br concentrations in bulk porewater cover a large range of 55 to 1'885 mg/L and 0.2 to 18 mg/L, respectively (Figs. 4.4-7 and 4.4-8). In the Br profile, the samples analysed by RWI show lower concentrations in the dry extracts (RWI SQ & PW) compared to the wet extracts (RWI PW and AD). No such difference between dry and wet extracts is seen in the Cl data obtained by RWI. The differences for Br may be related to drying process (e.g., attachment to organic matter), but this is not proven at the moment. The data from the two different labs (RWI, BRGM) are similar with two exceptions: the HRS samples from BRGM scatter and diverge to higher values compared to the trend set out by RWI, and the RWI samples especially in the Opalinus Clay tend to plot to the left of the BRGM samples. This latter difference disappears when calculating the bulk porewater concentrations of the wet extracts based on the pycnometer porosity instead of the water-loss porosity for both datasets, as shown in the right plot of Figs. 4.4-7 and 4.4-8. This implies that there is potentially a systematic difference in the measured water contents between RWI and BRGM, but not in the pycnometer porosity, and that the latter are thus possibly more appropriate to calculate concentrations per bulk porewater. As for the dry extracts the water contents were previously determined on the very same sample and so should be appropriate, it was not considered as meaningful to swith to the pycnometer porosity for these samples.

Both, the Cl and Br concentrations, show considerable scatter in the Hauptrogenstein as mentioned above with slight increasing trends in the Hauptrogenstein and Passwang Formation (but a tendency of a break between the two formations). There is a general decreasing trend from the Opalinus Clay down to the bottom of the Klettgau Formation (Figs. 4.4-7 and 4.4-8), reaching minimum values there. The trend is, however, not continuous, with two samples at the top of the Staffelegg Formation exceeding the values of the overlying Opalinus Clay. The Cl and Br profiles with the saturation correction for all samples (i.e., based on pycnometer porosity instead of water-loss porosity) show generally a smoother profile especially in the Opalinus Clay.

At this stage, these observed trends should be treated with care because the recalculated Cl and Br concentrations still need to be corrected for anion accessibility, which is further investigated in Chapter 5.

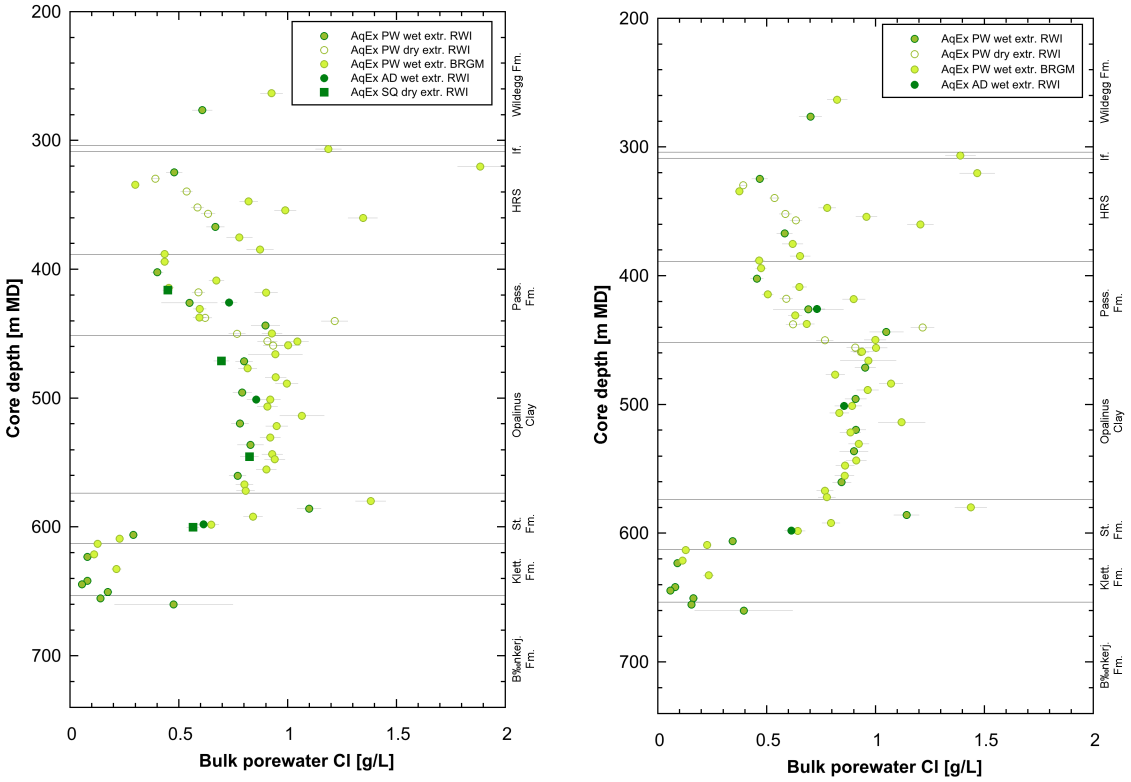

Fig. 4.4-7: Bulk porewater Cl concentrations versus depth from aqueous extracts of PW, AD and SQ samples

Right: RWI PW and AD and BRGM porewater volume is calculated with the pycnometer porosity for the wet extracts instead of the water-loss porosity (no pycnometer porosity is available for the SQ samples).

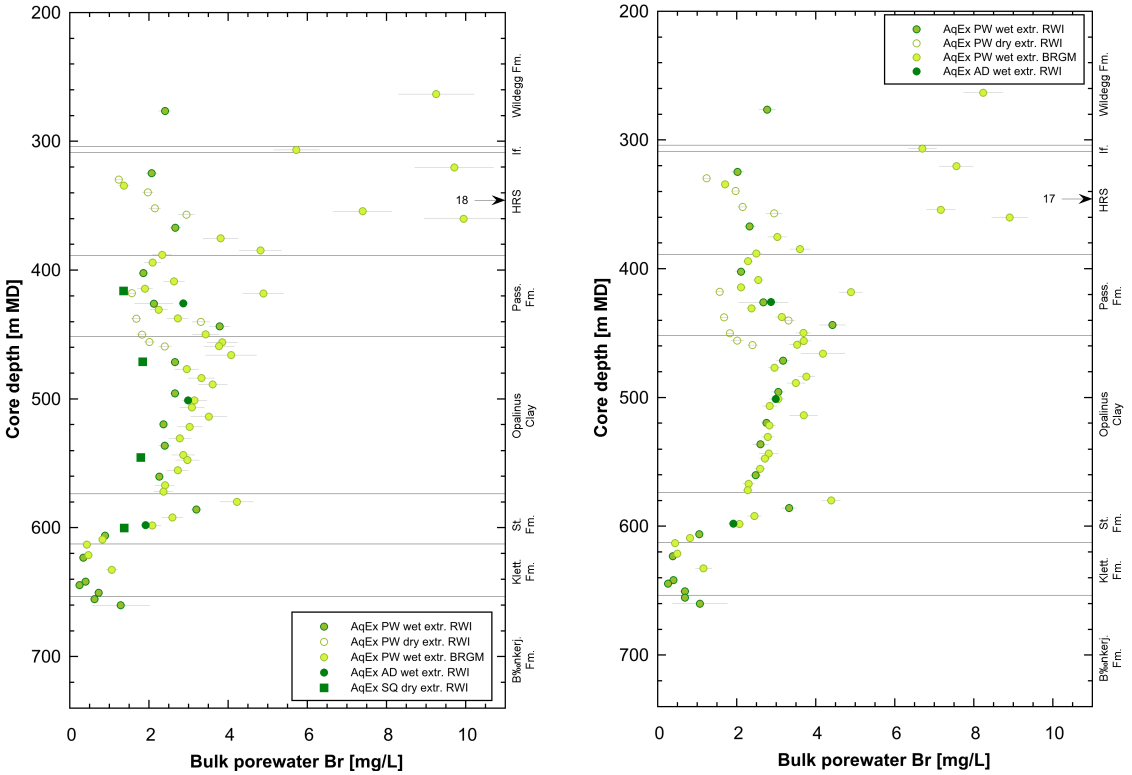

Fig. 4.4-8 Bulk porewater Br concentrations versus depth from aqueous extracts of PW, AD and SQ samples

Right: RWI PW and AD and BRGM porewater volume is calculated with the pycnometer porosity for the wet extracts instead of the water-loss porosity (no pycnometer porosity is available for the SQ samples).

4.5 Cation-exchange extraction data

Paul Wersin

Three samples used for advective displacement experiments (AD samples) were analysed at the University of Bern with the nickel triethylenediamine (Ni-en) extraction method to determine the cation exchange capacity (CEC) and the composition of the clay exchanger (for methodology see Waber (ed.) 2020). Material from end pieces above and below the AD core was mixed to obtain a representative sample for Ni-en extraction. A larger number of samples were studied by the team at PSI using the CsCl extraction method (see Section 5.6 and Marques Fernandes & Baeyens *in prep.*). The objective of the Ni-en extraction study was (i) to help to analyse the AD data (Section 4.7) and (ii) to compare and verify the PSI study with an alternative method.

The CEC can be derived in two ways: (1) From the consumption of the index cation (Ni in this case) during extraction and (2) from the sum of extracted cations (ΣCAT). Note that the latter includes (i) the exchangeable cations, (ii) cations dissolved in the porewater and (iii) cations released from potentially dissolving minerals (e.g. carbonates, sulphates) during extraction. Thus, in principle, the CEC derived from the sum of cations requires correction from contributions of (ii) and (iii). Corrected CEC and exchangeable cation data are discussed in Section 5.6, where the data from University of Bern is also compared with that of PSI. The analysis does not include ammonium, NH_4^+, known to be present in small but usually measurable amounts (e.g. < 1 – 2.4 mg/L in aqueous extracts, at $S/L \approx 1$).

Tab. 4.5-1 shows the Ni consumption and extracted cation data (Na, K, Ca, Mg, Sr, Ba) for solid/liquid ratios (S/L) around 1[6]. Anion data (F, Cl, Br, SO_4, NO_3) is depicted in Tab. 4.5-2. Note that Ni nitrate was added to the samples, which explains the high NO_3 contents.

Tab. 4.5-1: Cation data from Ni-en extracts at a S/L ratio around 1 (University of Bern data)
Fe content: < 0.001 mg/kg

Type	Depth	Formation	S/L	Na	K	Ca	Mg	Sr	Ba	ΣCAT	Ni cons.
	[m]		[g/g]	[meq/kg]							
AD	425.69	Passwang Fm.	0.872	32.2	4.5	30.5	17.4	1.0	0.003	85.5	95.2
AD	500.93	Opalinus Clay	0.858	40.0	4.6	30.7	15.6	1.0	0.010	92.0	94.8
AD	597.93	Staffelegg Fm.	0.892	37.4	4.8	33.0	14.6	0.5	0.005	90.3	97.9

Tab. 4.5-2: Anion data from Ni-en extracts at a S/L ratio around 1 (University of Bern data)

Type	Depth	Formation	S/L	F	Cl	Br	NO_3 [a]	SO_4
	[m]		[g/g]	[meq/kg]				
AD	425.69	Passwang Fm.	0.872	< 0.01	0.8	< 0.002	222.0	2.4
AD	500.93	Opalinus Clay	0.858	< 0.01	1.0	< 0.002	229.8	2.3
AD	597.93	Staffelegg Fm.	0.892	< 0.01	0.8	< 0.002	247.5	3.2

[a] Nitrate is part of the added Ni-en stock solution

The CEC derived from Ni consumption of the three AD samples lies in a narrow the range of 95 – 98 meq/kg_{rock} and is similar to the uncorrected sum of cations (86 – 92 meq/kg_{rock}). The depth profiles of Ni consumption and ΣCAT data indicate no trend (Fig. 4.5-1). No trend with clay-mineral content for the three samples, which vary between 35 and 52 wt.-%, is indicated either (Fig. 4.5-2).

Na and Ca are the main extracted cations, followed by Mg and K (Tab. 4.5-1). The molar Ca/Na ratio is about 0.8 for the OPA sample, the overlying and underlying samples in the Passwang Formation and Staffelegg Formation, respectively, display slightly higher ratios (Fig. 4.5-3). Mg correlates with Ca, thus the same trend is noted for the (Ca+Mg)/Na ratios (Fig. 4.5-3).

Speciation calculations on the Ni-en extracts were carried out with the PHREEQC Version 3 code (Parkhurst & Appelo 2013) and the PSI/Nagra thermodynamic database (Thoenen et al. 2014) assuming a temperature of 25 °C. The ethylene diamine complexes were taken from the MINTEC database (Allison et al. 1991) and included in the calculations. The concentration of ethylene diamine in the extracts, which was not analysed, was constrained by charge balance. The dissolved carbonate concentration (not measured) was constrained by assuming calcite equilibrium. The calculated TIC values are low, in the range of 0.12 – 0.15 mM (Tab. 4.5-3). The calculated partial pressures of CO_2 (P_{CO2}) and saturation indices for selected minerals are depicted in Tab. 4.5-3. The Ni-en extracts are clearly undersaturated with regard to the carbonate minerals dolomite and strontianite. They are also undersaturated with regard to the sulphate minerals gypsum and celestite, but either close to saturation or oversaturated with regard to barite.

[6] A water mass equal to the mass of the wet rock was added, leading to S/L (mass of dry rock /[mass of added water + porewater]) slightly below 1.

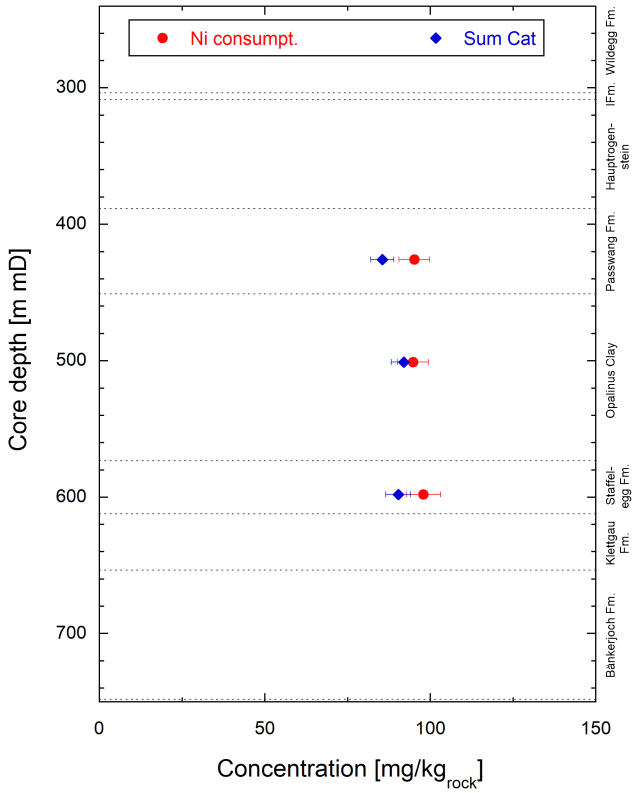

Fig. 4.5-1: Depth profile of Ni consumption and sum of cations (uncorrected, University of Bern data)

Errors reflect propagated analytical uncertainties.

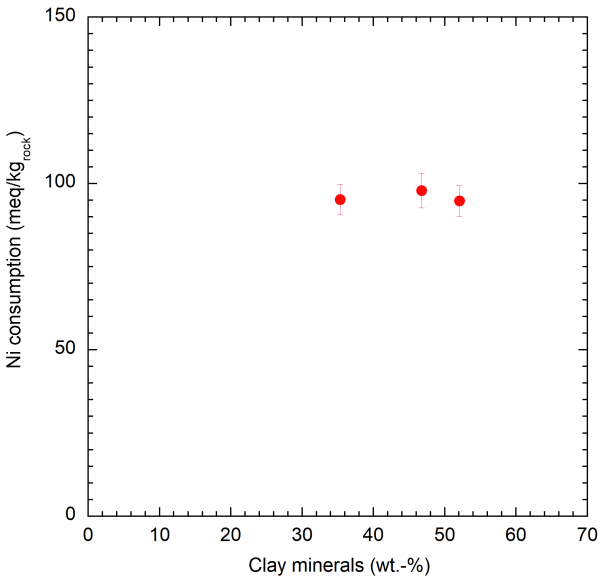

Fig. 4.5-2: Ni consumption vs. clay-mineral content (University of Bern data)

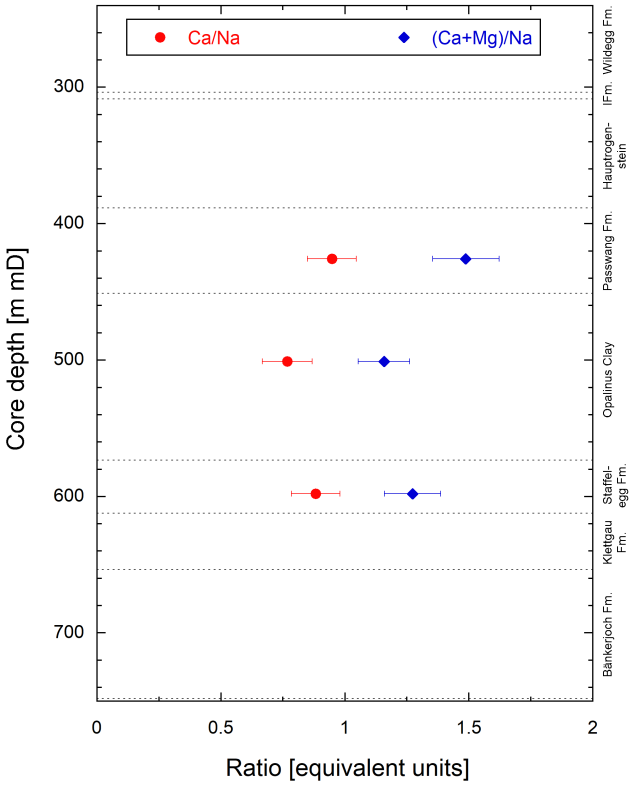

Fig. 4.5-3: Depth profiles of Ca/Na and (Ca+Mg)/Na ratios in Ni-en extracts (University of Bern data)

Errors reflect propagated analytical uncertainties.

Tab. 4.5-3: Calculated saturation indices of selected minerals, TIC log (P_{CO2}) for Ni-en extract solutions

Calcite saturation was assumed in the calculations.

Type	Depth [m]	Formation	Log (P_{CO2}) [bar]	TIC [mol/kg_w]	Gypsum	Celestite	Barite	Dolomite (ord)	Dolomite (dis)	Strontianite
AD	425.69	Passwang Fm.	-4.67	0.120	-1.44	-0.89	-0.05	-0.12	-0.67	-0.72
AD	500.93	Opalinus Clay	-4.47	0.151	-1.48	-0.93	0.42	-0.16	-0.71	-0.72
AD	597.93	Staffelegg Fm.	-4.50	0.144	-1.35	-1.12	0.19	-0.23	-0.78	-1.04

4.6 Data from squeezing experiments

Martin Mazurek

A small set of 4 samples from the interval Passwang-Formation – Staffelegg Formation were subjected to porewater squeezing. Photographs of the core samples are shown in Fig. 4.6-1. The mineralogical composition of the samples is listed in Tab. 4.6-1. Clay mineral contents are ≥ 39 wt.-% for all samples.

Tab. 4.6-1: Mineralogical composition of samples subjected to squeezing experiments

Empty field = mineral not identified.

Depth [m]	**Formation**	**Member**	**S** [wt.-%]	**C(inorg)** [wt.-%]	**C(org)** [wt.-%]	**Quartz** [wt.-%]	**K-feldspar** [wt.-%]	**Plagioclase** [wt.-%]	**Calcite** [wt.-%]	**Dolomite / Ankerite** [wt.-%]	**Siderite** [wt.-%]	**Magnesite** [wt.-%]	**Anhydrite** [wt.-%]	**Pyrite** [wt.-%]	**Clay minerals** [wt.-%]
416.08	Passwang Fm.	Rothenfluh Mb.	0.81	3.43	0.93	23	4	3	29					1.5	39
471.15	Opalinus Clay	'Sub-unit with silty calcareous beds'	0.66	1.01	1.22	23	2	3	8					1.2	62
545.41	Opalinus Clay	'Mixed clay-silt-carbonate sub-unit'	0.13	0.94	0.96	36	3	2	5	2				0.2	50
600.09	Staffelegg Fm.	Frick Mb.	1.68	0.7	0.92	16	1	1	6					3.1	72

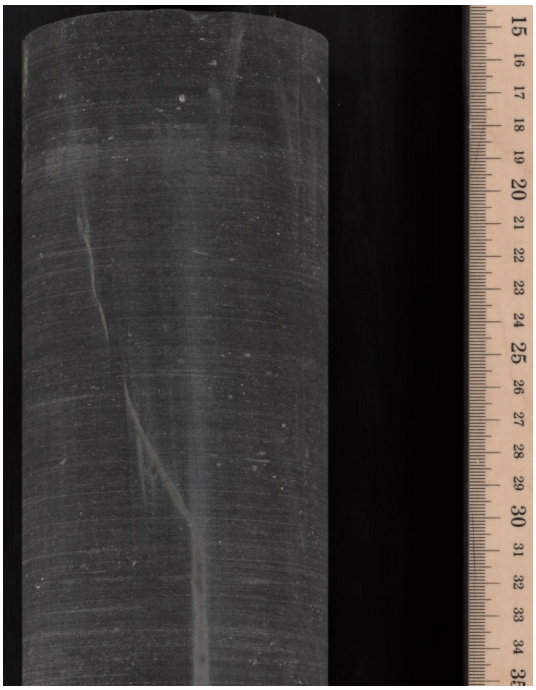

BOZ2 416.08

BOZ2 471.15

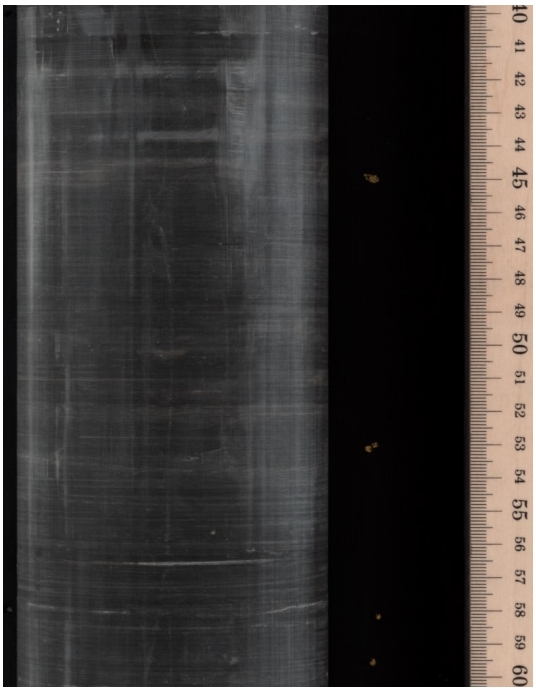

BOZ2 545.41

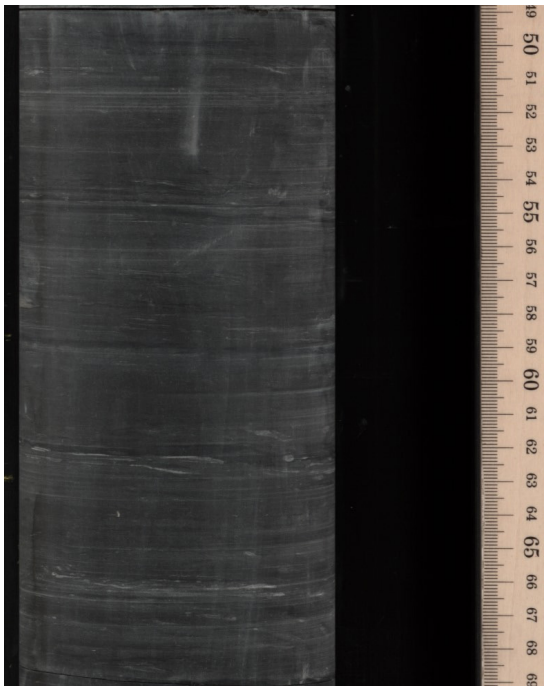

BOZ2 600.09

Fig. 4.6-1: Photographs of core samples subjected to squeezing

4.6.1 Mass recovery

The water masses obtained by squeezing are listed in Tab. 4.6-2 and shown graphically in Fig. 4.6-2 as a function of the squeezing pressure. Given the small number of samples, a correlation between the initial water content of the sample and the the total mass recovery, as observed in other squeezing campaigns, is not well established (Fig. 4.6-3). Samples yielded first water aliquots at 200 MPa, except for the sample from the Staffelegg Formation where 300 MPa were required to extract the first waters.

Given the fact that for 3 samples, a sufficient water mass was obtained in the pressure range 200 – 300 MPa, the experiments were terminated at this pressure, i.e. no waters were squeezed at higher pressures. The sample from the Staffelegg Formation was squeezed until the maximum pressure of 500 MPa.

Tab. 4.6-2: Water masses squeezed at different pressure steps

The initial water content was measured at CRIEPI on cut-off materials adjacent to the squeezed core, and this value was used here to calculate the initial mass of porewater in the sample. -: pressure step not applied.

Depth [m]	**Formation**	**Initial sample mass (CRIEPI)** [g]	**Initial wet water content (CRIEPI)** [wt.-%]	**Mass of porewater prior to squeezing (CRIEPI)** [g]	**Mass squeezed at P =**						**Total mass squeezed** [g]
					100 MPa [g]	**150 MPa** [g]	**200 MPa** [g]	**300 MPa** [g]	**400 MPa** [g]	**500 MPa** [g]	
416.08	Passwang Formation	429.36	4.71	20.22	0	-	1.06	1.46	-	-	2.52
471.15	Opalinus Clay	358.95	4.49	16.12	0	-	0.96	1.69	-	-	2.65
545.41	Opalinus Clay	442.97	5.41	23.96	0	-	2.31	1.30	-	-	3.61
600.09	Staffelegg Formation	429.05	3.80	16.30	0	-	0	0.41	0.93	1.00	2.34

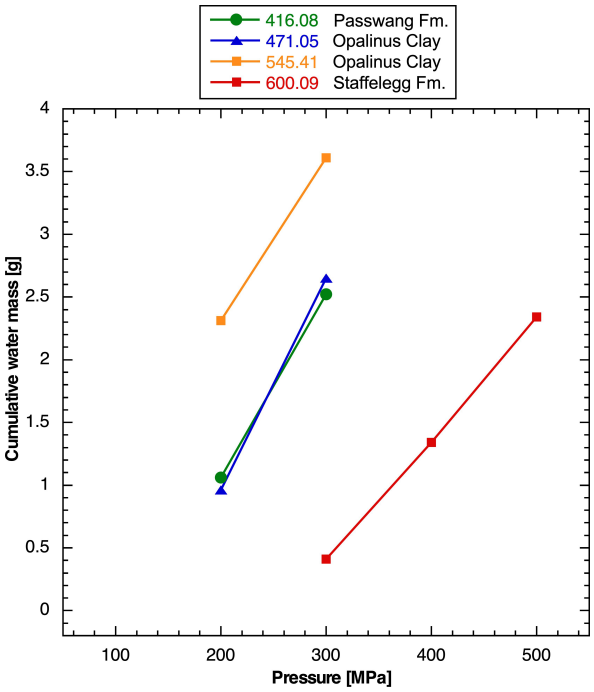

Fig. 4.6-2: Cumulative water masses obtained by squeezing as a function of the squeezing pressure

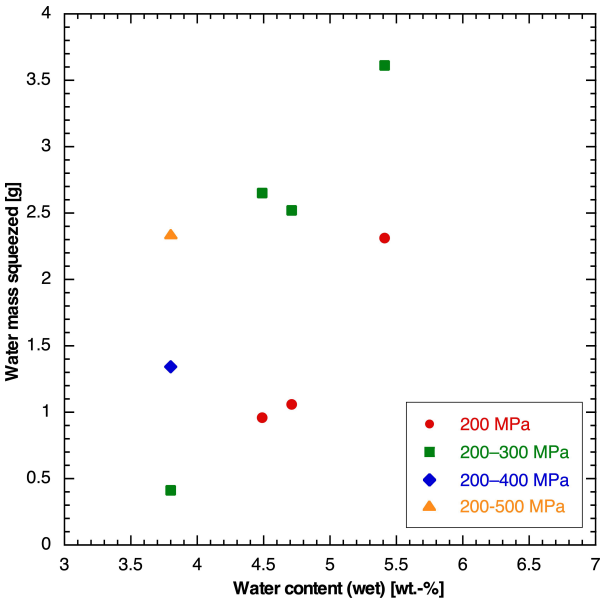

Fig. 4.6-3: Correlation of the original water content and the cumulative water mass obtained by squeeezing

4.6.2 Chemical composition of squeezed waters

The first squeezed aliquots yielded > 0.9 g water in 3 out of 4 cases, from which a complete dataset (major-ion composition, TIC/TOC, pH, water isotopes) could be obtained. For sample 600.09 from the Staffelegg Formation, which was difficult to squeeze, 0.4 g were obtained at the first pressure step at 300 MPa, resulting in a less complete dataset. However, sufficient water was squeezed at higher pressures.

The chemical compositions of squeezed waters are listed in Tab. 4.6-3 and shown graphically as a function of squeezing pressure in Fig. 4.6-4. Na is by far the most abundant cation. In the Dogger, SO_4 content is somewhat higher than Cl content (expressed in mass units), and this difference becomes even stronger in the Staffelegg Formation where Cl decreases but SO_4 increases.

The concentrations of monovalent ions Na, K, Cl and Br generally decrease with squeezing pressure, likely due to ion-filtration effects that become important at higher pressures (Mazurek et al. 2015). Ca and Mg remain near-constant with pressure or deviate slightly towards higher concentrations. As discussed in Mazurek et al. (2015) and Rufer & Mazurek (2018), the composition of the first water aliquot recovered from a sample is considered to be closest to that of the porewater, and these analyses are highlighted by bold print in Tab. 4.6-3. F concentrations, in particular in the first squeezed aliquots, are contaminated by F leached from the fiberglass filters and so are not representative of the porewater. For clarity, the subset of the data that is considered to be useful for further interpretation is summarised in Tab. 4.6-4.

Tab. 4.6-3: Chemical composition of squeezed waters: full dataset

Bold print indicates the selected ("best") aliquots. F concentrations, in particular in the first squeezed aliquots, are contaminated by F leached from the fiberglass filters and so are not representative of the porewater. n.a. = no analysis.

Depth [m]	**Formation**	**Pressure** [MPa]	**Squeezing time** [d]	**Mass squeezed** [g]	**Na** [mg/L]	**NH_4** [mg/L]	**K** [mg/L]	**Ca** [mg/L]	**Mg** [mg/L]	**Sr** [mg/L]	**F** [mg/L]	**Cl** [mg/L]	**Br** [mg/L]	**NO_3** [mg/L]	**SO_4** [mg/L]	**pH**	**TIC** [mg/L]	**TOC** [mg/L]	**TDS** [mg/L]	**Charge balance** [%]
416.08	Passwang Fm.	**200**	**3**	**1.06**	**1866**	**0.89**	**45.2**	**126**	**46**	**0.0**	**13.1**	**1341**	**3.8**	**12.62**	**2168**	**9.25**	**68.7**	**120.3**	**6092**	**1.5**
		300	2	1.46	1568	1.19	28.3	131	42	0.0	6.7	1036	3.4	7.02	2143	9.25	25.0	60.6	5155	1.6
471.15	Opalinus Clay	**200**	**3**	**0.96**	**2254**	**0.89**	**48.0**	**150**	**54**	**0.0**	**11.6**	**1790**	**5.4**	**11.47**	**2444**	**9.18**	**42.2**	**122.2**	**7106**	**2.5**
		300	3	1.69	1982	0.79	37.9	140	57	8.9	6.4	1490	4.5	4.85	2406	9.01	30.3	76.9	6369	2.0
545.41	Opalinus Clay	**200**	**4**	**2.31**	**2089**	**1.1**	**40.1**	**166**	**60**	**7.5**	**9.4**	**1678**	**4.2**	**6.61**	**2366**	**8.85**	**33.6**	**99.7**	**6698**	**2.6**
		300	2	1.30	1642	0.7	22.0	164	64	8.4	5.5	1322	3.5	7.25	2053	8.78	30.1	54.7	5500	1.6
600.09	Staffelegg Fm.	**300**	**3**	**0.41**	**2497**	**0.51**	**51.6**	**219**	**62**	**0.0**	**15.9**	**1315**	**2.5**	**8.18**	**3675**	**n.a.**	**n.a.**	**n.a.**	**7846**	**4.7**
		400	2	0.93	2281	1.09	33.7	292	73	8.0	6.0	1077	2.7	5.07	3935	8.94	25.5	49.8	7893	2.6
		500	2	1.00	2450	1.69	43.8	278	64	7.0	8.7	1204	2.8	5.78	4031	8.99	25.7	76.4	8303	2.6

Tab. 4.6-4: Chemical composition of squeezed waters: summary of selected analyses to be used for interpretation

n.a. = no analysis.

Depth [m]	**Formation**	**Pressure** [MPa]	**Squeezing time** [d]	**Mass squeezed** [g]	**Na** [mg/L]	**K** [mg/L]	**Ca** [mg/L]	**Mg** [mg/L]	**Sr** [mg/L]	**Cl** [mg/L]	**Br** [mg/L]	**NO_3** [mg/L]	**SO_4** [mg/L]	**pH**	**TIC** [mg/L]	**TOC** [mg/L]
416.08	Passwang Fm.	200	3	1.06	1866	45.2	126	46	0.0	1341	3.8	12.62	2'168	9.25	68.7	120.3
471.15	Opalinus Clay	200	3	0.96	2254	48.0	150	54	0.0	1790	5.4	11.47	2'444	9.18	42.2	122.2
545.41	Opalinus Clay	200	4	2.31	2089	40.1	166	60	7.5	1678	4.2	6.61	2'366	8.85	33.6	99.7
600.09	Staffelegg Fm.	300	3	0.41	2497	51.6	219	62	0.0	1315	2.5	8.18	3'675	n.a.	n.a.	n.a.

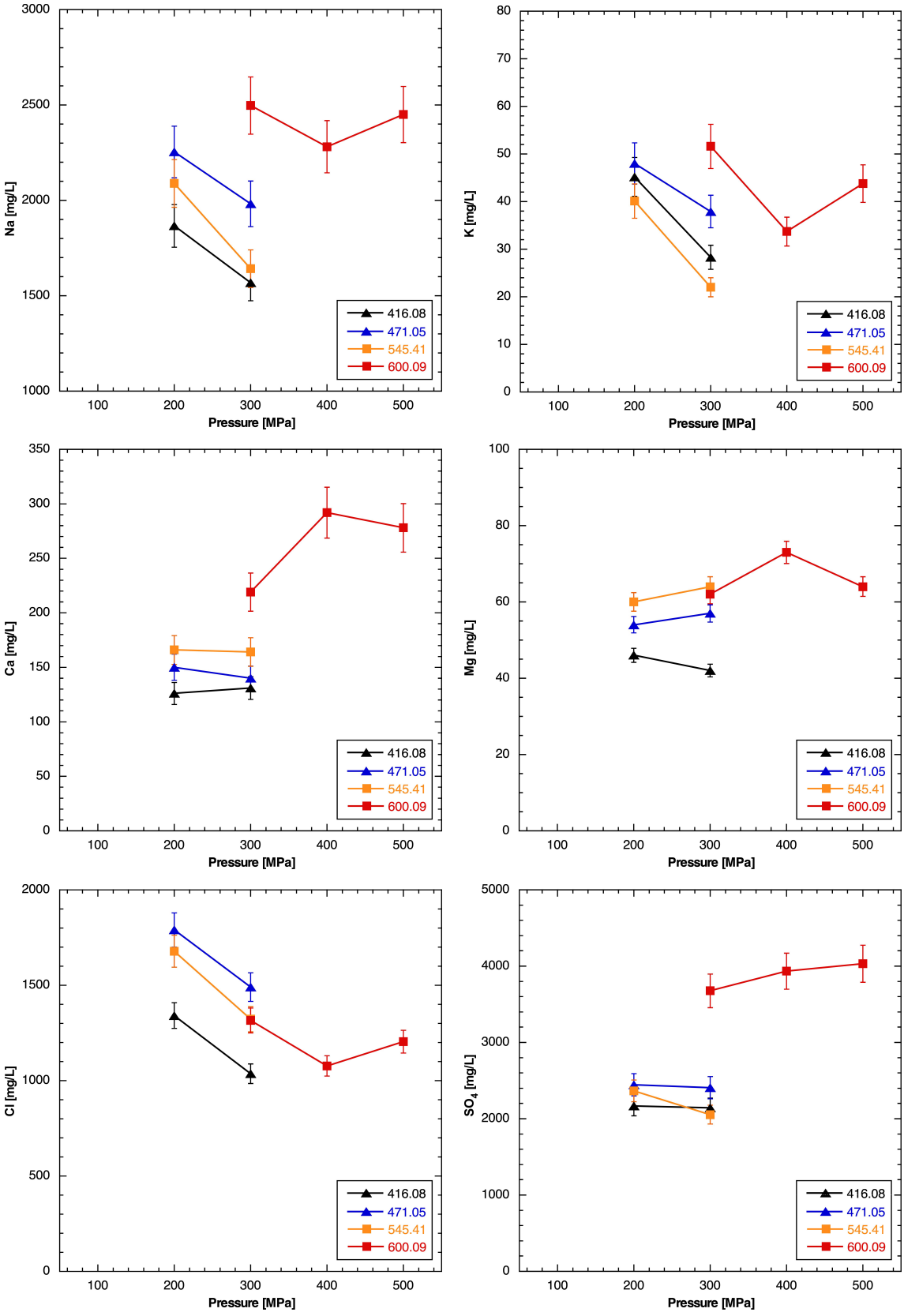

Fig. 4.6-4: Ion concentrations in squeezed waters as a function of squeezing pressure

Bars indicate analytical errors of ion-chromatography analysis.

4.6.3 Depth trends

Profiles with depth for various pore-water constituents are shown in Fig. 4.6-5. Given the fact that only 4 samples were studied, trends should preferably be studied in conjunction with data from other methods. Nevertheless, the following observations can be made:

- Na, Cl and SO_4 show limited variability with depth in the Dogger. In the Staffelegg Formation, the Na/Cl and SO_4/Cl ratios increase markedly, as does salinity.
- Ca and Mg contents increase with depth.
- The Br/Cl ratio is slightly below that of current seawater and further decreases with depth.
- The SO_4/Cl ratio is substantially higher than in seawater or in porewaters of boreholes from the Nördlich Lägern and Zürich Nordost areas.

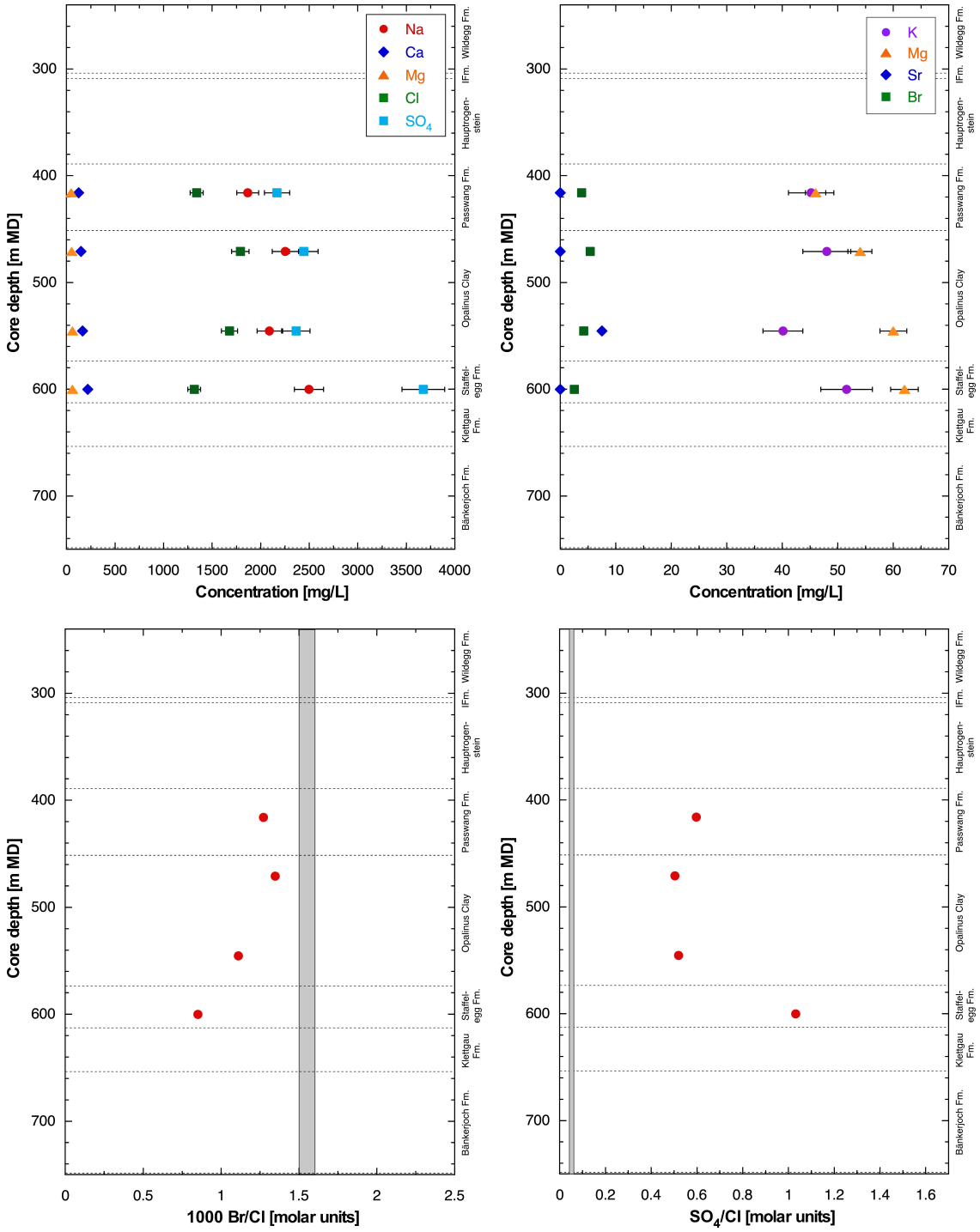

Fig. 4.6-5: Depth trends of ion concentrations and ion ratios in squeezed waters

Only the selected aliquots are shown for each sample. Bars indicate analytical errors of ion-chromatography analysis. Grey rectangles represent current seawater ratios. Zero entries for Sr refer to values below the quantification limit of around 10 mg/L.

4.6.4 Geochemical modelling and mineral saturation states

Mineral saturation indices for squeezed waters were calculated using PHREEQC V3 and the PSI/Nagra thermodynamic database at 25 °C (Thoenen et al. 2014) and are shown in Tab. 4.6-5.

- Squeezed waters are strongly oversaturated with respect to calcite, dolomite and magnesite, a feature already known from previous studies (e.g. Mazurek et al. 2015). The oversaturation is possibly due to the fact that mineral solubility at high pressures during squeezing is higher than at atmospheric pressure. Further, outgassing of CO_2 during the squeezing process increases the pH and the saturation indices of calcite and dolomite (Tournassat et al. 2015). Further outgassing my take place in the headspace of the sample vials during sample storage. The comparatively low calculated P_{CO2} suggest that some outgassing may have taken place, which also affects pH. However, this nevertheless does not markedly affect the obtained major-ion composition due to the large buffering capacity of the rock – water system in clay-rich lithologies. Last, lattice defects in carbonate minerals induced by deformation during squeezing might increase the solubility of these minerals. On the other hand, outgassing into the external atmosphere during sample storage in glass vessels is not considered to contribute to the low P_{CO2}. Such a process should also be seen by higher δ values of water isotopes, which is not the case (see Section 4.8), but this depends on the mode of water loss (via a gas phase, or via a liquid film). In Section 5.5.1 below, an attempt is made to restore the out-gassing by model calculations assuming equilibrium with calcite.
- A more limited oversaturation is seen for strontianite, together with a slight decrease of SI values with depth.
- The waters are close to saturation or slightly undersaturated with respect to celestite. They are undersaturated with respect to gypsum, but the degree of undersaturation becomes smaller with depth.
- Using the data from Tab. 4.6-3, squeezed waters are strongly oversaturated with respect to fluorite, which is a consequence of the contamination of F concentrations by the filter material. Therefore, no F data are listed in Tab. 4.6-4.

Tab. 4.6-5: Mineral saturation indices for squeezed waters

Bold print indicates the selected ("best") aliquots; n.a. = no analysis.

Depth [m]	Formation	Pressure [MPa]	pH	TIC [M]	Log (P_{CO2}) [bar]	SI Calcite	SI Aragonite	SI Dolomite (ordered)	SI Dolomite (disord.)	SI Strontianite	SI Magnesite	SI Gypsum	SI Anhydrite	SI Celestite	SI Fluorite
416.08	Passwang Fm.	**200**	**9.25**	**5.75E-03**	**-3.93**	**1.74**	**1.60**	**3.38**	**2.83**		**1.32**	**-0.75**	**-0.98**		**0.85**
		300	9.25	2.09E-03	-4.36	1.36	1.22	2.56	2.01		0.87	-0.69	-0.91		0.33
471.15	Opalinus Clay	**200**	**9.18**	**3.54E-03**	**-4.07**	**1.54**	**1.39**	**2.96**	**2.41**		**1.10**	**-0.65**	**-0.87**		**0.81**
		300	9.01	2.54E-03	-4.00	1.25	1.11	2.44	1.89	0.52	0.87	-0.66	-0.88	-0.13	0.28
545.41	Opalinus Clay	**200**	**8.85**	**2.82E-03**	**-3.78**	**1.23**	**1.09**	**2.35**	**1.80**	**0.35**	**0.80**	**-0.60**	**-0.82**	**-0.22**	**0.69**
		300	8.78	2.52E-03	-3.74	1.16	1.01	2.23	1.68	0.33	0.75	-0.61	-0.83	-0.18	0.26
600.09	Staffelegg Fm.	**300**	**n.a.**	**n.a.**							**0.55**	**-0.38**	**-0.60**		**1.19**
		400	8.94	2.14E-03	-4.02	1.34	1.20	2.40	1.85	0.24	0.73	-0.24	-0.46	-0.08	0.45
		500	8.99	2.16E-03	-4.08	1.36	1.21	2.39	1.84	0.22	0.71	-0.26	-0.48	-0.14	0.75

4.6.5 Water content and aqueous extraction of squeezed and adjacent unsqueezed core material

For the calculation of the Cl-accessible porosity fraction f_{Cl} (see below), the inventories of water and Cl in the rock prior to squeezing must be known. These data can be obtained by two alternative methods:

1. Measure the water content (by drying) and then the Cl content (by aqueous extraction) of the squeezed material (so-called POST data). From these data, the masses of water and Cl remaining in the sample after squeezing can be calculated. By adding the masses of squeezed water and Cl to these data, the respective contents prior to squeezing can be reconstructed.
2. Measure the water content (by drying) and Cl content (by aqueous extraction) of adjacent unsqueezed material some 10 cm away (so-called PRE data).

Both approaches have advantages and disadvantages:

- Method 1 has the advantage that all measurements are performed on the same material, so potential heterogeneity is not an issue. On the other hand, the reconstruction of the water and Cl inventories is less direct and assumes that the dead volume of the system is negligible (which is likely the case[7]). The results are listed in Tab. 4.6-6.
- Method 2 directly yields the desired data – no addition of two measurements is needed – but relies on the assumption that the measurement performed on adjacent material is also representative for the squeezed material itself. The assumption of homogeneity incurs some degree of uncertainty. Moreover, the material used for the PRE measurements (typically a 8 – 10 cm long piece of core) has been exposed to the atmosphere for a few minutes during sample preparation (dry sawing) prior to being re-sealed again. Results are shown in Tab. 4.6-7.

Tab. 4.6-6: Water contents and results of aqueous-extraction tests on previously squeezed samples (method 1, POST data).

Depth [m]	**Formation**	**Water content (wet) of squeezed sample** [wt.-%]	**Mass of porewater in squeezed sample** [g]	**Aqueous extraction of squeezed sample**				
				Mass of dry rock [g]	**Mass of added water** [g]	**S/L** [g/g]	**Cl** [mg/$L_{extract\ solution}$]	**Br** [mg/$L_{extract\ solution}$]
416.08	Passwang Fm.	4.18	17.83	30.21	29.90	1.010	14.8	0.050
471.15	Opalinus Clay	3.74	13.32	29.99	29.89	1.003	26.8	0.071
545.41	Opalinus Clay	4.29	18.84	29.98	29.88	1.003	27.9	0.061
600.09	Staffelegg Fm.	3.44	14.70	29.95	29.86	1.003	17.3	0.045

[7] A sensitivity calculation was performed on the impact of dead volume. Assuming a dead volume of 1 mL results is an anion-accessible porosity fraction that is 0.01 – 0.04 higher than the value without consideration of a dead volume. The most strongly expressed shift is found in samples where only a small water volume was squeezed, while it becomes insignificant for samples with a good water yield.

Tab. 4.6-7: Water contents and results of aqueous-extraction tests on material adjacent to squeezed samples (method 2, PRE data)

Depth [m]	**Formation**	**Water content (wet)** [wt.-%]	**Aqueous extraction of virgin material adjacent to squeezed sample**				
			Mass of dry rock [g]	**Mass of added water** [g]	**S/L** [g/g]	**Cl** [mg/L$_{extract\ solution}$]	**Br** [mg/L$_{extract\ solution}$]
416.08	Passwang Fm.	4.725	30.254	29.912	1.011	22.5	0.068
471.15	Opalinus Clay	5.038	30.298	29.893	1.014	37.4	0.099
545.41	Opalinus Clay	5.310	30.091	29.891	1.007	46.5	0.101
600.09	Staffelegg Fm.	3.869	29.726	29.865	0.995	22.6	0.055

4.6.6 Chloride-accessible porosity

The Cl-accessible porosity fraction f_{Cl} can be estimated from:

$$f_{Cl} = \frac{C_{Cl\ in\ bulk\ porewater}}{C_{Cl\ in\ squeezed\ water}}$$

$C_{Cl\ in\ squeezed\ water}$ is taken from Tab. 4.6-4, assuming that these data represent the concentrations in the anion-accessible pore space. $C_{Cl\ in\ bulk\ porewater}$ can be obtained using the two alternative methods described in Section 4.6.5. According to method 1, the masses of Cl and water obtained by squeezing and by drying/aqueous extraction of the squeezed material are added. The formalism is documented in more detail in Mazurek et al. (2021), and the results are listed in Tab. 4.6-8.

Alternatively, applying method 2, $C_{Cl\ in\ bulk\ porewater}$ can be obtained directly by drying/aqueous extraction of adjacent, unsqueezed rock according to:

$$C_{Cl\ in\ bulk\ porewater} = \frac{C_{Cl\ in\ extract\ solution}}{S/_L\ w_d}$$

using the data listed in Tab. 4.6-7 (w_d = water content relative to dry rock). The results are shown in Tab. 4.6-9.

The resulting Cl-accessible porosity fractions obtained by the two methods are also listed in Tabs. 4.6-8 and 4.6-9. They are shown as a function of the clay-mineral content in Fig. 4.6-6. For 3 of the 4 samples, results obtained by the two methods agree closely. A slight discrepancy is identified for the sample 471.15 from the 'Sub-unit with silty calcareous beds' of the Opalinus Clay. As seen in Fig. 4.6-1, this sample contains numerous silty lenses and beds, which contribute to an increased heterogeneity on the cm scale. Thus, the observed discrepancy is attributed to sample heterogeneity that affects f_{Cl} calculated using method 2. Overall, method 1 is considered to be the preferred way to calculate f_{Cl}, given the fact that all measurements refer to identical materials and so heterogeneity plays no role.

Values of f_{Cl} lie in the range 0.43 – 0.47, except for the sample from the Passwang Formation. In spite of its low clay-mineral content, this sample shows a remarkably low anion accessibility of 0.33. Note that a sample from the same stratigraphic level (Rothenfluh Member) in the BOZ1-1 core yielded a similarly low accessibility of 0.34 (Wersin et al. 2022). Also note that limestones from the Rothenfluh Member are outliers when it comes to pore-space architecture. As shown in Section 4.3.5 and in Fig. 4.3-17, the average pore radius is unusually small, consistent with a strong anion exclusion effect.

Tab. 4.6-8: Cl-accessible porosity fractions derived from squeezing and aqueous-extraction experiments using method 1 to obtain $C_{Cl\ in\ bulk\ porewater}$

Depth [m]	**Formation**	**Total mass of squeezed Cl** [mg]	**Mass of Cl in aq. extract of squeezed core** [mg]	**Porewater mass squeezed** [g]	**Water mass remaining in squeezed core** [g]	**Cl in bulk porewater** [mg/L]	**Cl-accessible porosity fraction f_{Cl}** [-]
416.08	Passwang Fm.	2.93	5.97	2.52	17.83	437	0.33
471.15	Opalinus Clay	4.24	9.15	2.65	13.32	838	0.47
545.41	Opalinus Clay	5.60	11.71	3.61	18.84	771	0.46
600.09	Staffelegg Fm.	2.74	7.09	2.34	14.70	577	0.44

Tab. 4.6-9: Cl-accessible porosity fractions derived from squeezing and aqueous-extraction experiments, using method 2 to obtain $C_{Cl\ in\ bulk\ porewater}$

Depth [m]	**Formation**	**Cl concentration in bulk porewater (in adjacent unsqueezed rock)** [mg/L]	**Cl-accessible porosity fraction f_{Cl}** [-]
416.08	Passwang Fm.	448	0.33
471.15	Opalinus Clay	696	0.39
545.41	Opalinus Clay	824	0.49
600.09	Staffelegg Fm.	564	0.43

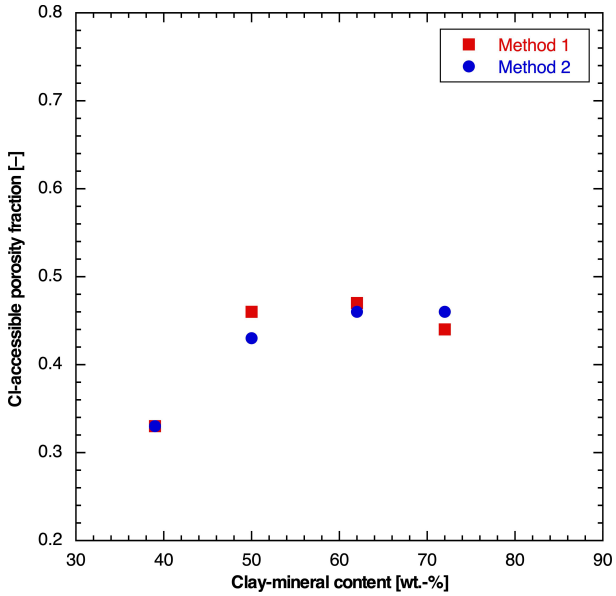

Fig. 4.6-6: Cl-accessible porosity fractions derived from squeezing experiments as a function of the clay-mineral content

See text for explanations regarding the two methods.

4.6.7 Stable isotopic composition of squeezed water

Results of stable water-isotope analyses are listed in Tab. 4.6-10 and shown as a function of depth in Fig. 4.6-7. The following observations can be made:

- Within any sample, the variation of the δ values with squeezing pressure is small (often within analytical error).
- As far as one can tell on the basis of 4 samples, both isotopes show a curved profile with a maximum in the Opalinus Clay. The decrease of δ values is particularly evident towards the Keuper.
- In a plot $\delta^{18}O$ vs. $\delta^{2}H$ (Fig. 4.6-8), the shallower samples are located on the right side of the global ($\delta^{2}H = 8\ \delta^{18}O + 10$, Craig 1961) and the local ($\delta^{2}H = 7.55\ \delta^{18}O + 4.8$, Kullin & Schmassmann 1991) meteoric water lines. The deeper samples lie close to or at the meteoric water lines.
- The same information is illustrated in Fig. 4.6-9 by the depth trend of deuterium excess ($\delta^{18}O - 8\ \delta^{2}H$), which increases systematically with depth.

Tab. 4.6-10: Stable isotopic composition of squeezed waters

The aliquots selected for interpretation are shown in bold.

Depth [m]	**Formation**	**Pressure** [MPa]	**$\delta^{18}O$** [‰ VSMOW]	**$\delta^{2}H$** [‰ VSMOW]	**D excess** [‰]
416.08	Passwang Formation	**200**	**-6.28**	**-47.0**	**3.3**
		300	-6.33	-46.7	3.9
471.15	Opalinus Clay	**200**	**-5.74**	**-42.2**	**3.7**
		300	-5.82	-42.7	3.9
545.41	Opalinus Clay	**200**	**-6.24**	**-42.4**	**7.5**
		300	-6.38	-42.3	8.7
600.09	Staffelegg Formation	**300**	**-8.16**	**-53.7**	**11.5**
		400	-8.22	-54.3	11.4
		500	-8.17	-53.9	11.5

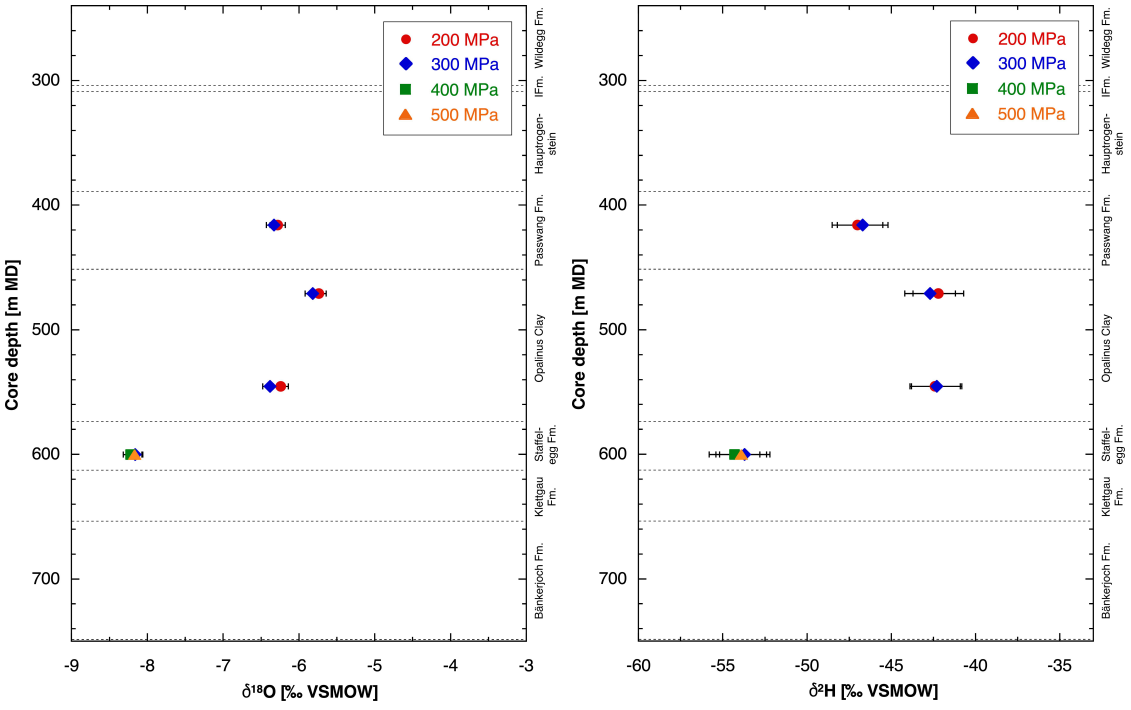

Fig. 4.6-7: Depth trends of $\delta^{18}O$ and $\delta^{2}H$ in squeezed waters

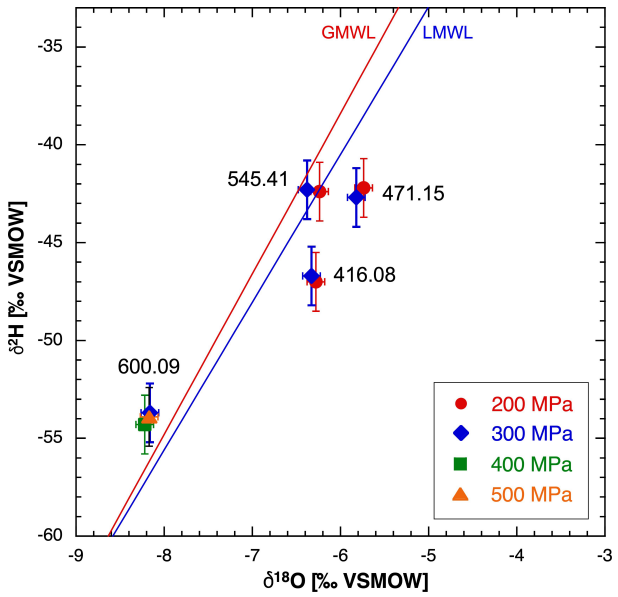

Fig. 4.6-8: Plot of $\delta^{18}O$ vs. $\delta^{2}H$ for squeezed waters

GMWL = Global Meteoric Water Line, LMWL = Local Meteoric Water Line. Numbers indicate sample depths in m.

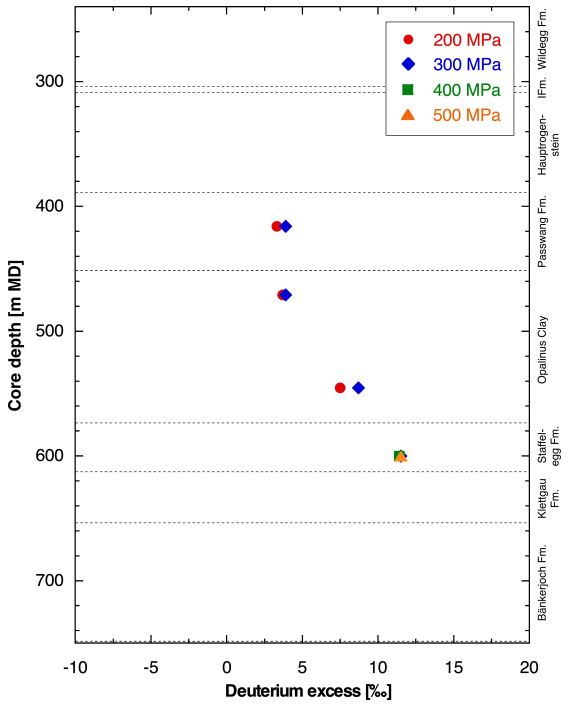

Fig. 4.6-9: Depth trend of deuterium excess in squeezed waters

4.7 Data from advective displacement experiments

Carmen Zwahlen, Andreas Jenni, Mirjam Kiczka, Urs Mäder & H. Niklaus Waber

Advective displacement (AD) experiments are a methodology for a comprehensive physico-chemical characterisation, including porewater chemistry and certain transport properties (details in method report, Waber (ed.) 2020). This section presents a data summary, more details where important, and short discussions where appropriate. The full datasets are provided in Appendix B. Integration of the data into context and depth profiles is included in Chapter 5.

Three samples from the Opalinus Clay and the clay-rich confining units were processed. All experiments were successful, subjected to a similar analytical programme, with differences mainly related to the duration of each experiment (numbers of sampled fluid aliquots). The extent of pre-and post-mortem characterisation of core material was optimised based on gained experience from former BUL1-1, TRU1-1, MAR1-1 and BOZ1-1 investigations. The programme fulfilled the planned work, but partially provided longer durations of advective displacement than requested. The duration of the percolation period was 118 – 125 days, transporting 0.8 – 0.9 pore volumes of fluid.

The salinity in this borehole is significantly lower than in all previous TBO boreholes but similar to BOZ1-1. A feature not observed in boreholes BUL1-1 and TRU1-1 but in some experiments from MAR1-1, BOZ1-and BOZ2-1 are very high nitrate concentrations eluted initially during advective displacement. At BOZ2-1, this is particularly the case for the sample from the Opalinus Clay and the Staffelegg Formation and this is discussed in Section 4.7.5.4, and further below.

4.7.1 Sample material and overview of analytical work

The three sample cores (Fig. 4.7-1) span 170 m of clay-rich confining and host rock units 426 – 598 m depth), from the Passwang («Brauner Dogger») to the Staffelegg Formation and include one sample from the Opalinus Clay.

X-ray computed tomography (CT) was performed on a medical scanner (Waber (ed.) 2020) for sample selection (Fig. 4.7-2) and detection of disturbing features (fractures, pyrite accumulations, macro-fossils, etc.). Dry cutting was used for obtaining a central core segment for AD experiments (yellow in Fig. 4.7-2), and adjacent 2 discs for accompanying characterisation (green in Fig. 4.7-2). The central core segment was turned on a lathe from 95 mm to 80 mm in diameter. Tab. 4.7-1 lists all analytical work performed on the three samples.

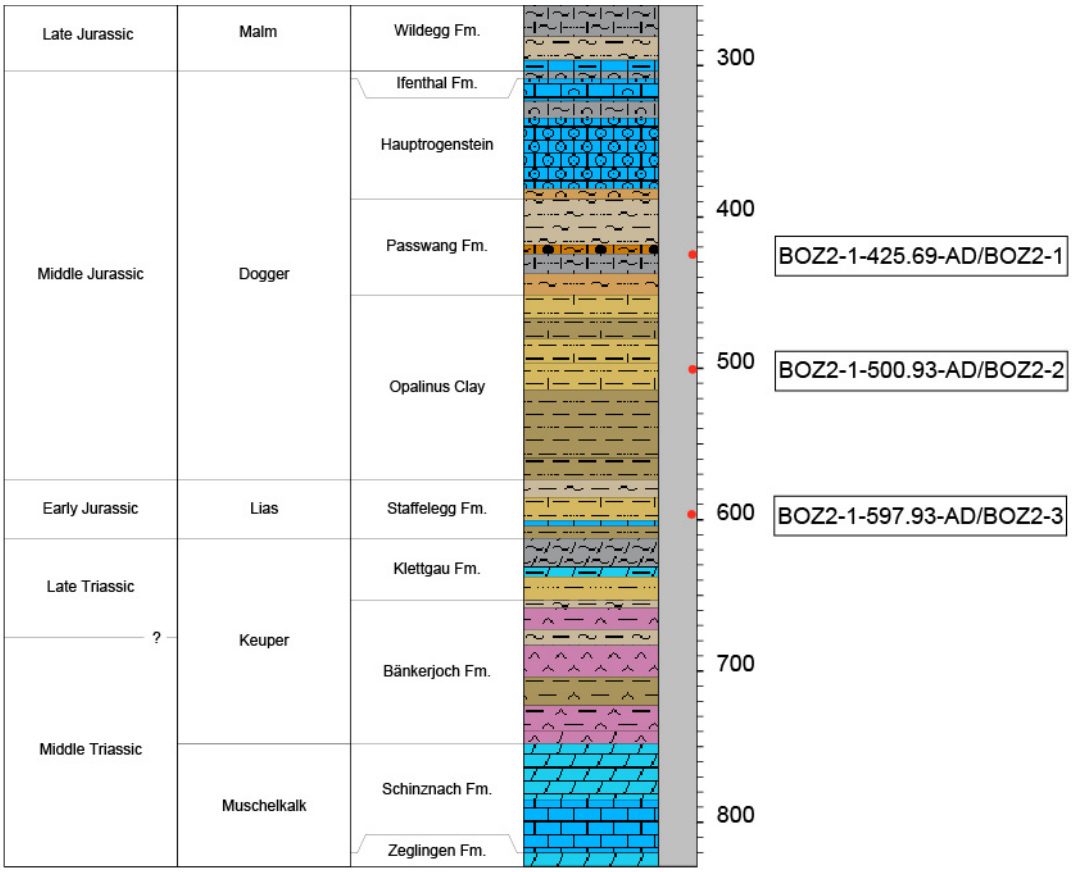

Fig. 4.7-1: Location of samples used for advective displacement experiments (red dots)
Short labels are consecutively numbered laboratory abbreviations.

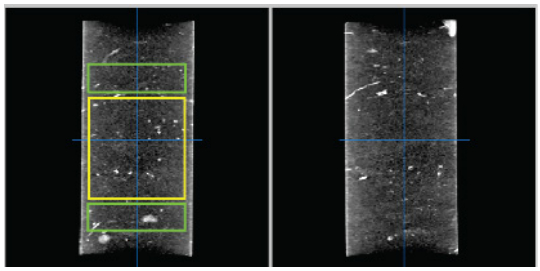

BOZ2-1-425.69-AD (Passwang Fm.)

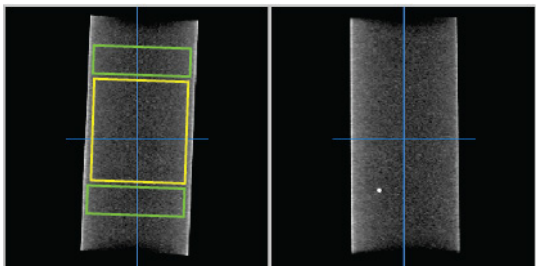

BOZ2-1-500.93-AD (Opalinus Clay)

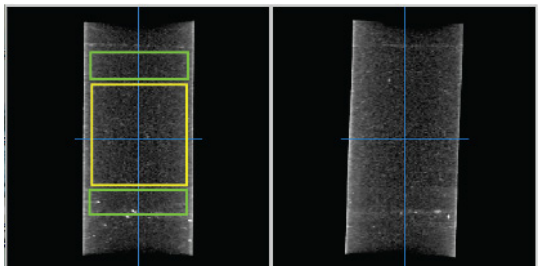

BOZ2-1-597.93-AD (Staffelegg Formation)

Fig. 4.7-2: X-ray CT images of AD samples

Central sections parallel to core axis at right angle. Grey scale range setting is 1'700 – 2'500 HU. Yellow segments are used for advective displacement, green segments for pre-characterisation. Low X-ray absorbance represents clay/quartz-rich sections (darker grey), slightly lighter grey indicates carbonate-richer parts, siderite is brighter, and pyrite is white (strongest absorbance). Black lines/gaps represent fractures.

Tab. 4.7-1: Summary of analytical work perfomed on samples for advective displacement experiments

Parameter	**BOZ2-1**	**BOZ2-2**	**BOZ2-3**
Sample ID RWI	BOZ2-1-425.69-AD	BOZ2-1-500.93-AD	BOZ2-1-597.93-AD
Lab sample ID	BOZ2-1xx-AD	BOZ2-2xx-AD	BOZ2-3xx-AD
Depth [m]	425.69	500.93	597.93
Geological unit	Passwang Formation	Opalinus Clay	Staffelegg Formation
Member / sub-unit	Waldenburg + lower part of Brüggli Member	'Mixed clay-silty-carbonate sub-unit'	Frick Member
AD_exp	y	y	y
Pre_WC	1+1	1+1	1+1
Pre_M	y	y	y
Pre_V,A,L	y	y	y
Pre_Min	1	1	1
Pre_Clay	1	1	1
Pre_AqEx	1+1	1+1	1+1
Pre_Ni-en	ave	ave	ave
Post_WC	5	5	5
Post_M	y	y	y
Post_V,A,L	y	y	y
Post_AqEx	2	2	2
Post_Ni-en	n	n	n
Abras_Drilling_Fl	n	n	n

y = yes = done; n = no = not done; integer numbers refer to the number of samples processed; +: samples from above (left number) and below (right number) a core were processed; Pre: sample pre-characterisation; Post: post-mortem characterisation; WC: water content; M: mass; V,A,L: core volume, sectional area and length; Min: mineralogy; Clay: clay mineralogy; AqEx: aqueous extracts; Ni-en: cation selectivity with Ni-en method; Post_WC: post-mortem water content determined along a profile with 5 segments; AD_exp: complete analysis of fluid sample aliquots collected during advective displacement; ave: average of two samples.

4.7.2 Conditions of advective displacement experiments

Sample preparation was performed according to Waber (ed.) (2020). The overview table (Tab. 4.7-2) presents some experiment specific parameters such as sample processing dates, storage time and other characteristic times like arrival of first fluid drop and its electric conductivity. Numbers of samples taken and analysed are listed as well as average pressures for confining and injection. The number of pore volumes percolated are based on the water content determined from pre-characterisation. Infiltration pressure of the artificial porewater (APW) was on average 46 bar, pressurised by He. The hydraulic gradients are large, 5'000 – 6'000 m_{H2O}/m (sample dimensions are in Tab. 4.7-4). Experiments were started within 24 – 30 days of sample delivery. The time until arrival of a first fluid drop at the electric conductivity cell (outflow, before sampling syringe) was 8 – 10 days after start of infiltration.

Confining pressure was on average 58 – 62 bar, pressurised by Ar on water (Tab. 4.7-2). The gas collected in gas-tight glass vials (with needle and septum) prior to the arrival of the first fluid drop, as well as the head space in selected syringes containing gas and fluid, was analysed by mass spectrometry (Entracers GmbH and Hydroisotop GmbH, results in Appendix B). In addition, the density of the gas could be derived from high-precision weighing. Assuming all O_2 originates from air that is entrapped during preparation (in filters and in dead-space), the air proportion in the gas is calculated and all air components (mainly N_2) are subtracted from the measurements. The results are summarised below:

- Apart from air (and He used as carrier gas), Ar dominates the exfiltrating gas composition, especially at early times. Ar content is far above compositions observed in other gas measurements of out-gassed rock samples (e.g. Schlattingen-1 borehole). The Ar must therefore originate from the confining system, although it is unclear how this gas penetrates the core insulation (inner Teflon tape, outer Latex double sleeve). From literature it is clear that Latex is not strictly gas-tight and it may be envisaged that Ar dissolves into Latex at the outer interface, permeates across the latex membrane, and ex-solves again and migrates towards the low-pressure outflow. The sleeve appears to become much more gas tight with time, because gas outflow is observed to rapidly decrease with time. In the beginning the gas migration might be fast along a small desaturated zone at the core rim. This desaturated zone is gradually saturated leading to a water dominated flow, which is slower. The interaction of noble gases with the porewater chemistry is expected to be negligible. There is no indication from the isotopic composition of the sampled aliquots that confining water did also penetrate into the sample core.
- At later infiltration stages, but still before APW breakthrough, gas exfiltration decreases and N_2 dominates the gas composition. These very small amounts of N_2 are inferred to originate from the initial porewater present in the core samples.

Approaching APW breakthrough, the low density (relative to air) of the minor volumes of exfiltrating gas indicates the expected presence of He, which is used to pressurise the infiltrating APW and dissolves therein in the infiltration tank at approximately 46 bar infiltration pressure. The pore pressure in the core decreases from 46 bar at the bottom to 1 bar at the top, where the degassing He is caught in the sampling syringe. Some He may also get trapped in the pore space of the core samples. This effect is expected to be small, because the total weight of the cores increases during the experiment (Tab. 4.7-4).

Tab. 4.7-2: Conditions of advective displacement experiments

Parameter	**BOZ2-1**	**BOZ2-2**	**BOZ2-3**
Depth [m]	425.69	500.93	597.93
Geological unit	Passwang Formation	Opalinus Clay	Staffelegg Formation
Drilled	21.09.2020	23.09.2020	27.09.2020
Delivered	05.10.2020	05.10.2020	05.10.2020
Prep_AD	29.10.2020	29.10.2020	05.11.2020
Injection	30.10.2020	30.10.2020	06.11.2020
First drop	07.11.2020	09.11.2020	16.11.2020
Days to first drop	8.3	9.7	9.7
Initial gas [mL]	9.3	3.2	6.4
End_AD	04.03.2021	04.03.2021	04.03.2021
Duration [d]	124.7	124.7	117.6
Pore-volumes	0.8	0.8	0.8
EC_initial (25 °C) (max. in 1st 24 h) [mS/cm]	12.3	13.5	7.8
Filter	PEEK	PEEK	PEEK
AD-samples	10	11	10
AD-samp_chem	9	10	9
AD-samp_isotopes	9	10	9
in-line pH	6	6	6
P_Conf [bar]	62	58	62
P_Inf [bar]	46	46	46
Gradient [mH_2O/m]	5'329	5'317	5'304

4.7.3 Mineralogy and petrophysical properties

For each core, the mineralogy was determined on the sum of subsamples cut adjacent to the core segment used for the AD experiments (Tab. 4.7-1). Results are summarised in Tab. 4.7-3 and plotted in Section 4.2. Samples cover a range of clay-mineral contents of 35 – 52 wt.-%, calcite contents of 10 – 18 wt.-%, and quartz contents of 26 – 37 wt.-%. Of the clays, the dominant minerals are illite (13 – 18 wt.-%), illite/smectite mixed layers (11 – 16 wt.-%), and kaolinite (5 – 17 wt.-%). The ratio of (illite/smectite+smectite)/(total_clay) is rather uniform in the range 0.30 – 0.32.

Carbon, sulphur and nitrogen analysis are also included. Pyrite contents are moderately low (0.2 – 1 wt.-%) because pyrite-rich lithologies were avoided based on X-ray CT characterisation (Fig. 4.7-2). More details, including end-member clays, are included in Appendix B.

Tab. 4.7-3: Mineralogy of advective displacement samples, including C, S and N analyses

Parameter	**Unit**	**BOZ2-1**	**BOZ2-2**	**BOZ2-3**
Depth	[m]	425.69	500.93	597.93
Geological unit		Passwang Formation	Opalinus Clay	Staffelegg Formation
S	[wt.-%]	0.4	b.d.	0.1
C(inorg)	[wt.-%]	2.3	1.7	1.2
C(org)	[wt.-%]	0.6	0.8	0.7
N	[wt.-%]	b.d.	0.06	0.04
Quartz	[wt.-%]	37	26	35
K-feldspar	[wt.-%]	6	4	5
Plagioclase	[wt.-%]	2	3	2
Calcite	[wt.-%]	18	10	10
Dolomite / Ankerite	[wt.-%]	b.d.	b.d.	b.d.
Siderite	[wt.-%]	1	4	b.d.
Anhydrite	[wt.-%]	b.d.	b.d.	b.d.
Celestite	[wt.-%]	b.d.	b.d.	b.d.
Pyrite	[wt.-%]	0.8	1.0	0.2
Clay minerals	**[wt.-%]**	**35**	**52**	**47**
Illite	[wt.-%]	14	13	18
Illite/smectite ML (85-90)	[wt.-%]	4	13	10
Illite/smectite ML (75-80)	[wt.-%]	5	0	3
Illite/smectite ML (50-70)	[wt.-%]	3	3	2
Illite/smectite ML (20-40)	[wt.-%]	b.d.	b.d.	b.d.
Smectite	[wt.-%]	b.d.	b.d.	b.d.
Kaolinite	[wt.-%]	5.0	16.9	8.3
Chlorite	[wt.-%]	1.7	2.0	2.8
Chl/Sm ML (85-95)	[wt.-%]	3.7	3.7	3.5
Total illite/smectite	[wt.-%]	**11**	**16**	**14**
(tot_ill_sm+sm)/(total_clay)		0.32	0.31	0.30
(tot_ill+ill/sm+sm)/(total_clay)		0.71	0.57	0.69

b.d.: below detection

A plethora of petrophysical parameters can be derived from sample dimensions, mass, water content, and changes in these parameters determined before and after an AD experiment (Tab. 4.7-4). These quantities include porosity, bulk density, grain density, water uptake during the experiments, and unsaturated porosity (saturation ratio). The relationships are given in Waber (ed.) (2020). Note that the water content determined for pre-characterisation is based on 2 sub-samples adjacent to the AD core segment.

The calculation of the initial corrected water content is based on the assumption, that the desaturation of the sample material from the pre analysis is the same as determined for the post-mortem core. The saturation state of the core is calculated based on the post-mortem water content and the initial and final core volume and mass. Thus, water related to the regularly observed slight core expansion was explicitly taken into account. The core volume increases by 0.3 – 0.5% (Tab. 4.7-4) during AD experiments, accompanied by a water uptake of 1.3 – 3.2 g. Accounting for volume expansion, there remains a small water uptake that must reflect an initially small volume of unsaturated porosity, ranging from 1.3 to 2.4 ml, or a saturation ratio in the range of 0.95 – 0.97. Therefore, the initial state is essentially saturated for all samples within measurement uncertainty.

Tab. 4.7-4: Core dimensions and derived petrophysical parameters

Parameter	**Unit**	**BOZ2-1**	**BOZ2-2**	**BOZ2-3**
Depth	[m]	425.69	500.93	597.93
Geol. unit		Passwang Formation	Opalinus Clay	Staffelegg Formation
Pre_Core_M	[g]	**1'100.34**	**1'100.61**	**1'092.11**
Pre_Core_DM	[cm]	8.02	8.01	8.02
Pre_Core_L	[cm]	8.64	8.68	8.59
Pre_Core_A	[cm^2]	50.53	50.42	50.45
Pre_Core_V	[cm^3]	436.41	437.61	433.34
Post_Core_M	[g]	**1'103.97**	**1'104.85**	**1'095.46**
Post_Core_DM	[cm]	8.03	8.02	8.02
Post_Core_L	[cm]	8.67	8.70	8.60
Post_Core_A	[cm^2]	50.60	50.50	50.56
Post_Core_V	[cm^3]	438.71	439.40	434.74
Delta_M	[g]	**3.63**	**4.24**	**3.35**
Delta_Core_DM	[cm]	0.005	0.006	0.008
Delta_Core_L	[cm]	0.034	0.022	0.010
Delta_Core_A	[cm^2]	0.068	0.079	0.107
Delta_Core_V	[cm^3]	**2.296**	**1.794**	**1.400**
Delta_Core_V-%	[%]	0.526	0.410	0.323
Pre_Bulk_WD	[g/cm^3]	**2.521**	**2.515**	**2.520**
Post_Bulk_WD	[g/cm^3]	**2.516**	**2.514**	**2.520**
Delta_Bulk_WD	[g/cm^3]	-0.005	-0.001	0.000
Delta_Bulk_WD-%	[%]	-0.195	-0.025	-0.016
Pre_GD	[g/cm^3]	**2.706**	**2.706**	**2.698**
Post_GD	[g/cm^3]	**2.709**	**2.718**	**2.703**
Delta_GD	[g/cm^3]	0.003	0.012	0.005
Corr_Pre_GD	[g/cm^3]	**2.700**	**2.701**	**2.690**
Pre_WCw		**0.0429**	**0.0445**	**0.0416**
Post_WCw		**0.0448**	**0.0472**	**0.0427**
Delta_WCw		0.0019	**0.0027**	0.0011
Corr_Pre_WCw		**0.0417**	**0.0435**	**0.0398**
Pre_H_2O_Core	[g]	**47.19**	**48.99**	**45.47**
Post_H_2O_Core	[g]	**49.49**	**52.15**	**46.78**
Delta_H_2O_Core	[g]	2.30	**3.16**	1.31
Corr_Pre_H_2O_Core	[g] or [mL]	**45.86**	**47.92**	**43.43**
Unsat_Vol	[g] or [mL]	1.33	2.44	1.95
Pore_Vol_tot	[mL]	47.19	50.36	45.38
Sat_ratio		**0.97**	**0.95**	**0.96**
Pre_Poro_WL		**0.1081**	**0.1120**	**0.1049**
Post_Poro_WL		**0.1128**	**0.1187**	**0.1076**
Delta_Poro_WL		0.0047	0.0067	0.0027
Delta_Poro_WL-%	[%]	4.33	6.02	2.56
Corr_Pre_Poro_WL		**0.1051**	**0.1095**	**0.1002**
Corr_Pre_Poro_tot		**0.1081**	**0.1151**	**0.1047**
Delta_Corr_Poro_WL-%		-2.82	-2.19	-4.48

_L = length; _A = area; _V = volume; _M = mass; WD = wet density; GD = grain density; WCw = water content rel. to wet mass; _WL = water loss

There are significant differences in water content measured in adjacent samples (pre-characterisation) and in the core itself (post-mortem) of 3 – 6% relative, which are reduced to 2 – 5% if accounting for core expansion (Fig. 4.7-3). This leads to different values of bulk wet density, water-loss porosity and grain density (assuming saturated conditions) derived from pre-characterisation and post-mortem data. This spread is larger than measurement uncertainties and illustrates that the largest contribution to uncertainty is sample heterogeneity for parameters that depend on water content. Differences in water content commonly correlate with differences in clay-mineral content, such that this heterogeneity is mainly an issue of lamination in fine-grained sediments.

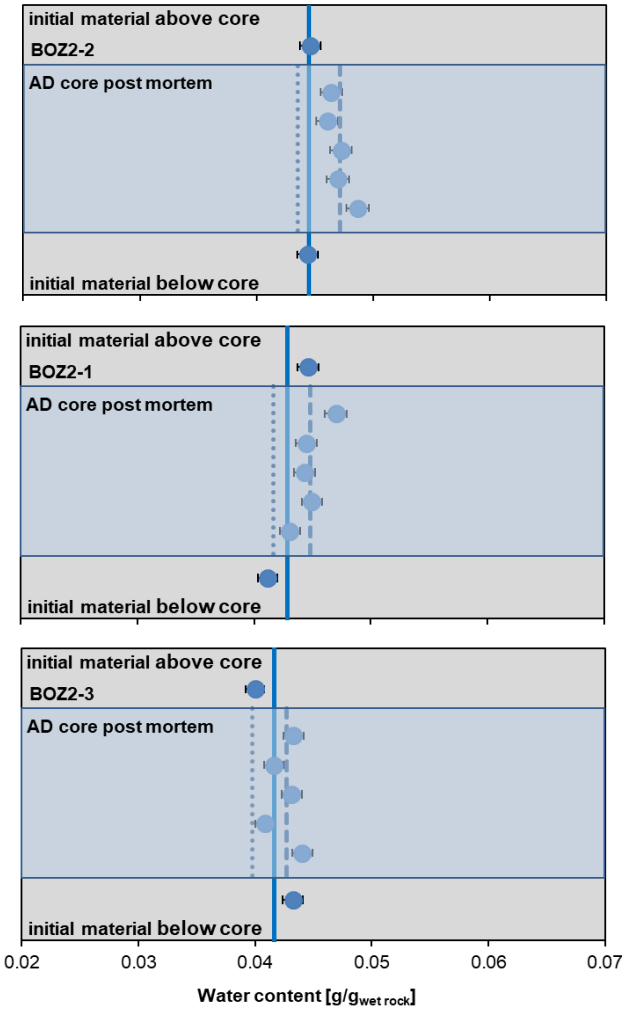

Fig. 4.7-3: Details of water content measurements before and after AD experiments

BOZ2-1 = BOZ2-1-425.69-AD (Passwang Formation); BOZ2-2 = BOZ2-1-500.93-AD (Opalinus Clay); BOZ2-3 = BOZ2-1-597.93-AD (Staffelegg Formation). Vertical lines indicate the value for pre-characterisation (solid line), average of post-mortem characterisation (dashed line) and the corrected initial water content (dotted line). Error bars refer to measurement uncertainty of 2%.

4.7.4 Aqueous extracts, CEC and cation selectivity of AD samples

Aqueous extracts, CEC and cation selectivity determinations were carried out within the pre-characterisation and post-mortem analysis. Detailed analyses are provided in Appendix B. Methods are the same as used for other core samples (Waber (ed.) 2020), with the exception of sample masses for water content that may have been smaller than used for regular core sample analysis. Averaged pre- and post-characterisation data – also used for integrative data plots – are presented in this section. Averaging refers to aqueous extraction measurements of pieces above and below the segment used for the AD experiments (indicated in Fig. 4.7-2 and Tab. 4.7-5). For CEC and cation selectivity, the pieces were combined in equal proportions and analysed as one sample.

All averaged aqueous extract solutions (Tab. 4.7-5) from pre-characterisation processed at $S/L \approx 1$ contain low concentrations of NH_4 (up to 2.8 mg/L) and NO_3 (0.77 – 1.67 mg/L, but 5.7 mg/L in sample BOZ2-1). The factor $(1/WC_w \cdot L/S_w)$ refers to the scaling factor required to scale aqueous concentrations for conservative components to porewater concentrations (i.e., at water content).

Characteristic molar ion ratios (Tab. 4.7-6) do not follow a systematic trend with depth, except for the Br/Cl ratio, which decreases with depth. Tab. 4.7-7 shows that the aqueous extract solutions are at or very close to calcite saturation, but far from dolomite saturation except for the sample BOZ2-1 which is in equilibrium with dolomite. Extracts are distinctly undersaturated with respect to sulphates and strontianite. TIC was used as input for the carbon system, because the titrated alkalinity would also include acetate. However, the calculated alkalinity agrees well with the measured one due to low acetate concentrations in samples from this borehole.

Tab. 4.7-5: Composition of aqueous extract solutions from pre-characterisation

Parameter	**Unit**	**BOZ2-1**	**BOZ2-2**	**BOZ2-3**
Depth	[m]	425.69	500.93	597.93
Geological unit		Passwang Formation	Opalinus Clay	Staffelegg Formation
averaging		top+base (1+1)	top+base (1+1)	top+base (1+1)
$1/WC_w*L/S_w$		24.31	23.54	24.07
Rock wet	[g]	30.47	30.27	30.21
Water	[g]	30.39	30.37	28.99
WC_w	[g/g_{wet}]	0.043	0.045	0.042
S/L ($S_d/(L+PW)$)		0.920	0.912	0.957
pH at titration		9.30	8.67	8.89
Na	[mg/L]	157	213	182
NH_4	[mg/L]	2.78	1.77	1.64
K	[mg/L]	5.83	5.77	4.99
Ca	[mg/L]	2.16	2.55	1.91
Mg	[mg/L]	0.443	0.559	0.405
Sr (OES)	[mg/L]	< 0.25	< 0.25	< 0.25
Ba (OES)	[mg/L]	< 0.025	< 0.025	< 0.025
F	[mg/L]	4.17	2.66	4.46
Cl	[mg/L]	30	36	26
Br	[mg/L]	0.12	0.13	0.08
NO_3	[mg/L]	5.57	1.67	0.77
SO_4	[mg/L]	156	170	204
Alk (tit)	[meq/L]	3.06	5.44	3.31
Alk as HCO_3	[mg/L]	150.0	276.7	170.5
TOC	[mg/L]	12.90	19.75	15.55
TIC	[mg/L]	29.6	54.5	33.6
lactate	[mg/L]	< 20	< 20	< 20
acetate	[mg/L]	25.00	21.70	< 20
propionate	[mg/L]	< 20	< 20	< 20
formate	[mg/L]	< 20	< 20	< 20

Tab. 4.7-6: Cation ratios and details of carbon system in aqueous extract solutions from pre-characterisation

Parameter	**Unit**	**BOZ2-1**	**BOZ2-2**	**BOZ2-3**
Depth	[m]	425.69	500.93	597.93
Geological unit		Passwang Formation	Opalinus Clay	Staffelegg Formation
Br/Cl*1'000	[mol/mol]	1.74	1.55	1.38
SO_4/Cl	[mol/mol]	1.90	1.73	2.95
Ca/Mg	[mol/mol]	2.95	2.77	2.86
Ca/Sr	[mol/mol]	Sr < 0.25	Sr < 0.25	Sr < 0.25
(Ca+Mg)/(Na+K)	[eq/eq]	0.015	0.014	0.012
Alk (tit)	[meq/L]	3.06	5.44	3.31
TIC	[meq/L]	2.46	4.53	2.79
acetate	[meq/L]	0.423	0.368	< 0.3
TOC	[mg/L]	12.9	19.8	15.6
acetate (as C)	[mg/L]	10.18	8.83	< 8.14

Tab. 4.7-7: Saturation indices calculated for aqueous extract solutions from pre-characterisation

Parameter	**Unit**	**BOZ2-1**	**BOZ2-2**	**BOZ2-3**
Depth	[m]	425.69	500.93	597.93
Geological unit		Passwang Formation	Opalinus Clay	Staffelegg Formation
Charge	[eq/kg_w]	4.9E-06	2.7E-04	6.1E-05
%-Error		0.03	1.41	0.38
Acetate	[eq/kg_w]	4.2E-04	3.7E-04	< 3.0E-04
Ionic strength	[mol/kg_w]	9.00E-03	1.13E-02	1.03E-02
tot_alk	[eq/kg]	2.87E-03	4.70E-03	2.97E-03
pH		9.30	8.67	8.89
log P_{CO2}	[bar]	-4.19	-3.26	-3.70
SI(calcite)		0.17	-0.08	-0.20
SI(dolomite)		0.00	-0.46	-0.73
SI(gypsum)		-2.97	-2.87	-2.90
SI(celestite)		-5.55	-5.54	-5.45
SI(strontianite)		-3.68	-4.01	-4.01
SI(anhydrite)		-3.19	-3.09	-3.13

PSI/Nagra 2012 thermodynamic database (Thoenen et al. 2014), calculated in PHREEQC for 25 °C, using ordered dolomite; kgw = kg water; charge = Σ(cation charge) – ׀Σ(anion charge)׀ ; %-error = 100*charge / (Σ(cation charge) + ׀Σ(anion charge)׀).

Aqueous extracts of all cores were also produced after termination of the experiments. A thin disc (13 – 19 mm) from the top and base of each core was processed according to the protocols used for pre-characterisation. The base of the core represents the inlet of the artificial porewater (APW), whereas the top represents the outflow to sampling. The two may yield different results depending on the overall progress of fluid percolation (different concentrations in inlet sample compared to outlet), and averaging is therefore meaningless.

Results (Tab. 4.7-8) show that Br (not present in the APW) was effectively flushed out of each core, whereas other minor anionic components were buffered to some extent (e.g. F, NO_3).

The Cl concentrations scaled to bulk porewater in the post-mortem aqueous extracts increase from top to bottom (or remain constant in BOZ2-3) as expected from the higher Cl concentration in the APW (Tab. 4.7-8).

The initially observed TOC and acetate in the pre-analysis were partially flushed out as seen in the post-mortem data, except for BOZ2-3 where acetate and TOC increase slightly, and BOZ2-2 where TOC increased at the top. The cation concentrations increased in general from pre- to post-analysis, but cation fractions need to be interpreted in more detail considering ion-exchange processes. Sr concentrations increased significantly from pre- to post-analysis. A more in-depth analysis will be required to reconcile differences between extracts from pre-characterisation and post-mortem analysis.

Calculation of speciation and saturation indices (Tab. 4.7-9) of the aqueous extract solutions from Tab. 4.7-8 are all below calcite saturation, and far from dolomite saturation. All extracts are distinctly undersaturated with respect to sulphates and strontianite. TIC was used as input for the carbon system.

Tab. 4.7-8: Composition of aqueous extract solutions from post-mortem characterisation

Parameter	**Unit**	**BOZ2-1**		**BOZ2-2**		**BOZ2-3**	
Depth	[m]	425.69		500.93		597.93	
Geological unit		Passwang Formation		Opalinus Clay		Staffelegg Formation	
averaging		top post-mortem	base post-mortem	top post-mortem	base post-mortem	top post-mortem	base post-mortem
$1/WC_w*L/_{Sw}$		22.47	24.61	22.73	21.84	24.42	23.99
Rock wet	[g]	30.18	30.09	30.31	30.06	30.03	30.15
Water	[g]	30.47	30.59	30.58	30.50	30.44	30.54
WC_w	[g/g_{wet}]	0.047	0.043	0.046	0.049	0.043	0.044
S/L ($S_d/(L+PW)$)		0.902	0.903	0.904	0.895	0.905	0.904
pH at titration		8.80	8.90	8.30	8.50	8.40	8.70
Na	[mg/L]	178	191	242	245	246	210
NH_4	[mg/L]	3.48	4.16	1.72	1.57	1.83	2.17
K	[mg/L]	5.96	7.30	7.93	7.27	8.29	8.27
Ca	[mg/L]	1.86	2.02	3.37	3.22	3.42	2.48
Mg	[mg/L]	0.522	0.567	0.823	0.814	0.774	0.587
Sr (OES)	[mg/L]	0.087	0.088	0.146	0.135	0.082	0.049
Ba (OES)	[mg/L]	< 0.025	< 0.025	< 0.025	< 0.025	< 0.025	< 0.025
F	[mg/L]	3.89	3.45	2.20	2.27	3.98	3.97
Cl	[mg/L]	85	115	74	119	118	119
Br	[mg/L]	0.02	< 0.016	0.03	< 0.016	0.04	< 0.016
NO_3	[mg/L]	7.24	1.04	72.80	12.00	82.50	13.70
SO_4	[mg/L]	141	150	156	175	191	167
Alk (tit)	[meq/L]	2.59	2.31	4.21	3.87	2.46	2.30
Alk as HCO_3	[mg/L]	158.0	140.9	256.9	236.1	150.1	140.3
TOC	[mg/L]	12.95	9.98	24.90	12.90	18.98	14.00
TIC	[mg/L]	32.1	29.5	50.8	46.8	31.4	28.0
lactate	[mg/L]	0.393	< 0.2	1.090	< 0.2	0.884	0.324
acetate	[mg/L]	2.66	0.96	4.11	1.84	4.11	1.25
propionate	[mg/L]	< 0.2	< 0.2	< 0.2	< 0.2	< 0.2	< 0.2
formate	[mg/L]	0.258	0.237	0.754	0.300	0.817	0.510

Tab. 4.7-9: Saturation indices calculated for aqueous extract solutions obtained post-mortem

Parameter	**Unit**	**BOZ2-1**		**BOZ2-2**		**BOZ2-3**	
Depth	[m]	425.69		500.93		597.93	
Geological unit		Passwang Formation		Opalinus Clay		Staffelegg Formation	
Position		top post-mortem	base post-mortem	top post-mortem	base post-mortem	top post-mortem	base post-mortem
Charge	[eq/kg_w]	-2.7E-04	-3.6E-04	1.7E-04	-1.4E-04	-2.6E-04	-6.6E-05
%-Error		-1.64	-2.01	0.80	-0.62	-1.15	-0.34
Acetate	[eq/kg_w]	4.5E-05	1.6E-05	7.0E-05	3.1E-05	7.0E-05	2.1E-05
Ionic strength	[mol/kg_w]	9.82E-03	1.06E-02	1.26E-02	1.30E-02	1.33E-02	1.14E-02
tot_alk	[eq/kg]	2.84E-03	2.67E-03	4.27E-03	3.99E-03	2.66E-03	2.44E-03
pH		8.80	8.90	8.30	8.50	8.40	8.70
log P_{CO2}	[bar]	-3.62	-3.76	-2.92	-3.15	-3.23	-3.58
SI(calcite)		-0.29	-0.20	-0.34	-0.21	-0.45	-0.33
SI(dolomite)		-0.78	-0.61	-0.94	-0.67	-1.20	-0.94
SI(gypsum)		-3.04	-3.00	-2.78	-2.76	-2.69	-2.87
SI(celestite)		-2.64	-2.63	-2.42	-2.42	-2.59	-2.85
SI(strontianite)		-1.15	-1.10	-1.24	-1.12	-1.61	-1.57
SI(anhydrite)		-3.27	-3.22	-3.00	-2.98	-2.91	-3.09

PSI/Nagra 2012 thermodynamic database (Thoenen et al. 2014), calculated in PHREEQC for 25 °C, using ordered dolomite; kgw = kg water; charge = Σ(cation charge) – |Σ(anion charge)| ; %-error = 100*charge / (Σ(cation charge) + |Σ(anion charge)|).

Cation exchange capacities and cation occupancies determined by the Ni-en method (Waber (ed.) 2020) were performed on one precombined sample for each core from the two samples used for aqueous extracts. The results are also presented and interpreted in Section 4.5. Tab. 4.7-10 shows uncorrected (for porewater contribution and mineral dissolution/precipitation) capacities of 86-92 meq/kg (dry rock) with errors of up to ~ ± 4%. Ni consumption is up to 10% higher than the sum of cations. Ammonium was not measured but is expected to be present on the exchanger judged by the presence of up to 3 mg/L of NH_4 in the aqueous extracts performed at the same *S*/*L* ratio (Tab. 4.7-5). The high nitrate concentrations derive from the Ni-en solution. The negative charge balance arises from the lack of incorporating ethylendiamine complexes from the Ni-en solution into the calculation (Tab. 4.7-10).

The non-detectable Br concentrations agree with non-detectable Br concentrations in aqueous extracts. Interestingly, the SO_4/Cl ratios are significantly and systematically lower in the Ni-en solutions compared to the aqueous extracts, suggesting that there is either a sulphate source in the aqueous extracts, which does not dissolve in the Ni-en solutions, or a sink in the Ni-en solutions (complexation).

The cation occupancies derived from Ni-en extracts and applying a correction for the porewater contribution are presented in Section 4.5.

Tab. 4.7-10: Composition of Ni-en extract solutions and related parameters from pre-characterisation

Parameter	**Unit**	**BOZ2-1**	**BOZ2-2**	**BOZ2-3**
Depth	[m]	425.69	500.93	597.93
Geological unit		Passwang Formation	Opalinus Clay	Staffelegg Formation
averaging		1 averaged sample	1 averaged sample	1 averaged sample
$1/WC_w*L/S_w$		25.59	25.03	25.82
Rock wet	[g]	30.40	30.12	30.01
Solution	[g]	32.06	32.22	31.01
WC_w	[g/g_{wet}]	0.04	0.04	0.04
S/L ($S_d/(L+PW)$)		0.87	0.86	0.89
pH (initial)		8.30	8.30	8.30
Ni (initial)	[mg/L]	5748	5748	5970
pH (final)		8.36	8.26	8.28
Na	[mg/L]	691	838	732
K	[mg/L]	165	166	160
Mg	[mg/L]	197	173	151
Ca	[mg/L]	571	561	562
Sr	[mg/L]	38.8	38.1	18.3
Ba	[mg/L]	0.196	0.619	0.280
Fe	[mg/L]	< 0.05	< 0.05	< 0.05
Ni	[mg/L]	2965	2907	3245
F	[mg/L]	1.07	0.62	1.08
Cl	[mg/L]	27	33	23
Br	[mg/L]	< 0.16	< 0.16	< 0.16
NO_3	[mg/L]	12855	12995	13059
SO_4	[mg/L]	107	100	130
TDS	[mg/L]	17619	17812	18082
Charge %-error	[%]	-7.51	-7.51	-6.63
Na	[meq/kg_d]	32.2	40.0	37.4
K	[meq/kg_d]	4.5	4.6	4.8
Mg	[meq/kg_d]	17.4	15.6	14.6
Ca	[meq/kg_d]	30.5	30.7	33.0
Sr	[meq/kg_d]	0.95	0.95	0.49
Ba	[meq/kg_d]	0.003	0.010	0.005
Fe	[meq/kg_d]	0.000	0.000	0.000
SumCat	[meq/kg_d]	85.5	92.0	90.3
SumCat_err	[meq/kg_d]	3.50	3.80	3.70
Ni_cons	[meq/kg_d]	95.2	94.8	97.9
Ni_cons_err	[meq/kg_d]	4.60	4.60	5.20
Br/Cl	[mol/mol*1'000]	-	-	-
SO_4/Cl	[mol/mol]	1.45	1.13	2.06

kg_d = kg dry rock

4.7.5 Chemical and isotopic evolution of displaced porewater aliquots

An artificial porewater (APW) composition was injected to force advective displacement. The outflow of each experiment was continuously sampled in small syringes (Waber (ed.) 2020). These syringe aliquots were analysed for chemical and water isotopic composition. Hydraulic conductivity was evaluated for each sampled aliquot (Darcy's law), and any expelled gas was also recorded, although gas-tightness is commonly good, but cannot be ensured for a syringe sampling system. Most data for each experiment are included in tables and graphs in this section, and more details are provided in Appendix B.

According to the method of advective displacement (Mäder 2018), it is expected that the first few sampled aliquots are of similar composition and represent the displaced porewater from the sample core. After this, a gradual breakthrough of the injected APW should be observed, until full breakthrough of conservative components (e.g. Cl, Br), given enough time.

4.7.5.1 Artificial porewater used for advective displacement

In the absence of constraining data, an artificial porewater composition (Tab. 4.7-11) was chosen that was based on work performed for the deep geothermal well Schlattingen-1 (advective displacement experiments detailed in Mäder & Waber 2017). The composition was calculated with PHREEQC for 25 °C, to be saturated with respect to calcite and dolomite, and a partial pressure of CO_2 of $10^{-2.2}$ bar. This partial pressure was imposed by bubbling with an Ar/CO_2 gas mixture during mixing and again when the fluid reservoir was filled before the experiments started. A recipe with the appropriate amounts of PA-grade chemicals is given in Tab. 4.7-12.

Deuterium was added as a water tracer for advective-diffusive transport, aiming for a δ^2H of approximately +100 ‰ (VSMOW). There is no Br contained in the APW and therefore bromide-breakout can be used as an anionic tracer in the case of significant Br concentrations in the porewater. If the Cl concentration in the APW is significantly different from the displaced early aliquots, Cl breakthrough forms an additional anionic tracer for transport.

All three experiments were fed from PFA-coated fluid tanks containing the APW from the same batch 3. The pressurised head space of the tanks was filled with He after bubbling with the Ar/CO_2 gas mixture mentioned above. The composition of the APW is therefore identical for all experiments.

Tab. 4.7-11: Composition and recipe for the artificial porewater

Parameter	**Unit**	**Recipe**	**Calculated** *	**Measured**	**Compounds**
pH		7.19		7.38	
Na	[mg/L]	3'989	3'988	4'059	NaCl; $NaHCO_3$; Na_2SO_4
NH_4	[mg/L]			< 10	
K	[mg/L]	79.4	79.3	78.7	KCl
Ca	[mg/L]	503	504	506	$CaCl_2 \cdot 2H_2O$
Mg	[mg/L]	226	226	208	$MgCl_2 \cdot 6H2O$
Sr (OES)	[mg/L]			< 0.25	
Ba	[mg/L]			< 0.25	
Si	[mg/L]			< 2.5	
Al	[mg/L]			0.279	
F	[mg/L]			< 1.6	
Cl	[mg/L]	5'992	5'986	5'826	$CaCl_2 \cdot 2H_2O$; KCl; $MgCl_2 \cdot 6H_2O$
Br	[mg/L]			< 1.6	
NO_3	[mg/L]			5.25	
SO_4	[mg/L]	2'305	2'303	2'132	Na_2SO_4
TOC	[mg/L]			7.4	
TIC	[mg/L]	29.3	29.32	28.0	$NaHCO_3$
lactate	[mg/L]			< 20	
acetate	[mg/L]			< 20	
propionate	[mg/L]			< 20	
formate	[mg/L]			< 20	
$\delta^{18}O$	[‰ VSMOW]		-11.43	-11.52	
$\delta^{2}H$	[‰ VSMOW]	100	91.9	90.8	D_2O

* Calculated from the weighed-in chemical compounds; pH measured; CO_2-Ar bubbling not taken into account.

Tab. 4.7-12: Recipe for the artificial porewater for a 2-litre batch

Chemical	**Manufacturer**	**Grade**	**Recipe**		**Weighed in**
			[g/kgw]	[g/2 kgw]	[g/2 L]
$NaHCO_3$	Merck	p.a.	0.2051	0.4101	0.4102
$CaCl_2 \cdot 2\ H_2O$	Merck	p.a.	1.8465	3.6930	3.6944
KCl	Merck	p.a.	0.1514	0.3029	0.3026
$MgCl_2 \cdot 6\ H_2O$	Merck	p.a.	1.8907	3.7814	3.7827
NaCl	Merck	p.a.	7.1916	14.3831	14.3838
Na_2SO_4	AnalaR NORAMAPUR	Ph.Eur.	3.4089	6.8177	6.8114
D_2O (100%)	Roth	> 99.8% D	0.0310	0.0620	0.0607

4.7.5.2 Physical conditions, hydraulic conductivity, sampling, and pore volume equivalents

All core samples were subjected to 55 – 63 bar hydraulic confining pressure, and an infiltration pressure of initially around 48 bar set by a He headspace. The infiltration pressure was gradually decreasing with time (displaced APW, and any small He leak), and was replenished repeatedly until the end of the last experiments. The pressure range covered 43 – 48 bar.

Temperature conditions were stable without diurnal fluctuations, ranging seasonally from 21.5 to 25.5 °C. Critical temperature-sensitive measurements, such as electric conductivity, pH and hydraulic conductivity, were temperature-compensated, either intrinsically or explicitly (details in Waber (ed.) 2020).

Hydraulic conductivity referenced to 25 °C was evaluated for all sampled aliquots based on sample mass and Darcy's law (detailed data in Appendix B, method in Waber (ed.) 2020). Earliest aliquots commonly show lower apparent hydraulic conductivities due to the expulsion of gas from the dead volume in the outflow, and any small unsaturated volume in the sample core itself. All cores (Fig. 4.7-4) share an increasing hydraulic conductivity, followed by a slight decrease to a steady-state value, if sufficient run-time was provided. The values for the early conductivity and that measured towards the end of the experiments (Tab. 4.7-13) span a narrow range from 0.8 – 1.7 × 10^{-13} m/s. This conductivity refers to a direction perpendicular to bedding and a sample length of 8 – 9 cm, measured at very large hydraulic gradients (Tab. 4.7-2). A gradual but rather minor decrease after an early maximum value may be due to slow sample consolidation, and this was also observed in earlier work (Mäder 2018). These latter values are most representative for in situ conditions, although the confining stress of 60 bar (6 MPa) in the experiments is still considerably less than the lithostatic stresses at 426 – 598 m depth.

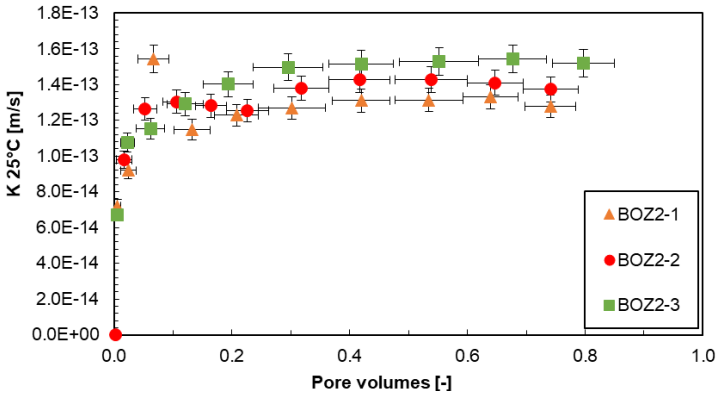

Fig. 4.7-4: Evolution of hydraulic conductivity during advective displacement experiments

BOZ2-1 = BOZ2-1-425.69-AD (Passwang Formation); BOZ2-2 = BOZ2-1-500.93-AD (Opalinus Clay); BOZ2-3 = BOZ2-1-597.93-AD (Staffelegg Formation). Pore volume fractions relate to transport time based on water content. Experiment duration is 118 – 125 days. Horizontal length of symbol bar covers the sampling interval, vertical bars are an estimate of combined uncertainties.

Tab. 4.7-13: Hydraulic conductivity of AD samples

Parameter	**Unit**	**BOZ2-1**	**BOZ2-2**	**BOZ2-3**
Depth	[m]	425.69	500.93	597.93
Geological unit		Passwang Formation	Opalinus Clay	Staffelegg Formation
Early_K (25 °C)	[m/s]	1.54E-13	1.30E-13	1.40E-13
Late_K (25 °C)	[m/s]	1.28E-13	1.37E-13	1.52E-13

The time axis for all data representations of sequential fluid aliquots is converted to pore volume fractions by dividing the cumulative sample mass (volume) by the water content of the core. In this way, experiments with very different hydraulic conductivities or different water contents can be represented in a meaningful way for transport. There may be some minor ambiguities in the case where water contents from pre-characterisation deviate from the true water content of a sample core, or if a significant initial unsaturated porosity fraction would be present. The chosen approximation is sufficient for a visual presentation of the data.

Sampled aliquots (mass) plotted versus pore volume fraction (time) provides an overview of all syringe samples taken for all three AD experiments (Fig. 4.7-5). For each experiment 10 to 11 samples were collected.

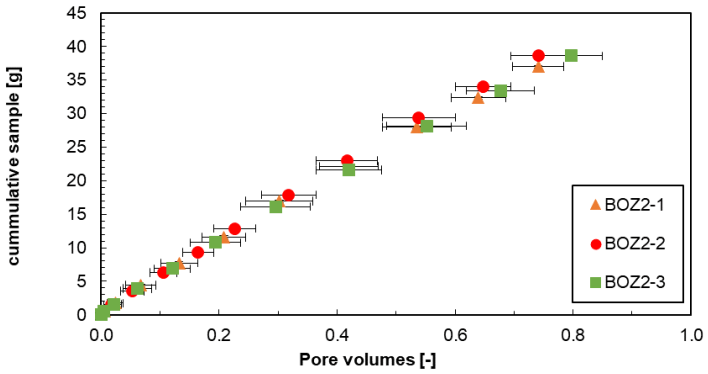

Fig. 4.7-5: Sampling schedule and sample volumes taken

BOZ2-1 = BOZ2-1-425.69-AD (Passwang Formation); BOZ2-2 = BOZ2-1-500.93-AD (Opalinus Clay); BOZ2-3 = BOZ2-1-597.93-AD (Staffelegg Formation). Each data point represents a syringe aliquot taken, with the horizontal bar indicating the duration for sampling, here converted to pore volume fraction percolated. Different slopes reflect different volumetric flow rates scaled by porosity.

4.7.5.3 Inline measurement of electric conductivity and pH

Electric conductivity (EC) was continuously monitored in all experiments (Fig. 4.7-6, Waber (ed.) 2020, for method). Conductivity cells were initially calibrated but may show a drift to varying extent over time due to electrode corrosion, commonly resulting in low apparent readings. Therefore, electric conductivity values are only meant to provide an indication of salinity but are not used quantitatively.

The electric conductivities show three different trends: In BOZ2-1 the values describe a narrow range between 14 and 16 mS/cm (22 °C laboratory reference) and remain below the APW throughout the experiment. The two cores BOZ2-2 and BOZ2-3 show an anomalous behaviour with EC values rising well above the injected APW at the same time as the nitrate concentration increases (Fig. 4.7-11). In BOZ2-2, the EC values drop below the APW value after 0.3 pore volumes, whereas in BOZ2-3, the values remain at a value above the APW. Values below the APW might be due to either a mixture between porewater and APW or corrosion effects of the electrode. Corrosion may not only affect the inner surface of the flow-through electrodes but may also lead to diffusion-dominated short-circuits between the two electrodes. A linear correlation between the ionic strength of the sampled aliquots and the EC data in BOZ2-2 suggests that the EC data represents changes in porewater composition rather than corrosion effects.

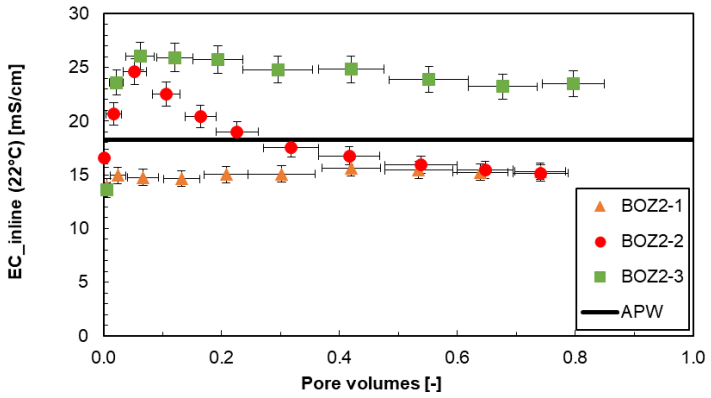

Fig. 4.7-6: Evolution of electric conductivity (22 °C) during advective displacement experiments

BOZ2-1 = BOZ2-1-425.69-AD (Passwang Formation); BOZ2-2 = BOZ2-1-500.93-AD (Opalinus Clay); BOZ2-3 = BOZ2-1-597.93-AD (Staffelegg Formation). Pore volume fractions relate to transport time based on water content. Experiment duration is 118 – 125 days. Horizontal length of symbol bar covers the sampling interval, vertical bars are an estimate of combined uncertainties.

The aim was to measure pH inline three times before/after sampling of the first four aliquots, and less frequently at later times (method in Waber (ed.) 2020). Measurements took 12 – 24 hrs in most cases, to ensure that the dead volume of the very small flow-through pH cell was sufficiently flushed given the very slow flow rates of the experiments. The micro-electrode was left installed in the flow-through cell and was checked before and after each pH measurement period with a standard solution. The initial calibration was made at pH 7 and 9, and simple drift checks and corrections were made with a standard solution at pH 7. The electrode slope was checked from time to time and was found to remain remarkably stable. In most cases, drift corrections over 12 – 24 hrs were ≤ 0.1 pH units. The overall uncertainty is difficult to assess because these small electrodes may respond to manipulations at the flow-through cell (response to small strains) and also small gas bubbles may temporarily affect readings. It is estimated that an error of ± 0.2 pH units is appropriate for most measurements. pH values of early aliquots are also tabulated below (Tab. 4.7-14).

These in-line pH measurements (Fig. 4.7-7) are rather tricky and require careful handling of the equipment. Criteria to accept a value include a small drift and a reasonably well-defined pH-plateau, as well as a stable non-zero electric conductivity (no gas bubbles). It cannot be excluded that for long measurement durations some effect from outgassing or ingassing of CO_2 may

influence the readings. The measurements for each experiment span a range of less than 0.5 pH units and point to a systematic trend over the duration of each experiment, thus indicating that random errors or disturbed signals are not a dominant feature. The in-line pH values from BOZ2-3 form an exception and vary over 0.8 pH units due to an apparent outlier at the end of the experiment. More details are discussed further below.

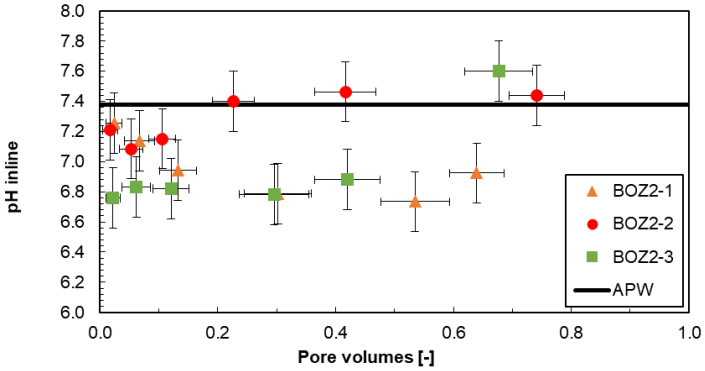

Fig. 4.7-7: Evolution of inline pH during advective displacement experiments

BOZ2-1 = BOZ2-1-425.69-AD (Passwang Formation); BOZ2-2 = BOZ2-1-500.93-AD (Opalinus Clay); BOZ2-3 = BOZ2-1-597.93-AD (Staffelegg Formation). Pore volume fractions relate to transport time based on water content. Experiment duration is 118 – 125 days. Horizontal length of symbol bar covers the sampling interval, vertical bars are an estimate of combined uncertainties.

4.7.5.4 Evolution of major and minor components

Evolution of concentrations with progress of percolation are shown in Figs. 4.7-8 to 4.7-13. Select analytical data for the first two aliquots sampled are summarised in Tab. 4.7-14 further below, with full details in Appendix B. The composition of the earliest aliquots displaced from the core samples are the most representative for the pore fluid extracted, and this is highlighted and interpreted in Section 4.7.5.5.

The displaced **major component Cl** presents a continous increase towards the APW in all three experiments and an exceptionally sharp increase in the first few samples in BOZ2-3. The major component **SO_4** behaves differently in all three experiments: the concentration starts above the APW in BOZ2-1 and decreases to values below the APW. In BOZ2-2 the sulphate concentrations start below the APW and increase slightly towards the APW after an initial drop in concentrations. In BOZ2-3 the SO_4 concentration starts also above the APW and decreases smoothely towards APW values.

The cations Na, Ca, Mg are initially less concentrated in the outflow than in the injected APW in BOZ2-1 and increase steadily towards it (Fig. 4.7-8). In BOZ2-2 and BOZ2-3 there are initially elevated Ca, Na and Mg concentrations above the APW that compensate for the exceptionally high nitrate, both decreasing with ongoing percolation (also see Tab. 4.7-10). In this case, nitrate forms a major component and is a carrier for anion charge along with chloride and sulphate (also see Tab. 4.7-10). BOZ2-1 is the sole sample with major ion concentrations (exept SO_4) that form an early plateau, whereas in the remaining experiments there is an initial drop or rise in major ion concentrations or a contineous rise towards the APW.

The same information as depicted in Fig. 4.7-8 is summarised for selected components for all three experiments (Fig. 4.7-9). A choice was made to use average compositions of the first two analysed aliquots to best represent the porewater composition. The resulting porefluid compositions are summarised in Tab. 4.7-15 (Section 4.7.5.5) and are also used in the integrative plots in Chapter 5.

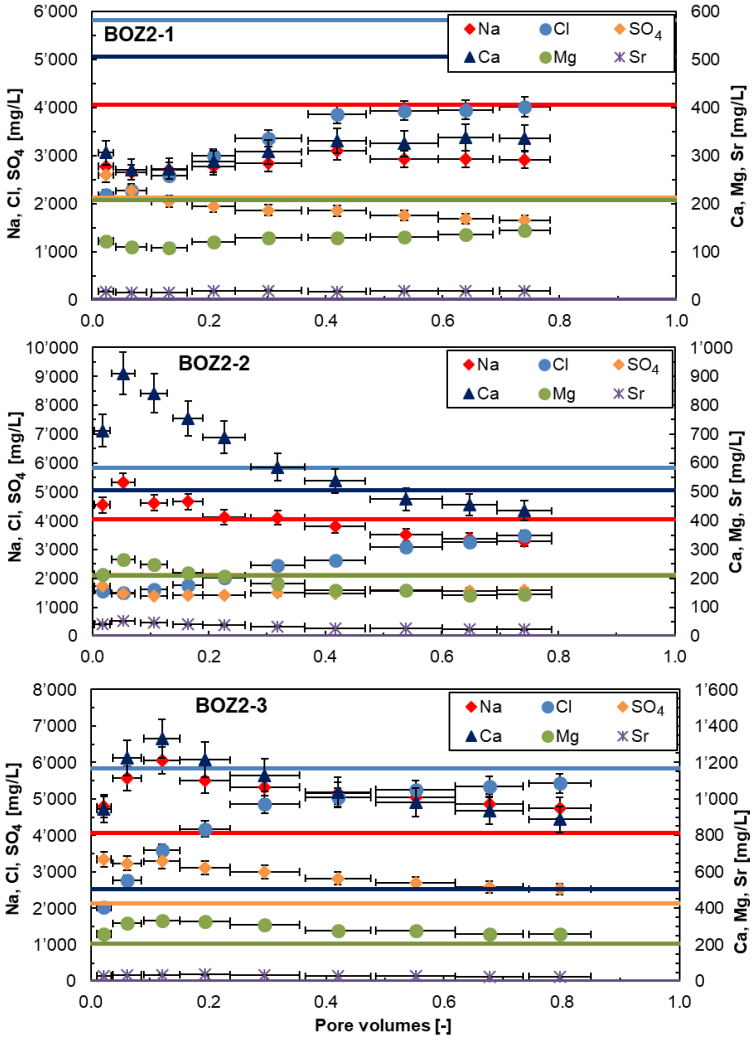

Fig. 4.7-8: Evolution of major components during advective displacement experiments

BOZ2-1 = BOZ2-1-425.69-AD (Passwang Formation); BOZ2-2 = BOZ2-1-500.93-AD (Opalinus Clay); BOZ2-3 = BOZ2-1-597.93-AD (Staffelegg Formation). Pore volume fractions relate to transport time based on water content. Experiment duration is 118 – 125 days. Horizontal length of symbol bar covers the sampling interval, vertical bars are an estimate of combined uncertainties. Horizontal lines represent the composition of the injected APW.

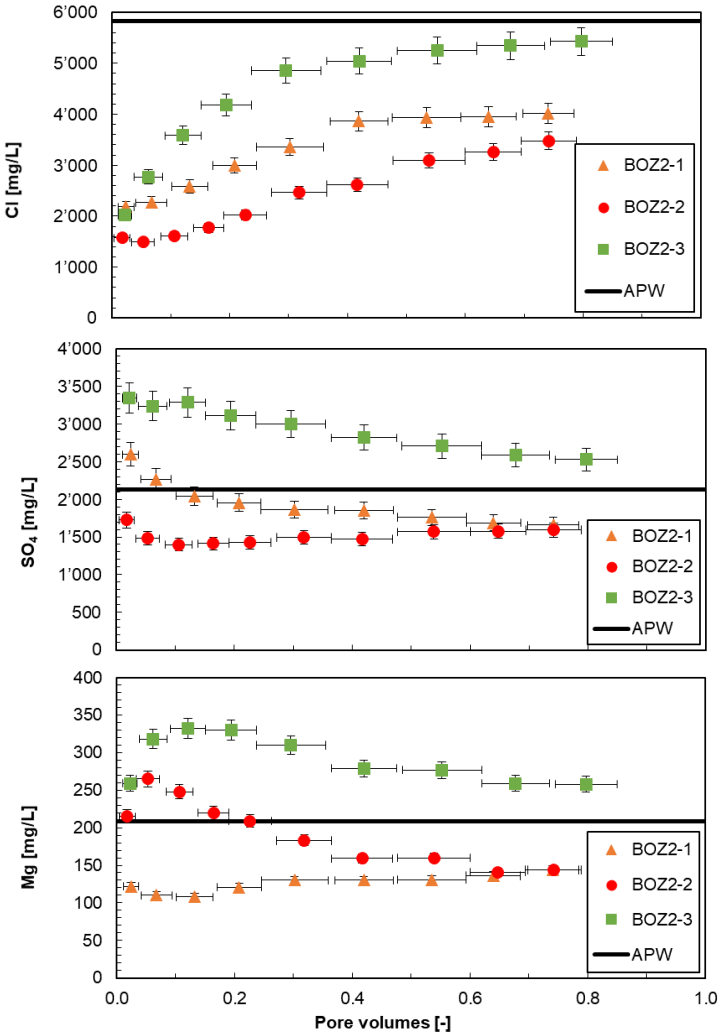

Fig. 4.7-9: Evolution of Cl, SO_4 and Mg during advective displacement experiments

BOZ2-1 = BOZ2-1-425.69-AD (Passwang Formation); BOZ2-2 = BOZ2-1-500.93-AD (Opalinus Clay); BOZ2-3 = BOZ2-1-597.93-AD (Staffelegg Formation). Pore volume fractions relate to transport time based on water content. Experiment duration is 118 – 125 days. Horizontal length of symbol bar covers the sampling interval, vertical bars are an estimate of combined uncertainties. Horizontal lines represent the composition of the injected APW.

Of the **minor components (Br, NO_3, K, Sr, Si)**, only potassium is present in the injected APW. Its concentration pattern shows an increase towards the APW in BOZ2-1 (Fig. 4.7-10). The other two experiments have a more complicated K concentration pattern with an initial increase and subsequent drop to a near constant concentration after 0.4 pore volumes. Bromide is gradually decreasing (details in Fig. 4.7-11) until being flushed out completely in all experiments. This can be used as a reversed break-through of an anionic tracer (see below). Dissolved silica elutes at 2 – 5 mg/L, in some cases slightly decreasing with time. Sr concentrations remain nearly constant in sample aliquots from BOZ2-1 but show an initial sharp increase and subsequent decrease in BOZ2-2 and BOZ2-3, despite not being present in the APW. The Sr behaviour in the latter two experiments is presumeably also related to the nitrate effect mentioned above that affects also Mg, Ca and Na.

Nitrate is a major component in the early aliquots in experiments BOZ2-2 and BOZ2-3 (Opalinus Clay and Staffelegg Formation). For these samples, the maximum values reach up to 11 g/L already in the first couple of aliquots, followed by a regular decrease (Fig. 4.7-10, Tab. 4.7-14, Appendix B). The elution of NO_3 in BOZ2-1 (Figs. 4.7-10 and 4.7-11, Tab. 4.7-14, Appendix B) starts at 800 mg/L and decreases to 4 mg/L over the course of the experiment. The origin of nitrate is still unknown, but a reactive nitrogen phase is suspected (associated with solid organic matter), which is not mobilised during comparably short and anaerobic aqueous extracts. There, only the samples from the Passwang Formation (BOZ2-1) show exceptionally high nitrate concentrations of 6 mg/L (other formations < 2 mg/L, Tab. 4.7-5). But aqueous extracts of post-mortem samples from the Opalinus Clay (BOZ2-2) and Staffelegg Formation (BOZ2-3) show nitrate concentrations up to 83 mg/L (Tab. 4.7-8), generally higher at the outlet side than at the inlet of the core. This indicates a nitrogen mobilisation during the AD experiment. Ammonium (NH_4) is near or below a detection limit of 10 mg/L in all exfiltrated sample aliquotes. Although the exact mechanism of nitrate mobilisation, presumably by oxidation from kerogen-bound nitrogen, is unclear, the substantial additional anion charge introduced must be balanced by cations, as mentioned above.

Ba and Al were measured by ICP-OES but always below detection limits. The detection limits depend on dilution factors and were 0.25 mg/L for Ba, and 0.25 – 2.5 mg/L for Al.

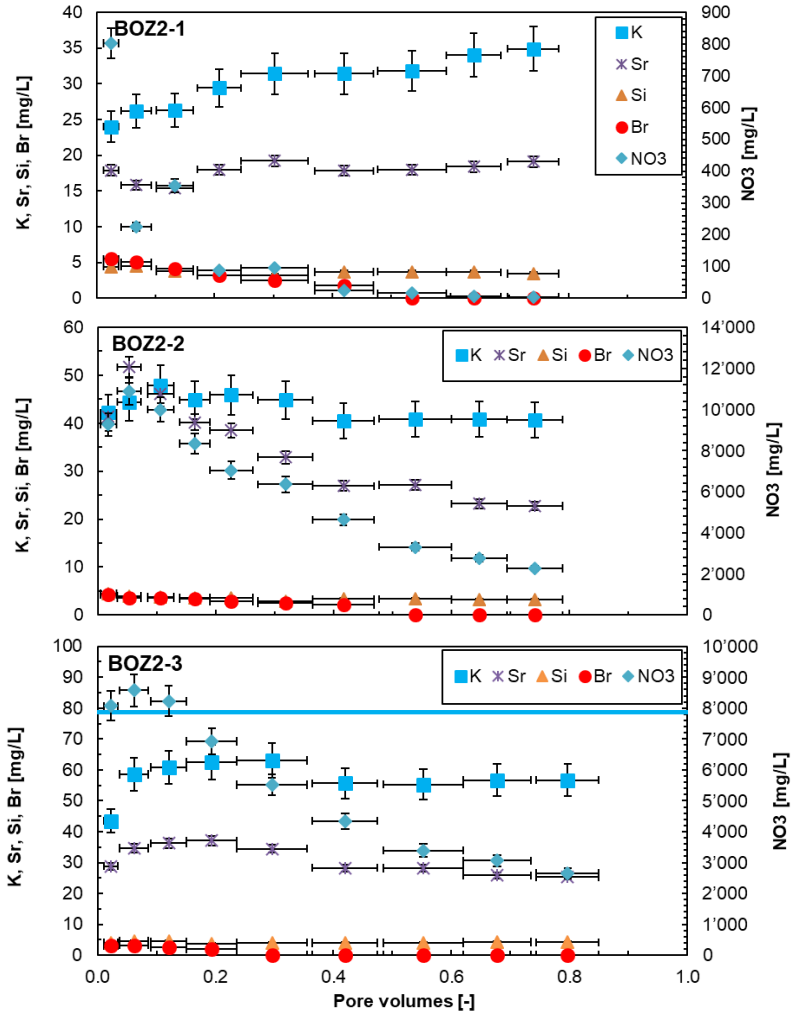

Fig. 4.7-10: Evolution of minor components during advective displacement experiments

BOZ2-1 = BOZ2-1-425.69-AD (Passwang Formation); BOZ2-2 = BOZ2-1-500.93-AD (Opalinus Clay); BOZ2-3 = BOZ2-1-597.93-AD (Staffelegg Formation). Pore volume fractions relate to transport time based on water content. Experiment duration is 118 – 125 days. Horizontal length of symbol bar covers the sampling interval, vertical bars are an estimate of combined uncertainties. Horizontal line represent the composition of the injected APW for K (0 for others).

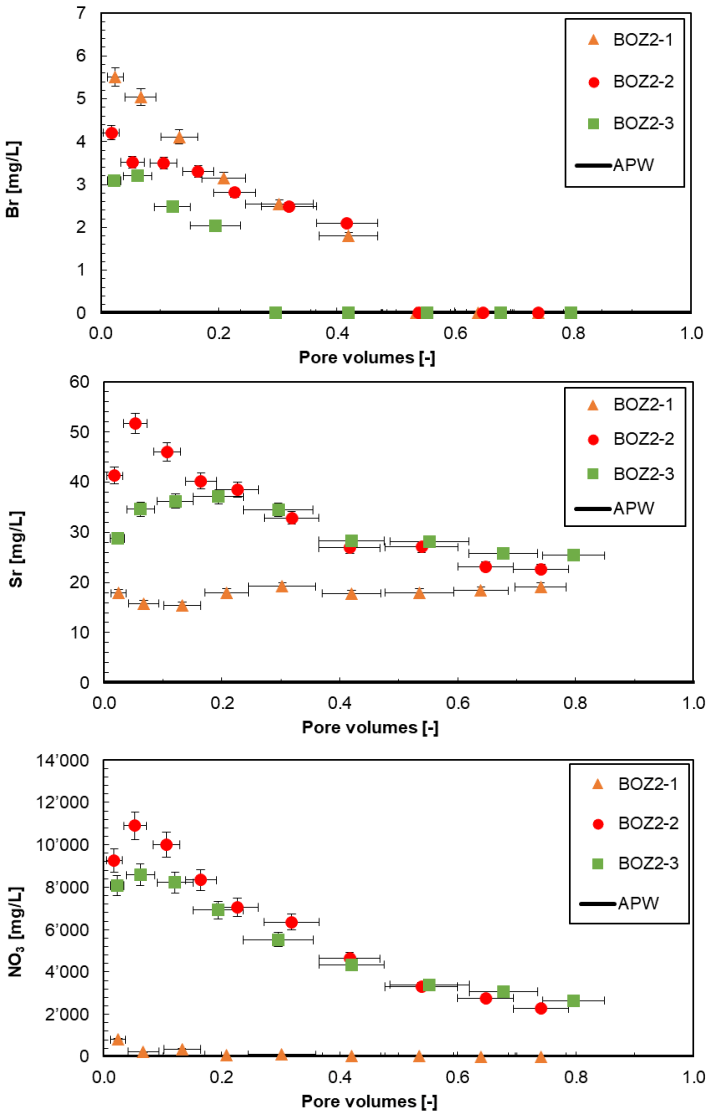

Fig. 4.7-11: Evolution of select minor components during advective displacement experiments

BOZ2-1 = BOZ2-1-425.69-AD (Passwang Formation); BOZ2-2 = BOZ2-1-500.93-AD (Opalinus Clay); BOZ2-3 = BOZ2-1-597.93-AD (Staffelegg Formation). Pore volume fractions relates to transport time based on water content. Experiment duration is 118 – 125 days. Horizontal length of symbol bar covers the sampling interval, vertical bars are an estimate of combined uncertainties. Br, Sr and NO_3 in the APW are 0. Br concentrations below detection are plotted at 0.

The **carbon system (TIC, TOC, TC, LMWOA)** shares as a common feature of all experiments that relatively large TOC concentrations are eluted initially (235 – 850 mg/L) that gradually decrease to 16 – 125 mg/L with progressive percolation (Fig. 4.7-12, Tab. 4.7-14 shows averages of first 2 aliquots). TOC clearly dominates the dissolved carbon inventory (TC) at early times. The TOC cannot be explained by low-molecular-weight organic acids (LMWOA), since acetate, propionate and formate are below the limit of detection in all three experiments.

Aqueous extracts (Tab. 4.7-5) imply TOC values of 300 – 500 mg/L when scaled to porewater content, which almost covers the range observed in the early aliquots. Aqueous extracts carried out post-mortem (Tab. 4.7-8) show similar TOC concentrations compared to the initial state and

in case of BOZ2-2 and BOZ2-3 even a slight increase at the top end of the experiment. The former observations are similar to previous work, with samples from the Schlattingen-1 geothermal well (Mäder & Waber 2017) and also TBO borehole BUL1-1 (Mazurek et al. 2021), TRU1-1 (Aschwanden et al. 2021), MAR1-1 (Mäder et al. 2021) and BOZ1-1 (Wersin et al. 2022).

TIC elutes initially at much lower concentrations than TOC, but covers a wide range of concentrations, and trends for each experiment are dissimilar to some extent (Figs. 4.7-12 and 4.7-13). Microbial activity might influence TIC/TOC, either in the syringe itself (i.e. during sampling/storage) or at the surface of the core sample, whereby a part of organic carbon might be oxidised to inorganic carbon, e.g. coupled with sulphate reduction.

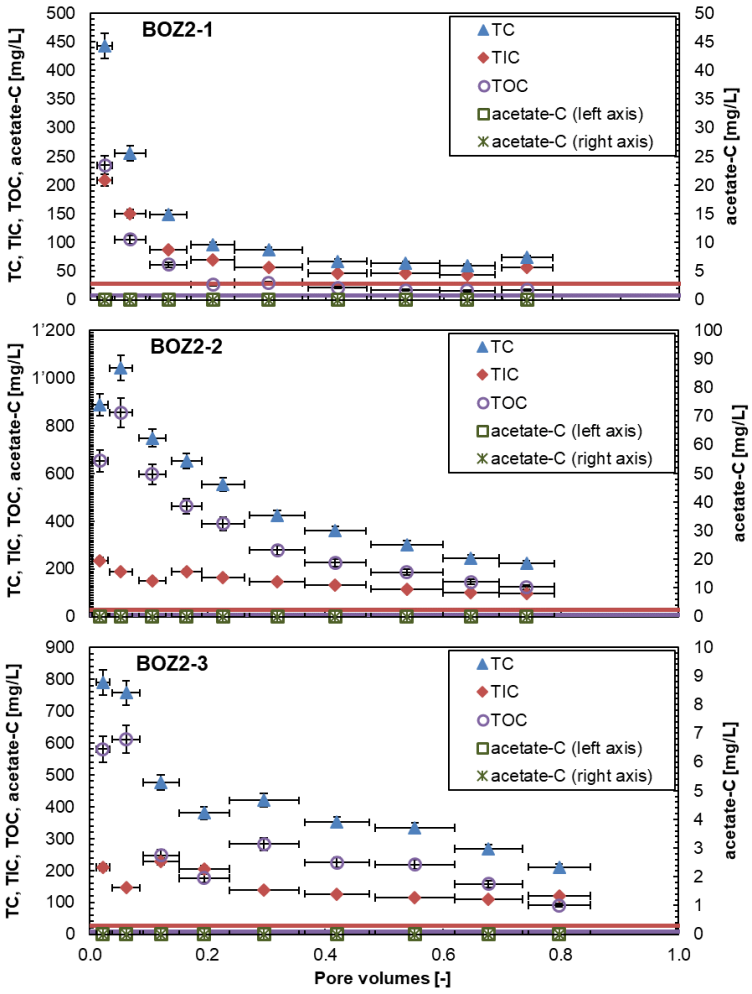

Fig. 4.7-12: Evolution of carbon system during advective displacement experiments

BOZ2-1 = BOZ2-1-425.69-AD (Passwang Formation); BOZ2-2 = BOZ2-1-500.93-AD (Opalinus Clay); BOZ2-3 = BOZ2-1-597.93-AD (Staffelegg Formation). Pore volume fractions relate to transport time based on water content. Experiment duration is 118 – 125 days. Horizontal length of symbol bar covers the sampling interval, vertical bars are an estimate of combined uncertainties. Horizontal lines represent the composition of the injected APW.

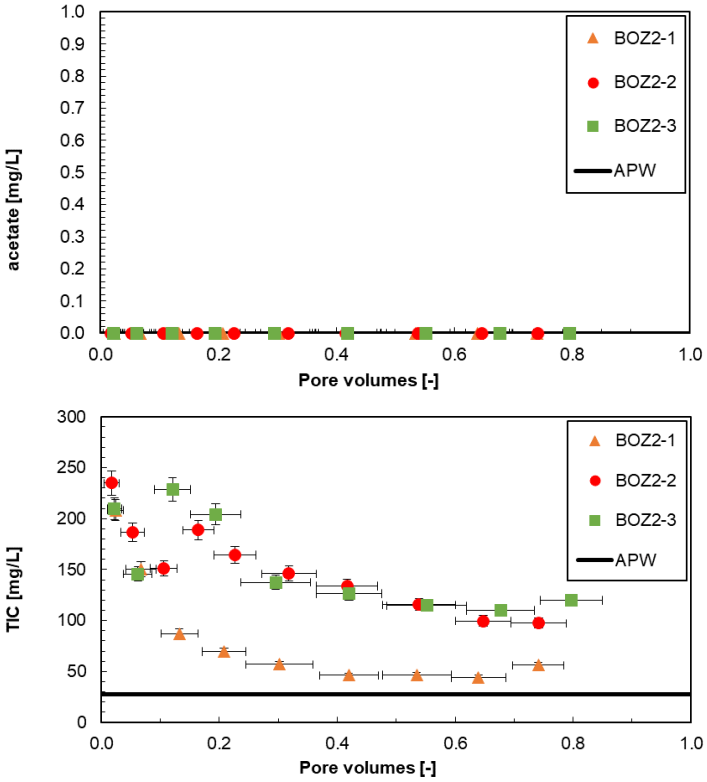

Fig. 4.7-13: Evolution of select carbon components during advective displacement experiments

BOZ2-1 = BOZ2-1-425.69-AD (Passwang Formation); BOZ2-2 = BOZ2-1-500.93-AD (Opalinus Clay); BOZ2-3 = BOZ2-1-597.93-AD (Staffelegg Formation). Pore volume fractions relate to transport time based on water content. Experiment duration is 118 – 125 days. Horizontal length of symbol bar covers the sampling interval, vertical bars are an estimate of combined uncertainties. Horizontal lines represent the composition of the injected APW. Concentrations below detection (acetate) are plotted at 0.

The **measurement of pH** was performed in-line between some of the sampling intervals (setup in Waber (ed.) 2020; *cf.* Section 4.7.5.3) and in the laboratory when syringe aliquots were prepared/preserved for analysis. The latter was done in most cases very shortly after sampling (one to a few hours), or after a few days of storage. The total range covered for all samples, in-line and laboratory, is 6.7 – 7.6 (Fig. 4.7-14), both showing similar spreads. In BOZ2-1 there is a systematic offset between the in-line and laboratory measured pH with the in-line pH presenting lower values. This can be explained by outgasing of CO_2 during the laboratory measured pH leading to higher values.

The laboratory measured pH presents some increasing and decreasing trends with variations of 0.2 – 0.6 pH units. The calculated partial pressure of CO_2 is larger than atmospheric in the aliquots, and this bears the potential for outgassing and resultant supersaturation with respect to calcite, and a possibility for some loss of Ca and TIC by precipitation.

It should be noted that in samples with the large initial nitrate concentrations (BOZ2-2 and BOZ2-3) there is some uncertainty regarding the generation of this dissolved nitrate. Depending on the processes, this could also affect pH values. While the pH may still be representative of the porewater of the experiment, it may deviate from the undisturbed state.

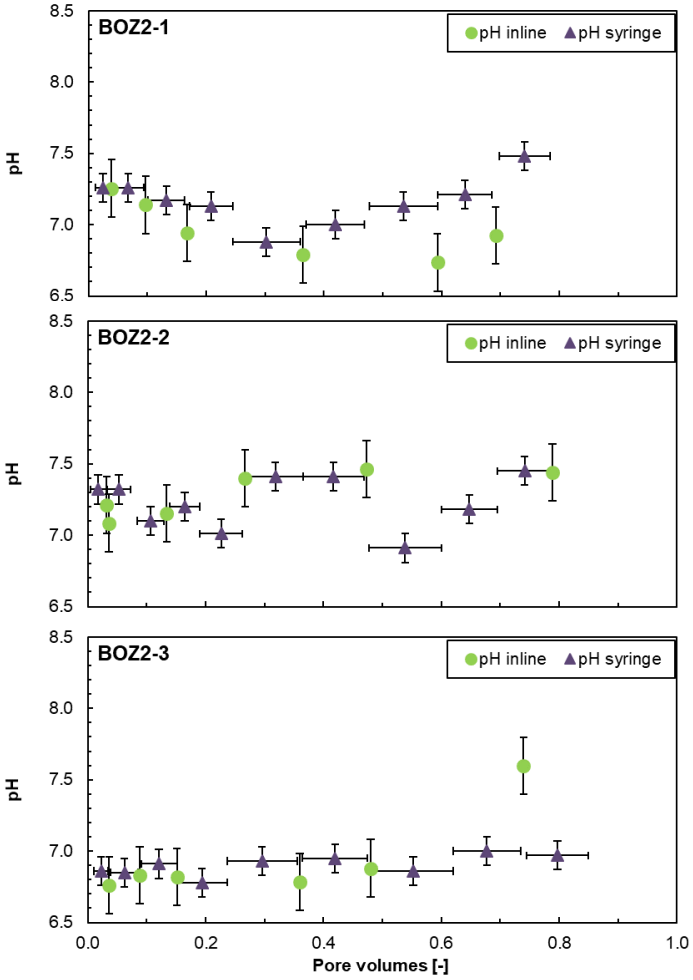

Fig. 4.7-14: Evolution of pH during advective displacement experiments

BOZ2-1 = BOZ2-1-425.69-AD (Passwang Formation); BOZ2-2 = BOZ2-1-500.93-AD (Opalinus Clay); BOZ2-3 = BOZ2-1-597.93-AD (Staffelegg Formation). Pore volume fractions relate to transport time based on water content. Experiment duration is 118 – 125 days. Horizontal length of symbol bar covers the sampling interval, vertical bars are an estimate of combined uncertainties.

4.7.5.5 Early displaced aliquots representing the porewater composition

Early displaced aliquots were generally obtained by averaging the first two measured samples (Tab. 4.7-15). Interpretation of these early displaced aliquots as being representative of the in situ porewater, contained in the core at the time of the experiment, requires integration and interpretation of the entire dataset supported with geochemical calculations. Comprehensive reactive transport simulations are expected to further restrict the initial porewater compositions, as well as the transport properties of the cores. Only speciation calculations are included in this data report

for the early compositions. Speciation calculations for all individual syringes are provided in Appendix B. The laboratory pH values were used for the speciation calculations. TIC was used as a constraint for inorganic carbon. In case of BOZ2-2 and BOZ2-3 there are high nitrate concentrations already in the first syringes which is indicative for a disturbed porewater (Tab. 4.7-14).

Tab. 4.7-14: Composition of earliest two aliquots from advective displacement experiments

Parameter	**Unit**	**BOZ2-1**	**BOZ2-2**	**BOZ2-3**
Depth	[m]	425.69	500.93	597.93
Sample ID RWI		BOZ2-1-425.69-AD	BOZ2-1-500.93-AD	BOZ2-1-597.93-AD
Lab sample ID		BOZ2-1xx-AD	BOZ2-2xx-AD	BOZ2-3xx-AD
Geological unit		Passwang Formation	Opalinus Clay	Staffelegg Formation
pH inline	[-]	7.20	7.15	6.80
pH lab	[-]	7.26	7.32	6.86
Na	[mg/L]	2'716	4'939	5'174
K	[mg/L]	25.1	43.3	51.1
Ca	[mg/L]	288.5	811	1'085
Mg	[mg/L]	116	240	288.5
Sr	[mg/L]	16.9	46.5	31.7
Ba	[mg/L]	< 0.25	< 0.25	< 0.25
Si	[mg/L]	4.46	4.20	4.33
Al	[mg/L]	< 2.5	< 2.5	< 2.5
F	[mg/L]	1.97	< 1.6	1.12
Cl	[mg/L]	2'226	1'533	2'396
Br	[mg/L]	5.3	3.865	3.145
NO_3	[mg/L]	514	10'084	8'322
SO_4	[mg/L]	2'432	1'602	3'291
TOC	[mg/L]	169.9	753.3	595.5
TIC	[mg/L]	179.3	210.75	177.8
lactate	[mg/L]	< 20	< 20	< 20
acetate	[mg/L]	< 20	< 20	< 20
propionate	[mg/L]	< 20	< 20	< 20
formate	[mg/L]	< 20	< 20	< 20
$\delta^{18}O$	[‰VSMOW]	-6.31	-6.87	-6.92
$\delta^{2}H$	[‰VSMOW]	-48.1	-49.8	-50.9

n.a.: not analysed

The speciation calculations (Tab. 4.7-15) reveal a cation charge surplus (positive 'Charge') that is not large and partially explained by significant TOC concentrations that were not included in the speciation. TIC was used as constraint for inorganic carbon. The aliquots are all significantly oversaturated with respect to calcite and also dolomite. Such oversaturation may result from shifts in pH linked to potential ingassing or outgassing of CO_2 during sampling and storage. Alternatively, the large TOC (and TC) contents pose analytical difficulties to obtain TIC, and associated errors may be larger than commonly assigned to TIC measurements.

Saturation is also reached or slightly exceeded for celestite and in the case of BOZ2-2 also for strontianite. Gypsum saturation is only reached in the lower-most formation (Staffelegg Formation, BOZ2-3). The implication is that the ion-activity products ($[Sr]\cdot[SO_4]$) and ($[Ca]\cdot[SO_4]$) are controlling factors, but this does not necessarily mean that these minerals are also present in the core before the experiments. There are larger SO_4, Ca and Sr concentrations in the the early aliquots than in the APW except for BOZ2-2 with SO_4 and BOZ2-1 with Ca concentrations below the APW (Figs. 4.7-8 and 4.7-11). The high initial SO_4 and Ca concentrations in BOZ2-3 can explain the saturation with respect to gypsum. The high initial Ca concentration in BOZ2-2 and BOZ2-3 can be explained by the high nitrate elution which either cause calcite dissolution and/or induce cation exchange reactions.

A more in-depth analysis and interpretation will have to be carried out, including reconstructions by geochemical modelling.

Tab. 4.7-15: Saturation state of earliest two aliquots from advective displacement experiments

Parameter	**Unit**	**BOZ2-1**	**BOZ2-2**	**BOZ2-3**
Depth	[m]	425.69	500.93	597.93
Geological unit		Passwang Formation	Opalinus Clay	Staffelegg Formation
Charge	[eq/kg_w]	7.6E-03	2.2E-02	2.3E-02
%-Error		2.96	4.22	4.15
Acetate	[eq/kg_w]	< 3.4E-4	< 3.4E-4	< 3.4E-4
Ionic strength	[mol/kg_w]	0.16	0.29	0.32
tot_alk	[eq/kg_w]	1.4E-02	1.7E-02	1.3E-02
pH (Lab)		7.26	7.32	6.86
log P_{CO2}		-1.45	-1.47	-1.14
SI(calcite)		0.62	1.18	0.68
SI(dolomite-o)		1.16	2.18	1.11
SI(dolomite-d)		0.61	1.63	0.56
SI(gypsum)		-0.42	-0.29	0.08
SI(celestite)		0.06	0.19	0.27
SI(strontianite)		-0.17	0.39	-0.41
SI(anhydrite)		-0.64	-0.51	-0.13

PSI/Nagra 2012 thermodynamic database (Thoenen et al. 2014), calculated in PHREEQC for 25 °C; dolomite-o: ordered dolomite; dolomite-d: disordered dolomite; charge = Σ(cation charge) – |Σ(anion charge)| ; %-error = 100*charge / (Σ(cation charge) + |Σ(anion charge)|).

4.7.5.6 Initial values and evolution of stable water isotope composition

Common to all three experiments (Fig. 4.7-15) is a relatively smooth evolution of $\delta^{18}O$ towards the APW value with progress of percolation. Unlike some major chemical components (e.g. chloride), the breakthrough trend starts immediately with the first sample aliquot. The percolated pore volume is limited in all experiments and therefore no complete breakthrough of the APW is reached.

The behaviour for $\delta^{2}H$ is distinctly different and shows initially a reverse trend towards more negative values that goes through a minimum at 0.1 – 0.45 pore volumes (BOZ2-1 and BOZ2-3 experiments). In experiment BOZ2-2 (Opalinus Clay) the $\delta^{2}H$ remains at a minimum until the end of the experiment. The extent of breakthrough is much less compared to $\delta^{18}O$ for reasons that may not be intuitively obvious and are not yet resolved in detail, however, a couple of hypotheses are discussed further below.

The stable isotope composition in $\delta^{18}O$ versus $\delta^{2}H$ coordinates (Fig. 4.7-16) for experiment BOZ2-3 displays a slightly curved data array extending from the earliest and isotopically light ($\delta^{2}H$) or heaviest ($\delta^{18}O$) aliquot towards the APW isotopic composition. For the two other experiments, the evolution towards the APW is distinctly retarded and samples initially follow the global meteoric water line before the trend bends towards the APW. Earliest aliquots of all three experiments (on right side of arrays) define a trend just below the global meteoric water line.

One hypothesis for the difference in breakthrough curves of $\delta^{18}O$ and $\delta^{2}H$ is that there is an effect from dry cutting the core surfaces during sample preparation. This may induce evaporation of small amounts of porewater in the close vicinity of the cut surfaces, thus, enriching the residual porewater in heavy isotopes. Percolation would then first yield isotopically heavy signatures, which are then gradually mixed with the unaffected porewater signature, and increasingly also affected by the breakthrough of the traced APW (ca. +100 ‰ VSMOW for $\delta^{2}H$ and -11.5 ‰ VSMOW for $\delta^{18}O$). This would explain qualitatively the observed initial trends for $\delta^{2}H$, but not the prolonged delay of the APW breakthrough compared to $\delta^{18}O$. In the case of the oxygen isotopes, the APW is significantly lighter than the in situ porewater and accordingly, the trend of $\delta^{18}O$ will always decrease as a function of replaced pore volumes (i.e., first by mixing with the non-evaporated and heavier porewater and later with the APW). This could explain the apparent immediate breakthrough behaviour. In older studies, wet cutting was used rather than dry cutting, and this led to a small component of contamination by tap water for the early extracted water isotopes (Mäder & Waber 2017). However, the early aliquots in the BOZ2-1 and BOZ2-2 experiments are isotopically lighter than neighbouring isotopic exchange experiments (Fig. 5.7-1), contradicting the potential evaporation effect. For experiment BOZ2-3 the evaporation effect on the initial aliquots can not be ruled out.

Another possibility is admixing an isotopically light H and O component along with the nitrate and TOC mobilisation into the porewater. In particular, any microbial activity in the core or on its surface, which might be involved in the high mobilisation of nitrate and TOC as well as the degradation of organic matter into TIC, can induce a isotopically light signature.

Furthermore, precipitation of hydrous minerals that may be induced by advective displacement may affect the water isotopic composition in the progressing experiment.

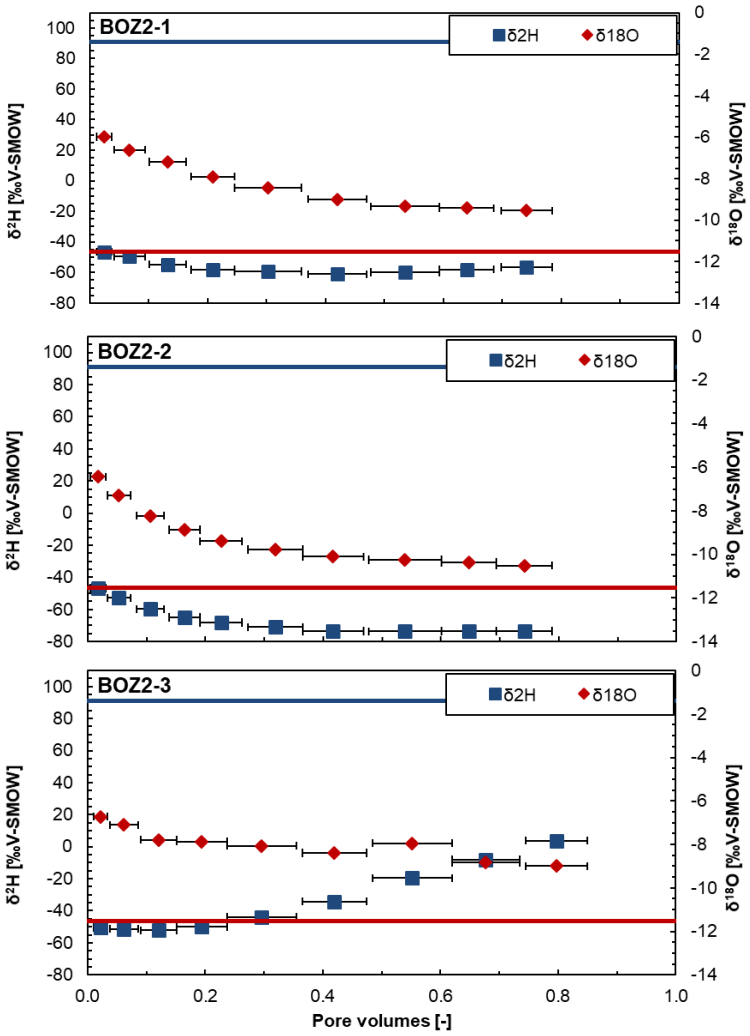

Fig. 4.7-15: Evolution of δ^2H and $\delta^{18}O$ during advective displacement experiments

BOZ2-1 = BOZ2-1-425.69-AD (Passwang Formation); BOZ2-2 = BOZ2-1-500.93-AD (Opalinus Clay); BOZ2-3 = BOZ2-1-597.93-AD (Staffelegg Formation). Pore volume fractions relate to transport time based on water content. Experiment duration is 118 – 125 days. Horizontal length of symbol bar covers the sampling interval. Measurement errors are 1.5 ‰ for δ^2H and 0.1 ‰ for $\delta^{18}O$. Lines denote concentrations of APW.

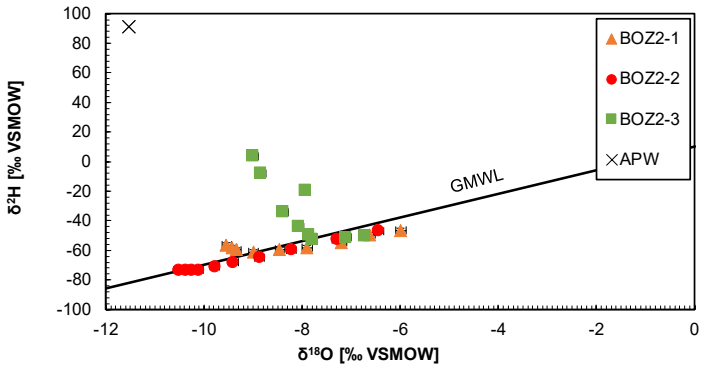

Fig. 4.7-16: Stable isotope composition of aliquots from advective displacement experiments

BOZ2-1 = BOZ2-1-425.69-AD (Passwang Formation); BOZ2-2 = BOZ2-1-500.93-AD (Opalinus Clay); BOZ2-3 = BOZ2-1-597.93-AD (Staffelegg Formation). Measurement errors are 1.5 ‰ for δ^2H and 0.1 ‰ for $\delta^{18}O$. GMWL is the global meteoric water line. 1st aliquots are located the furthest to the right, and evolve towards the left.

4.7.6 Derivation of anion-accessible porosity

There are several ways by which chloride and bromide accessible porosity fractions may be obtained. The principle is the same: namely the ratio between the anion concentration obtained from aqueous extracts scaled to porewater content divided by that obtained from earliest aliquots from the percolation experiments (discussion in Waber (ed.) 2020 and Mäder 2018). There are some variants depending on how water contents were measured and averaged, or how inferred initial desaturation is taken into account. In the case where a full or well-advanced breakthrough in chloride is captured, such a ratio may also be obtained by post-mortem aqueous extracts (top and base) and the latest aliquots sampled before the end of the experiments (for the outlet / top), or the injected APW (for the inlet / base). Normally, bromide drops below detection and only the chloride data can be evaluated for post-mortem datasets. The bromide data commonly is more 'noisy'.

The top two data lines (Tab. 4.7-16) list the average concentrations (Cl, Br) for the first two displaced aliquots as shown in Tab. 4.7-14. The third line lists the concentration of Cl in the last syringe sampled (for post-mortem evaluation). The following three lines list different Cl concentrations from the pre-characterisation up-scaled to water content: for the sample from above the AD core (_upscaled_top), for the sample from below (_upscaled_base) and a corrected and averaged value (top and base). The correction compensates for a small amount of water loss (unsaturated volume) commonly observed and evaluated from a measured net water uptake. The net water uptake is the measured water uptake (mass gain of the core during the experiment) corrected for a commonly measured small volume increase during the experiment (Section 4.7.3 and Tab. 4.7-4). The correction hinges on the assumption that sample treatment for the AD core and the off-cuts share the same history (core handling, storage, sample preparation) and therefore also potentially underwent similar water losses. These corrections are rather small, with small net water uptakes. The following three lines contain the same data for Br. The observed range in up-scaled concentrations is an indication of heterogeneity, mainly in clay-mineral content. A homogeneous sample with respect to the degree of anion-exclusion should yield the same up-scaled Cl or Br concentrations, despite differences in water content. A consistent proportion of anion-accessible porosity would then be evaluated regardless of choosing a sample from the top or from the base as a reference for the early displaced aliquots. The two data lines for Cl suffixed with _p-m are the up-scaled chloride concentrations evaluated post-mortem from aqueous extracts from the top of the core (outlet to sampling) and the base of the core (APW inlet).

The final data block (Tab. 4.7-16) lists the accessible porosity fraction obtained by various combinations and averaging. The first four lines list values that are derived without knowledge of the net water uptake. The next two lines, including the suffix _corr, indicate values obtained after applying a correction for net water uptake as mentioned above. The last two data lines represent the post-mortem evaluations of the top of the core (outlet) and the base of the core (inlet).

There is good agreement and a rather high degree of consistency among the different ways of evaluation and data derived from pre-characterisation within each experiment. The two post-mortem chloride accessible porosity fractions calculated for each core are consistent in itself, too, but differ significantly from the values calculated from the pre-characterisation and early porewater aliquots. Changes in accessible porosity fraction during the course of the experiment must be related to the changes in porewater composition, induced by the gradual replacement of the initial porewater by the injected APW. The effect of an early small unsaturated pore volume or of some sample consolidation during the experiment is considered minor based on the narrow range of hydraulic conductivities (Section 4.7.5.2). In general, an increasing ionic strength of the porewater is expected to increase the anion accessible porosity fraction due to the contraction of the width of the diffuse layer next to the negatively charged surfaces. For each of the three experiments however, the ionic strength of early displaced aliquots, late aliquots and the APW (0.23 mol/L) differs by less than 0.1 mol/L and might thus not provide a straight-forward explanation to the observed different pre- and post chloride accessbile porosity fractions. More complex, not yet understood, effects of the porewater composition, such as the chloride content itself, as well as the prevailing anions and cations appear to influence the chloride accessible porosity considerably. Hence, the Cl accessible porosity fraction derived from the pre-characterisation and early aliquots is generally recommended as the value to approach the in situ conditions at best and is here also selected for experiment BOZ2-1. A Cl accessible porosity fraction of 0.32 is obtained, which is on the lower side for a clay-mineral content of 35 wt.-% but compares well to the value of 0.31 for the Passwang Formation in the closeby TBO borehole BOZ1-1 (Wersin et al. 2022).

In contrast, the early evolution of the porewater aliquots in experiments BOZ2-2 and BOZ2-3 were highly affected by the increased nitrate concentration and associated processes such as presumably (microbial-) degradation of organics, dissolution of calcite and considerable gas production. Moreover, the aqueous extract sample taken before the start of the experiment appears uninfluenced by this disturbance, making a comparison of the pre-characterisation aqueous extract with the first porewater aliquots doubtful. The derived Cl-accessible porosity fraction are affected by experimentally induced artefacts, rather than in situ conditions. To account for this large uncertainty in the early porewater evolution, a choice was made to recommend for these two experiments the Cl accessible porosity based on the post-mortem AqEx of the base and the APW, for which the effect of nitrate was minimised. The value of 0.45 calculated for the Opalinus Clay sample is well in accordance to the range of 0.42 to 0.51 determined previously for Opalinus Clay with the same approach, and thus for the same APW porewater composition in the TBO boreholes BUL1-1 (Mazurek et al. 2021), TRU1-1 (Aschwanden et al. 2021), MAR1-1 (Mäder et al. 2021) and BOZ1-1 (Wersin et al. 2022). Similarly, the post-mortem value for the Staffelegg Formation fits in the range reported previously. The remaining uncertainty of the Cl-accessible porosity fraction associated with the different composition of the porewater compared with the APW can be quantified based on the comparison of pre- and post- Cl accessible porosity fractions of the previous boreholes, which are less than 0.09 and 0.17 for the Opalinus Clay and the Staffelegg Formation, respectively. In experiment BOZ2-1 (Passwang Formation), which was not significantly affected by the nitrate, the shift from porewater to APW increased the Cl accessible porosity fraction by 0.17, from 0.32 to 0.49. This latter difference appears to be rather large given a moderate change in ionic strength (from 0.16 to 0.22 M), and this should be further addressed in the context of an increasing number of measurements.

A reliable bromide accessible porosity could only be calculated for experiment BOZ2-1, because data for the other two experiments were presumeably affected by nitrate as discussed above, and Br is not present in the APW to be used in a post-mortem evaluation. The bromide accessible porosity fraction is with 0.53 significantly larger than the one for Cl. This was, to a lesser extent, also observed in some previous experiments, however, a good explanation for this is still lacking, except the Br may have some affinity for organic carbon components and these are seen to be disturbed during the early phase of advective displacement.

The accuracy is, in addition to the above discussed effect of porewater chemistry and nitrate, limited by the basic assumptions underlying the approach and by sample heterogeneity to some degree, mainly in clay-mineral content. The combined measurement uncertainties are dominated by the analytical error associated with Cl and Br concentrations but are probably not more than ± 10% for chloride.

Tab. 4.7-16: Chloride and bromide-accessible porosity fractions

Preferred values are shaded in blue; values in italic are unreliable due to interferences with nitrate.

Parameter	**Unit**	**BOZ2-1**	**BOZ2-2**	**BOZ2-3**
Depth	[m]	425.69	500.93	597.93
Geol. unit		Passwang Formation	Opalinus Clay	Staffelegg Formation
Cl-AD_ave (1-2)	[mg/L]	2226	1533	2396
Br-AD_ave (1-2)	[mg/L]	5.28	3.87	3.15
Cl_AD_last	[mg/L]	4014	3480	5425
Cl-AqEx-upscaled_top	[mg/L]	706	854	621
Cl-AqEx-upscaled_base	[mg/L]	759	855	606
Cl-AqEx-upscaled_ave_corr	[mg/L]	**712**	**814**	**588**
Br-AqEx-upscaled_top	[mg/L]	2.73	3.06	1.93
Br-AqEx-upscaled_base	[mg/L]	3.00	2.91	1.89
Br-AqEx-upscaled_ave_corr	[mg/L]	2.79	2.84	1.83
Cl-AqEx-upscaled_top_p-m	[mg/L]	1915	1682	2881
Cl-AqEx-upscaled_base_p-m	[mg/L]	2831	2599	2855
Cl-AqEx_top / Cl-AD_ave		0.32	*0.56*	*0.26*
Br-AqEx_top / Br-AD_ave		0.52	*0.79*	*0.61*
Cl-AqEx_ave / Cl-AD_ave		0.33	*0.56*	*0.26*
Br-AqEx_ave / Br-AD_ave		0.54	*0.77*	*0.61*
Cl-AqEx_ave_corr / Cl-AD_ave		**0.32**	*0.53*	*0.25*
Br-AqEx_ave_corr / Br-AD_ave		0.53	*0.74*	*0.58*
Cl_AqEx_p-m_top / Cl_last_AD		0.48	0.48	0.53
Cl_AqEx_p-m_base / Cl_APW		0.49	**0.45**	**0.49**

4.7.7 Transport properties marked by breakthrough of δ^2H, $\delta^{18}O$, Cl and Br

There are four components that can be used to elucidate on transport properties by their breakthrough behaviour, namely Cl, Br, and the water isotopes δ^2H and $\delta^{18}O$. Chloride is a good tracer in all three experiments, because the APW has a distinctly higher Cl concentration than the in-situ porewater. The resolution towards a full breakthrough is diminished because small differences between large concentrations can no longer be resolved. Bromide is a break-out tracer that is gradually flushed out of the core (no Br in the APW). Again, as a full break-out is approached, bromide concentrations tend to fall below the detection limit. Water tracers also feature a considerable contrast between the in situ porewater (Tab. 4.7-15) and the APW.

For comparison (Fig. 4.7-17), all breakthrough data are normalised to 1 and bromide is inverted to mimic a breakthrough behaviour. The normalised breakthrough of chloride, for example, is given by $1-(Cl-Cl_{APW})/(Cl_{PW}-Cl_{APW})$, where Cl_{PW} refers to the value of the early aliquots representing the in situ porewater composition (Tab. 4.7-14).

Chloride breakthrough is slower than that of bromide, except for BOZ2-3. This same behaviour was illustrated in earlier work by Mäder (2018), where a slightly faster breakthrough for Br was observed. This observation is at odds with the slightly larger reported Br-accessible pore fraction compared to Cl. A larger accessible pore fraction would tend to delay the Br breakthrough compared to Cl. Currently, no clear explanation of these discrepancy is possible. Bromide breakthrough cannot be tracked beyond the percolation progress where it drops below detection (seemingly missing points in Fig. 4.7-17). There is some ambiguity in dealing with data scatter that may be present in the first few syringe compositions (e.g. Br, Cl), and the choice made to define the initial value that is used for normalisation of breakthrough curves. Different choices may shift curves somewhat, but this is a minor effect for these relatively smooth data trends.

Fig. 4.7-18 illustrates the breakthrough behaviour of the Br/Cl molal ratio vs. time (pore volume fraction). Plotting the ratio removes some of the data scatter of the individual data series and illustrates similarities between the different experiments and thus also highlights any differences. The three experiments form a set of nearly parallel curves. The trends of decreasing Br/Cl ratios are mainly caused by the washing out of bromide (no Br in the injected APW), the increase in Cl concentrations towards the APW and to a minor extent by the small observed difference of Br transport vs. Cl transport properties (mentioned above). The offset between the Br/Cl ratio in the AqEx and the early aliquot, in particular in experiment BOZ2-3, visualises the discrepancy of Cl and Br accessible porosity fractions discussed in Section 4.7.6.

$\delta^{18}O$ is expected to break through more slowly compared to the anions Br and Cl. However, this is observed solely in experiment BOZ2-3. In experiment BOZ2-1, $\delta^{18}O$ breakthrough falls between Cl and Br breakthrough and is faster than both anions in BOZ2-2. δ^2H displays an anomalous behaviour during the early breakthrough, possibly for reasons discussed in Section 4.7.5. Deuterium lags considerably behind oxygen, in experiments BOZ2-1 and BOZ2-2 even lacking any clear breakthrough behaviour within the first 0.4 to 0.8 PV, suggesting some sort of retardation mechanism that is presently not understood (see Section 4.7.5). The unexpected breakthrough behaviour of $\delta^{18}O$ and δ^2H in experiments BOZ2-1, BOZ2-2, and (only δ^2H) BOZ2-3 cannot be explained currently; it is very likely related to the disturbances discussed in Section 4.7.5.

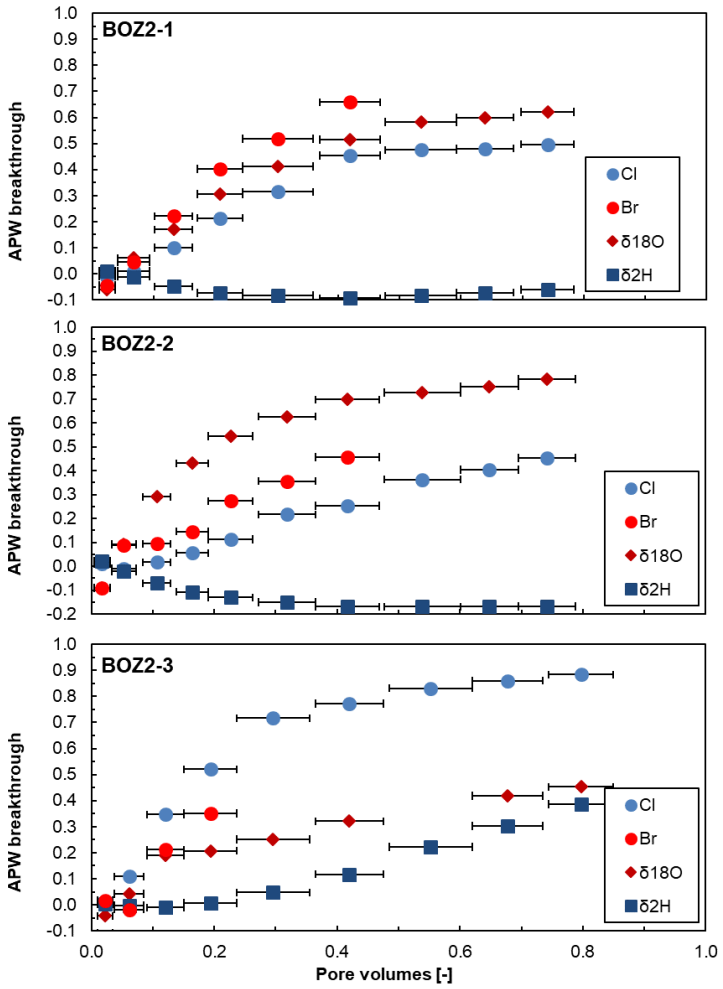

Fig. 4.7-17: Breakthrough of Cl, Br, δ^2H and $\delta^{18}O$ during advective displacement experiments

BOZ2-1 = BOZ2-1-425.69-AD (Passwang Formation); BOZ2-2 = BOZ2-1-500.93-AD (Opalinus Clay); BOZ2-3 = BOZ2-1-597.93-AD (Staffelegg Formation). Pore volume fractions relate to transport time based on water content. Experiment duration is 118 – 125 days. Horizontal length of symbol bar covers the sampling interval.

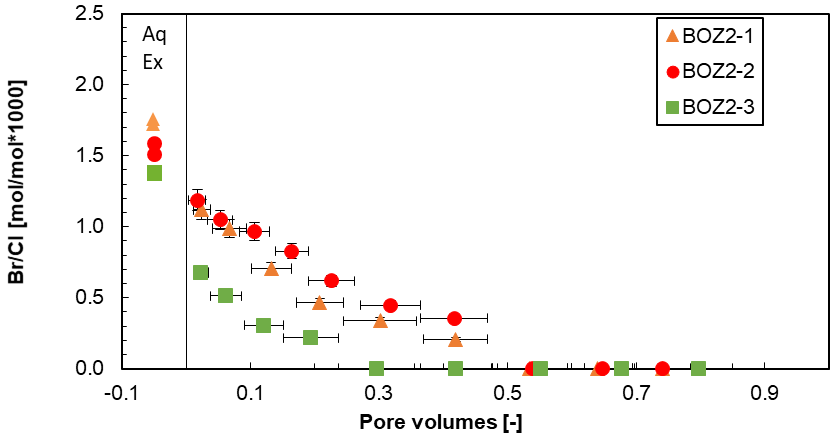

Fig. 4.7-18: Breakthrough of Cl/Br during advective displacement experiments

Data on left side (top graph, 'Aq Ex') are the ratios measured in the aqueous extracts perfomed for pre-characterisation. Ratios plotted at 0 correspond to later aliquots where Br concentration drops below detection. BOZ2-1 = BOZ2-1-425.69-AD (Passwang Formation); BOZ2-2 = BOZ2-1-500.93-AD (Opalinus Clay); BOZ2-3 = BOZ2-1-597.93-AD (Staffelegg Formation); APW = artificial porewater. Pore volume fractions relate to transport time based on water content. Horizontal length of symbol bar covers the sampling interval.

4.7.8 Concluding remarks and open issues

Three successful advective displacement experiments were conducted on samples from the clay-rich Dogger units and lower Liassic, especially focussing on the derivation of constraints for a representative porewater composition, and with less emphasis on transport properties. Thus, experimental duration was in general shorter than for the BUL1-1 borehole (Mazurek et al. 2021). Nevertheless, a systematic and consistent dataset on petrophysical and geochemical properties was obtained not only of value for the specific site characterisation but also for interpretation of porewater chemistry and chloride / bromide accessible porosity fractions across all TBO drilling sites.

Earliest displaced aliquots are representative of the porewater contained in the sample cores, possibly subject to some artefacts as discussed in Section 4.7.5, but these aliquots are not equally representative for the in situ porewater due to issues of drilling, unloading, handling and storage. Remarkably, early aliquots of 2 cores (BOZ2-2 & BOZ2-3) from the Opalinus Clay and Staffelegg Formation show large nitrate concentrations (8'070 – 10'900 mg/L) that gradually decrease at later sampling times, a feature not observed in samples from the BUL1-1 and TRU1-1 boreholes but in two samples from the MAR1-1 and in one from the BOZ1-1 boreholes. Corresponding aqueous extracts from post-mortem samples show still increased nitrate not completely flushed out, but not the normal aqueous extracts from pre-characterisation. The origin of this nitrate is likely the kerogenous solid organic matter, but the mechanisms of its mobilisation or liberation during the experiment are not known. There is relatively little data and experience to compare such findings.

While derived Cl and (probably) Br concentrations are robust with respect to such artefacts, the sulphate system in all aliquots appears to be controlled by celestite equilibrium. This either implies that such a control is imposed by these minerals being initially present, or that a disturbance causes to reach such a solubility-product control. In the latter case, the reconstruction

of the porewater sulphate concentration is more challenging, and also influences the carbonate system and clay-exchanger complex by ways of interdependent thermodynamic mass-action equilibria.

In BOZ2-2 and BOZ2-3 the mobilisation of nitrate compromises the data of all cations, the carbon system and stable isotopes. In these experiments the initial anion accessibility porosity fraction might be affected by the disrupted porewater chemistry. Although the Cl and Br concentrations are more robust, they might be affected by the change in the anion accessible porosity fraction (error of approximately 20%). Clearly, the erliest aliquots of these two experiments are strongly affected by nitrate and associated charge-balancing cations, and are thus not representative of in situ conditions, except for the chloride concentration.

Like in all earlier work, there are unusually high concentrations of TOC mobilised in the earliest aliquots, decreasing gradually to values more in line with aqueous extracts, but still at significant concentrations.

All three advective displacement experiments supplied a large amount of systematic, consistent and plausible data on petrophysical and geochemical properties of high quality. Samples covered a clay-mineral content of 35 – 52 wt.-%, with similar proportions of (illite/smectite + smectite) compared to total clay. The derived anion-accessible porosity fraction in the Passwang Formation is 0.32 for chloride and 0.53 for bromide. For the Opalinus Clay and the Staffelegg Formation the accessible porosity fractions derived using the post-mortem aqueous extracts are recommended (0.45 and 0.49, respectively). The hydraulic conductivities are similar for all core samples tested, but porosities differ and thus also volumetric fluxes induced by identical head gradients.

An unexpected feature – not yet understood – is the observed partly strongly delayed break-through of deuterium (δ^2H traced in the APW) compared to $\delta^{18}O$. The latter elutes more regularly, but in two of the three cores much too early than expected for a water tracer. This observation is suspected to be related to the elevated amount of nitrate and TOC measured in the sampled aliquots. It is possible that the mobilisation and degradation of organic matter linked to microbial activity evolving in the core enriched the porewater in light water isotopes.

There are no fundamental adaptations to the methods prompted by this study. The mechanical, hydraulic and electronic or sensor aspects of the experimental setup reliably performed for the duration of the experiments and even longer. Likewise, the analytical procedures were already optimised and adequate, naturally limited by very small sample volumes for some cases.

The large gas volumes exfiltrating mainly at the beginning of the experiments (Tab. 4-7-2), but in some cases continuing throughout the entire percolation period, cannot be explained by initial dead volumes and initially undersaturated porosity in the core, nor by He dissolved in the APW at the infiltration pressure (45 – 49 bar) and outgassing due to pressure decrease to 1 bar. During MAR1-1 and BOZ1-1 experiments, selective gas analysis revealed considerable volumes of Ar and Kr (when substituted for Ar) in the exfiltrating gas, which originates from the core confinement water, where Ar (or Kr) was used in the pressurised headspace. Therefore, a gas-free confining pressure system was installed starting with samples from the STA1-2 borehole. However, both Ar and He in the exfiltrating system do not significantly influence the solution composition.

In future experiments, a piston pump generates the confining pressure, where no gas phase is in contact with the confining fluid (water). Also, hydraulic diaphragm accumulators were introduced for future experiments that intrinsically separate the pressurised medium (water in our case) from the pressurised nitrogen reservoir by a thick rubber diaphragm.

4.8 Water-isotope data from diffusive-exchange experiments

Lukas Aschwanden, Thomas Gimmi

The porewater isotope composition ($\delta^{18}O$, $\delta^{2}H$) was derived by isotope diffusive-exchange experiments conducted on core material of 80 samples collected across an interval of 270.1 – 660.0 m depth. The obtained highly resolved profiles for $\delta^{18}O$ and $\delta^{2}H$ cover the lithologies from the Wildegg Formation of the Malm to the Bänkerjoch Formation of the Keuper.

Isotope diffusive-exchange experiments were conducted in two different laboratories for reasons of quality assurance and optimisation of data production time. Hydroisotop GmbH conducted experiments and analyses on 51 samples between 270.1 and 640.5 m, whereas 29 samples were investigated by the University of Bern (Rock-Water Interaction Group RWI) in the interval of 276.3 – 660.0 m.

The dataset of Hydroisotop GmbH is provided in their data report in Appendix C. The relevant data produced at the University of Bern are summarised in Appendix A.

4.8.1 Data evaluation

4.8.1.1 Experimental and analytical data

Both laboratories followed the experimental and analytical protocol given in Waber (ed.) (2020) and Appendix C. The evaluation of the experimental and analytical data underlying the derivation of the water stable isotope composition of the in situ porewater followed a standardised procedure as detailed below.

In order to qualify for a successful isotope diffusive-exchange experiment the following criteria had to be met (within the propagated analytical uncertainties) by the two experiments (so-called LAB[8] and NGW or ICE[9] experiments) conducted for one core sample:

- No severe leakage (evaporation). In most cases, the mass of the experiment container including rock and test water before and after experiment remained constant (± 0.04 g). If the loss of mass was > 0.04 g, corrections were applied to the measured isotope value of the equilibrated test water by Rayleigh-distillation calculations before calculating the porewater isotope ratio, assigning the mass loss to evaporation of the initial test water. If the correction of the $\delta^{18}O$ value for evaporation was > 0.5‰ VSMOW (typically meaning that the mass loss of test water was > 5% of the initial mass of testwater), the porewater isotope value was marked as less reliable.
- Reasonable mass ratio of porewater to test water yielding a change in the isotope signal of the test water after equilibration outside the propagated analytical uncertainty. Porewater to test water ratios as low as 0.1 – 0.2 render the calculated isotope composition of the porewater less reliable, whereas at porewater to test water ratios of < 0.1 it becomes unreliable. The mass of porewater in an experiment is defined by the mass of rock and its gravimetric water content. The latter is not known when starting an experiment.

---

[8] LAB: Experiments with laboratory tap water used as test water (same terminology for experiments performed at the University of Bern and Hydroisotop GmbH).

[9] NGW and ICE: Experiments using test water depleted in ^{18}O and ^{2}H (melt water of Antarctic ice cores). Different terminology for experiments performed at the University of Bern (NGW) and Hydroisotop GmbH (ICE).

- Limited mass transfer between rock and test water, i.e. 1) limited transfer of test water to rock (< 0.5 $m_{\text{test water}}$) caused either by high salinity of porewater compared to test water or hydrating mineral phases (e.g. anhydrite, halite) or 2) limited transfer of porewater to test water (< 0.02 g) caused by high salinity of test water compared to porewater. Such mass transfer between rock and test water may lead to isotope fractionation processes whose impacts on the experiments are poorly understood. Porewater isotope data not fulfilling these criteria are kept but classified as less reliable provided that the experiments do not show any further unconformities and that the calculated porewater isotope data and water contents derived from isotope mass balance agree well with those of neighbouring samples (i.e. within the propagated analytical uncertainty). If this is not the case (i.e. the data constitute outliers), the experiments are considered as failed.
- Stable isotope analyses of test water solutions within the required accuracy.

All of the 80 investigated samples (or 160 individual experiments) pass these criteria, however, for 10 samples the experimental data resulted in an elevated uncertainty of the calculated isotope composition of the in situ porewater. Two samples show minor evaporation of the test water (5 – 10%; corrected by Rayleigh-distillation calculations) during the experiments, five samples show minor transfer of porewater to test water, for one sample tiny pieces of rock material fell into the test water and two samples show a large transfer of test water to rock. Porewater isotope compositions calculated from these experiments are associated with somewhat larger uncertainties. These data are shown but marked with open symbols in the following graphs.

4.8.1.2 Calculation of porewater composition and water contents

Porewater $\delta^{18}O$ and $\delta^{2}H$ values were calculated using equation 76 in Appendix A in Waber (ed.) (2020) considering the ratio *q* of the gravimetric water contents of the individual subsamples used in the experiments (for details see Appendix A in Waber (ed.) 2020). Water contents could then also be calculated by mass balance from the porewater isotope values. The robustness of the calculated porewater $\delta^{18}O$ and $\delta^{2}H$ values was further tested according to the following criteria:

3. A relative difference of less than 20% between the water contents calculated from $\delta^{18}O$ and $\delta^{2}H$ data derived from the experiments with test water depleted in ^{18}O and ^{2}H (NGW/ICE subsamples).
4. A relative difference of less than 20% between the average water content calculated by isotope mass balance from $\delta^{18}O$ and $\delta^{2}H$ data and the average of the gravimetric water content of the two subsamples used in the experiments.

If the relative difference in the different water contents is larger than 20%, the calculated porewater $\delta^{18}O$ and $\delta^{2}H$ values are considered less reliable. Such data may still be used for further interpretation by accepting the larger propagated uncertainty; they are marked with open symbols in the following graphs.

All of the 80 samples that passed the experimental quality criteria (*cf.* Section 4.8.1.1; including samples with elevated experimental uncertainties) pass criterion 1 above (Fig. 4.8-1), however, 6 samples do not pass criterion 2 (Fig. 4.8-2). These samples do not show any experimental irregularities and thus, the failure of criterion 2 is likely attributed to lithological heterogeneity of the different subsamples used in the two experiments.

All samples that pass the above criterion 2 display a consistent, previously observed relationship between the average water content derived by isotope mass balance and the average of the gravimetric water content of the subsamples used in the experiments, the former being around 10% larger than the latter (Fig. 4.8-2). As the water content is generally well correlated with the clay-mineral content of the rocks (*cf.* Section 4.3), it was postulated that this difference might be associated with minor exchange with water of different isotope composition adsorbed on clay minerals (e.g. Pearson et al. 2003). However, no stringent explanation exists at the moment.

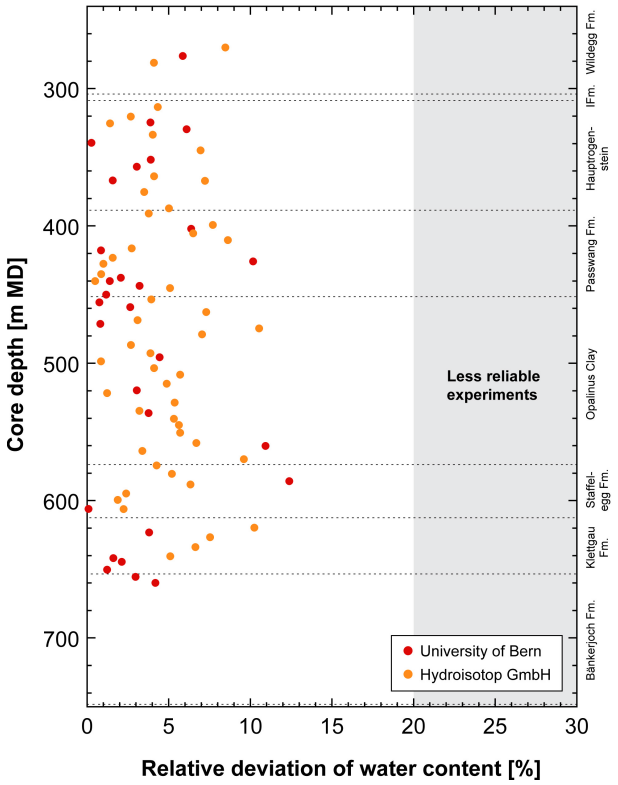

Fig. 4.8-1: Relative deviation of water contents obtained from $\delta^{18}O$ and $\delta^{2}H$ mass balance

The relative deviation is defined as the difference between the water contents calculated from the equilibrated $\delta^{18}O$ and $\delta^{2}H$ values, respectively, of the experiments with test water depleted in ^{18}O and ^{2}H (NGW or ICE, respectively) divided by the water content based on $\delta^{2}H$; it is expressed in %. Grey area: Relative deviation of water contents obtained from $\delta^{18}O$ and $\delta^{2}H$ mass balance is > 20%. For samples within this area the calculated porewater $\delta^{18}O$ and $\delta^{2}H$ values are considered less reliable.

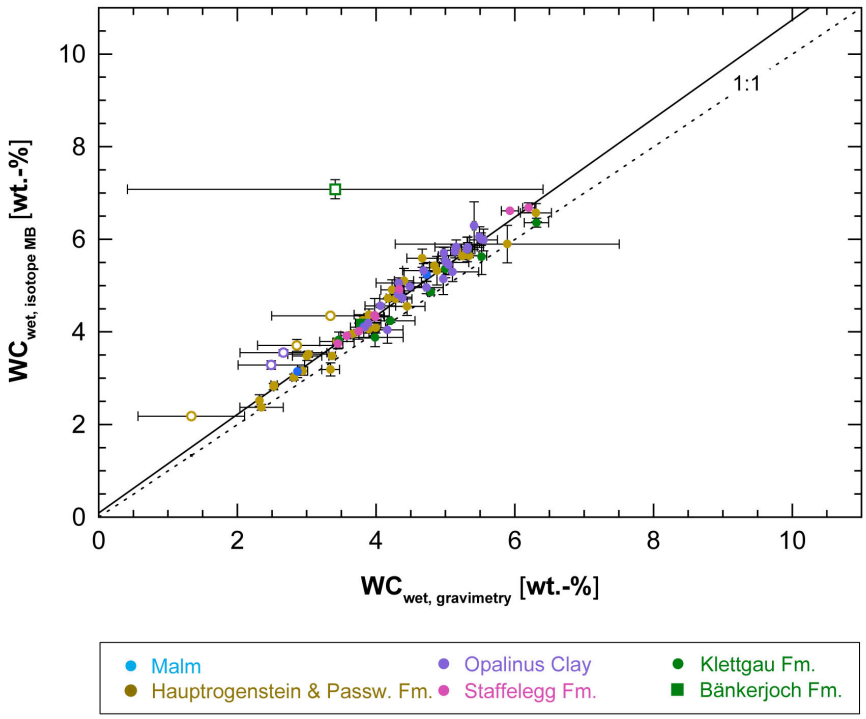

Fig. 4.8-2: Average water content obtained by water-loss at 105 °C ($WC_{wet,\ gravimetry}$) of subsamples LAB and NGW/ICE vs. average water content calculated from $\delta^{18}O$ and $\delta^{2}H$ mass balance from NGW/ICE diffusive-exchange experiments ($WC_{wet,\ isotope\ MB}$)

Open symbols refer to samples showing differences larger than 20% between the average water content derived by isotope mass balance and the average gravimetric water content of the two subsamples used in the experiment.

4.8.2 $\delta^{18}O$ and $\delta^{2}H$ values of porewater

4.8.2.1 Data comparison University of Bern – Hydroisotop GmbH

All the porewater isotope data that pass the various quality criteria are illustrated in Fig. 4.8-3 as a function of depth. Porewater $\delta^{18}O$ and $\delta^{2}H$ values from Hydroisotop GmbH and the University of Bern generally agree well within the propagated uncertainty. Nevertheless, across the clay-rich lithologies of the Passwang Formation and the Opalinus Clay porewater $\delta^{18}O$ values from the University of Bern are systematically slightly higher compared to those of Hydroisotop GmbH, whereas the $\delta^{2}H$ values agree better. The reasons for these differences are not known at this stage.

4.8.2.2 Depth profiles of porewater isotope composition

Both $\delta^{18}O$ and $\delta^{2}H$ values of the porewater show well defined, curved profiles across the interval Wildegg Formation – Klettgau Formation. Although both tracers indicate the same general trends, some differences exist. From the Malm across half of the Hauptrogenstein both $\delta^{18}O$ and $\delta^{2}H$ values sharply decrease towards a local minimum at around 340 m depth ($\delta^{18}O$ = –9.2 ‰ VSMOW; $\delta^{2}H$ = –66.6 ‰ VSMOW) where the trend reverses. The porewater isotope profile between the local minimum in the Hauptrogenstein and the Klettgau Formation indicates a bell-shaped curve with highest porewater $\delta^{18}O$ values at the top of the Opalinus Clay (–5.4 ‰ VSMOW) from where they increasingly become more negative across the Opalinus Clay and the Staffelegg Formation, approaching a minimum of –10.1‰ VSMOW in the Gruhalde Member of

the Klettgau Formation at 627 m depth. In contrast, porewater δ^2H values remain remarkably constant across the Opalinus Clay (at ~ –41.8 ‰ VSMOW). At its base they sharply decrease towards distinctly lower values in the Klettgau Formation. Across the remainder of the Klettgau Formation both $\delta^{18}O$ and δ^2H signatures of the porewater remain constant at very negative values.

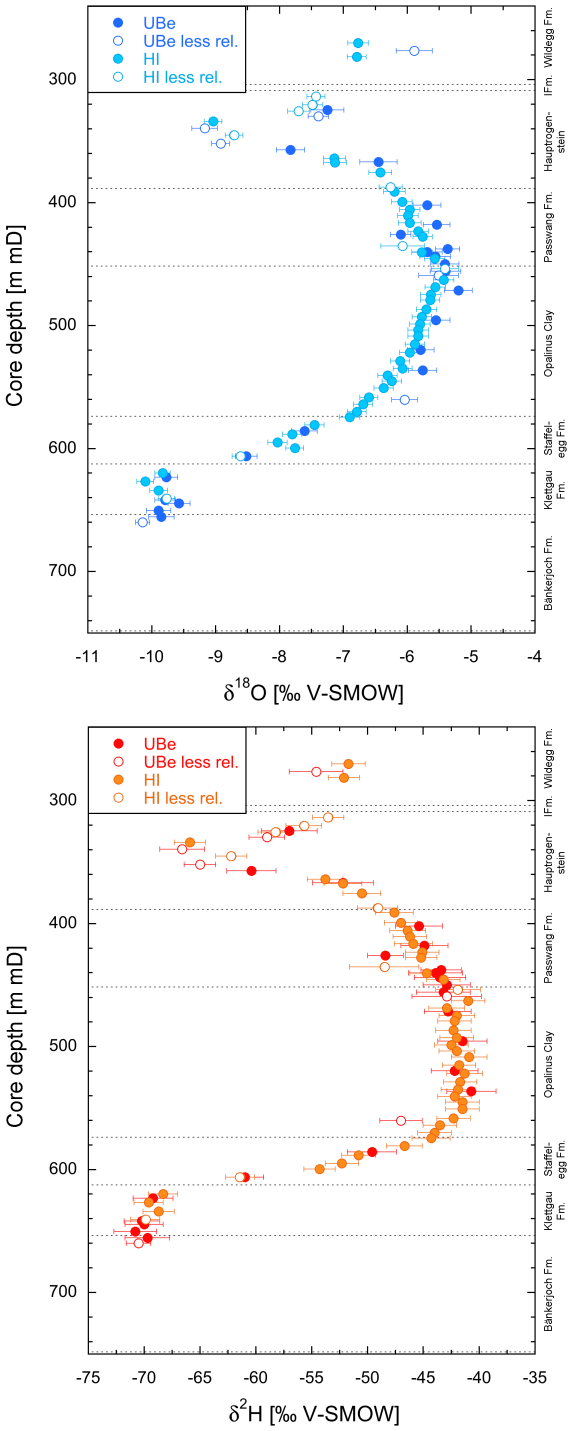

Fig. 4.8-3: Depth distribution of porewater $\delta^{18}O$ and δ^2H values obtained from isotope diffusive-exchange experiments

Open symbols refer to porewater isotope values which are less reliable owing to experimental artefacts (see text). Data produced at University of Bern (UBe) and at Hydroisotop GmbH (HI).

The different shapes of the $\delta^{18}O$ and $\delta^{2}H$ profiles are also illustrated in Fig. 4.8-4, which shows the depth profile of deuterium excess (defined as $\delta^{2}H - 8 \times \delta^{18}O$; deuterium excess is +10 ‰ for a sample that lies on the GMWL, lower values of deuterium excess reflect sample positions to the right of the GMWL in a plot of $\delta^{2}H$ vs. $\delta^{18}O$; note that the deuterium excess as used at this stage carries no direct implications about the palaeoclimate at the time of infiltration; it is the result of several interactions – some acting in the deep underground). Across the Wildegg Formation and the Hauptrogenstein deuterium excess shows significant scatter. In contrast, rather constant values are indicated in the underlying Passwang Formation (around 0.8 ‰). At the top of the Opalinus Clay deuterium excess starts to steadily increase and reaches a maximum in the Staffelegg Formation (12.7 ‰). Across the remaining Stafelegg Formation and the Klettgau Formation there is a general trend towards slightly lower values of deuterium excess, however, the scatter of the data is again large.

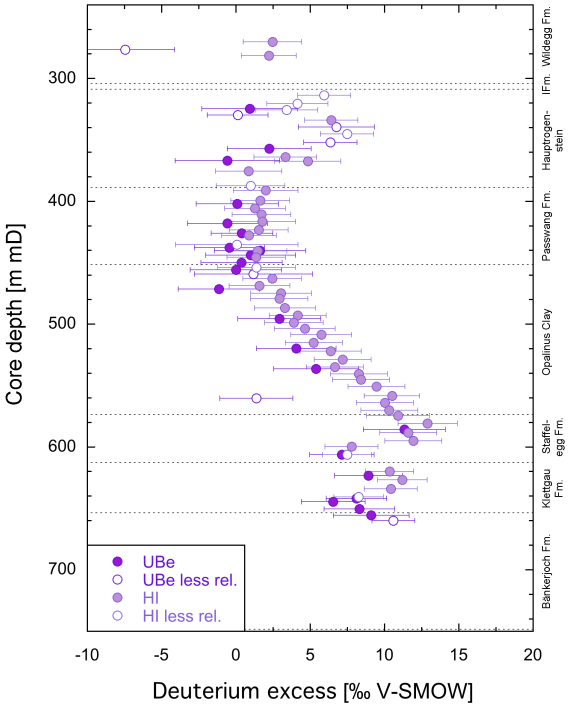

Fig. 4.8-4: Depth trend of deuterium excess in porewater based on the isotope diffusive exchange technique

Deuterium excess is +10‰ for a sample that lies on the GMWL. Lower values of deuterium excess reflect sample positions to the right of the GMWL in a plot of $\delta^{2}H$ vs. $\delta^{18}O$. Note that the deuterium excess as used at this stage carries no genetic implications about the origin of H_2O, e.g. on palaeo-climate at the time of infiltration. Open symbols refer to samples which are less reliable owing to experimental artefacts (see text). Data produced at University of Bern (Ube) and at Hydroisotop GmbH (HI).

4.8.2.3 $\delta^{18}O$ versus $\delta^{2}H$ and comparison with Global Meteoric Water Line

In the $\delta^{18}O$-$\delta^{2}H$-diagramm (Fig. 4.8-5) some remarkably regular and linear trends can be observed. Porewater isotope signatures of the few Malm samples fall to the right of the Global Meteoric Water Line (GMWL) and partly overlap with the porewater in the underlying «Brauner Dogger» (note that the term «Brauner Dogger» is used for the Dogger units overlying the Opalinus Clay). However, the latter spans a wide range of $\delta^{18}O$ and $\delta^{2}H$ values, linearly arrayed and deviating towards the right from the Global Meteoric Water Line. Across the underlying Opalinus Clay the porewater isotope composition continuously evolves towards $\delta^{18}O$ and $\delta^{2}H$-values that plot on the GMWL, indicating a dominant meteoric component in the latter porewaters. Similarly, the isotope compositions of the porewater in the Staffelegg have a meteoric signature, however, at distinctly more negative isotope values. At the base of the Staffelegg Formation, porewater $\delta^{18}O$ and $\delta^{2}H$ signatures sharply evolve to distinctly more depleted values in the Klettgau Formation and in the top of the Bänkerjoch Formation, still plotting on the GMWL.

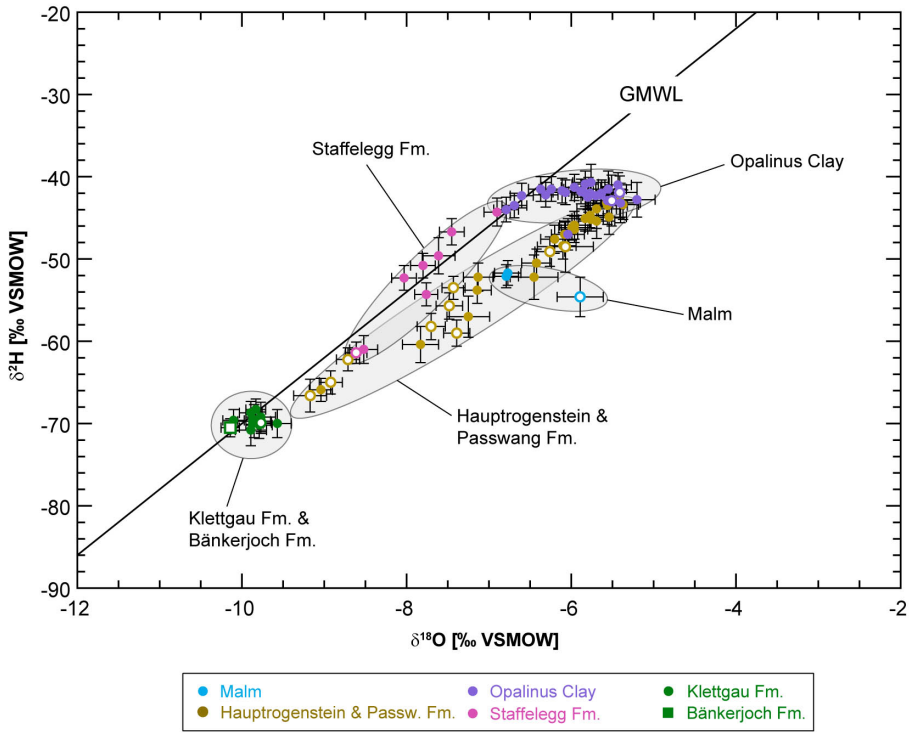

Fig. 4.8-5: $\delta^{2}H$ vs. $\delta^{18}O$ values of porewater obtained from isotope diffusive-exchange experiments

GMWL = Global Meteoric Water Line ($\delta^{2}H = 8 \times \delta^{18}O + 10$ ‰ VSMOW), open symbols refer to porewater isotope values which are less reliable owing to experimental artefacts (see text).

5 Discussion of porewater data

5.1 Chloride data and estimation of Cl^- and Br^--accessible porosity

Paul Wersin, Martin Mazurek, Thomas Gimmi, Carmen Zwahlen

Chloride, a major compound in the porewater, has been determined by squeezing (Section 4.6), advective displacement (Section 4.7) and aqueous extraction (Section 4.4). This anion is considered to behave as a conservative species with no or very limited interaction with the minerals. The same can be said for bromide, which occurs at much lower concentrations in the porewater. In argillaceous rocks, anions are repelled from the negative structural charge of the clay-mineral surfaces and are thus affected by ion exclusion. In other words, they only 'see' part of the total water-filled porosity, the fraction of which is often termed anion-accessible porosity (Pearson 1999, Pearson et al. 2003) or also 'free' porosity. Ion exclusion is not complete according to theory and depends on distance from charged surfaces, but here this simplifying assumption is made for adopting a simplest possible model.

Knowing the concentration of Cl per bulk (total) porewater in a sample from aqueous extraction ($C_{Cl\ in\ bulk\ porewater}$), the Cl-accessible porosity fraction, f_{Cl}, can be estimated from Cl measurements in squeezing ($C_{Cl\ in\ squeezed\ water}$) or advective displacement ($C_{Cl\ in\ adv.\ displaced\ water}$) experiments, assuming that the latter represent the composition of the 'free' porewater:

$$f_{Cl} = \frac{n_{anion-accessible}}{n_{total}} = \frac{C_{Cl\ in\ bulk\ pore\ water}}{C_{Cl\ in\ squeezed\ or\ adv.displaced\ water}}$$

$C_{Cl\ in\ bulk\ porewater}$ is calculated from

$$C_{Cl\ in\ bulk\ pore\ water} = \frac{C_{Cl\ in\ aq.extract}}{WC_{dry}\ {}^{S}/_{L}}$$

with C = concentration [mg/L], n = porosity [–], WC_{dry} = water content relative to dry rock mass [g/g], S/L = (dry) solid/liquid ratio of aqueous extraction experiment [g/g]. The Br-accessible porosities are derived in an analogous fashion.

The anion-accessible porosities have been derived according to the above equation for squeezed and advectively displaced porewaters (Tabs. 4.6-8, 4.6-9 and 4.7-16). Both methods enable to mobilise porewater that is thought to represent the mobile porewater and a proxy of the so-called "free" porewater (not affected by the negatively charged clay surface). It should be noted, however, that the two methods operate by entirely different mechanisms. Whereas porewater is mobilised by mechanical compaction implying a deformation of the porespace in the squeezing method, this is achieved by a strong hydraulic and pressure gradient and an artificial porewater in the advective displacement method. Thus, method-specific artefacts may be expected and likely not the same volume of the porespace is sampled by the two methods. In the case of Cl, experimental artefacts appear to be minor as suggested from previous studies (e.g. Mazurek et al. 2021). In the case of the squeezed waters it is generally assumed that the waters squeezed at the lowest pressure best reflect the in situ porewater (Mazurek et al. 2015, Wersin et al. 2016). For the advectively displaced waters, the first two aliquots are assumed to be the most representative of the in situ porewater (Section 4.7). One should keep in mind that the f_{Cl} for the two AD samples from the Opalinus Clay and the Staffelegg Formation had to be derived from the inlet side in

contact with the artificial porewater, because of an initial disturbance of the experiment by increased NO_3 contents. This disturbance was less pronounced for the uppermost AD sample from the Passwang Formation.

The derived values of the Cl-accessible porosity fraction (f_{Cl}) for the two datasets are shown as a function of the clay-mineral content in Fig. 5.1-1, with the SQ values derived according to the preferred method 1 (from POST data, see Section 4.6). Consistent porosity fractions are obtained from the two methods. The corresponding mean value from both methods is 0.42 ± 0.07[10]. This value is very similar to the mean value obtained for the BOZ1-1 borehole at clay-mineral contents > 25 wt.-%. This shows that most samples, i.e., those belonging to the Staffelegg Formation and Opalinus Clay scatter around a f_{Cl} value of 0.45 whilst the majority of samples from the (rather heterogeneous) Passwang Formation have clearly lower values of about 0.33 (see also Fig. 5.1.3 below). It is interesting to note that a very low mean pore size was determined from the N_2 data for a sample from the upper Passwang Formation (402.37 m, Rothenfluh Menber), making such lower accessibilities plausible. In contrast, higher accessibilities are expected in the iron ooliths from the Hauptrogenstein (i.e. 'Spatkalk'), as they show comparably large average pore sizes derived from the N_2 data.

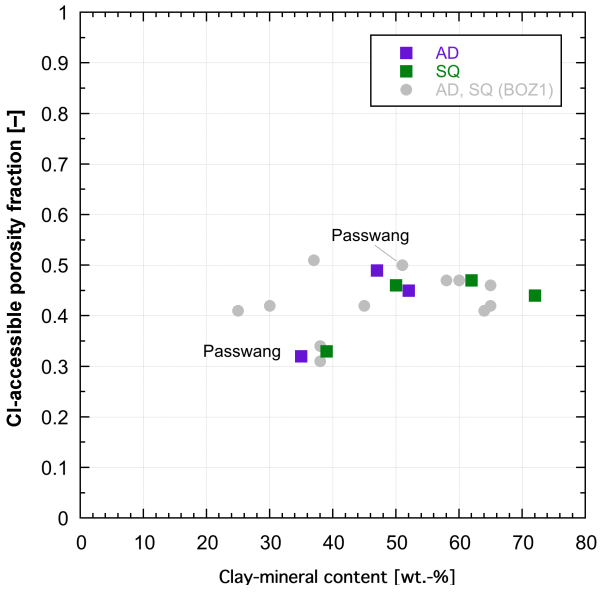

Fig. 5.1-1: Cl-accessible porosity fraction as a function of the clay-mineral content from AD and SQ data

The AD data for Opalinus Clay and Staffelegg Formation (with higher clay contents) had to be determined from post-mortem data of the inlet side and may be less certain (see text).

It should be noted that fewer f_{Cl} data are available for BOZ2-1 compared to the other boreholes. In particular, the dataset is limited to clay-mineral contents above 35 wt.-% and thus no dependence at lower clay-mineral contents can be derived. This would be important because within the sampled interval, the lithologies in the BOZ2-1 profile vary substantially. In order to derive a porewater profile for Cl, the anion accessibility in these lithologies must be known or assumed. Given the similarity with the BOZ1-1 data (which displays a significantly larger dataset) and their similar ionic strengths, we use the same relationship for BOZ2-1 to estimate anion-acessible

[10] Note that the average is pulled down by the two samples from the Passwang Formation.

porosities. Thus, for clay-mineral contents ≥ 25 wt.-% a uniform f_{Cl} value of 0.42 is considered. Below this clay-mineral content, a linear increase of f_{Cl} to a value of 1 at a clay-mineral content of zero is assumed. For BOZ1-1, diffusion data indicated lower anion accessible porosities for samples with clay-mineral contents ≥ 25 wt.-% (Wersin et al. 2022). Diffusion data for BOZ2-1, which focus on samples from the confining units, are currently not yet available. Data of previous boreholes (Mazurek et al. 2021, Aschwanden et al. 2021, Mäder et al. 2021) qualitatively support the assumed trend of f_{Cl}, which, however, certainly represents an oversimplification.

The fact that f_{Cl} shows considerable scatter when plotted against the clay-mineral content suggests that the latter is not the only parameter that determines anion accessibility. Mineralogical composition of the clay fraction, mean pore size, grain-size distribution, fabric and other factors are expected to affect anion accessibility as well. Note that the negative structural charge of the clays is predominately carried by the smectite and illite components. Furthermore, according to theory, anion accessibility also varies with the salinity and composition of the porewater, i.e., it is not just a material property. All these partly interdependent effects cannot be properly quantified at this stage, which severely limits the application of theoretical models.

An uncertainty range of ± 20% is considered for f_{Cl}, which is probably sufficient for clay-rich lithologies but may still be an underestimation for clay-poor rocks. This uncertainty propagates into the calculated Cl concentrations in the anion-accessible porewater, i.e., an error of ± 20% must be considered in addition to the propagated analytical error.

For Br, only advective displacement data are available. The derived f_{Br} values as a function of the clay-mineral content are illustrated in Fig. 5.1-2. As for f_{Cl}, the two values at higher clay-mineral contents (from Opalinus Clay and Staffelegg Formation) were derived from the inlet side of samples disturbed by increased NO_3 contents. The mean f_{Br} value for the 3 samples where these values could be derived is 0.68 ± 0.11. This is higher than the corresponding mean f_{cl} value for the same 3 AD samples (0.42 ± 0.09). The reason for this difference is not clear at this stage.

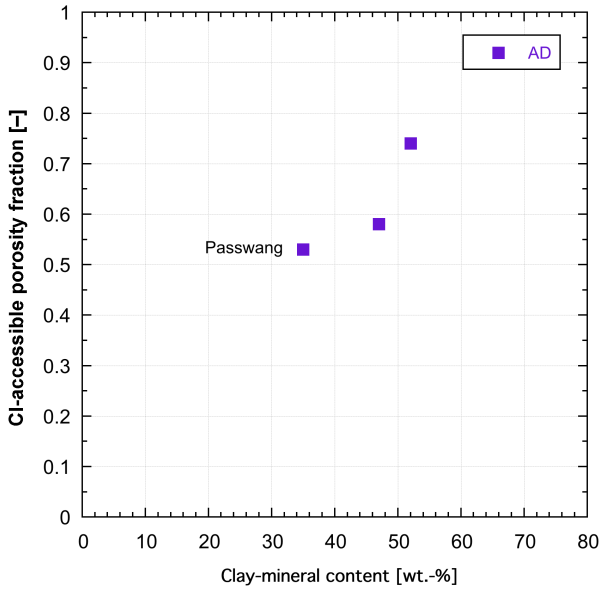

Fig. 5.1-2: Br-accessible porosity fraction as a function of the clay-mineral content derived from AD data

The AD data for the Opalinus Clay and the Staffelegg Formation (with higher clay-mineral contents) had to be determined from post-mortem data of the inlet side and may be less certain (see text).

Fig. 5.1-3 illustrates the Cl-accessible porosity fraction as a function of depth (depths for BOZ1-1 samples adjusted). Again, the consistency between the two AD and SQ datasets from BOZ2-1 and BOZ1-1 is evident. The few data points suggest an increasing trend of f_{Cl} with depth from the Passwang Formation to the upper Opalinus Clay, from where values remain approximately constant down to the Staffelegg Formation. The increasing trend in the upper part of the sequence is, however, not confirmed by AD and SQ data from BOZ1-1 (Fig. 5.1-3), even though broad consistency with the BOZ2-1 data exists as discussed above. The ensemble of data rather suggests constant f_{Cl} values across the Opalinus Clay. Lower f_{Cl} values are present in the Passwang Formation for four out of the five samples for the BOZ2-1 and BOZ1-1 datasets. However, local heterogeneity may be expected in view of the lithological heterogeneities in this formation. For example, two samples from BOZ1-1 located within a distance of 0.5 m have values of 0.31 and 0.50[11], respectively.

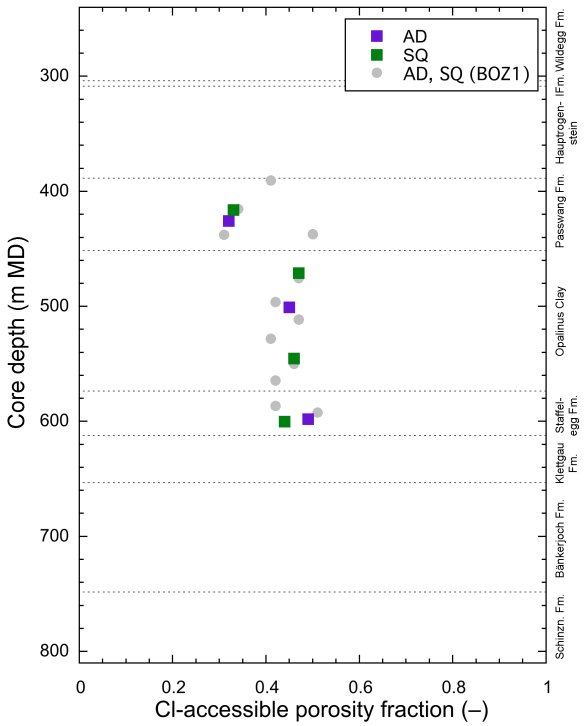

Fig. 5.1-3: Cl-accessible porosity fraction as a function of depth

The depths of the samples from the BOZ1-1 borehole are adjusted such that the top of Opalinus Clay matches between the two locations. The AD data for Opalinus Clay and Staffelegg Formation had to be determined from post-mortem data of the inlet side and may be less certain (see text).

[11] Note, however, that the lower value was obtained from the AD method, the higher value from the SQ method.

5.2 Chloride, bromide and Br/Cl profiles

Paul Wersin, Martin Mazurek, Thomas Gimmi, Carmen Zwahlen

The chloride profile depicted in Fig. 5.2-1 includes aqueous extraction data re-calculated to in-situ conditions assuming the relationship between clay-mineral content and f_{Cl} as discussed in Section 5.1. Aqueous extraction data were produced by BRGM and University of Bern. In the latter laboratory, some of the extractions were carried out on the same subsamples that had been used for water content determination (extracts on dried samples). The Cl concentrations obtained from squeezing and advective displacement, as well as those for the groundwater in the Hauptrogenstein, the Keuper and the Muschelkalk (Tab. 2-4; Lorenz *in prep.*), are also shown in Fig. 5.2-1. The error bars include the propagated analytical uncertainty and, for aqueous extraction data, an additional 20% that reflect the uncertainty related to f_{Cl} (see Section 5.1, Fig. 5.1-1).

Data from all three methods are consistent within the extended error bars[12]. In general, the Cl profile is well constrained and supported by the dense sampling, particularly in the Opalinus Clay and confining units. Thus, Cl concentrations display a mild increase from the Keuper aquifer accross the Klettgau Formation, followed by a marked increase in the Staffelegg Formation. Cl concentrations in the Opalinus Clay remain approximately constant at 1.5 – 2.5 g/L, but decrease across the Passwang Formation and the Hauptrogenstein, where they reach similar levels as the groundwater sample (~ 1 g/L). There is, however, considerable scatter of the BRGM data in the Hauptrogenstein. The reason for this scatter is unknown; it may be related to partly low porosities leading to larger uncertainties in porewater concentrations. Note, however, that the scatter is reduced when pycnometer porosities instead of water-loss porosities are considered (see below). Above the Hauptrogenstein, a slight increase towards the top of the cored sequence is indicated. Below the Keuper aquifer, the Cl levels appear to increase towards the Muschelkalk aquifer, but it should be noted that there are only a few samples from the uppermost part of this sequence (Bänkerjoch Formation).

There are two outliers with comparably large values at 579.80 m depth from the Rietheim Member (Posidonienschiefer) and at 585.84 m from the Frick Member. The same positive excursion at this location was already observed in previous boreholes, such as BUL1-1, TRU1-1 and MAR1-1. It appears that the anion-accessible porosity fraction estimated from the simple relationship described above, is not appropriate for these types of sediment.

When using the pycnometer porosity instead of the water-loss porosity for the calculation of porewater concentrations from aqueous extracts prepared from wet samples, as discussed in Section 4.4, the differences between the data analysed by University of Bern and by BRGM tend to become smaller (Fig. 5.2-1 below; for the data from dry extracts, the water content was known for the very same sample, so changing to pycnometer porosity is not meaningful for these samples). Overall, the profile appears smoother with clearer trends, but some outliers especially in the Hauptrogenstein or also in the upper Staffelegg Formation remain. Moreover, in the Opalinus Clay, re-calculated AqEx data are more shifted to higher values compared to AD and SQ data (although still within the estimated error).

The Cl profile is clearly influenced by the Keuper aquifer in the Klettgau Formation. This is also the case for the $\delta^{18}O$ and $\delta^{2}H$ profiles (Section 5.7). The upper part of the profile shows a bend in the Passwang Formation and reaches approximately constant concentrations towards the top of

[12] One should keep in mind that the AD values originate from experiments showing a somewhat (uppermost sample) or a clearly (lower two samples) increased NO_3 content, even though this probably does not affect Cl.

this formation at about 400 m depth (Fig. 5.2-1 above). Using the pycnometer porosities instead for the wet extracts, leads to a more gradual decrease in Cl levels up to the sampled Hauptrogenstein groundwater (Fig. 5.2-1 below). Using a lower anion-accessible porosity of 0.33 for the Passwang formation as discussed above would lead to calculated porewater concentrations between 1'215 and 2'811 mg/L (based on water-loss porosity) or between 1'380 and 3'180 mg/L (based on pycnometer porosity), with the largest values at the bottom of the Passwang Formation. Using a lower accessible porosity also at the bottom of the Passwang Formation may not necessarily be justified. In any case, the calculated concentrations in the Passwang Formation would increase by a factor of ~ 1.3 (for clay-mineral contents > 25 wt.-%) when using such lower accessible porosity, such that the decrease across the Passwang Formation would be less pronounced. It should be noted that the $\delta^{18}O$ and $\delta^{2}H$ profiles show a more gradual change in this interval, suggesting a clear influence by the aquifer in the Hauptrogenstein.

It is evident (Fig. 5.2-1) that the used average f_{Cl} value is somewhat too small for Opalinus Clay, as stated in Section 5.1, due to a bias towards some very low values for the Passwang Formation. The chloride contents in the Opalinus Clay may therefore be a bit lower than suggested by the scaled aqueous extracts, more in agreement with the SQ and AD samples in this region, i.e., 1'600 – 1'800 mg/L, rather than 1'800 – 2'000 mg/L (AqEx, water-loss porosity), or 2'000 – 2'200 mg/L (AqEx, pycnometer porosity).

In summary, a broadly consistent Cl profile above the Keuper aquifer is obtained from squeezing, advective displacement and aqueous extraction data. A well-defined profile is identified, with some scatter. This scatter is related predominantly to the uncertainty in anion-accessible porosity (which may not only vary as a function of the clay-mineral content) and to a lesser extent to the uncertainty in the water content. In this analysis, a simple relationship of the anion-accessible porosity with the clay-mineral content (as proxy of surface charge) based on squeezing and advective displacement data was used. It is worth noting that other relationships with the clay-mineral content (e.g. linear extrapolation from clay-mineral content < 40 wt.-%, or < 50 wt.-%) do no result in a less scattered profile.

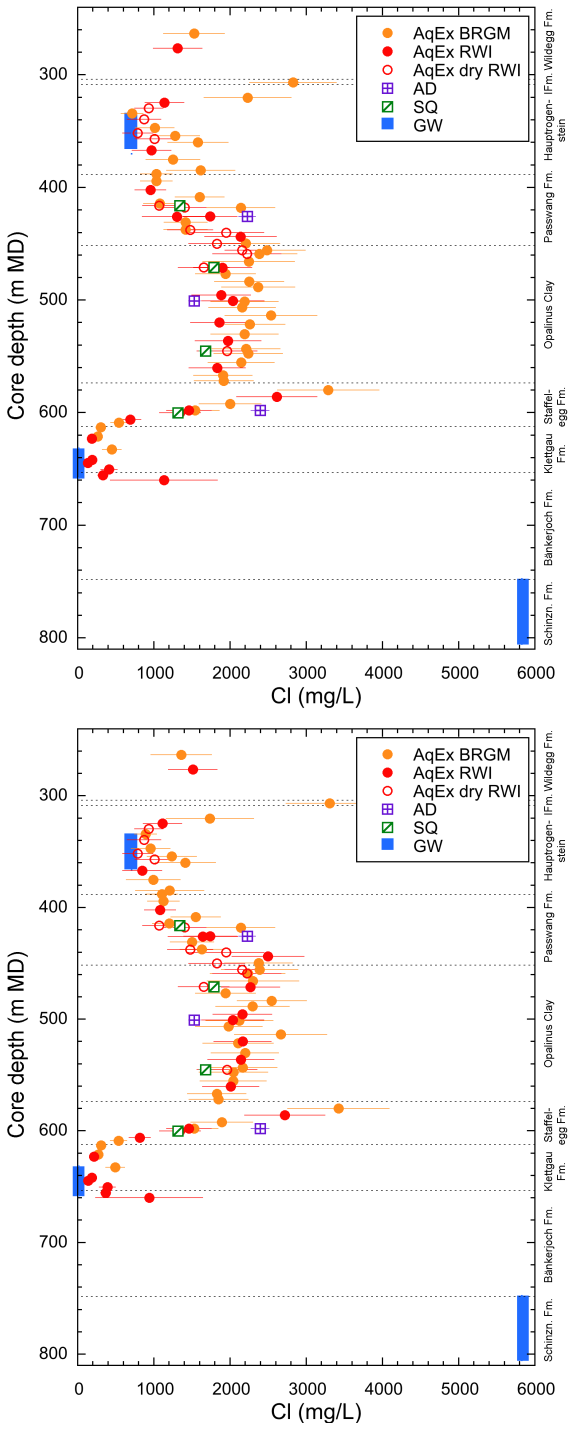

Fig. 5.2-1: Cl profile with data from squeezing, advective displacement, aqueous extraction, and groundwater samples

AqEx data recalculated from water-loss porosity (above) and, for wet extracts only, from pycnometer porosity (below).

Aqueous extraction data re-calculated to Cl-accessible porosity assuming the relationship between accessibility and clay-mineral content as discussed in Section 5.1. Error bars on the data from aqueous extraction include propagated analytical uncertainty plus another 20% that reflect the uncertainty related to f_{Cl}. The symbols for groundwater cover the packer intervals. See comment in text regading possible disturbance of AD values.

The Br profile (Fig. 5.2-2) reveals a similar shape as the one of Cl, albeit with somewhat more scatter, which is likely related to the larger analytical uncertainty of this minor element. Using the pycnometer porosity (Fig. 5.2-2 below) instead of the water-loss porosity (Fig. 5.2-2 above) to calculate porewater concentrations from aqueous extracts of wet samples (see discussion in Section 4.4) leads to less scatter and a better agreement between the data from University of Bern and from BRGM, as for Cl. Thus, an increasing trend from the Keuper aquifer to the top of Staffelegg Formation, followed by constant levels in the Opalinus Clay, decreasing levels in the Passwang Formation and constant levels in the Hauptrogenstein and lower Malm are noted. The decreasing trend in the Passwang Formation would also be modified as for Cl (increase of the concentrations by a factor of ~ 1.3 for samples with clay-mineral content > 25 wt.-%) by using a lower anion accessible porosity of 0.33. Below the Keuper aquifer, a similar increasing trend with depth as seen for Cl in the upper units of the Bänkerjoch Formation is observed, but the groundwater sample below does not reflect such an increasing trend. A closer look at the profile shows a larger difference between the AD and SQ data and the aqueous extract data as compared to the Cl profile. This is because the same scaling as for Cl was used, while according to AD data f_{Br} would tend to be larger than f_{Cl}. A closer look shows also an offset of the aqueous extract data prepared from dry samples relative to those prepared in the standard way from wet extracts (similar as in BOZ1-1; Wersin et al. 2022). This is more evident in the Br/Cl ratio (see below).

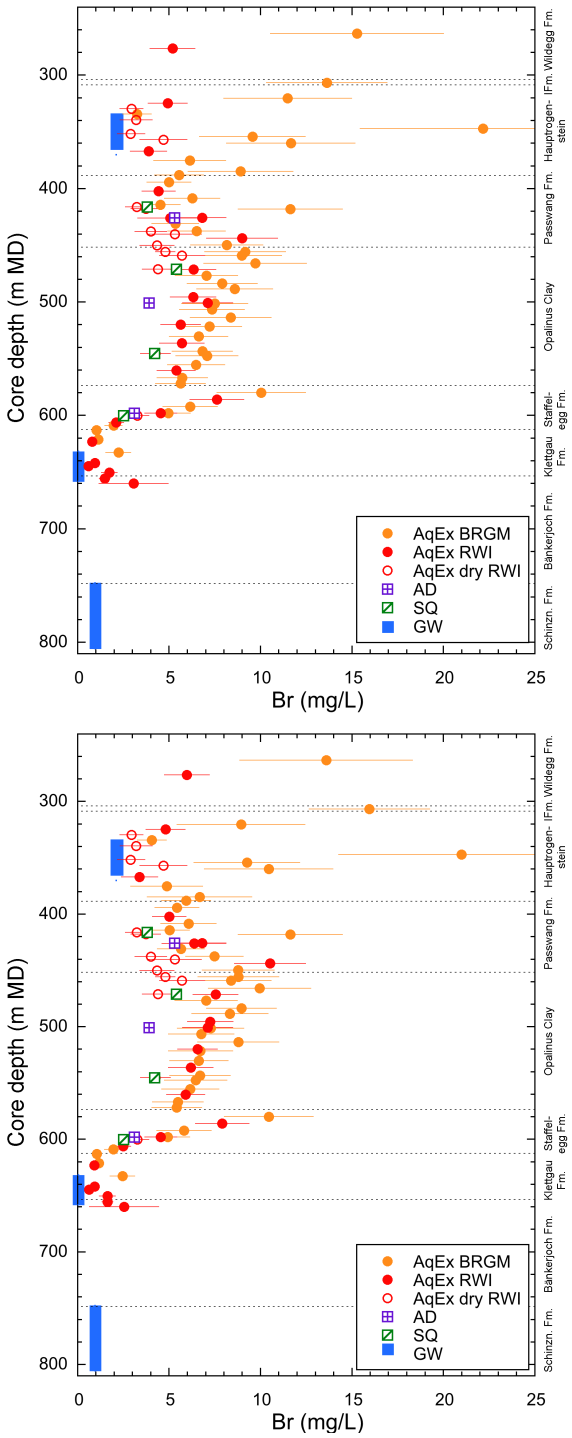

Fig. 5.2-2: Br profile with data from squeezing, advective displacement, aqueous extraction, and groundwater samples

AqEx data recalculated from water-loss porosity (above) and, for wet extracts only, from pycnometer porosity (below).

Aqueous extraction data in the Br profile re-calculated to Br-accessible porosity assuming the relationship between accessibility and clay-mineral content for Cl as discussed in Section 5.1. Error bars on Br data from aqueous extraction include propagated analytical uncertainty plus another 20% that reflect the uncertainty related to f_{Br}. The symbols for groundwater cover the packer intervals. See comment in text regading possible disturbance of AD values.

The Br/Cl profile (Fig. 5.2-3) shows less scatter than the individual Cl and Br profiles. This is mainly because heterogeneity and uncertainty related to anion-accessibility and water content do not affect the Br/Cl ratio, contrary to the individual concentrations. A strong increase from the Keuper aquifer (1'000*Br/Cl ≈ 1 mol/mol) in the Klettgau Formation, followed by a decrease towards the base of the Staffelegg Formation is noted. A slightly increasing trend in the Opalinus Clay can be discerned. Above the Opalinus Clay, rather constant Br/Cl ratios with some scatter up to the top of the cored section are indicated. There appears to be an offset between the "standard" AqEx data prepared from wet samples on the one hand and the AqEx prepared from dry samples and AD data and, to a lesser extent, also SQ data on the other hand. The reason for this offset is not clear at this stage. For instance, prior drying could reduce the extractability of Br, or performing an extract with a wet sample could lead to a mobilisation of Br bound to organic matter (see discussion in Section 4.4).

The groundwater sample of the Muschelkalk aquifer has a very low Br/Cl ratio, similar to what was found in the BOZ1-1 borehole. The Br/Cl ratios for the groundwater samples in the Haupt-rogenstein and especially in the Keuper tend to be lower than those obtained from aqueous extracts, especially from wet samples, for unknown reasons. A more systematic investigation, for instance regarding any potential mobilisation of Br during aqueous extracts, would be needed to clarify this issue.

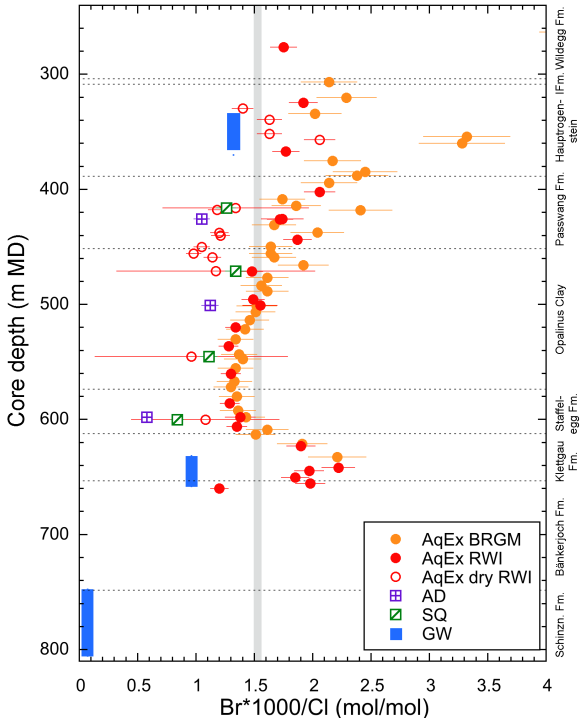

Fig. 5.2-3: 1'000*Br/Cl (molar units) profile with data from squeezing, advective displacement, aqueous extraction, and groundwater samples

Grey bar: range in modern seawater. The propagated uncertainty for SQ data assumes the same analytical uncertainty as for the other samples (4% for Cl). The symbols for ground-water cover the packer intervals. See comment in text regading possible disturbance of AD values.

5.3 Sulphate and SO_4/Cl profiles

Paul Wersin, Martin Mazurek, Thomas Gimmi

Sulphate data from squeezing, advective displacement, aqueous extraction and groundwaters (last sample; Lorenz, *in prep.*) are illustrated in Fig. 5.3-1. Data from aqueous extraction were re-calculated to concentrations in bulk porewater (Fig. 5.3-1 above) or to concentrations in anion accessible porewater (using the same accessibility as for Cl, Fig. 5.3-1 below), assuming conservative behaviour of sulphate. This assumption is not true at least in anhydrite-bearing lithologies in the Bänkerjoch Formation where mineral dissolution contributed to SO_4 concentrations in the extracts, as is evident from the AqEx sample at 659.95 m depth with a re-calculated unrealistically high SO_4 concentration of 100 g/L (not shown in Fig. 5.3-1).

SO_4 concentrations based on squeezing and advective displacement yield distinctly lower and less scattered values in comparison to the concentrations per bulk water or per accessible porewater re-calculated from aqueous extraction. A closer look at the sequence Passwang Formation – Staffelegg Formation reveals consistent concentrations between squeezing and advective displacement data. These exhibit a slightly increasing trend in the lower part of the sequence, followed by approximately constant concentrations (2.5 – 3 g/L) from the lower part of the Opalinus Clay up to the top of the cored sequence.

In this sequence, the porewater thus shifts from a more Na-Cl dominated to a somewhat more Na-SO_4 dominated chemistry.

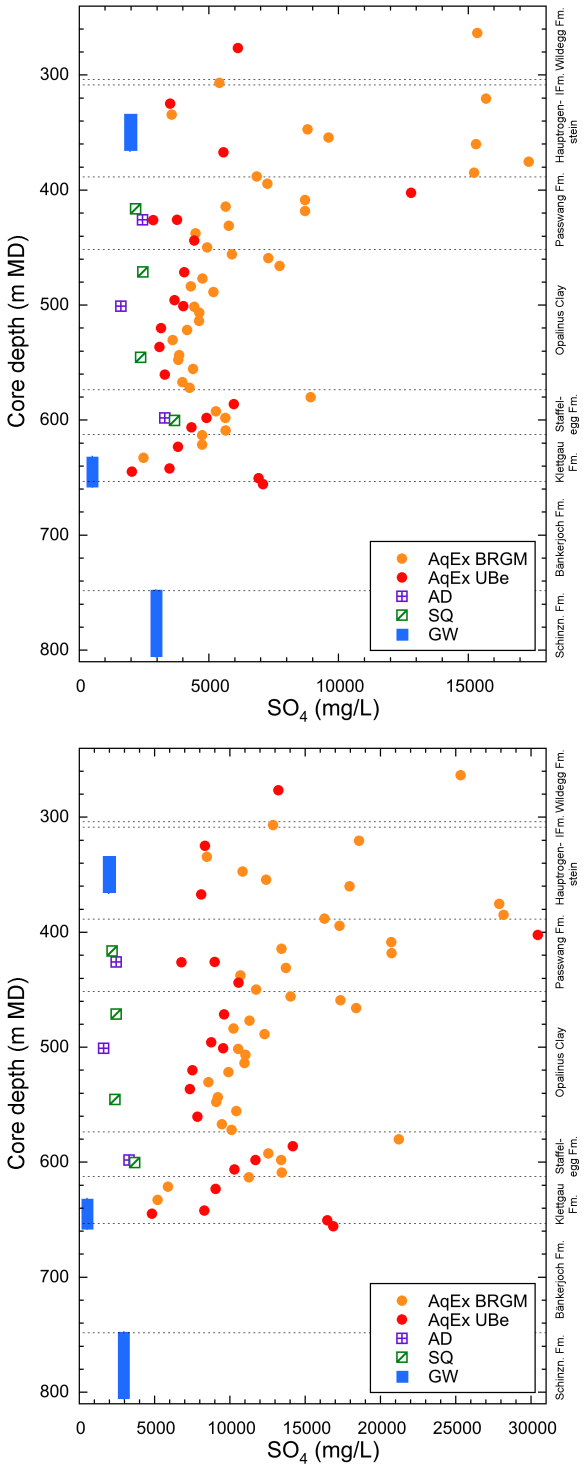

Fig. 5.3-1: SO_4 profiles with data from squeezing, advective displacement, aqueous extraction, and groundwater samples

AqEx data re-calculated to bulk porosity (above), AqEx data re-calculated to anion-acessible porosity (below)

Aqueous extraction data re-calculated to contents in bulk porewater using water content. Aqueous data re-calculated to SO_4-accessible porosity assuming the same relationship between accessibility and clay-mineral content as applied above for Cl. The symbols for groundwater cover the packer intervals.

The re-calculated aqueous extraction concentrations exhibit systematically higher and more variable concentrations than the SQ and AD data. The discrepancy between aqueous extraction and squeezing/advective displacement data becomes even larger when anion exclusion is considered, e.g. by assuming the same relationship between anion-accessible porosity and clay-mineral content as that applied for Cl (Fig. 5.3-1 below). However, it should be noted that the anion-exclusion effect of SO_4 in the considered rocks is not well known. From double layer theory, the exclusion of SO_4 in clayrocks is predicted to be higher because of its higher charge (Gimmi & Alt-Epping 2018). On the other hand, SO_4 has a larger tendency to form weak complexes, such as with alkaline earths, thus partly compensating the charge effect. Also, data for selenate in Opalinus Clay from Mont Terri suggest a similar diffusion regime as for Cl (Gimmi et al. 2014), even though no exact values for anion accessibility are available. A similar discrepancy between squeezing or advective displacement data on the one hand and aqueous extraction data on the other hand has been observed for other boreholes, such as Schlattingen-1 (Wersin et al. 2013), the BUL1-1 borehole (Mazurek et al. 2021), the TRU1-1 borehole (Aschwanden et al. 2021) as well as in in the Mont Terri Rock Laboratory (Wersin et al. 2021). In the latter case, waters sampled from packed-off boreholes exhibited similar sulphate concentrations and SO_4/Cl ratios as waters squeezed from nearby drillcores. The reason for the higher sulphate levels derived from aqueous extraction compared to squeezing or advective displacement data is not understood at this stage, in spite of a recent systematic aqueous extraction study on Opalinus Clay including Mont Terri and BUL1-1 samples (Debure & Gailhanou 2019, Aschwanden & Wersin 2020).

The porewaters from squeezed samples are slightly undersaturated with respect to celestite (SI: –0.08 to –0.22), while those from advectively displaced samples are somewhat oversaturated (SI: 0.06 to 0.27). Celestite could be identified in some samples of the matrix of the Opalinus Clay and overlying formation samples at Mont Terri and Schlattingen-1 by a combined SEM/microprobe study (Jenni et al. 2019). Samples from advective displacement and squeezing are generally undersaturated with regard to gypsum, and gypsum is not thought to play a role in this issue.

The depth profile of SO_4/Cl ratios (Fig. 5.3-2) shows similar trends as the SO_4 profile. The general discrepancy between AD and SQ data on the one hand and AqEx data on the other are clearly evident and not discussed further. In the Dogger part, SO_4/Cl ratios in AD and SQ data remain distinctly below 1, scattering around 0.5. The overlying groundwater samples from the Passwang Formation displays a SO_4/Cl molar ratio close to 1. In the underlying Staffelegg Formation, the two AD and SQ samples range between 0.5 and 1, which may reflect a strongly increasing trend with depth, as suggested from the AqEx data. The groundwater sample from the underlying aquifer shows a high SO_4/Cl ratio of ~ 14. Note that SO_4/Cl ratios are generally much higher than that of modern seawater (0.052) (red line in Fig. 5.3-2 below).

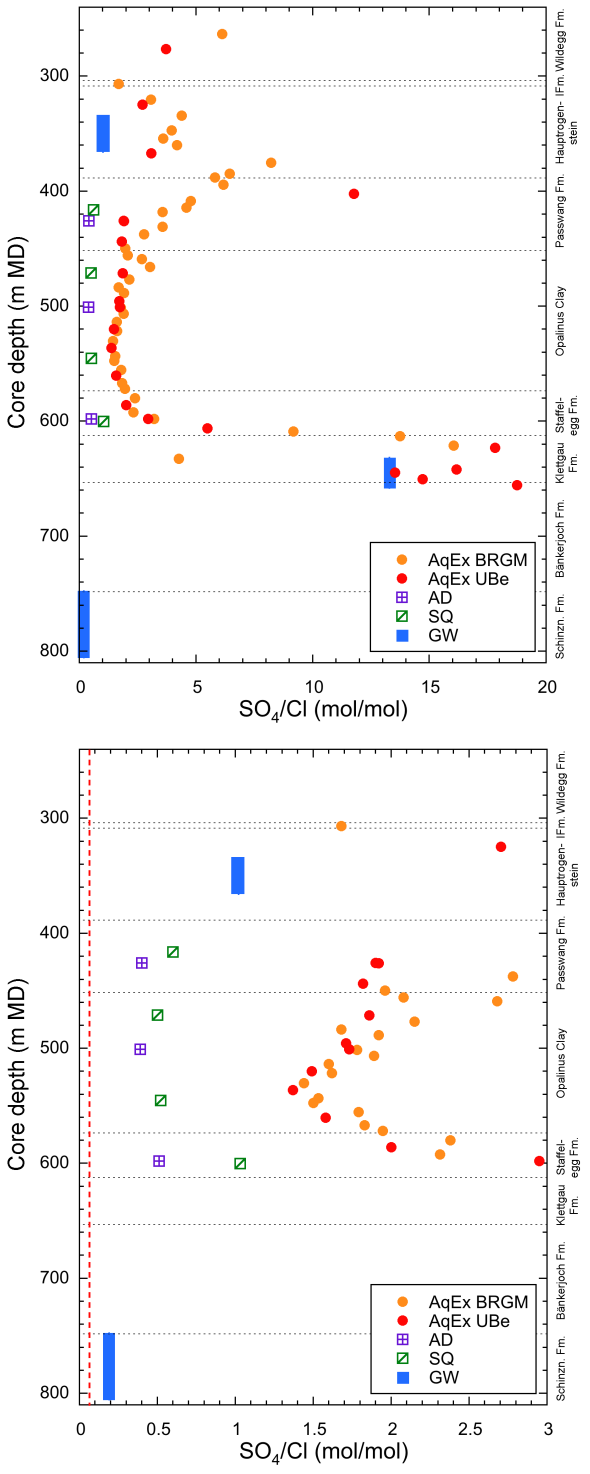

Fig. 5.3-2: Profiles showing molar SO_4/Cl ratios obtained from different methods at different scales

The red line in the plot below indicates the value of modern seawater (0.052). The symbols for groundwater cover the packer intervals.

5.4 Cation concentrations in porewaters

Paul Wersin, Eric Gaucher, Thomas Gimmi

Squeezing and advective displacement are the two methods that yield direct information on the cation concentrations in the porewater. Moreover, these can be estimated by simple modelling from the cation exchange data, notably from the cation occupancies on the exchanger. Aqueous extraction data, on the other hand, do not enable straightforward determination of porewater cations because of their modification via cation exchange and mineral reactions during the extraction process.

Both the squeezing and advective displacement method may potentially induce changes in porewater composition, thus also affecting cation composition and distribution. Data from previous boreholes and the Mont Terri rock laboratory, however, suggest, that using not too high squeezing pressures and very early samples in the case of squeezing and advective displacement, respectively, experimental artefacts are relatively minor (e.g., Wersin et al. 2016, Wersin et al. 2021), or at least some level of consistency between AD and SQ data is obtained (Mazurek et al. 2021, Aschwanden et al. 2021, Mäder et al. 2021). It should be pointed out that microbial processes probably occured during the AD experiments of BOZ2-1, as indicated for example by anomalous nitrate levels in the samples (Section 4.7, especially samples at 500.93 and 597.93 m). This obviously also affects the cationic charge.

Depth profiles for Na, Ca, Mg, K and Sr in porewater are illustrated in Fig. 5.4-1. Overall, a differentiated picture regarding consistency between AD and SQ datasets can be seen. Looking at first at the main cations Na, Ca and Mg, the top AD sample from the Passwang Formation lies within the general trend depicted by the four SQ samples: a slightly increasing trend with depth from the Passwang Formation down to the Staffelegg Formation. The main cation in terms of cationic charge is Na followed by Ca and Mg. The two lower AD samples clearly fall off this trend, exhibiting significantly higher concentrations of these cations. This is related to their anomalous nitrate concentrations as illustrated in Fig. 5.4-2. Whereas the cationic charge of Na^+ is compensated almost entirely by Cl^- and SO_4^{2-} for SQ samples and the top AD sample, this is not the case for the two lower AD samples, where an anion charge deficit is evident. (Fig. 5.4-2 above). The remaining anionic charge is in fact carried by nitrate (Fig. 5.4-2 below), produced presumably via microbial processes during the experimental procedure (Section 4.7). The Sr data follows same trends as the other divalent cations Ca and Mg (Fig. 5.4-1). For K, the consistency of both datasets is generally rather good, suggesting that the microbial processes leading to high nitrate levels did not strongly affect the concentrations of this monovalent cation.

The Ca/Na molar ratio shows constant values of about 0.04 for all samples, except for the two AD samples affected by high nitrate levels. Note that the groundwaters from the bounding aquifers (last sample; Lorenz *in prep.*) display a similar Ca/Na ratio (Fig. 5.4-3). For the two samples with anomalous nitrate levels, preferential release of Ca (and other divalent cations) over Na is indicated. This appears to be related to microbial processes and resulting carbonate mineral dissolution (see next Section) having occurred during the AD experiments.

The relationships of cations and their consistency with exchangeable cation populations are further discussed in Section 5.6.

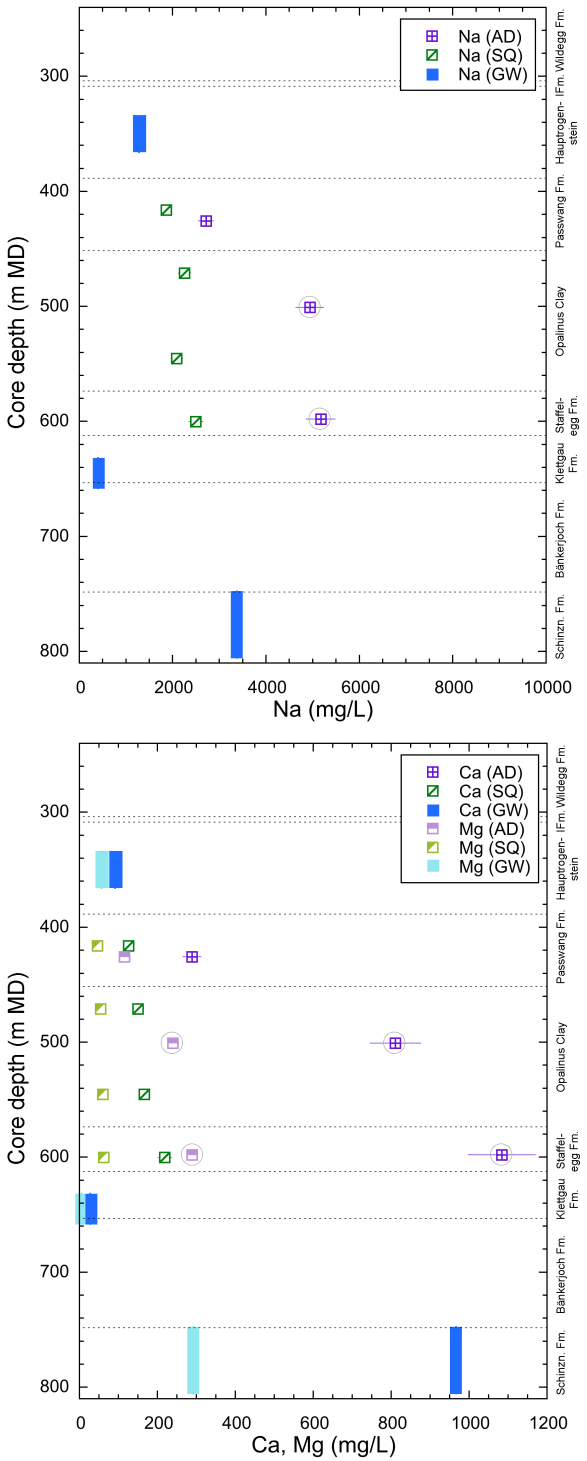

Fig. 5.4-1: Profiles for Na, Ca, Mg, K and Sr in porewater with data from squeezing, advective displacement and groundwater samples

The values of the AD samples, and especially those of the lower two (circled), are most likely disturbed by microbial reactions (see text and Fig. 5.4-2). The symbols for groundwater cover the packer intervals.

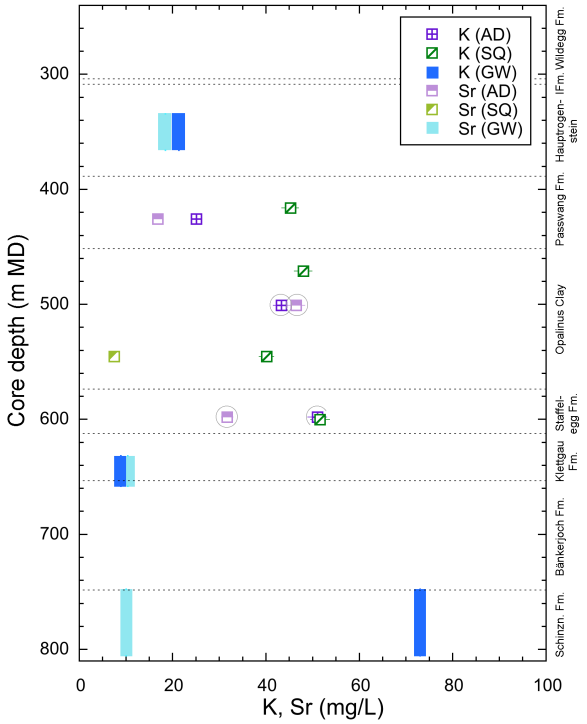

Fig. 5.4-1: (continued)

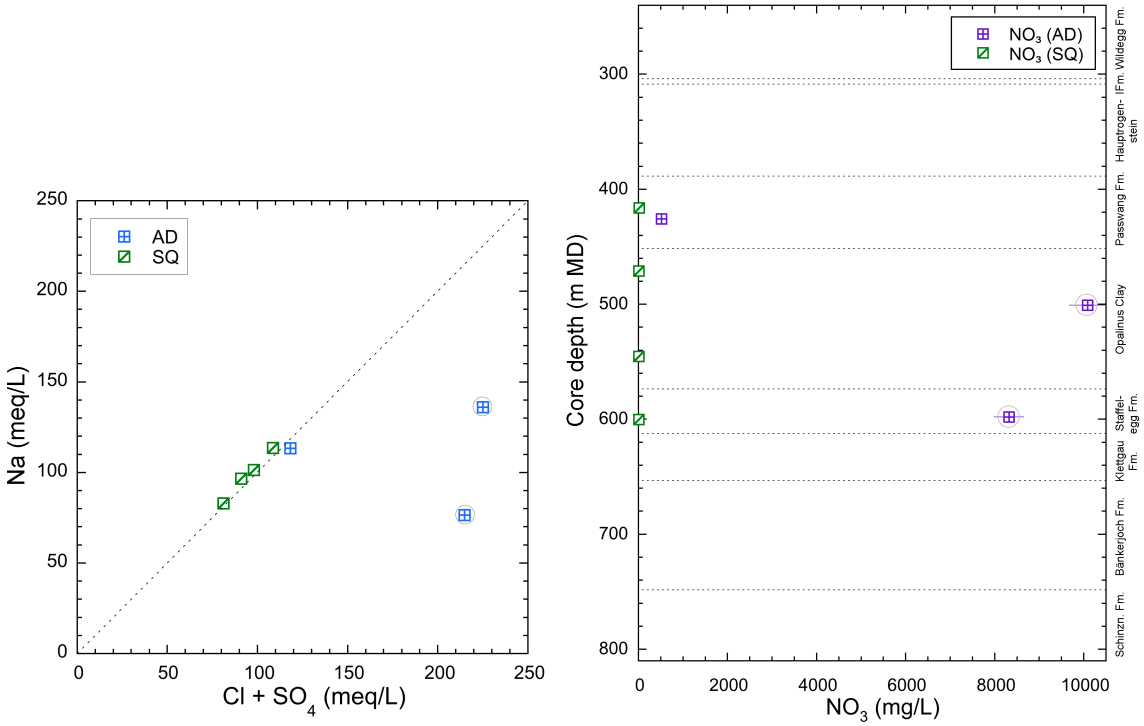

Fig. 5.4-2: AD and SQ data; $Cl + SO_4$ concentrations vs. Na concentrations (meq/L) (above); NO_3 concentrations as a function of depth (below)

Dashed line in plot above: 1:1 relationship between $Cl + SO_4$ concentration and Na concentration. The values of the AD samples, and especially those of the lower two (circled), are most likely disturbed by microbial reactions (see text).

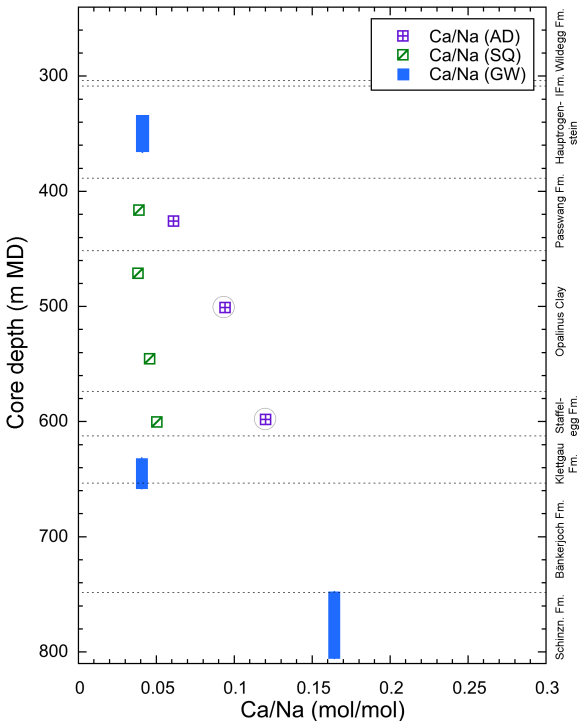

Fig. 5.4-3: Ca/Na ratio (molar units) for SQ and AD samples and groundwater

The values of the AD samples, and especially those of the lower two (circled), are most likely disturbed by microbial reactions (see text and Fig. 5.4-2). The symbols for groundwater cover the packer intervals.

5.5 Dissolved carbon species (inorganic, organic), alkalinity, pH and P_{CO2}

Paul Wersin, Eric Gaucher, Thomas Gimmi

5.5.1 Dissolved inorganic carbon, alkalinity, pH and P_{CO2}

The two methods yielding information on the carbonate system of the porewater are squeezing and advective displacement. Notably, with the two methods TIC, alkalinity (determined by titration) and pH can be measured. Alkalinity may include other compounds (e.g. low-molecular organic acids) than carbonate species (HCO_3^-, CO_3^{2-}) and thus TIC is considered to be a more reliable parameter for constraing the carbonate system of the porewaters (Wersin et al. 2021).

Knowing pH and TIC, the (dissolved) carbonate system is entirely constrained (at constant temperature and pressure) according to Gibbs phase rule and the CO_2 partial pressure can be calculated. It should be noted that it is not straightforward to obtain reliable measurements on these parameters which are prone to perturbations. For example, degassing of CO_2 during the squeezing process may alter pH and TIC parameters[13] (Tournassat et al. 2015, Wersin et al. 2021). In the case of advective displacement, an important perturbation that may arise is related to microbial activity inducing high nitrate levels (Section 4.7.5). Equilibrium with calcite, omni-present in the sedimentary sequence, imposes a further constraint on pH/P_{CO2}. Thus, from the measured Ca, TIC and pH, the saturation state with regard to calcite can be calculated, providing a plausibility test regarding the carbonate system. It is worth noting, however, that calculated saturation indices for calcite close to zero do not a priori confirm that measured parameters, such as pH and TIC reflect in situ conditions. In fact, perturbations during the experimental procedure might lead to a new equilibrium with calcite at different pH/P_{CO2} conditions.

Tab. 5.5-1 shows the measured pH, TIC data together with the derived P_{CO2} and saturation index for calcite from speciation calculations with PHREEQC. Note that for the AD experiments, pH was measured in-line and after sampling, but only in-line pH is considered here (differences between these two measurements are rather small). In general, pH values for AD are in the range of 6.2 – 6.7, whereas those for SQ are much higher, in the range of 8.8 – 9.2, as also illustrated in Fig. 5.5-1 (above, closed symbols). Conversely, TIC values are higher for AD (15 – 18 mM) compared to SQ (2 – 6 mM), even for the uppermost AD sample where NO_3 concentrations were less elevated. Regarding P_{CO2}, measured AD data indicate values of –1.1 to –1.4 bar in log units, whereas much lower values (–3.8 to –4.1) are derived for SQ data, as also illustrated in Fig. 5.5-1 (below, closed symbols). All samples are oversaturated with regard to calcite.

The P_{CO2} data obtained from pH/TIC measurements represent rather extreme values relative to the expected ones (about –2 to –3 log(bar); Wersin et al. 2021). Thus, P_{CO2} values from AD appear too high, which is likely related to the microbial perturbation leading to high nitrate levels up to almost 200 mM (Tab. 5.5-1). Although the details of the nitrate-producing pathway remain unknown at present, it is reasonable to assume that it involved a redox process with the production of acidity. This in turn would have led to the dissolution of carbonates and the production of CO_2 and alkalinity, as schematically illustrated by the following reaction:

$$2CaCO_3 + 3H^+ \rightarrow 2Ca^{2+} + HCO_3^- + CO_2(g) + H_2O$$

[13] But alkalinity is not affected by changes in CO_2 partial pressures as long as no dissolution/precipitation reaction occurs.

This would explain both the high TIC and P_{CO2} derived from the AD data[14]. In the case of SQ data, CO_2 degassing, which is known phenomeon occuring during the squeezing process, may explain high pH, and increase of CO_3^{2-} activity (leading to calcite oversaturation), schematically represented by the two reactions (where ↑ represents degassing):

$$HCO_3^- \rightarrow CO_2(g)\uparrow + OH^-$$

$$2\ HCO_3^- \rightarrow CO_2(g)\uparrow + CO_3^{2-} + H_2O$$

Tab. 5.5-1 Measured pH and TIC as well as calculated P_{CO2}, $SI_{calcite}$ and pH from AD and SQ experiments (see text)

Method	**Depth**	**From measured parameters**				**Calculated**		**Nitrate**
		pH	**TIC**	**log P_{CO2}**	**SI calcite**	**log P_{CO2}**	**pH**	
	[m]		[mmol/L]	[bar]	[–]	[bar]		[mmol/L]
AD	469.40	7.20	15.06	-1.39	0.55			8.36
AD	516.72	7.15	17.90	-1.32	1.00			165.87
AD	575.26	6.80	15.12	-1.09	0.61			137.07
SQ	494.48	9.25	5.75	-3.93	1.74	-1.68	7.24	0.20
SQ	516.27	9.18	3.54	-4.07	1.54	-2.07	7.40	0.19
SQ	554.36	8.85	2.82	-3.78	1.23	-2.30	7.49	0.11
SQ	590.32	9.00	2.14	-4.08	1.28	-2.46	7.55	0.13

[14] This process would also explain the elevated Ca concentrations (Section 5.4).

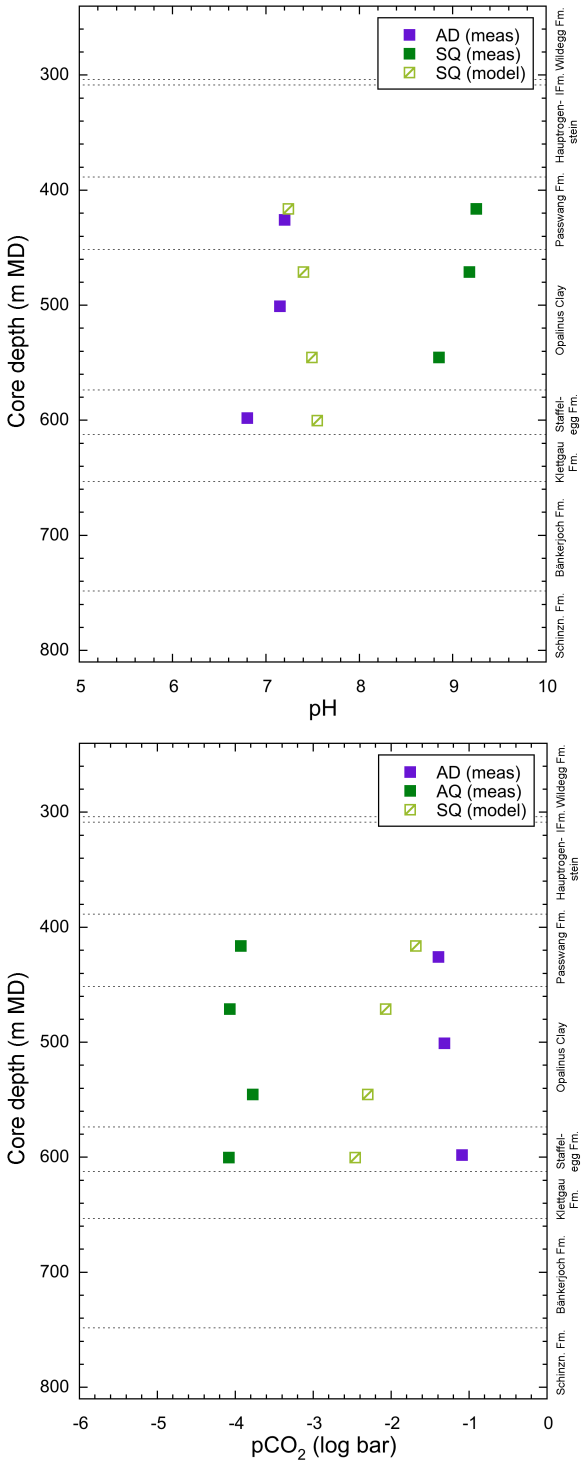

Fig. 5.5-1: pH (above) and P_{CO2} values (below) from AD and SQ (see text)

Solid symbols: measured pH, P_{CO2}: calculated from measured pH and TIC. Open symbols: models based on calcite equilibrium (see text).

Assuming that SQ samples were affected by CO_2 outgassing during the experimental procedure, CO_2 was added until attainment of calcite saturation with aid of PHREEQC. This leads to higher pH and lower P_{CO2} values, depicted as open symbols in Fig. 5.5-1. The calculated pH/P_{CO2} values seem to be in a reasonable range (pH 7.2 – 7.5, log (P_{CO2}) –1.7 to –2.5) according to previous pH/P_{CO2} data in Opalinus Clay (Wersin et al. 2021). This supports the hypothesis that the carbonate system was mainly affected by CO_2 degassing and much less by carbonate dissolution during the squeezing procedure.

In summary, both AD and squeezing data indicate perturbed P_{CO2} conditions. Re-calculating P_{CO2} and pH assuming calcite equilibrium seems to lead to reasonable values in the case of SQ.

5.5.2 Dissolved organic carbon

Information on dissolved organic carbon is available from advective displacement (AD) and squeezing (SQ) data as well as from aqueous extracts of AD cores (AqEx-AD):

1. SQ: TOC
2. AD: TOC, low molecular-weight organic acids (LMWOA)
3. AqEx-AD: low molecular-weight organic acids (LMWOA)

Moreover, the (solid) organic carbon content (C_{org}) from the corresponding SQ and AD samples is available besides those from PW, RP, DI, and OD samples.

Before discussing the dissolved organic carbon data it is worth mentioning some general points: The organic carbon in the sedimentary rock consists of refractory kerogen and only a small fraction is extractable by solvents (< 1%). The water soluble-organic carbon is even smaller, thus for example reaching a few mg C/L in the porewater of Opalinus Clay at Mont Terri or in the Callovo-Oxfordian Formation sampled from seepage boreholes (Courdouan Merz 2008, Courdouan et al. 2007a and b). Higher concentrations (several tens to hundreds of mg C/L) are generally measured in porewaters extracted from core samples, such as from squeezing or advective displacement (Wersin et al. 2013, Wersin et al. 2021). In the case of aqueous extracts, a significant amount of organic carbon is released to the solution. This indicates that a fraction of the "solid" carbon fraction is mobilised during the extraction process. It also suggests the preferential release of loosely bound small organic molecules.

The TOC concentrations from AD and SQ data are shown in Fig. 5.5-2 (above). The SQ data show rather constant levels of 100 – 120 mg/L for the three samples (note that no TOC data was acquired for the lowermost sample). Regarding AD data, the top sample from the Passwang Formation displays a similar TOC concentration, but the two lower ones, affected by high nitrate levels, display much higher TOC levels above 600 mg/L. This underlines that microbial perturbation also affected TOC contents of these two lower samples. The solid organic carbon profile (Fig. 5.5.2 below) show C_{org} amounts of ~ 1 wt.-% in the Opalinus Clay and somewhat lower amounts in the adjacent formations. A few limestone samples from the Hauptrogenstein contain rather elevated levels. The TOC data do not show any correlation with the corresponding C_{org} values.

The concentrations of the measured LMWOA are below detection for the three AD samples (LWMOA were not measured in SQ samples). The fact that acetate is below detection (< 20 mg/L) is conspicuous, since acetate levels were generally rather elevated in samples from previous boreholes, constituting a significant fraction of the TOC. This difference might also be related to the microbial activity in the AD cores by which acetate would have been transformed.

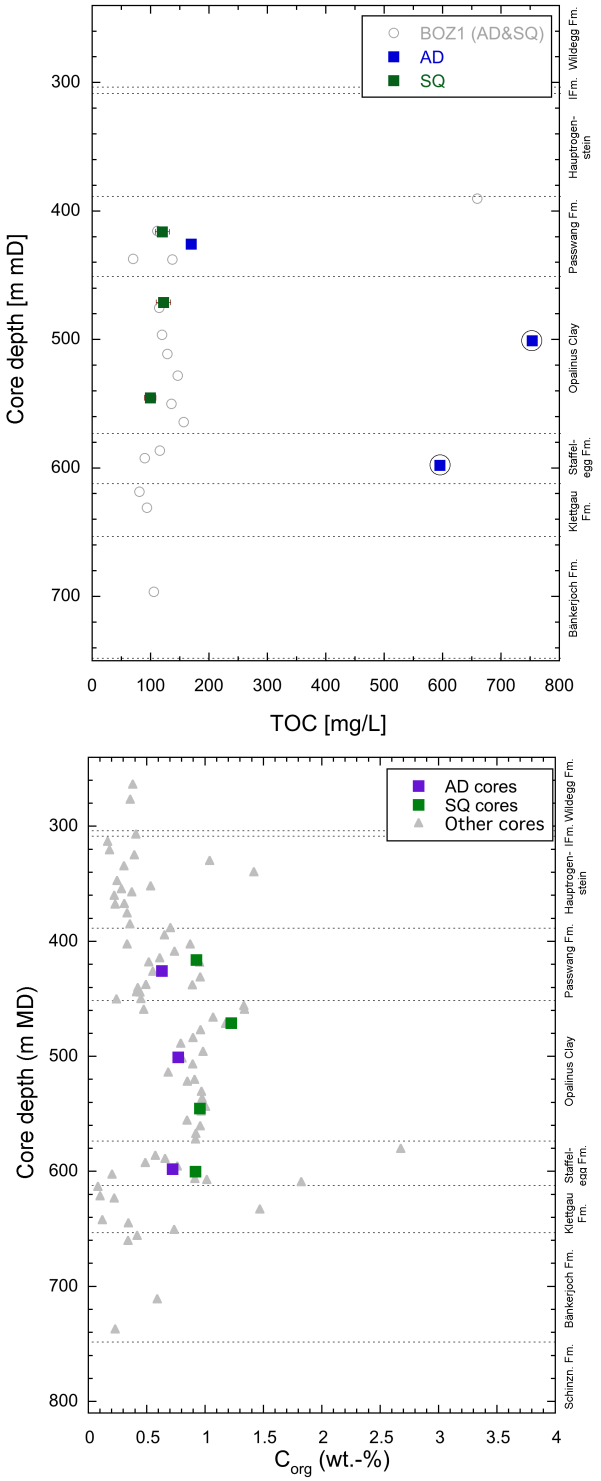

Fig. 5.5-2: TOC concentrations (above) from AD and SQ and organic carbon content in rock (below) in AD, SQ and other cores

The values of the AD samples from BOZ2-1, and especially those of the lower two (circled), are most likely disturbed by microbial reactions (see text and Fig. 5.4-2).

5.6 Cation exchange capacity and exchangeable cation population

Paul Wersin

5.6.1 Corrected exchangeable cation data

As mentioned in Section 4.5, in order to obtain the exchangeable cation concentrations, the extracted cation data need to be corrected for cations dissolved in the porewater and the cations released from (potential) mineral dissolution. As shown from previous work (e.g. Hadi et al. 2019) and also indicated from speciation calculations presented in Section 4.5 (Tab. 4.5-4), carbonate mineral dissolution is minimised with the appropriate S/L ratio, extraction time and pH conditions. Such conditions were applied to the University of Bern dataset.

Two correction methods for cations dissolved in the porewater were applied based on the concentrations of the main anions chloride and sulphate (Bradbury & Baeyens 1998, Hadi et al. 2019). The first correction method ($NaCl/Na_2SO_4$) attributes dissolved Cl and SO_4 from the Ni-extracts to Na and leaves the other cations unchanged. The second method ($NaCl/CaSO_4$) attributes Cl to Na and SO_4 to Ca, leaving the other cations unchanged. In both methods, the CEC is calculated from the sum of cations (ΣCAT) minus the concentrations (normalised to meq/kg_{dry_rock}) of Cl and SO_4. The corresponding data are shown in Tab. 5.6-1. The relative difference between the uncorrected and corrected sums of extracted cations (ΣCAT) is 4% for all three samples.

The values for the corrected ΣCAT are close to those of Ni consumption, albeit generally slightly lower by –6% to –14%. The good match between the two datasets supports the validity of the correction procedure for deriving the CEC based on the sum of cations.

Fig. 5.6-1 shows the CEC parameters as function of the clay-mineral content. Regarding Ni consumption, no clear trend can discern but the sum of cations suggests the expected increasing trend of CEC with clay-mineral content. It should be noted that the difference in clay-mineral content between the samples is rather small. Previous boreholes containing larger datasets, such as for example BOZ1-1, show a clear correlation between CEC (Ni consumption, sum cations) and clay-mineral content (Mazurek et al. 2021, Aschwanden et al. 2021, Mäder et al. 2021, Wersin et al. 2022). Further correlations are discussed in the following section where data from PSI is included.

The exchangeable cations are expressed as cation fractional occupancies (in equivalent fractions) in Tab. 5.6-1. Na and Ca are the main exchangeable cations, followed by Mg and K. The Sr occupancies are considerably lower (0.6 – 1.2% of the CEC).

Tab. 5.6-1: Sum of cations and cation occupancies obtained from Ni-en extraction after correction (University of Bern data)

First line for each sample indicates fractional cation occupancies (fr.oc.; in equivalent units) obtained by the $NaCl/Na_2SO_4$ correction method, the second line those obtained by the $NaCl/CaSO_4$ method.

Type	**Depth** [m]	**Formation**	**Clay-mineral content** [wt.-%]	**Sum CAT raw** [meq/kg_{rock}]	**Sum CAT corr.** [meq/kg_{rock}]	**Na** fr.oc.	**K** fr.oc.	**Ca** fr.oc.	**Mg** fr.oc.	**Sr** fr.oc.
AD	521.06	Passwang Fm.	35	85.5	82.3	0.35 0.38	0.05	0.37 0.34	0.21	0.012
AD	576.32	Opalinus Clay	52	92.0	88.7	0.41 0.44	0.05	0.35 0.32	0.18	0.011
AD	645.48	Staffelegg Fm.	47	90.3	86.4	0.39 0.42	0.06	0.38 0.35	0.17	0.006

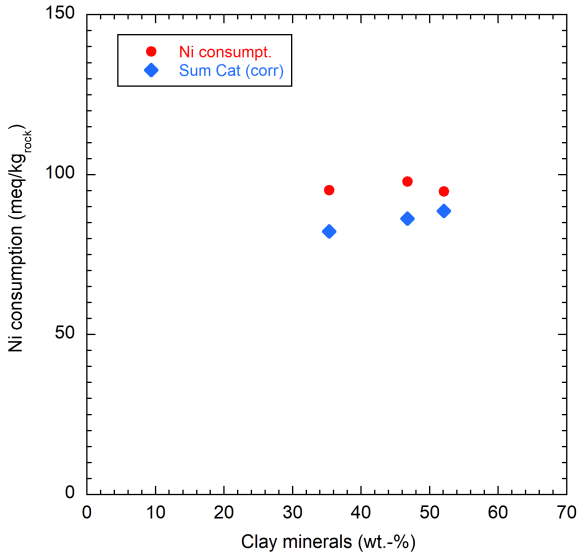

Fig. 5.6-1: Ni consumption and sum of (corr.) cations as a function of the clay-mineral content (data of University of Bern)

5.6.2 Comparison with data from PSI

A dataset including 10 samples from the BOZ2-1 borehole was elaborated by PSI (Marques Fernandes & Baeyens *in prep.*). Samples originated from the Passwang Formation down to the Staffelegg Formation. In a first step, the CEC at PSI was estimated for all samples from Ni consumption with the Ni-en extraction method. Subsequently, the main dataset was generated via CsCl extraction, from which the CEC and the exchanger population were obtained. The CEC was derived by subtracting the anion equivalents (Cl, SO_4, HCO_3/CO_3) from those of the cations (Na, Ca, Mg, K, NH_4, Sr). Cl inventories were determined in separate aqueous extraction experiments. The exchanger population was derived by two correction methods: (1) attributing Cl and SO_4 to Na and TIC to Ca, and (2) attributing Cl to Na and SO_4 and TIC to Ca. Note that these two methods are analogous to the ones used for the University of Bern samples presented above, except for the additional consideration of TIC. The contribution of the latter is less relevant in the case of the University of Bern data (see Tab. 4.5-4) because of the much higher solid/liquid ratios and thus a lower contribution of mineral dissolution to measured cation concentrations.

The conditions applied in the different extraction methods of PSI and University of Bern are compared in Tab. 5.6-2. Important differences of the PSI methods relative to that of the University of Bern are (i) the lower solid/liquid ratios, (ii) the smaller amount of solid mass and (iii) the more variable concentration of the index cation depending on the expected CEC.

Tab. 5.6-2: Extraction conditions applied by University of Bern and PSI

	University of Bern	**PSI**	**PSI**
Extraction method	Ni-ethylenediamine	Ni-ethylenediamine	CsCl
Initial extract solution concentration	98 – 102 mmol/L	3 mmol/L	34 mmol/L
Solid/liquid ratio	~ 0.9 kg/L	~ 0.032 kg/L	0.05 – 0.11 kg/L
Amount of solid used	~ 30 g	~ 1 g	~ 1.3 – 4.3 g [a)]
Extraction time	24 h	24 h	24 h
Final pH	8.3 – 8.5	7.7 –7.8	8.7 – 9.2
Sample disaggregation	Disintegration by hand to a few mm^3 pieces	Milled and passed through 1 mm sieve	Milled and passed through 1 mm sieve
Sample storage time prior to preparation	1 – 14 days	Several months [b)]	Several months [b)]
Extraction in glovebox	Yes	No	Yes

[a)] S/L ratio adjusted to obtain the expected index cation consumption-to-CEC ratio.

[b)] In glovebox.

Cation exchange capacity and corrected sum of extracted cations

The Ni-en consumption and the corrected ΣCAT data (the latter from Ni-en extraction in the case of University of Bern (UniBe) and CsCl extraction in the case of PSI) are shown in Fig. 5.6-2. From the comparison of these two datasets, the following findings can be derived:

- The CEC values obtained from Ni consumption exhibit consistent values for both datasets (to the degree the small number of samples permits a comparison; Fig. 5.6-2 above). In this context, it should be noted that the two datasets were not performed on the same samples, thus CEC variations at similar depths due to mineralogical variation can be expected.
- The CEC values obtained from the corrected sum of cations indicate somewhat less consistency between University of Bern and PSI datasets (Fig. 5.6-2 below) relative to Ni consumption data. Values obtained by University of Bern suggest slightly lower values for the upper two samples.
- In the case of University of Bern data, the corrected ΣCAT data are generally slightly lower than Ni consumption (by –14 to –6%), whereas the PSI data show the opposite (+4 to +17%).
- In general, both datasets show the expected positive trend between clay-mineral content and CEC, both for Ni consumption and corrected sum of cations (Fig. 5.6-3). There is one sample at 402.15 m with 35 wt.-% clay minerals from the Passwang Formation (Rothenfluh Member) that falls off the trend and displays a rather high CEC. Note that the relative proportions of the illite and smectite end-members in the clay fraction are particularly high in the Rothenfluh Member (65 – 69%), whereas the proportion of kaolinite is low in comparison to the adjacent units.
- The trend improves when illite content or smectite content is considered instead of clay-mineral content (not shown). In fact, the CEC is primarily induced by the structural negative charge of these minerals, whereby the negative charge carried by smectite is about four times larger than that of illite. The correlation between the sum of illite and 4× smectite content and the CEC is clearly superior to that exhibited by the clay-mineral content, as illustrated in Fig. 5.6-4. Note that the outlier sample from the previous graph now lies within the general trend (see previous point).

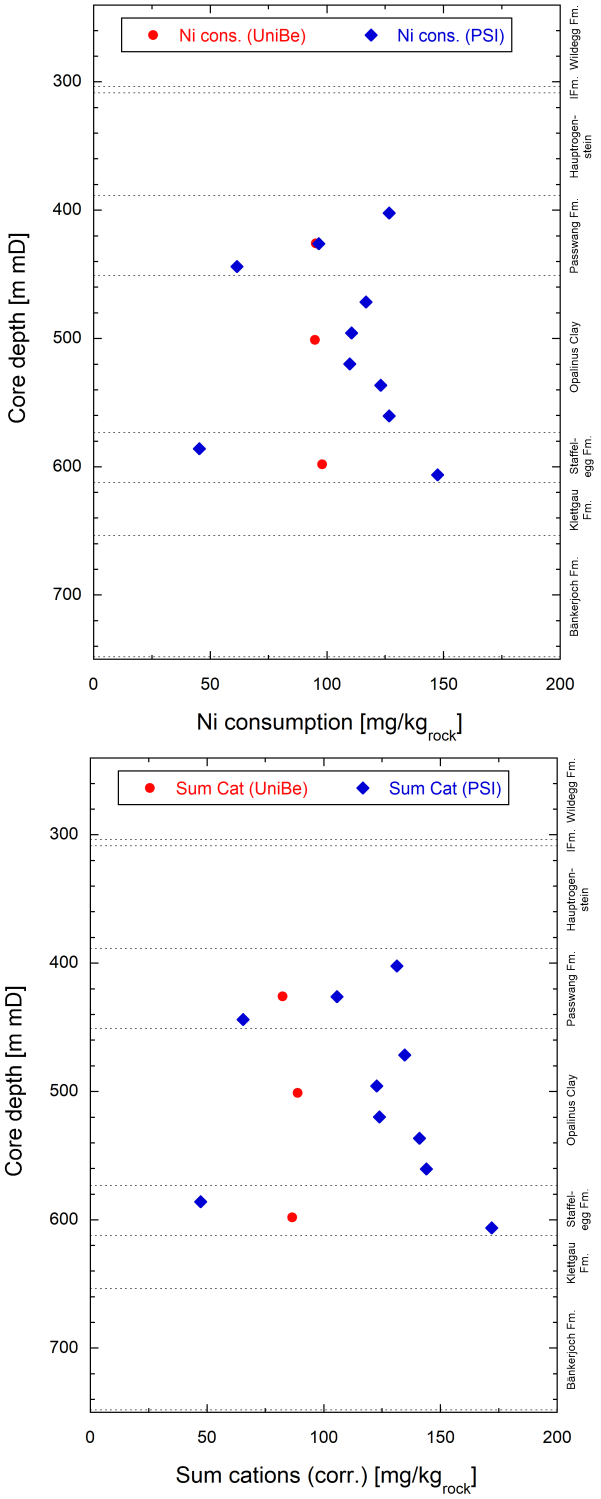

Fig. 5.6-2: Comparison of CEC data from University of Bern and from PSI; Ni consumption data (above) and corrected sum of cations data (below)

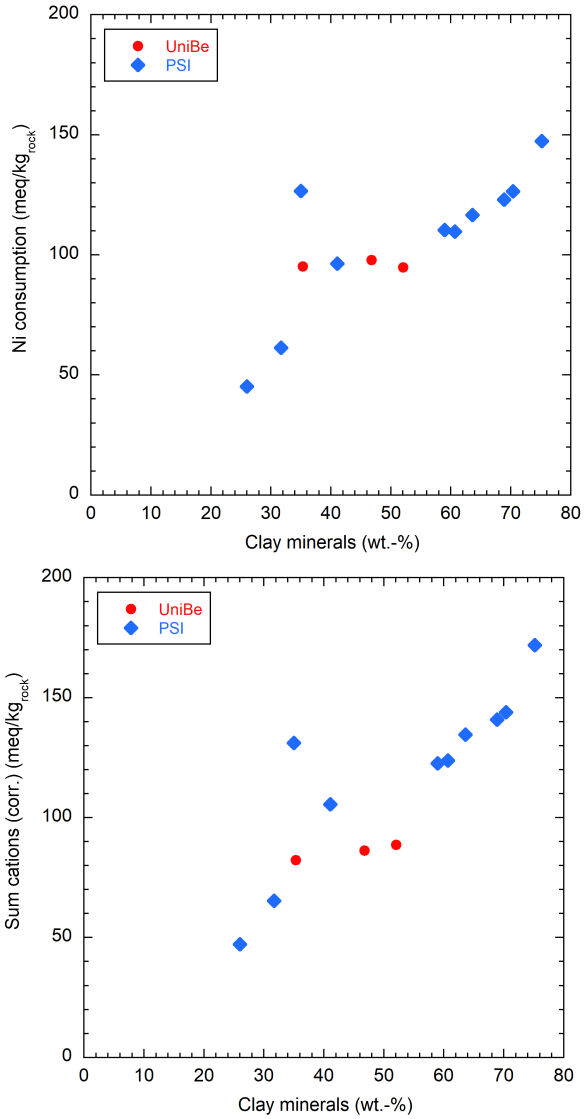

Fig. 5.6-3: CEC data as a function of the clay-mineral content; Ni consumption data (above) and corrected sum of cations (below)

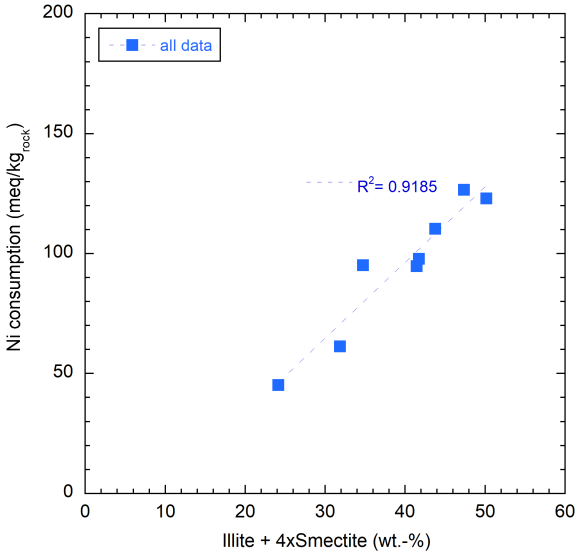

Fig. 5.6-4: Ni consumption as function of the sum of illite end-member content and 4× smectite end-member content.

Note that illite and smectite contents were not measured for all samples.

Exchangeable cation occupancies

The advantage of comparing fractional cation occupancies rather than the extracted cation concentrations is that they are normalised to the sum of cations (as proxy for the CEC) and do not directly depend on the clay-mineral content of the sample.

Fig. 5.6-5 shows the Na and Ca occupancies derived from the two correction methods. Note that in method 1 Cl and SO_4 are attributed to Na, whereas in method 2, SO_4 and, in the case of PSI data, also TIC is attributed to Ca. Thus, the Na fraction is minimised in method 1 and maximised in method 2, while the opposite is true for Ca. Besides the two datasets, the calculated occupancies from the SQ and AD porewater data are shown. The calculations were done with the PHREEQC simulator and the well-established single-site cation exchange model for Opalinus Clay (Pearson et al. 2011, Wersin et al. 2016).

Comparison of "measured" University of Bern and PSI exchangeable cation data illustrates consistent trends for all measured exchangeable cations, except for K, as illustrated in Figs. 5.6-5 to 5.6-7. The cation occupancies back calculated from AD and SQ porewater analyses support the overall trends, but the Na occupancies are systematically higher and those of divalent cations lower than those of the "measured" data. The reason for this deviation is not clear at this stage. The "calculated" data alone from AD and SQ appear to be consistent although AD data were partly affected by microbially induced nitrate generation. Thus, this perturbation cannot explain the difference between "calculated" and "measured" data. Note that in the case of BOZ1-1, "calculated" data from AD/SQ and "measured" data were more in-line compared to BOZ2-1 data.

For K, PSI data display systematically higher occupancies, which is related to the extraction by CsCl mobilising a larger pool of K present in the illite fraction. The same mismatch was already observed in previous boreholes (Mazurek et al. 2021, Aschwanden et al. 2021, Mäder et al. 2021).

In the case of Na and (to a lesser extent) of Ca, University of Bern data display slightly higher occupancies than the PSI data. The reason is not the generally higher extracted amount of these cations, but rather the higher amount of K extracted by the PSI method and, albeit less, the contribution of NH_4, which lowers the fraction of the other cations. The Ca/Na ratio generally shows better agreement between the two datasets (Fig. 5.6-8). The difference between the datasets corrected by method 1 and 2, respectively, increases towards the top of the sequence. In fact, the datasets obtained from method 1 exhibit a shift to higher Ca/Na and (Ca+Mg/Na) ratios in the Passwang Formation, whereas this is less pronounced when correction method 2 is applied.

The Mg/Ca ratio is constant over most of the profile (Fig. 5.6-9 above), but slightly increases in the Passwang Formation. The Sr/Ca ratio profile shows a slight increase from the Staffelegg Formation. Towards the Passwang Formation. There are two outliers from the general trend, at 585.84 m and at 402.15 m, the reason of which is unclear at this stage.

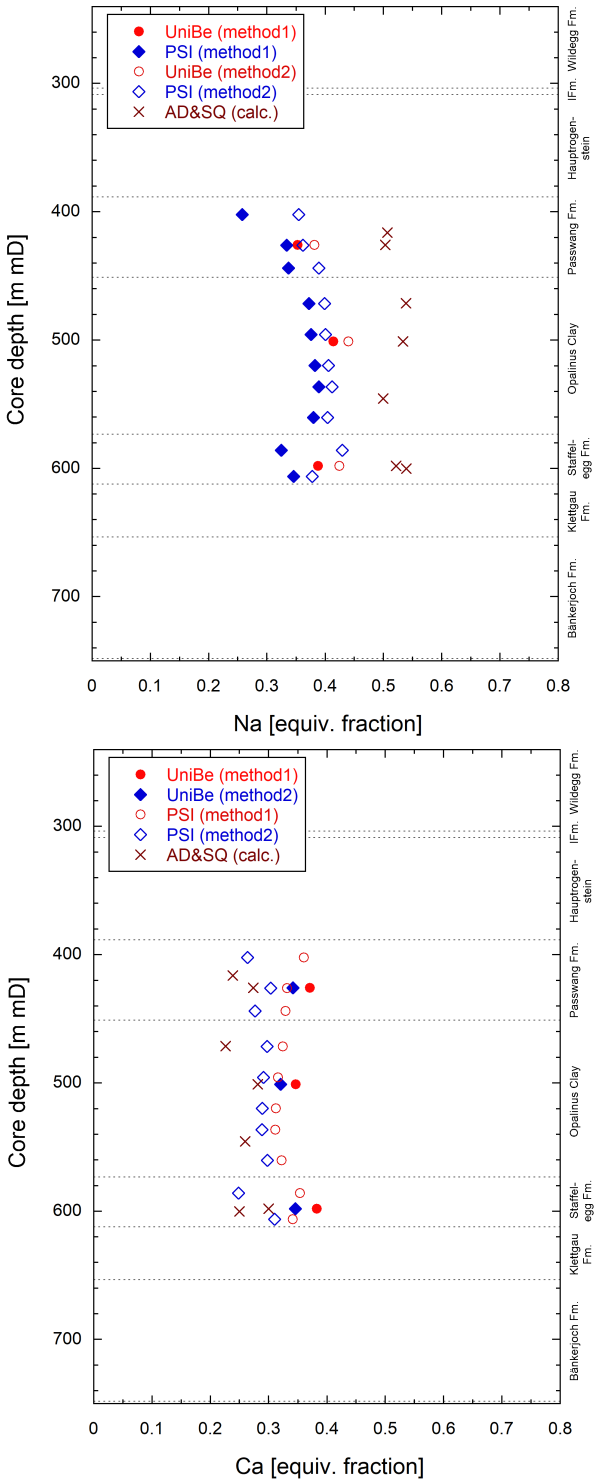

Fig. 5.6-5: Na (above) and Ca (below) occupancies according to University of Bern and PSI data and "back calculated" from AD/SQ data

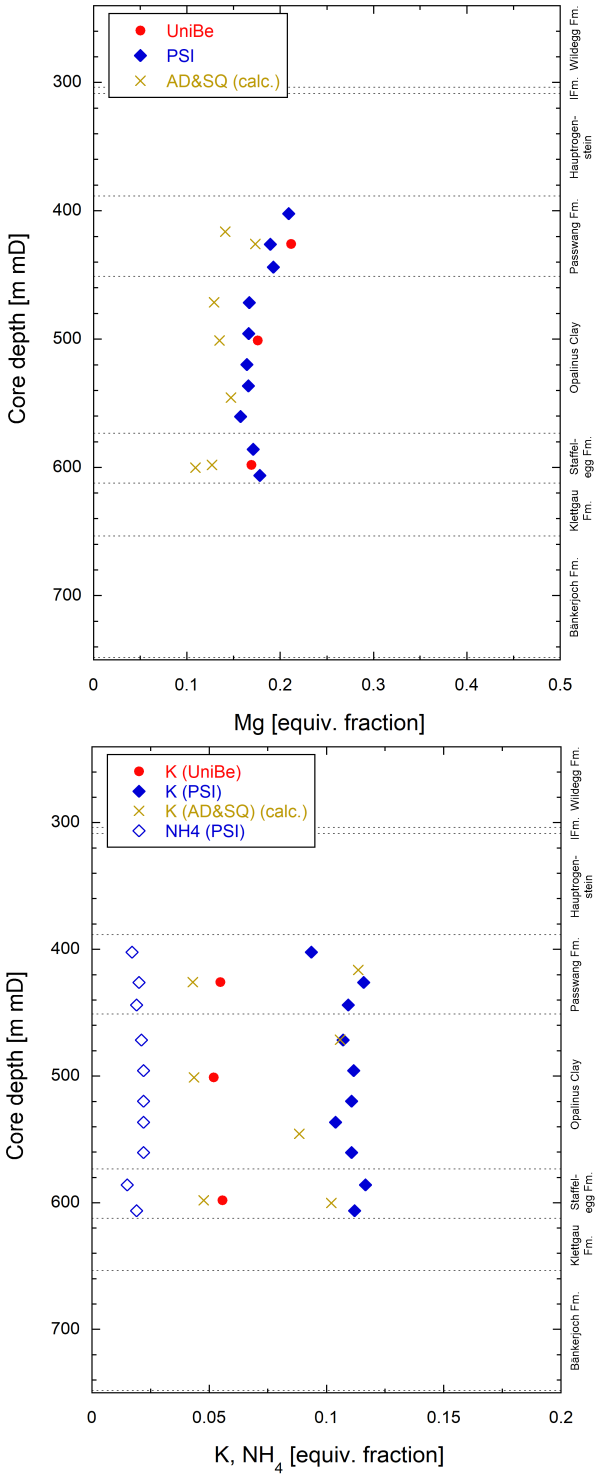

Fig. 5.6-6: Mg (above) and K, NH_4 (below) occupancies according to Uni versity of Bern and PSI data and "back calculated" from AD/SQ data

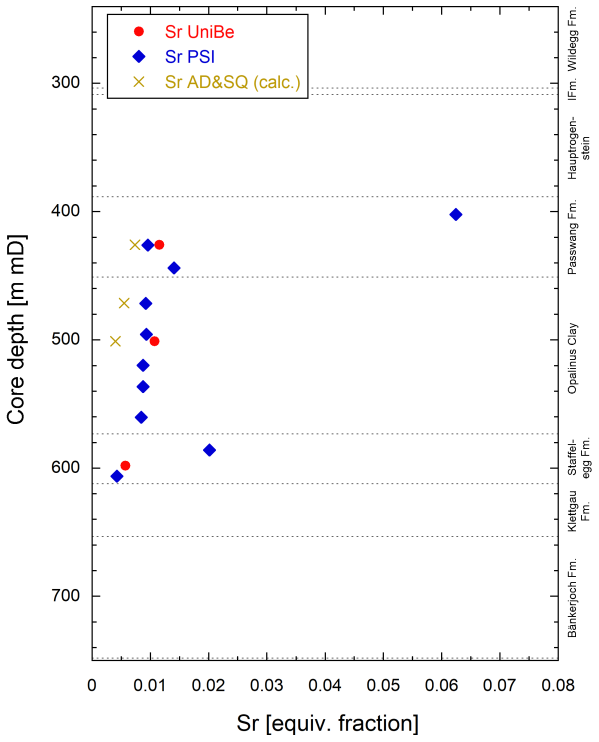

Fig. 5.6-7: Sr occupancies according to University of Bern and PSI data and "back calculated" from AD/SQ data

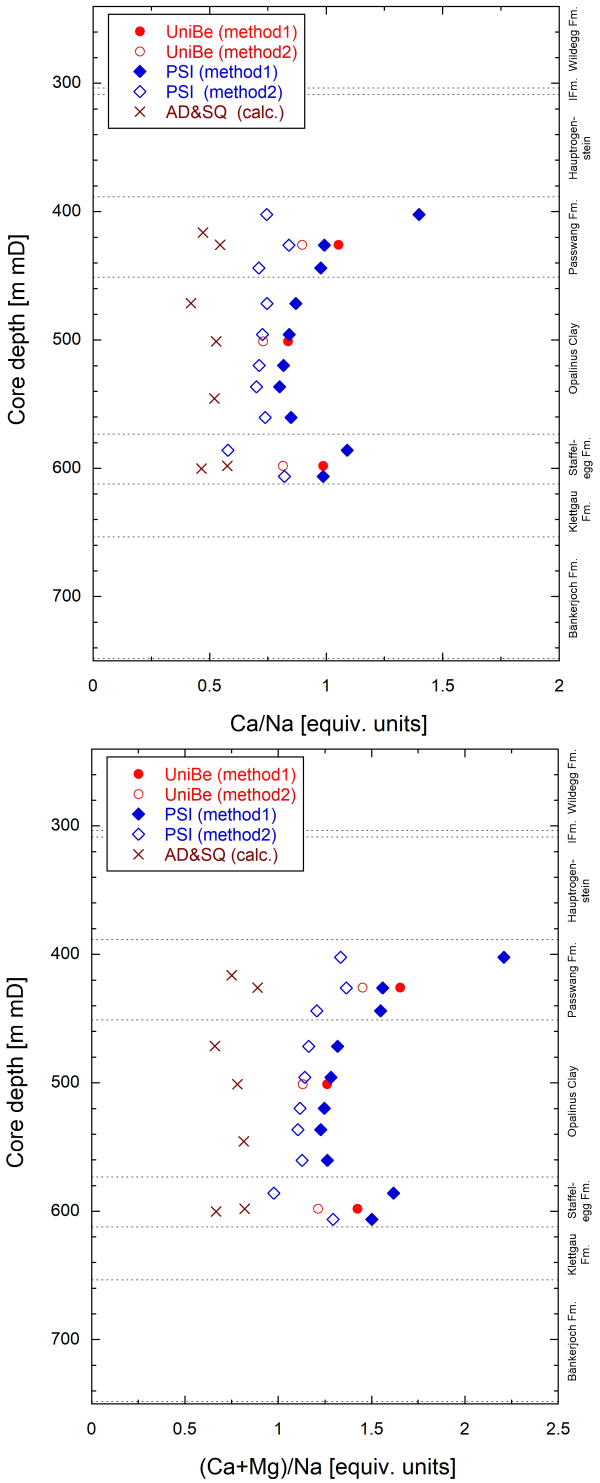

Fig. 5.6-8: Ca/Na ratios (above) and (Ca+Mg/Na) (below) according to University of Bern and PSI data and "back calculated" from AD/SQ data

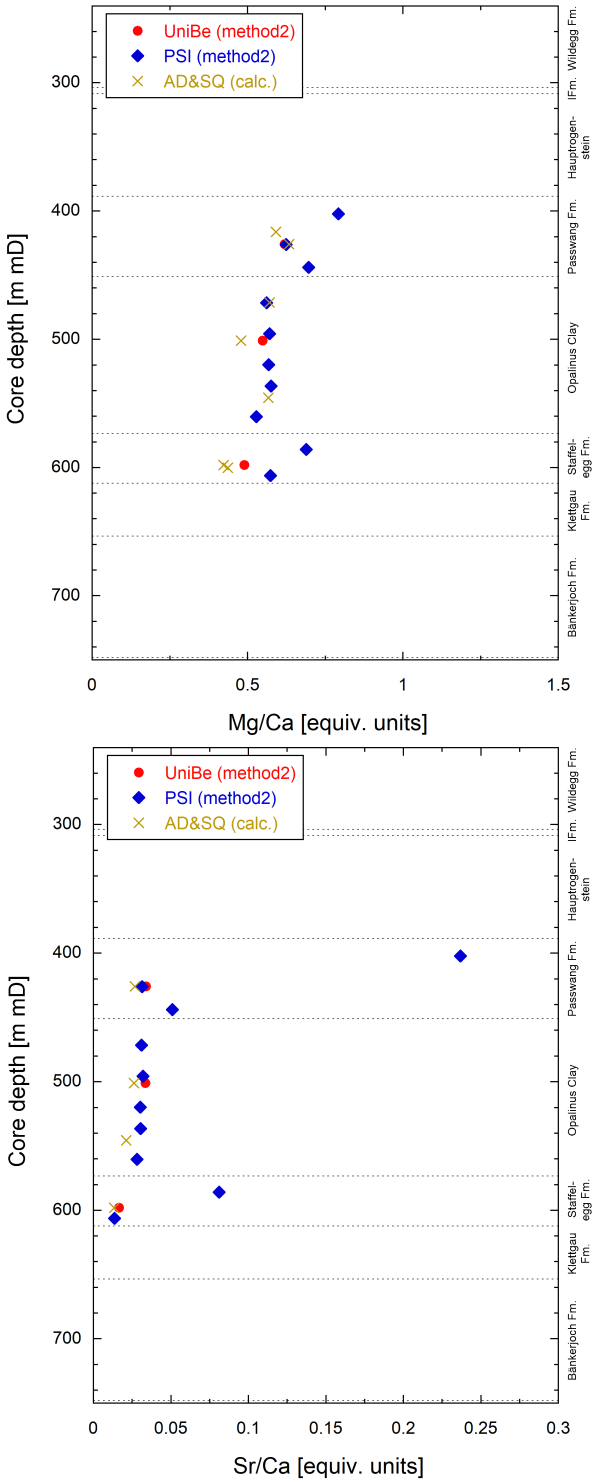

Fig. 5.6-9: Mg/Ca ratios (above) and Sr/Ca ratios (below) according to University of Bern and PSI data and "back calculated" from AD/SQ data

Extracted anions

The amounts of Cl and SO_4 extracted are illustrated in Fig. 5.6-10. Note that for PSI data, Cl data from aqueous extraction are shown, because CsCl was used for extraction of exchangeable cations. These Cl data compare well with those analysed in the Ni-en extracts of University of Bern. Both these datasets agree with the (larger) AqEx dataset of University of Bern which is also illustrated in Fig. 5.6-11 (left). Regarding SO_4, the University of Bern data shows agreement between aqueous and Ni-en extracts. The SO_4 data from PSI, which were obtained from CsCl extraction, exhibit somewhat higher concentrations relative to the University of Bern dataset, but follow the same trend. It thus appears that the CsCl extraction led to higher release of SO_4 compared to the University of Bern extraction procedures. This difference was not noted in the previous boreholes, such as BOZ1-1. Perhaps the higher SO_4 in the PSI extracts in BOZ2-1 were induced by pyrite oxidation. The very high SO_4 content of the sample at 402.15 m depth is possibly affected by celestite, as this sample has also an elevated Sr inventory (Marques Fernandes & Baeyens *in prep.*)

The Cl data reveal a curved shape with strongly decreasing concentrations from the top and the bottom of the Opalinus Clay, respectively. The Cl profile is discussed in more detail in Sections 4.4.3 and 5.2.

The extracted SO_4 levels are generally somewhat higher (on an equivalent basis) relative to Cl. They are rather constant in the Opalinus Clay but display an increasing trend with depth from the footwall of this formation. There is one outlier at 402.15 m in the Passwang Formation.

Total inorganic carbon (TIC) measured in the PSI extracts is 5 – 17 $mmol/kg_{dry\ rock}$. TIC was not measured in the University of Bern extracts but calculated to be below 1 $mmol/kg_{dry\ rock}$ based on the assumption of calcite equilibrium (Tab. 4.5-4). The higher TIC in the PSI extracts is explained by the lower S/L ratio, which induces a higher proportion of dissolved carbonate from carbonate minerals.

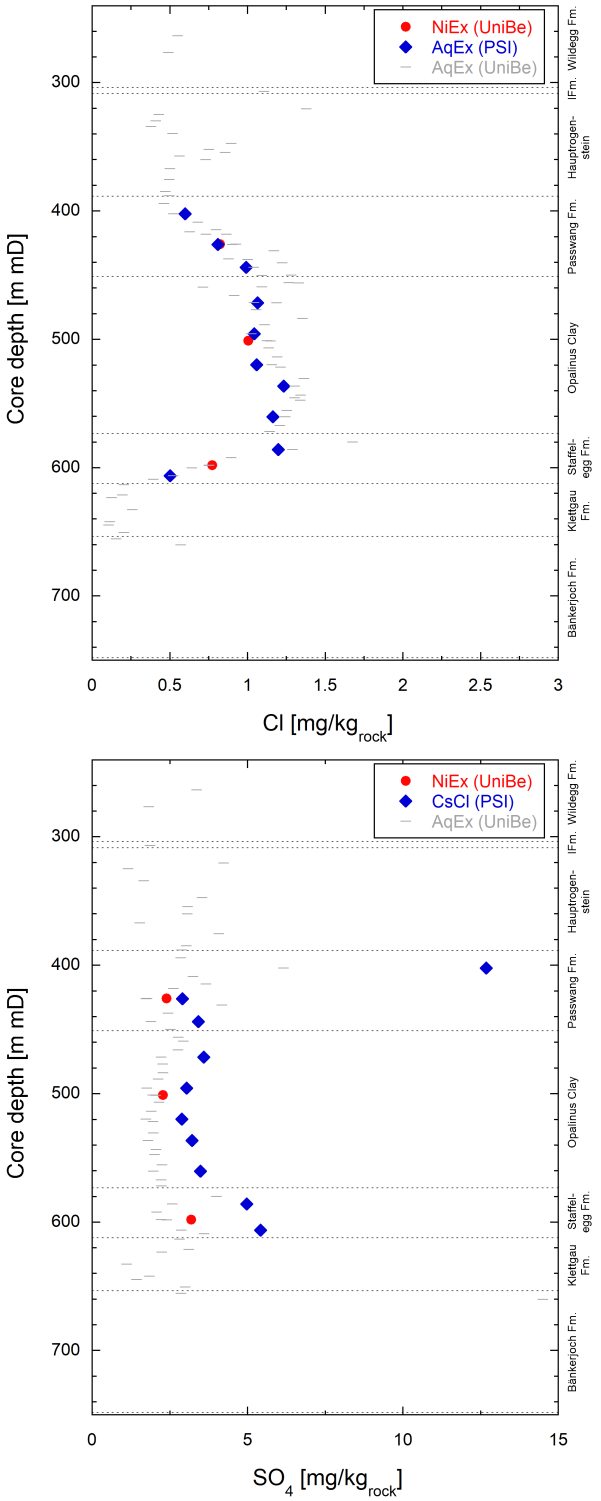

Fig. 5.6-10: Extracted Cl (above) and SO_4 (below) according to University of Bern and PSI data

5.7 Stable water isotopes

Lukas Aschwanden & Thomas Gimmi

5.7.1 Comparison between different methods for the determination of stable porewater isotope compositions

The porewater oxygen and hydrogen isotope compositions were determined using three different methods including isotope diffusive-exchange (Section 4.8), advective displacement (Section 4.7) and high-pressure squeezing (Section 4.6). Data of the three techniques are available for the section 410 – 600 m where clay-rich rocks dominate, and all methods can be applied. For the clay-poor rocks of the Malm and the Keuper only data from isotope diffusive-exchange experiments are available. For the advective displacement technique, the average of the first two displaced solution aliquots is considered as being most representative for the in situ porewater. For the squeezed water, the one obtained at the lowest squeezing pressure (200 MPa or 300 MPa) is considered as being most representative for the in situ porewater.

All the porewater isotope data, together with those for the groundwater samples from the Hauptrogenstein aquifer, the Keuper aquifer, and the Muschelkalk aquifer (*cf.* Section 2.3), are shown in Fig. 5.7-1 as a function of depth. For isotope data from isotope diffusive-exchange experiments the error bars reflect the propagated experimental and analytical uncertainty; for isotope data from advective displacement and high-pressure squeezing experiments only the analytical error is illustrated. In general, there is a good agreement (within the uncertainty) between porewater $\delta^{18}O$ and $\delta^{2}H$-values obtained from isotope diffusive-exchange experiments and high-pressure squeezing, whereas some differences exist for advectively displaced waters: There is approximate agreement between the three methods in the Passwang Formation, whereas in the Opalinus Clay advectively displaced water shows distinctly lower $\delta^{18}O$ and $\delta^{2}H$ values than those obtained by isotope diffusive-exchange experiments. In the Staffelegg Formation advectively displaced water shows distinctly higher $\delta^{18}O$ values than those obtained by the other two methods, whereas $\delta^{2}H$ values agree with the other methods. The reason for this behaviour is currently unknown. However, the breakthrough curves of the water tracers obtained from the AD experiments, notably those from the upper two samples and less so from the lowermost sample, showed peculiarities which were not observed in earlier investigations, and which could not be explained (*cf.* Section 4.7.8, probable disturbance by decomposition of organic matter). Accordingly, all three AD isotope values should be considered as less reliable for the moment.

5.7.2 Comparison with groundwater data and depth profiles

In the Hauptrogenstein of BOZ2-1 porewater isotope values indicate distinct local minima of $\delta^{18}O$ and $\delta^{2}H$ at around 334 – 352 m depth. A groundwater sample could be collected from the packed-off interval at 334.30 – 365.93 m depth whose $\delta^{18}O$ and $\delta^{2}H$ signatures (–7.86 ‰ VSMOW and –57.2 ‰ VSMOW, respectively; *cf.* Section 2.3) seem distinctly enriched compared to the average of porewater obtained from samples within the packed-off interval. However, mud logging indicates that the most transmissive zone is located in the lowermost part of the packed-off interval (mud losses at 351.5 – 370.0 m; Dossier I) where the isotope composition of the groundwater and porewater agree well. The mud loss is likely caused by a joint at 351.7 m (log depth; see Section 2.5 or Dossier V, Section 5.1). Proceeding from the local minima of porewater $\delta^{18}O$ and $\delta^{2}H$ values in the Hauptrogenstein, adjacent porewaters indicate rather steep gradients towards heavier values upwards and downwards. Such steep gradients indicate that the isotope signal in the groundwater is geologically young, or that effective diffusion coefficients in this part are relatively low.

The $\delta^{18}O$ and $\delta^{2}H$ values of groundwater from the Keuper aquifer agree well with those of the porewater obtained from the samples in the packed-off interval and from nearby samples, representing minima of $\delta^{18}O$ and $\delta^{2}H$. Between the Keuper and the Hauptrogenstein aquifer the porewater isotope profiles show continuous, bell-shaped curves with highest porewater $\delta^{18}O$ and $\delta^{2}H$ values in the Opalinus Clay indicating that the evolution of the porewater isotope signatures in this interval are clearly dominated by exchange with the confining water-conducting zones.

As described in Section 4.8, although both $\delta^{18}O$ and $\delta^{2}H$ values of the porewater indicate the same general trends between the aquifers in the Hauptrogenstein and the Klettgau Formation, some differences exist: $\delta^{18}O$ values reach a maximum at the top of the Opalinus Clay from where they increasingly become more negative across the Opalinus Clay and the Staffelegg Formation, whereas porewater $\delta^{2}H$ values remain remarkably constant across the Opalinus Clay and then sharply decrease in the lowermost Opalinus Clay and the Staffelegg Formation. This different behaviour may reflect inherited trends from the initial porewater isotope profiles (i.e., before activation of the confining aquifers) with rather constant $\delta^{2}H$ but $\delta^{18}O$ values decreasing with depth across the low-permeability formations of the Dogger and the Liassic. Interestingly, similar differences, partly less pronounced, were observed in data from other boreholes (Mazurek et al. 2021, Aschwanden et al. 2021, Mäder et al. 2021, Wersin et al. 2022) or even in the older data from Benken (Gimmi & Waber 2004, Gimmi et al. 2007).

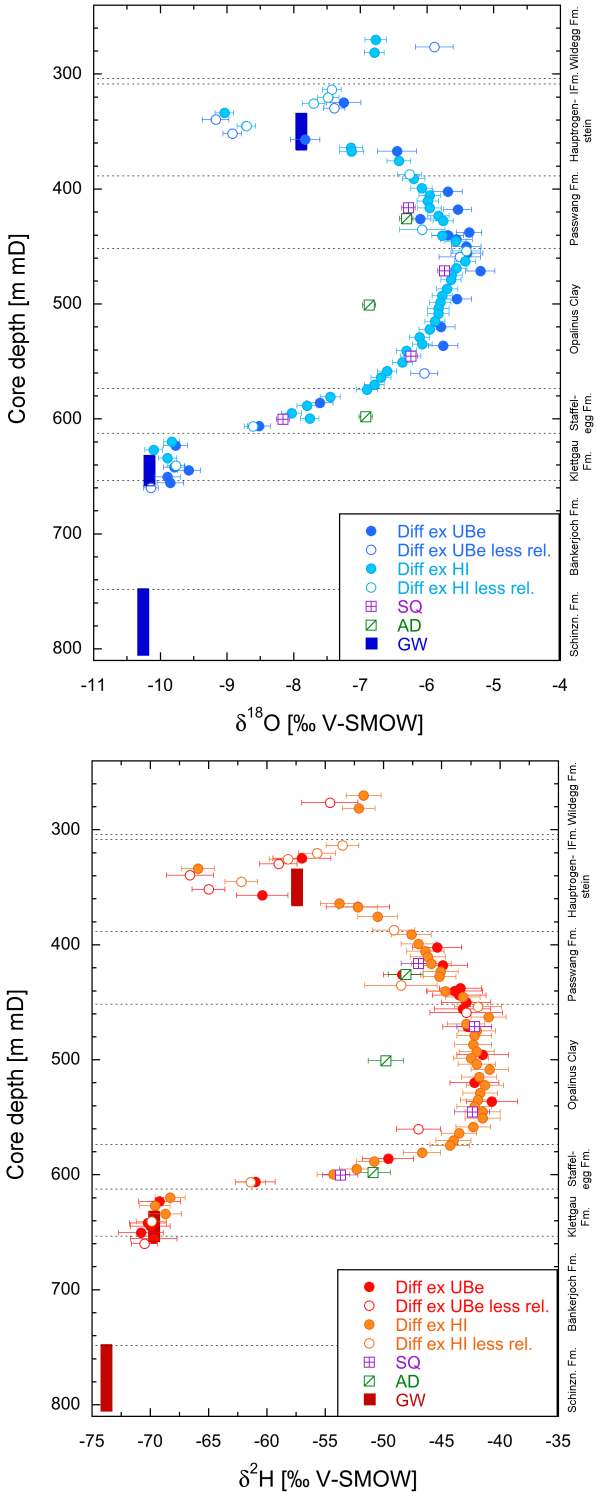

Fig. 5.7-1: Depth trends of $\delta^{18}O$ and $\delta^{2}H$ in groundwater and porewater derived by all techniques

Diff ex: diffusive exchange; SQ: squeezing; AD: advective displacement; GW: groundwater. Open symbols refer to porewater isotope values which are less reliable owing to experimental artefacts (*cf.* Section 4.8). Horizontal bars indicate propagated analytical errors (diffusive exchange) or simple analytical errors (squeezing, advective displacement). Groundwater data are from Lorenz (*in prep.*); the symbol extends over the packer interval.

5.7.3 $\delta^{18}O$ versus $\delta^{2}H$ and comparison with Global Meteoric Water Line

Fig. 5.7-2 illustrates all data in a $\delta^{18}O$ vs. $\delta^{2}H$ diagram. Such diagrams provide information on, e.g., climatic conditions during recharge and indications on water-rock interactions or mixing of different water components. The distribution of the Deuterium excess versus depth is presented in Fig. 5.7-3.

In the upper part of the cored borehole section, porewater isotope compositions evolve towards a local minimum in the Hauptrogenstein (solid red arrow 1 in Fig. 5.7-2), thereby approaching the GMWL in the range of modern recharge. Note that modern recharge does not only refer to recent or post-galcial recharge but rather recharge under climatic conditions similar to recent conditions (e.g., during an interglacial period in the Quaternary). In the remainder of the Hauptrogenstein and the Passwang Formation the porewater isotope composition evolves towards more enriched $\delta^{18}O$ and $\delta^{2}H$ signatures (solid red arrow 2 in Fig. 5.7-2). These trends behave remarkably linear and they follow a seawater dilution line (assuming the minima of $\delta^{18}O$ and $\delta^{2}H$ at around 340 m depth as an approximation for the depleted end-member), however, slightly shifted towards the right. At the base of the Passwang Formation the linear trend described above abruptly breaks and the porewater composition starts to continuously evolve towards values that fall on the GMWL in the lower parts of the Opalinus Clay (solid red arrow 3 in Fig. 5.7-2). This suggests a significant meteoric component in the latter porewaters. Across the Staffelegg Formation the porewater isotope composition evolves along the GMWL, from $\delta^{18}O$ and $\delta^{2}H$ values more enriched than those of modern recharge (solid red arrow 4 in Fig. 5.7-2) towards most negative values in the water conducting zone of the Klettgau Formation, falling into the range of modern recharge (solid red arrow 5 in Fig. 5.8-2). Overall, these trends indicate that the isotopic composition of the porewaters in the Jurassic sediments evolved from the original seawater by exchange with water in the overlying or underlying formations, possibly by water-rock interactions, and finally by the exchange with the present-day confining aquifers.

The profile of the Deuterium excess (Fig. 5.7-3) reflects the above observations: While values between ~ 0 – 5 are observed in the Hauptrogenstein and the Passwang Formation, values near +10 (the value for data lying on the GMWL) are approached in the lower part of the sequence. Similar values are also seen in the Keuper (+11.7) and the Muschelkalk groundwater (+8.3). The porewater values in the lower Staffelegg Formation and the Klettgau Formation tend to be slightly lower than the values in the Keuper groundwater, reflecting $\delta^{18}O$ porewater values in this region somewhat higher than those in the groundwater. The shape of the Deuterium excess profile is similar to that of the BOZ1-1 borehole, with similar values in the Klettgau Formation (including the Keuper aquifer in BOZ2-1) but larger values from the upper part of the Staffelegg Formation towards the Hauptrogenstein (including the aquifer in BOZ2-1). The differences in the upper part are mainly caused by somewhat larger $\delta^{18}O$ values in BOZ1-1 compared to BOZ2-1 and by the influence of the Hauptrogenstein aquifer.

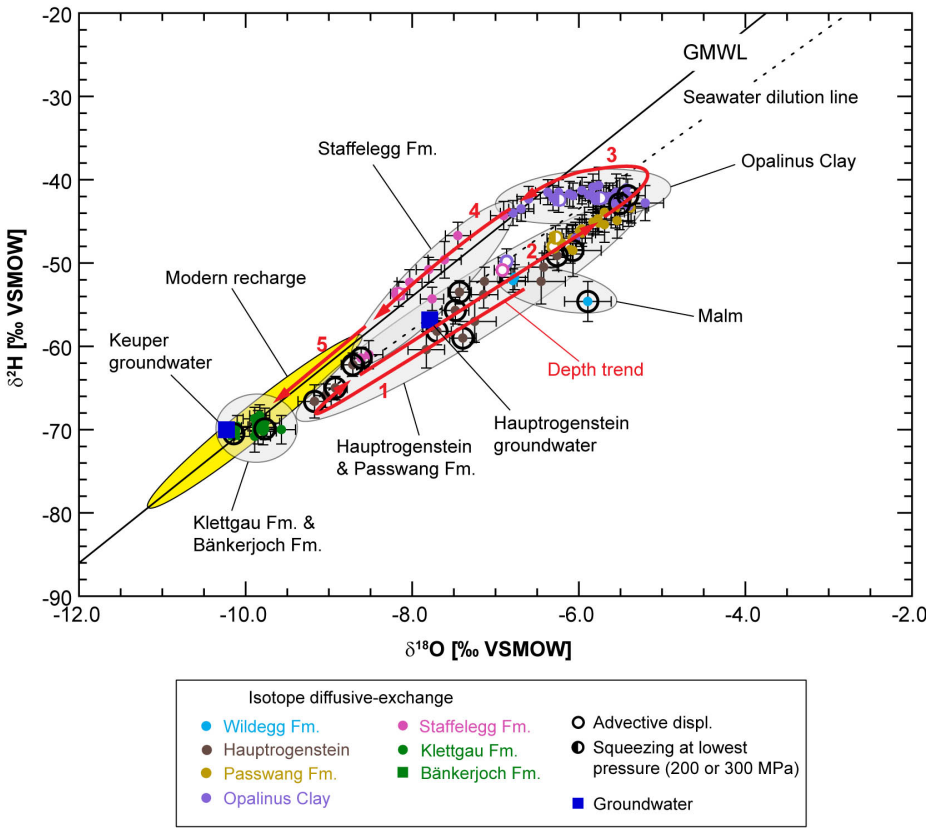

Fig. 5.7-2: $\delta^{18}O$ vs. $\delta^{2}H$ for groundwater and porewater derived by all techniques

Bars indicate propagated analytical errors (diffusive exchange) or simple analytical errors (squeezing, advective displacement). Groundwater data are from Lorenz (2021). GMWL = Global Meteoric Water Line (defined as $\delta^{2}H = 8\ \delta^{18}O + 10$; Craig 1961). Range of modern recharge from Kullin & Schmassmann (1991). Samples in black circles are less reliable owing to experimental artefacts (*cf.* Section 4.8). See text for details on the numbering of red arrows.

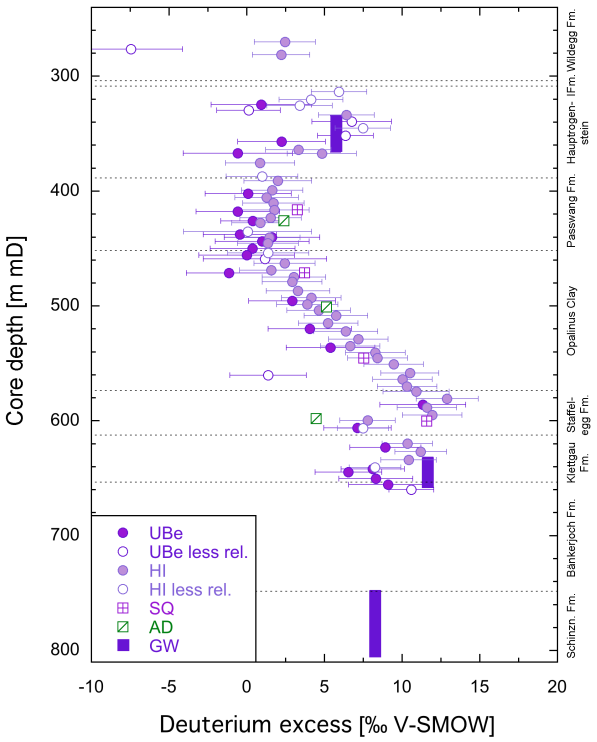

Fig. 5.7-3: Depth trends of the Deuterium excess in groundwater and porewater derived by all techniques

Deuterium excess is +10 ‰ for a sample that lies on the GMWL. Note that the D-Excess of porewater has no implication on the paleo-climatic conditions during infiltration. Diff ex: diffusive exchange; SQ: squeezing; AD: advective displacement; GW: groundwater. Open symbols refer to porewater isotope values which are less reliable owing to experimental artefacts (*cf.* Section 4.8). Horizontal bars indicate propagated analytical errors. Groundwater data are from Lorenz (*in prep.*); the symbol extends over the packer interval.

6 Final remarks and main conclusions

RWI team

High-quality cores could be extracted from the BOZ2-1 borehole as planned between the bottom of the Wildegg Formation and the top of the Zeglingen Formation. Groundwater could be sampled from the centre of the Hauptrogenstein, the Klettgau Formation (upper Keuper) and the Muschelkalk. Only few further porewater samples were taken from units below the Keuper aquifer, down to the top of the Bänkerjoch Formation. The porewater samples enabled to acquire high quality mineralogical, petrophysical and porewater data using a well-established procedure. Drilling operations proceeded without major problems down to a maximum depth of 829 m (Zeglingen Formation, Muschelkalk). Relevant drilling mud losses occurred at a depth of ~ 352 m MD in the Hauptrogenstein (related to a single open subvertical fracture observed in the cores) and at depths from 805 m to 829 m MD in the Schinznach Formation and Zeglingen Formation (caused by steeply dipping open fractures observed in the cores).

As in previous boreholes, a number of systematic depth trends are observed for the contents of clay minerals, quartz and calcite (and, in the lower Hauptrogenstein, of dolomite). The ratio of the illite-to-kaolinite end-member clays also shows a systematic variation, including low and largely constant values in the Opalinus Clay but markedly higher values in the Staffelegg and Passwang Formations. Sections of the Ifenthal Formation and parts of the 'Spatkalk' are macroscopically brownish, which is due to considerable contents of goethite. Samples from these sections have distinct characteristics, such as high grain density.

The depth trends of mineral contents correlate well with those of petrophysical parameters. Water content and porosity correlate positively with clay-mineral content, even though the correlation is far from perfect. This indicates that apart from clay-mineral content, other rock characteristics, such as depositional environment and pore-space architecture, have an influence on porosity. Some samples containing goethite or dolomite fall off the trend and show higher porosities. This is also the case for limestones of the lower Hauptrogenstein.

Nitrogen adsorption data were obtained for 10 samples from the upper and lower confining units of Opalinus Clay only. The samples show strong lithological difference, but the trends of the external specific surface area (BET, N_2 adsorption) match with those observed for the larger data-set from the BOZ1-1 borehole, that is, a broadly positive correlation with clay-mineral contents and a weaker correlation with water contents. The ironoolithic sample from the upper Hauptrogenstein ('Movelier Beds' and 'Spatkalk') exhibits comparably small surface area, but large water content, and thus also a comparably large average pore size derived from N_2 adsorption. In contrast, the limestone sample from the Rothenfluh Member in the Passwang Formation exhibits a comparably large surface area but a small water content, and thus a very low average pore size. This is probably the reason for the rather low anion-accessible porosity observerd for samples from this section, even though they have a comparably low clay mineral content. In general, radii of external pores derived from N_2 adsorption tend to be smallest in clay-rich lithologies.

Drilling fluid contamination was not identified in any aqueous extraction samples. It was noticed that aqueous extraction on dried rock yielded substantially lower Br concentrations compared to extracts conducted on wet rock. This might be related to complexation with transformed organic matter during the heating to 105 °C, but further investigations would be needed to check this hypothesis.

Porewater $\delta^{18}O$ and $\delta^{2}H$ values exhibit generally a characteristic curved shape between the Hauptrogenstein and the Klettgau Formation. In the upper part of the cored borehole section, porewater isotope compositions evolve towards a local minimum at around 330 – 340 m depth

(located just at or above the upper end of the packed-off interval, slightly above the transmissive zone in the Hauptrogenstein aquifer at around 352 m depth) thereby approaching the GMWL in the range of modern recharge. In the remainder of the Hauptrogenstein and the Passwang Formation the porewater isotope composition evolves – at relatively steep gradients – towards more enriched $\delta^{18}O$ and $\delta^{2}H$ signatures. In a $\delta^{2}H$ vs. $\delta^{18}O$ diagram, the porewater isotope trends in the Hauptrogenstein and the Passwang Formation behave remarkably linear, and they follow a seawater dilution line. This trend abruptly breaks at the base of the Passwang Formation, where the porewater $\delta^{18}O$ values start to continuously decrease while the $\delta^{2}H$ values remain about constant, such that the data tend to fall on the GMWL in the lower parts of the Opalinus Clay. This suggests a significant influence of a meteoric signature in the latter porewaters. Moreover, the different behaviour of $\delta^{18}O$ and $\delta^{2}H$ values may reflect inherited trends resulting from the earlier evolution (i.e., before activation of the confining aquifers) with rather constant $\delta^{2}H$ but $\delta^{18}O$ values decreasing with depth across the low-permeability formations of the Dogger and the Liassic. Across the Staffelegg Formation the porewater isotope composition evolves along the GMWL, from $\delta^{18}O$ and $\delta^{2}H$ values more enriched than those of modern recharge towards most negative values in the water conducting zone of the Klettgau Formation, falling into the range of modern recharge. Overall, these trends indicate that the isotopic composition of the porewaters in the Jurassic sediments evolved from the original seawater by exchange with water in the over- and underlying formations, possibly by water-rock interactions, and finally by the exchange with the present-day confining aquifers in the Hauptrogenstein and the Klettgau Formation.

Anion-accessible porosities could be derived from squeezed (SQ) and advectively displaced (AD) porewaters. These yielded consistent Cl-accessible porosity fractions (f_{Cl}) with a mean value of ~ 0.42 ± 0.07. This is very similar to the values derived for the BOZ1-1 borehole, in which more data, notably also at low clay-mineral contents are available. Based on this similarity, the same linear relationship of f_{Cl} with clay-mineral content at a clay-mineral content ≤ 25 wt.-% was used for BOZ2-1 to derive Cl and Br concentrations per accessible porewater from aqueous extraction.

Broadly consistent Cl and Br profiles are revealed from squeezing, advective displacement and re-calculated aqueous extraction data. Using pycnometer instead of water-loss porosities when scaling the aquous extract data to concentrations per bulk porewater or accessible porewater leads to slightly smoother profiles and a better match of University of Bern and BRGM data. The Cl and Br profiles show a curved shape between the Klettgau Formation and the Passwang Formation, with constant Cl concentrations of ~ 2.5 g/L in the Opalinus Clay. They are bounded by the lower aquifer and upper aquifer in the Keuper and Hauptrogenstein, respectively. Analogous profiles were derived for $\delta^{18}O$ and $\delta^{2}H$ (see above). There is no indication of the presence of an active aquifer in the Passwang Formation. Below the Keuper aquifer, the few Cl and Br concentrations suggest an increasing trend towards the Muschelkalk aquifer, which would be in line with the Cl concentration, but not really the Br concentration in the aquifer.

The depth profile of the Br/Cl ratio reveals consistency between the three datasets AqEx, SQ and AD. It shows less scatter than that of Cl or Br, due to the fact that no assumptions on anion accessibility need to be made and the uncertainty regarding recalculation to the rock porosity cancels out. From the Keuper aquifer, the Br/Cl ratio indicates a strong increase followed by strong decrease in the Klettgau Formation. In the Staffelegg Formation and Opalinus Clay, values remain more constant, but display an increasing trend and more scatter in the upper lying formations. There is an offset of the "dry" AqEx and AD (and partially also SQ data) relative to the "standard" AqEx data, and the aquifer data tend to be slightly lower than the porewater values. The reasons for both observations are unclear at this stage.

The sulphate data obtained from SQ and AD, which covers the Passwang Formation to the Staffelegg Formation, are consistent. The corresponding SO_4 profile indicates slightly decreasing concentrations from the upper to the lower units. Conversely, AqEx data yield systematically

higher and more variable concentrations, as has been observed in the previous boreholes and the Mont Terri Rock Laboratory. SO_4/Cl ratios deduced from SQ and AD are approximately constant (~ 0.5 in molar units) in the Passwang Formation and Opalinus Clay, but appear to increase below towards the Keuper aquifer.

Cation data representative of the porewater could be obtained from SQ and AD data although two of three AD samples were affected by high nitrate levels and showed perturbed cation distributions. The other samples indicated an increasing trend with depth for the main cations Na, Ca and Mg from the Passwang Formation to the Staffelegg Formation. Na follows the same trend as Cl in the upper part of the profile, but diverges from Cl further down, where SO_4 contributes significantly to the anionic charge. K does not seem to follow any trend with dept (for Sr there are not sufficient data available to deduce any trend).

The cation exchange capacity (CEC) correlates with the clay-mineral content. An even better correlation can be deduced with the sum of illite and smectite end-member mineral contents, the main carriers of the CEC. The main exchangeable cations are Na and Ca, followed by Mg and K. The exchanger composition (cation occupancies) is approximately constant across the sampled sequence (Staffelegg Formation – Passwang Formation). The exchanger composition determined from extraction methods exhibits the same trends as the "calculated" exchanger compositon obtained from modelling of the SQ and AD porewater data, but the latter data show somewhat higher Na/Ca ratios.

The porewaters in the Opalinus Clay and bounding formations from BOZ2-1 are the most dilute of all boreholes investigated so far, but only slightly less saline than BOZ1-1 and of similar composition as that borehole in the same siting area. Maximum Cl concentrations are ~ 2.5 g/L. Note that the porewaters have a larger share of SO_4 and a higher SO_4/Cl ratio than those of the other siting regions NL and ZNO. The porewaters are of Na-Cl-SO_4 type (according to the nomenclature of Jäckli 1970) in the Passwang Formation and Opalinus Clay, shifting to Na-SO_4-Cl type in the Staffelegg Formation.

The pH/P_{CO2} conditions deduced for the SQ and AD data appear somewhat perturbed due to CO_2 exchange during the experiments in case of SQ and due to microbial processes resulting in elevated nitrate concentrations in the case of AD. Reasonable pH/P_{CO2} conditions could be estimated from simple modelling considering CO_2 exchange during the SQ experiments.

SQ data and the AD sample not too much perturbed by high nitrate production yield consistent TOC concentrations of 100 – 120 mg C/L. These concentrations, however, are not thought to fully reflect in situ porewater conditions, but rather the easily mobilisable fraction from the solid organic matter.

An in-depth interpretation and comparison with data from boreholes from other siting areas is beyond the scope of this report. Here, a short summary of a few points is presented:

- In the BOZ2-1 borehole, groundwater samples could be extracted from packed-off sections in the Hauptrogenstein, in the upper Keuper and in the Muschelkalk. In the BOZ1-1 borehole, a groundwater sample could only be obtained from from the Muschelkalk.
- Tracer profiles as well as structural observations clearly confirm the presence of active aquifers in the centre of the Hauptrogenstein and in the Klettgau Formation of the upper Keuper (no tracer data were determined in the Bänkerjoch Formation towards the Muschelkalk aquifer). In the BOZ1-1 borehole, tracer profiles indicated an active aquifer in the upper Keuper as well, but not in the Hauptrogenstein.

- From the few currently available SQ and AD data, the f_{Cl} value seems to be in a similar range as in the BOZ1-1 borehole (~ 0.42 for clay-mineral contents > 25 wt.-%; lower value of ~ 0.32 in the Passwang Formation). No data from diffusion experiments are currently available for the BOZ2-1 borehole.
- The porewaters in the Opalinus Clay and confining units from the BOZ2-1 borehole are even somewhat more dilute than those in the BOZ1-1 borehole and thus represent the most dilute in all investigated boreholes so far, with chloride contents in the range of 1.5 – 2.5 g/L. The share of sulphate and the SO_4/Cl ratio, however, is larger than in iother siting regions.
- The maximum delta-values of the stable water isotopes are only slightly lower compared to maximum values in other boreholes.

7 References

Allison, J.D., Brown, D.S. & Novo-Gradac, K.J. (1991): MINTEQA2/PRODEFA2, a geochemical assessment model for environmental systems: Version 3.0 user's manual. Environmental Research Laboratory, Office of Research and Development, U.S. Environmental Protection Agency, 106 p.

Aschwanden, L. & Wersin, P. (2020): Experimental study of sulphate in the Opalinus Clay: Results from extraction tests. Nagra Arbeitsbericht NAB 20-17.

Aschwanden, L., Camesi, L., Gimmi, T., Jenni, A., Kiczka, M., Mäder, U., Mazurek, M., Rufer, D., Waber, H.N., Wersin, P., Zwahlen, C. & Traber, D. (2021): TBO Trüllikon-1-1: Data report Dossier VIII. Rock properties, porewater characterisation and natural tracer profiles. Nagra Arbeitsbericht NAB 20-09.

Bradbury, M.H. & Baeyens, B. (1998): A physicochemical characterisation and geochemical modelling approach for determining porewater chemistries in argillaceous rocks. Geochim. Cosmochim. Acta 62, 783-795.

Charpentier, D., Tessier, D. & Cathelineau, M. (2003): Shale microstructure evolution due to tunnel excavation after 100 years and impact of tectonic paleo-fracturing. Case of Tournemire, France. Engineering Geology 70, 55-69.

Courdouan Merz, A. (2008): Nature and reacivity of dissolved organic matter in clay formations evaluated for the storage of radioactive waste. PhD thesis. ETH Zurich.

Courdouan, A., Christl, I., Meylan, S., Wersin, P. & Kretzschmar, R. (2007a): Characterization of dissolved organic matter in anoxic rock extracts and in situ pore water of the Opalinus Clay. Applied Geochemistry 22, 2926-2939.

Courdouan, A., Christl, I., Meylan, S., Wersin, P. & Kretzschmar, R. (2007b): Isolation and characterization of dissolved organic matter from the Callovo-Oxfordian formation. Applied Geochemistry 22, 1537-1548.

Craig, H. (1961): Isotopic variations in meteoric waters. Science 133, 1702-1703.

Debure, M. & Gailhanou, H. (2019): GD experiment: Experimental study of sulphate in Opalinus Clay. Unpubl. Mont Terri Technical Note. Mont Terri Project, Switzerland.

Egli, D., Mosar, J., Ibele, T. & Madritsch, H. (2017): The role of precursory structures on tertiary deformation in the Black Forest – Hegau region. International Journal of Earth Sciences 106, 2297-2318.

Gaboreau, S., Prêt, D., Tinseau, E., Claret, F., Pellegrini, D. & Stammose, D. (2011): 15 years of in situ cement–argillite interaction from Tournemire URL: Characterisation of the multi-scale spatial heterogeneities of pore space evolution. Appl. Geochem. 26, 2159-2171.

Gimmi, T. & Alt-Epping, P. (2018): Simulating Donnan equilibria based on the Nernst-Planck equation. Geochim. Cosmochim. Acta 232, 1-13.

Gimmi, T. & Waber, H.N. (2004): Modelling of tracer profiles in porewater of argillaceous rock in the Benken borehole: Stable water isotopes, chloride and chlorine isotopes. Nagra Technical Report NTB 04-05.

Gimmi, T., Waber, H.N., Gautschi, A. & Rübel, A. (2007): Stable water isotopes in pore water of Jurassic argillaceous rocks as tracers for solute transport over large spatial and temporal scales. Water Resour. Res. 43, W04410, doi:10.1029/2005WR004774.

Gimmi, T., Leupin, O.X., Eikenberg, J., Glaus, M., Van Loon, L.R., Waber, H.N., Wersin, P., Wang, H.A.O., Grolimund, D., Borca, C.N., Dewonck, S., Wittebroodt, C. (2014): Anisotropic diffusion at the field scale in a four-year multi-tracer diffusion and retention experiment – I: Insights from the experimental data. Geochim. Cosmochim. Acta 125, 373-393.

Hadi, J., Wersin, P., Mazurek, M., Waber, H.N., Marques Fernandes, M., Baeyens, B., Honty, M., De Craen, M., Frederickx, L., Dohrmann, R. & Fernandez, A.M. (2019): Intercomparison of CEC method within the GD project. Mont Terri Technical Report TR 2017-06. Mont Terri Project, Switzerland.

Isler, A., Pasquier, F. & Huber, M. (1984): Geologische Karte der zentralen Nordschweiz 1:100'000. Herausgegeben von der Nagra und der Schweiz. Geol. Komm.

Jäckli, H. (1970): Kriterien zur Klassifikation von Grundwasservorkommen. Eclogae geol. Helv. 63/2, 389-434.

Jenni, A., Aschwanden, L., Lanari, P., de Haller, A. & Wersin, P. (2019): Spectroscopic investigation of sulphur-containing minerals in Opalinus Clay. Nagra Arbeitsbericht NAB 19-23.

Kullin, M. & Schmassmann, H. (1991): Isotopic composition of modern recharge. *In:* Pearson F.J., Balderer, W., Loosli, H.H., Lehmann, B.E., Matter, A., Peters, Tj., Schmassmann, H.-J. & Gautschi, A. (1991): Applied Isotope Hydrogeology – A Case Study in Northern Switzerland. Studies in Environmental Science 43, Elsevier, Amsterdam, 65-89.

Lorenz, G.D. (*in prep.*): Borehole BOZ2-1 (Bözberg-2-1): Fluid sampling and analytical hydrochemical data report. Unpubl. Nagra Interner Bericht.

Mäder, U. (2018): Advective displacement method for the characterisation of porewater chemistry and transport properties in claystone. Geofluids 2018, Article ID 8198762, doi.org/10.1155/2018/8198762

Mäder, U. & Waber, H.N. (2017): Results of advective displacement / multi-component transport experiments from claystone samples of the Schlattingen borehole. Nagra Arbeitsbericht NAB 17-16.

Mäder, U., Aschwanden, L., Camesi, L., Gimmi, T., Jenni, A., Kiczka, M., Mazurek, M., Rufer, D., Waber, H.N., Wersin, P., Zwahlen, C. & Traber, D. (2021): TBO Marthalen-1-1: Data report Dossier VIII: Rock properties, porewater characterisation and natural tracer profiles. Nagra Arbeitsbericht NAB 21-20.

Madritsch, H. & Hammer, P. (2012): Characterisation of Cenozoic brittle deformation of potential geological siting regions for radioactive waste repositories in Northern Switzerland based on structural geological analysis of field outcrops. Nagra Arbeitsbericht NAB 12-41.

Marques Fernandes, M. & Baeyens, B. (*in prep.*): Sorption measurements of Cs, Ni, Eu, Th and U on rock samples of Opalinus Clay and confining geological units from deep boreholes at the potential siting regions for a deep geological repository for radioactive waste in Switzerland: Jura Ost, Nördlich Lägern and Zürich Nordost. Nagra Technical Report NTB 22-02.

Mazurek, M. (2017): Gesteinsparameter-Datenbank Nordschweiz – Version 2. Nagra Arbeitsbericht NAB 17-56.

Mazurek, M. & Aschwanden, L. (2020): Multi-scale petrographic and structural characterisation of the Opalinus Clay. Nagra Arbeitsbericht NAB 19-44.

Mazurek, M., Oyama, T., Wersin, P. & Alt-Epping, P. (2015): Pore-water squeezing from indurated shales. Chemical Geology 400, 106-121.

Mazurek, M., Aschwanden, L., Camesi, L., Gimmi, T., Jenni, A., Kiczka, M., Mäder, U., Rufer, D., Waber, H.N., Wanner, P., Wersin, P. & Traber, D. (2021): TBO Bülach-1-1: Data Report Dossier VIII: Rock properties, porewater characterisation and natural tracer profiles. Nagra Arbeitsbericht NAB 20-08.

Monnier, G., Stengel, P.T. & Fies, J. (1973): Une méthode de mesure de la densité apparente de petits agglomérats terreux – Application à l'analyse des systèmes de porosité du sol. Ann. Agron. 24.

Naef, H., Büchi, M., Bläsi, H.R., Deplazes, G. & Gysi, M. (2019): Lithology Manual – Lithological description of drill cores and cuttings in Northern Switzerland. Nagra Arbeitsbericht NAB 19-11.

Nagra (2008): Vorschlag geologischer Standortgebiete für das SMA- und das HAA-Lager. Geologische Grundlagen. Nagra Technischer Bericht NTB 08-04.

Nagra (2014): SGT Etappe 2: Vorschlag weiter zu untersuchender geologischer Standortgebiete mit zugehörigen Standortarealen für die Oberflächenanlage. Geologische Grundlagen. Dossier II: Sedimentologische und tektonische Verhältnisse. Nagra Technischer Bericht NTB 14-02.

Parkhurst, D.L. & Appelo, C.A.J. (2013): Description of input and examples for PHREEQC Version 3: A computer program for speciation, batch-reaction, one-dimensional transport, and inverse geochemical calculations. No. 6-A43. US Geological Survey.

Pearson, F.J. (1999): What is the porosity of a mudrock? *In*: Aplin, A.C., Fleet, A.J. & Macquaker, J.H.S. (eds.): Muds and Mudstones: Physical and Fluid Flow Properties. Geological Society, London, Special Publications 158, 9-21.

Pearson, F.J., Arcos, D., Bath, A., Boisson, J.Y., Fernandez, A.M., Gäbler, H.E., Gaucher, E., Gautschi, A., Griffault, L., Hernan, P. & Waber, H.N. (2003): Mont Terri project – geochemistry of water in the Opalinus Clay formation at the Mont Terri rock laboratory. Federal Office for Water and Geology Rep. 5, Bern, Switzerland.

Pearson, F.J., Tournassat, C. & Gaucher, E.C. (2011): Biogeochemical processes in a clay formation in situ experiment: Part E – Equilibrium controls on chemistry of pore water from the Opalinus Clay, Mont Terri underground research laboratory, Switzerland. Applied Geochemistry 26, 990-1008.

Pietsch, J. & Jordan, P. (2014): Digitales Höhenmodell Basis Quartär der Nordschweiz – Version 2013 (SGT E2) und ausgewählte Auswertungen. Nagra Arbeitsbericht NAB 14-02.

Rufer, D. (2019): Field Manual: Drillcore sampling for analytical purposes. Nagra Arbeitsbericht NAB 19-13.

Rufer, D. & Mazurek, M. (2018): Pore-water extraction and characterization: Benchmarking of the squeezing and adapted isotope diffusive exchange methods. NWMO Technical Report NWMO-TR-2018-14. Nuclear Waste Management Organization, Toronto, Canada.

Thoenen, T., Hummel, W., Berner, U. & Curti, E. (2014): The PSI/Nagra Chemical Thermodynamic Database 12/07. PSI Bericht Nr. 14-04, Paul Scherrer Institut, Villigen, Switzerland.

Thommes, M., Kaneko, K., Neimark, A.V., Olivier, J.P., Rodriguez-Reinoso, F., Rouquerol, J. & Sing, K.S. (2015): Physisorption of gases, with special reference to the evaluation of surface area and pore size distribution (IUPAC Technical Report). Pure and Applied Chemistry 87, 1051-1069.

Tournassat, C., Vinsot, A., Gaucher, E.C. & Altmann, S. (2015): Chemical conditions in clay-rocks. *In:* Tournassat, C., Steefel, C.I., Bourg, I.C. & Berrgaya, F. (eds.): Natural and Engineered Clay Barriers. Developments in Clay Science 6, Chapter 3, 71-100. Elsevier.

Van Loon, L.R. & Glaus, M.A. (*in prep.*): Diffusion measurements of HTO, $^{36}Cl^-$ and $^{22}Na^+$ on rock samples of Opalinus Clay and confining geological units from deep boreholes at the potential siting regions for a deep geological repository for radioactive waste in Switzerland: Jura Ost, Nördlich Lägern and Zürich Nordost. Nagra Technical Report NTB 22-01.

Waber, H.N. (ed.) (2020): SGT-E3 deep drilling campaign (TBO): Experiment procedures and analytical methods at RWI, University of Bern (Version 1.0, April 2020). Nagra Arbeitsbericht NAB 20-13.

Wersin, P., Mazurek, M., Waber, H.N., Mäder, U.K., Gimmi, T., Rufer, D. & de Haller, A. (2013): Rock and porewater characterisation on drillcores from the Schlattingen borehole. Nagra Arbeitsbericht NAB 12-54.

Wersin, P., Mazurek, M., Mäder, U.K., Gimmi, T., Rufer, D., Lerouge, C. & Traber, D. (2016): Constraining porewater chemistry in a 250 m thick argillaceous rock sequence. Chemical Geology 434, 43-61.

Wersin, P., Pekala, M., Mazurek, M., Gimmi, T., Mäder, U.K., Jenni, A., Rufer, D. & Aschwanden, L. (2021): Porewater chemistry of Opalinus Clay: Methods, modelling & buffering capacity. Nagra Technical Report NTB 18-01.

Wersin, P., Aschwanden, L., Camesi, L., Gaucher, E.C., Gimmi, T., Jenni, A., Kiczka, M., Mäder, U., Mazurek, M., Rufer, D., Waber, H.N., Zwahlen, C. & Traber, D. (2022). TBO Bözberg-1-1: Data report Dossier VIII: Rock properties, porewater characterisation and natural tracer profiles. Nagra Arbeitsbericht NAB 21-21.